ORSAY
N° D'ORDRE:

UNIVERSITÉ DE PARIS-SUD
U.F.R. SCIENTIFIQUE D'ORSAY

THÈSE

Présentée pour obtenir

le GRADE de DOCTEUR EN SCIENCE DE L'UNIVERSITÉ PARIS XI

Par

Zdenko MACHALA

Sujet:

Les décharges électriques continues et transitoires, induites par streamer, sous pression atmosphérique, pour la destruction des composés organiques volatils (COV)

Soutenue le 18 décembre 2000 devant la Commission d'examen:

M. Jacques AMOUROUX *Professeur à l'Université Paris VI, France*	rapporteur
M. Marc FITAIRE *Professeur à l'Université Paris XI, France*	examinateur
M. František HANIC *Directeur de recherche à l'Académie Slovaque des Sciences, Slovaquie*	rapporteur
M. Peter LUKÁČ *Professeur à l'Université Comenius à Bratislava, Slovaquie*	examinateur
M. Emmanuel MARODE *Directeur de recherche au CNRS, Orsay, France*	examinateur
Mme Marcela MORVOVÁ *Chercheur et professeur à l'Université Comenius à Bratislava, Slovaquie*	examinateur
M. Serge VACQUIE *Directeur de recherche au CNRS, Toulouse, France*	rapporteur

Continuous and transient electrical discharges, streamer triggered, at atmospheric pressure, for the removal of Volatile Organic Compounds (VOC).

Abstract: The thesis presents two new types of streamer-induced electric discharges operating in the non-uniform electric field in air at atmospheric pressure. These discharges are applied to the removal of Volatile Organic Compounds (VOC) – important atmospheric pollutants. One of them is the high pressure glow discharge (HPGD) whose exceptional feature is to be pulseless, in contrast with an usual high pressure case to be self pulsing. It has physical properties similar to those of the normal low pressure glow discharge. The second discharge regime, the transient spark (TS), uses the streamer-to-spark transition. However, by limiting the spark phase to a very short time interval, it cannot reach the local thermodynamic equilibrium. Both discharges generate a non-thermal plasma with a gas temperature in the range of 1000 to 2000 K.

The effects of these discharges to VOC (cyclohexanone and toluene) contained in a buffer gas (usually air) have been investigated in various reactors and under various conditions. Achieved removal efficiencies and energy costs, as well as formed products, depend on many factors, particularly on the injected energy (energy density), the gas components (e.g. moisture) and, of course, on the discharge and reactor type. Optimal conditions for pollutant removal specific for each discharge type have been determined. It is shown that mechanisms associated with heterogeneous effects of the Cu electrode surfaces together with active nitrogen species are responsible for low energy costs (under 100 eV/molecule) and a low production of CO_2 and other gaseous species, but a dominant formation of condensed products based on amino acids.

The small pilot-scale reactor (50 Nm^3/h) working with TS discharge has been successfully applied to the removal of cyclohexanone in the mixture with other VOC, with no noxious gas output. This validates a possibility of application of such a type of discharge reactor for larger industrial scales.

Les décharges électriques continues et transitoires, induites par streamer, sous pression atmosphérique, pour la destruction des composés organiques volatils (COV).

Résumé: La thèse présente deux nouveaux types des décharges électriques induites par streamer, opérés en champ électrique non-uniform dans l'air à la pression atmosphérique. Elles sont appliquées à la destruction de Composés Organiques Volatiles (COV) – des polluants gazeux importants. Une de ces décharges est la décharge luminescente (glow) haute pression (HPGD) avec la propriété exceptionnelle d'être continue, contrairement au cas habituel en haute pression d'être auto-pulsée. Elle possède des propriétés physiques similaires à la décharge luminescente basse pression normale. L'autre décharge est une étincelle transitoire (TS), qui se fonde sur le passage du streamer vers la formation d'un arc. Elle s'obtient en limitant la durée de la phase d'arc de telle sorte qu'elle deviennent trop courte pour que s'établissent des conditions d'équilibre thermodynamique local. Les deux décharges génèrent un plasma non-thermique, avec une température du gaz se situant entre 1000 et 2000 K.

L'action de ces décharges sur les COV (cyclohexanone et toluène) contenus dans le gaz vecteur (habituellement air) dans plusieurs réacteurs et sous conditions diverses sont étudiées. Les taux de destruction et les rendements énergétiques atteints, ainsi que les produits créés dépendent de nombreux facteurs, dont les principaux sont l'énergie injectée (la densité d'énergie), la composition du gaz (par exemple vapeur d'eau) et, bien sûr, le type de décharge et de réacteur. Les conditions optimales de fonctionnement pour la destruction des polluants spécifiques pour le type de la décharge ont été déterminés. Il est montré que des mécanismes associés aux effets hétérogènes sur la surface des électrodes en Cu combinés aux espèces activées d'azote sont ce qui définit les rendements énergétiques bas (inférieur à 100 eV/molécule) et la production diminuée de CO_2 et d'autres produits gazeux, mais la formation dominante de produits condensés fondés sur des acides aminées.

Le petit réacteur en échelle pilot (50 Nm^3/h), fonctionnant avec la décharge TS, donne des résultats acceptables dans la dégradation du cyclohexanone en mélange d'autres COV sans, pour autant, laisser des résidus gazeux nocifs. Cela démontre la possibilité d'application de tel réacteurs aux échelles industrielles.

Kontinuálne a prechodové elektrické výboje indukované streamerom, za atmosférického tlaku, na odstraňovanie prchavých organických látok (VOC)

Abstrakt: Dizertačná práca prezentuje dva nové typy streamerom indukovaných elektrických výbojov pracujúcich v nehomogénnom elektrickom poli vo vzduchu pri atmosférickom tlaku. Tieto výboje sú aplikované na odstraňovanie prchavých organických látok (VOC) – významných atmosférických znečistenín. Jedným z nich je vysokotlaký tlecí výboj (HPGD), s výnimočnou vlastnosťou byť bezpulzný (kontinuálny), hoci výboje pri atmosférickom tlaku sú obyčajne auto-pulzné. Fyzikálnymi vlastnosťami zodpovedá normálnemu tleciemu výboju pri nízkom tlaku. Druhým výbojom je prechodová iskra (TS), ktorá funguje v režime prechodu streamera do iskry, avšak v dôsledku časovej limitácie iskorvej fázy sa v nej nestihne dosiahnuť lokálna termodynamická rovnováha. Obidva výboje generujú non-termálnu plazmu s teplotou plynu v intervale 1000-2000 K.

Vplyvy týchto výbojov na VOC (cyclohexanón and toluén) v nosnom plyne (obyčajne vzduch) boli skúmané vo viacerých reaktoroch a za rôznych podmienok. Dosiahnuté účinnosti a energetické náklady, rovnako ako formované produkty závisia od mnohých faktorov, predovšetkým od vloženej energie (hustote energie), zložiek plynu (napr. vlhkosť) a samozrejme typu výboja a reaktora. Boli zistené optimálne podmienky procesu deštrukcie polutantov, charakteristické pre každý výboj. Ukázalo sa, že mechanizmy spojené s heterogénnymi efektami na povrchoch Cu elektród spolu s aktívnym dusíkom sú zodpovedné za nízke energetické náklady procesu (pod 100 eV/molekula) a zníženú produkciu CO_2 a iných plynných látok, avšak dominantnú tvorbu kondenzovaných produktov na báze aminokyselín.

Malý reaktor v pilotnej škále (50 Nm^3/h), pracujúci s výbojom TS bol úspešne aplikovaný na deštrukciu cyklohexanónu v zmesi s inými VOC, bez výstupu škodlivých plynov. Tým sa overila možnosť použitia takého typu výbojového reaktora vo väčšej priemyselnej mierke.

REMERCIEMENTS

Cette étude a été effectuée en parallèle au sein de l'Equipe Décharges Electriques et Environnement (EDEE) du Laboratoire de Physique des Gaz et Plasmas (LPGP) de l'Université Paris-Sud XI à Gif sur Yvette, France et à l'Institut de Physique de Faculté des Mathématiques et Physique de l'Université Comenius (MFF UK) à Bratislava, Slovaquie. Merci à Messieurs **Emmanuel Marode** et **J.-P. Borra**, l'ancien et le nouveau responsables de l'EDEE et à Messieurs **Mirko Černák** et **Branislav Sitár**, l'ancien et le nouveau responsables de l'Institut de Physique, de m'avoir accueilli et permis de travailler dans leurs équipes. Je remercie également l'ancien et le nouveau directeurs du LPGP, Messieurs **Claude Deutch** et **Jean Bretagne** et le doyen de MFF UK, Monsieur **Ľudovít Fischer**, ainsi que les recteurs des deux universités, Messieurs **Alain Gaudemer** et **Ferdinand Devínsky**, pour avoir accepté que je suive mes études doctorales sous cette forme. Je tiens à remercier aussi les gouvernements français (représenté par l'ambassade de France en Slovaquie) et slovaque, qui m'ont attribué les bourses d'études.

J'adresse ma chaleureuse reconnaissance surtout à mes deux directeurs de thèse: Monsieur **Emmanuel Marode**, directeur de recherche au CNRS et Madame **Marcela Morvová**, chercheur et maître de conférence à MFF UK. J'ai en haute estime leurs qualités scientifiques et expérimentales, leurs connaissances, leurs idées, leur patience et le temps qu'ils ont consacré à ce travail. Nos nombreuses discussions, les relations amicales, ainsi que leur sens de l'humour et leur aide étaient pour moi un grand enrichissement, et pas seulement sur le plan scientifique.

Que Messieurs **Serge Vacquié** et **František Hanic**, directeurs de recherche au CNRS de l'Université Paul Sabatier à Toulouse et à l'Académie Slovaque de Sciences à Bratislava, ainsi que Messieurs **Jacques Amouroux** et **Július Krempaský**, professeurs à l'Université Pierre et Marie Curie, Paris VI et à l'Université Technique Slovaque à Bratislava, trouvent ici ma reconnaissance pour l'honneur qu'ils m'ont fait en acceptant d'être les rapporteurs de ce travail. Je remercie également Messieurs **Marc Fitaire** et **Peter Lukáč**, professeurs à l'Université Paris-Sud à Orsay et à l'Université Comenius à Bratislava d'avoir accepté de faire partie du jury de soutenance de cette thèse en France.

Ma gratitude appartient aussi à ceux, qui m'ont fait profiter de leur savoir ou de leur matériel et qui m'ont donné des conseils scientifiques divers et leur soutien moral, surtout aux chercheurs suivants : **Robert Haug**, **Gildas Hartmann**, **Djamal Djermoune**, **Jean-Pascal Borra**, **Marie-Pierre Jaffrezic**, **Pavel Veis**, **Imrich Morva**, **Elena Brežná**, **Štefan Matejčík** et **Anna Polášková**.

Mes remerciements vont également aux assistants ingénieurs et autres personnels des laboratoires, particulièrement à Madame **Micheline Palierne** pour sa constante disponibilité et son soutien et à Messieurs **Michel Cottet-Dumoulin** et **Alain Péchard** pour l'intérêt qu'ils ont porté sur mon travail et la réalisation technique des nombreux montages. Je suis reconnaissant aussi à Messieurs **Roger Hahn**, **Guy Orine** et **Guy Ermende** pour leur disponibilité et leurs compétences techniques et à l'administratrice du laboratoire français **Dominique Goullieux**, qui m'a aidé à surmonter les obstacles administratifs.

Je tiens à remercier tous les doctorants et étudiants des deux laboratoires, récents ou déjà partis. Ce sont eux qui m'ont accueilli dans une ambiance amicale et avec qui j'ai partagé « les hauts et les bas » des jeunes chercheurs. Je vais nommer au moins ceux, avec qui j'ai directement coopéré et qui m'ont aidé dans les difficultés scientifiques, techniques ou concernant la vie pratique: **Philippe Dessante**, **Nathalie Deschamps**, **Emmanuel Odic**, **Ludovic Parissi**, **Sandrine Dupré**, **Sophie Delaveau**, **Séverine Bousquet**, **Marielle Dhainaut**, **Christian Deniset**, **Ramzi Hadaji**, **Bernhard Kreissl** et **Bénédicte Lemieux-Dudon** du côté français, ainsi que **Karol Hensel**, **Martin Kurdel**, **Róbert Gašparík**, **Mário Janda**, **Eva Guldanová** et **Peter Macko** du côté slovaque.

Merci à mon beau-frère **Marek Discantiny** de son aide dans les phases finales de la rédaction de thèse. Que ma **mère**, toute ma famille et mes amis, qui ont attentivement suivi mes succès et non-succès, trouvent ici également le témoignage de ma reconnaissance.

Enfin, je tiens à exprimer ma chaleureuse gratitude, ma reconnaissance, mon admiration et ma compréhension à mon épouse **Zuzka**, qui m'a tout le temps fidèlement accompagné et soutenu, pendant les séjours en France aussi bien que chez nous, en Slovaquie. C'est elle qui m'a toujours aidé, en particulier dans les phases finales de la rédaction, et qui a, du fait de cette thèse, pratiquement sacrifié ses études doctorales. Je remercie également ma fille **Monika** qui a souvent souffert de l'absence de son père. J'essaierai de leur compenser tout ce temps.

Mais ma plus humble gratitude appartient à notre **Dieu**, bon et puissant, qui m'a béni, a été tout le temps auprès de moi et qui m'a donné les aptitudes et la force d'aboutir.

POĎAKOVANIE

Táto práca bola vykonávaná paralelne na Ústave fyziky Matematicko-fyzikálnej fakulty Univerzity Komenského (MFF UK) v Bratislave na Slovensku a na Oddelení elektrických výbojov a environmentu (EDEE) Laboratória fyziky plynov a plazmy (LPGP) Univerzity Paríž-Juh v Gif sur Yvette vo Francúzsku. Ďakujem bývalému i súčasnému riaditeľovi Ústavu Fyziky doc. **Mirkovi Černákovi** a prof. **Branislavovi Sitárovi**, ako aj bývalému a súčasnému vedúcemu EDEE Dr. **Emmanuelovi Marodovi** a Dr. **J.-P. Borrovi** za prijatie a umožnenie pracovať na svojich oddeleniach. Rovnako ďakujem dekanovi MFF UK doc. **Ľudovítovi Fischerovi** a bývalému i súčasnému riaditeľovi LPGP Dr. **Claudovi Deutchovi** a Dr. **Jeanovi Bretagnovi**, ako aj rektorom oboch zainteresovaných univerzít prof. **Ferdinandovi Devínskemu** a p. **Alainovi Gaudemerovi** za umožnenie doktorandského štúdia touto formou. Moja vďaka patrí tiež slovenskej i francúzskej vláde (reprezentovanej Francúzskou ambasádou na Slovensku), ktoré mi poskytli štipendium na toto štúdium.

Predovšetkým však chcem vyjadriť svoju vrelú vďaku a ocenenie mojim dvom školiteľom: doc. **Marcele Morvovej**, samostatnej vedeckej pracovníčke na Ústave fyziky MFF UK a Dr. **Emmanuelovi Marodovi**, vedúcemu výskumu v LPGP (CNRS). Vysoko si vážim ich vedecké kvality a experimentálne skúsenosti, rozhľadenosť, nápady, trpezlivosť a čas, ktoré zasvätili tejto práci. Naše nespočetné odborné diskusie a priateľský vzťah, rovnako ako ich zmysel pre humor a mnohoraká pomoc z ich strany boli pre mňa veľkým prínosom, a to nielen vo vedeckej oblasti.

Moje ocenenie nech prijmú páni doc. **František Hanic** a Dr. **Serge Vacquié**, vedúci výskumu na Slovenskej Akadémii Vied a v CNRS na Univerzite Paul Sabatier v Toulouse, rovnako ako páni prof. **Július Krempaský** a prof. **Jacques Amouroux**, profesori na Slovenskej Technickej Univerzite Bratislave a Univerzite Pierre a Marie Curie, Paríž VI, a to za česť, ktorú mi prejavili, keď sa podujali oponovať túto rozsiahlu prácu. Takisto ďakujem pánom prof. **Petrovi Lukáčovi** a prof. **Marcovi Fitairovi**, profesorom na Univerzite Komenského v Bratislave a Univerzite Paríž-Juh v Orsay za prijatie účasti v komisii obahjoby tejto práce vo Francúzsku.

Moja vďaka patrí aj tým, ktorí mi pomáhali v odborných otázkach a poskytovali svoj materiál, cenné rady a morálnu podporu. Sú nimi najmä títo výskumní pracovníci: doc. **Pavel Veis**, Dr. **Imrich Morva**, doc. **Elena Brežná**, doc. **Štefan Matejčík**, Dr. **Anna Polášková**, Dr. **Robert Haug**, Dr. **Gildas Hartmann**, Dr. **Djamal Djermoune**, Dr. **Jean-Pascal Borra** a Dr. **Marie-Pierre Jaffrezic**.

Ďakujem tiež technickým a administratívnym pracovníkom, najmä pani **Micheline Palierne** za jej disponibilitu, pomoc a podporu a pánom **Michelovi Cottet-Dumoulinovi** a **Alainovi Péchardovi** za ich záujem o moju prácu a promptnú technickú realizáciu mnohých zariadení. Ďalej ďakujem pánom Dr. **Rogerovi Hahnovi**, **Guy Orinovi** a **Guy Ermendovi** za možnosť využiť ich technické zdatnosti a administratívnej pracovníčke **Dominique Goullieux**, ktorá mi pomáhala prekonávať byrokratické problémy.

Ďalej by som rád poďakoval všetkým súčasným i už skončeným doktorandom a študentom na oboch pracoviskách. Práve s nimi som nadviazal priateľské vzťahy a zdieľal úspechy i strasti mladých výskumníkov. Vymenujem aspoň tých, s ktorými som úzko spolupracoval a ktorí mi pomáhali pri experimentálnych, odborných i bežného života sa týkajúcich problémoch: **Karol Hensel**, **Martin Kurdel**, Dr. **Róbert Gašparík**, **Mário Janda**, **Eva Guldanová** a **Peter Macko** za slovenskú stranu a Dr. **Philippe Dessante**, Dr. **Nathalie Deschapms**, Dr. **Emmanuel Odic**, Dr. **Ludovic Parissi**, **Sandrine Dupré**, **Sophie Delaveau**, **Séverine Bousquet**, **Marielle Dhainaut**, **Christian Deniset**, Dr. **Ramzi Hadaji**, Dr. **Bernhard Kreissl** a **Bénédicte Lemieux-Dudon** za francúzsku stranu.

Ďakujem svojmu švagrovi **Markovi Discantinymu** za pomoc v záverečných fázach písania práce. Nech prijmú moju vrúcnu vďaku aj moja **mama**, celá moja rodina i priatelia, ktorí s napätím sledovali moje úspechy i neúspechy.

A napokon chcem vyjadriť svoju veľkú vďaku, uznanie, ocenenie, obdiv a pochopenie svojej manželke **Zuzke**, ktorá ma celý čas verne sprevádzala a podporovala, či už počas pobytov vo Francúzsku, alebo doma na Slovensku. Práve ona mi všemožne pomáhala, najmä v záverečných fázach písania práce a dá sa povedať, že ako obetu tejto práci priniesla svoje doktorandské štúdium. Rovnako ďakujem našej dcérke **Monike**, ktorá sa musela často uspokojiť s otcovou neprítomnosťou. Pokúsim sa im obom tento čas vynahradiť.

Moja najväčšia vďaka však patrí nášmu mocnému a dobrému **Bohu**, ktorý celý čas pri mne stál, a obdaril ma schopnosťami, silou a požehnaním.

TABLE OF CONTENTS

GENERAL INTRODUCTION

Global warming of the Earth, atmospheric pollution (ozone layer depletion, acid rains, smog), contaminated soil, pollution of surface and underground water, dying of some kinds of organisms etc. are pre-eminent environmental problems facing the world today. All these problems grew up during the last century, especially the last decades, due to the increasing demands of civilisation. Of course, every distortion of a natural equilibrium on the Earth by human activities does not stay without less or more serious, but often catastrophic consequences.

Most of the serious global and local environmental problems are directly associated with the atmospheric pollution. Industry and transport are essential sources responsible for the emissions of sulphur and nitrogen oxides, volatile organic compounds, carbon monoxide and dioxide, dust particles and other atmospheric pollutants. These emissions cause acid rains, a smog formation, an increase of tropospheric but a decrease of stratospheric ozone (ozone layer), they contribute to the enhanced greenhouse effect etc. Some of these problems (e.g. acid rains) have already been reduced in many industrial countries, however, others become more and more critical. The need of atmospheric pollution control is indispensable.

A variety of techniques can be used for this purpose. Many of them are old and can be considered as conventional. However, their certain practical limitations open the field for various innovative approaches offering solutions for some environmental problems of the atmospheric pollution. Techniques based on the plasma state of matter, especially non-thermal (low temperature) plasmas, find successfully their applications in the pollution control. This field has grown dramatically in recent years and is still in a stage of the laboratory as well as the industrial research. Many new types of air pollutants have been tackled, new kinds of plasma reactors have been developed, and existing kinds have been greatly improved. Chapter 1 is dedicated to plasmas, electric discharges, physico-chemical aspect of the processes occurring in plasmas and various plasma environmental applications, especially for the reduction of atmospheric emissions.

Volatile Organic Compounds (VOC) belong to the most important atmospheric pollutants of natural, but mainly atropogeneous origin. They participate in the processes of the atmospheric photochemical pollution (smog formation), halogenated hydrocarbons are responsible for the depletion of the ozone layer and many of them contribute to the enhanced greenhouse effect, hence global warming of our planet. VOC emissions into the atmosphere became an increasing environmental concern. However, only limited progress has been made up to now regarding their abatement. Non-thermal plasmas offer a novel approach to this

problem. They are able to compete with conventional techniques of VOC reduction. Various types of electric discharges and electron beams are used to generate suitable plasmas in these techniques. Everything concerning VOC, together with the state of art of plasma VOC reduction and associated physico-chemical processes is discussed in chapter 2.

The development of new kinds of electric discharges and plasmochemical reactors applicable for VOC destruction will be the main objective of this thesis. In the experimental part of this work we introduce two new types of electric discharges operating in air at atmospheric pressure. They generate non-thermal plasmas of some specific features, something different from other known and frequently used discharges, but also convenient for the VOC removal. The discharges have been named the high pressure glow discharge (HPGD) and the transient spark (TS), both of them are induced by a streamer in the non-homogeneous electric field (usually point-to-plane geometry). The experimental investigation of their physical properties based especially on the emission spectroscopy in UV-visible region and mechanisms of their function are dealt in chapters 3 and 4.

Our experimental study continues to chapter 5 where these discharges are applied for the VOC removal, namely cyclohexanone and toluene as VOC representatives. We present a large comparative study where the chemical effects of plasmas generated by these discharges operated in various reactors and under various electric parameters, gas flow and gas composition conditions are investigated. Evaluation of the discharge and VOC removal parameters such as removal efficiency, energy density and energy costs enables to compare used discharge regimes and reactors. A special attention is paid to the precise analysis of the process products appearing in all phases (in particular by means of IR absorption spectroscopy). The process is optimised not only from the viewpoint of VOC removal and its parameters, but also with regard to the nature of the products.

Novel optimised techniques of VOC removal by HPGD and TS are proposed, together with a suitable design of the laboratory-scale reactors, specific for each discharge. They can be included among other plasma VOC removal techniques. Successful tests of the pilot-scale discharge reactor working with TS discharge (chapter 6) are a practical industrial application of this research.

Finally, appendices give some additional information on the conversion of concentration units (1), theoretical bases of the UV-VIS emission spectroscopy and determination of rotational and vibrational temperatures (2) and theoretical and practical bases of the IR absorption spectroscopy (3).

This work has been effectuated in parallel in the Equipe of Electric Discharges and Environment of the Laboratory of Physics of Gases and Plasmas, CNRS (associated to the University Paris-Sud) in Gif sur Yvette, France as well as in the Institute of Physics at Faculty of Mathematics and Physics of Comenius University in Bratislava, Slovakia.

1.

PLASMA AND ITS ENVIRONMENTAL APPLICATIONS

1.1 SOME GENERAL FACTS ON PLASMA

1.1.1 Introduction

The term plasma has been initially introduced by Irving Langmuir, to qualify a fully, or almost fully, ionised gas. Afterwards, it has been applied to all situations where a gas is partially ionised. Let us recall what exactly means an ionised gas. When a solid is heated the thermal motion of its atoms (or molecules) increases with the temperature, until a break of its crystal lattice happens, and usually a liquid is formed. Again, if a liquid is heated enough, particles vaporise and a gas is formed. The next step appears when a gas is heated that the collisions among particles become strong enough to knock some of their electrons off. These electrons become free and an ionised gas or a plasma is formed, qualified sometimes as the "fourth state of matter".

It is I. Langmuir, the Nobel laureate who pioneered the scientific study of ionised gases and gave this new state of matter the name "plasma". In Greek πλασμα means a 'mouldable substance' or a 'jelly'. Indeed, the mercury arc plasma with which he worked diffused throughout the glass vacuum chamber, filling it like jelly in a mould. [Gls95]

As already introduced, the plasma state is said to be established when the gas is ionised, i.e. it is composed of neutral (atoms, molecules), as well as ionised particles (electrons, ions), and when ions and electrons are sufficiently numerous to dominate the behaviour of the system. A plasma has unique properties. It is an electric conductor where both ions and electrons are free to move. Charge separation between ions and electrons gives rise to electric fields, and flows of charged particles give rise to currents and magnetic fields.

It is estimated that plasma exists as a normal state of 99 % of all matter in the universe. This state forms the nuclei and atmospheres of stars, interstellar and interplanetary space, solar wind and solar corona, van Allen belts, Earth's ionosphere, etc. However, in common life we meet just a small fraction of all plasmas in the universe, such as flames, lightning, gas discharges in the fluorescent tubes, seldom auroras, but usually we do not realise that plasma is concerned. In every case, natural as well as laboratory plasmas are subjects of a research for fields like astrophysics, aeronomy, chemistry etc. Controlled thermonuclear fusion and magneto-hydrodynamic energy converters are a promising energy source for future. Nowadays, various plasmas find numerous applications in industry e.g. surface treatment of materials, plasma molecular synthesis and decomposition, etching,

depositions etc. Environmental plasmas applications become more frequent as well, for example the pollution control (flue gas cleaning, treatment of wastewater, contaminated lands etc.), sterilisation purposes in medicine and many others.

Low temperature plasma applicable for flue gas cleaning from organic atmospheric pollutants will be a concern of this work.

1.1.2 The Debye shielding – a scientific definition of plasma

Let us consider a substance composed of positive and negative charges, likewise an ionised gas. These charges react to each other, they 'feel' each other due to the electric forces. The "feeling" distance is however not that existing for an isolated specie in a free space. Indeed, in a plasma, each positive charge is shielded by negative charges and vice versa so that the distance into which the potentials of an individual charge is felt is smaller than in free space, of the order of a specific distance called the Debye length. This concept comes from the Debye-Hückel theory for charge shielding (originally developed for strongly dissociated substances such as electrolytes) and assumes a Maxwell-Botzmann distribution functions of the various species velocities.

The situation in an ionised gases is somehow specific, because the most important and frequent charged particles are electrons and positive ions. Electrons are 3-4 orders of magnitude lighter than positive ions ($m_{H+} \approx 2000 m_e$), thus their mean velocity and consequently their kinetic temperature T_e are much higher than those of positive ions. Said in the language of Debye charge shielding, light electrons are able to react on the kinetic motion of positive ions and to shield their charge, while heavy positive ions are not able to follow the kinetic motion of electrons, they keep their homogeneous spatial distribution with concentration N_+.

Debye length λ_D (distance into which Debye charge shielding occurs) in plasmas is given by the equation:

$$\lambda_D = \sqrt{\frac{\varepsilon_0 k}{e^2 N_+} T_e} \tag{1.1.1}$$

where T_e is the kinetic temperature of electrons, N_+ is the concentration (density) of positive ions, $\varepsilon_0 = 8.854\times10^{-12}$ F/m is the permittivity of vacuum, $e = 1.609\times10^{-19}$ C is the elementary charge and $k = 1.38\times10^{-23}$ J.K^{-1} is the Botzmann constant. The Debye length for a

plasma is also called the shielding distance. For distances below λ_D the individual charges play a dominant role, but beyond λ_D the total electric field, and hence the influence of individual charges is reduced to zero and collective effects dominate.

Plasmas, although composed of charged particles, macroscopically behave as neutral. They satisfy the so called 'condition of quasineutrality', i.e. the concentrations of electrons and positive ions being macroscopically equal:

$$N_e = N_+ \tag{1.1.2}$$

Concentration of positive ions N_+ in the expression for Debye length (1.1.1) can be thus replaced by the concentration of electrons N_e.

Now we can exactly define the term plasma*: Plasma is an ionised gas, macroscopically neutral, where charge shielding occurs. Its dimensions have to be much larger than the Debye length* in order that the plasma inside is shielded from the outer electric field. Another formulation says that the number of couples of charged particles in a sphere with diameter λ_D (Debye sphere) must not be lower than 1. Even more simply, *plasma is an ionised gas with a collective behaviour of charged particles, individual charges being shielded*. [Gls95, Mrr68, Mrt95]

1.1.3 Types of plasmas

Plasma is characterised by several parameters, the basic ones are the density of the neutral N_g and charged particles N ($N = N_e = N_+$ from the quasineutrality condition) and the temperatures of the neutral and charged particles T_g, T_e and T_+ respectively. Other useful parameters are the electric conductivity, mobility of charged particles, etc.

1.1.3.1 Weakly and strongly ionised plasma

According to the density of charged particles one speaks about:

- Weakly ionised plasma with the density of neutrals much higher than the density of charged particles ($N_g >> N$). Basic interactions occur at short distances (polarisation forces). The electric conductivity depends on N.

- Strongly ionised plasma with the density of neutrals lower than the density of charged particles ($N_g < N$). Interactions occur at long distances. The electric conductivity is independent from N.

1.1.3.2 Thermal and non-thermal plasma

Temperature is a macroscopic quantity which reflects a mean value of the kinetic energy of the species. We have to introduce two terms: complete and local thermodynamic equilibrium (CTE and LTE).

Complete thermodynamic equilibrium (CTE) means that temperature and other macroscopic characteristics (pressure, concentration) of all present species are equilibrated ($T_g = T_e = T_+$). They obey the Maxwell-Boltzmann statistics (distribution functions), the Saha's equation (the degree of ionisation depends on the temperature) and the Planck's law, i.e. the plasma radiates like a black body. The principle of detailed equilibrium, i.e. the reversibility of all running processes at a microscopic level (the forward reaction is exactly balanced by the reverse reaction) is characteristic for plasmas in CTE.

However, plasma in CTE is very difficult to achieve, because even when all species are thermodynamically equilibrated, the radiation usually escapes from the plasma, the system is not fully isolated, thus the Planck law of radiation is not satisfied. We define the so called local thermodynamic equilibrium (LTE) which has the same conditions as the CTE except the Planck law. The collisional processes are micro-reversible, but not the radiative processes. LTE characterises the collisional plasma, i.e. the plasma where collisions among the particles prevail over the radiation. The temperature describing the LTE is that which describes the distribution function of the species dominating the reaction rate, in laboratory plasmas this is the electron temperature T_e. Temperatures of all species are equilibrated ($T_g \approx T_e \approx T_+$). [Mrr68]

Plasmas in CTE or LTE are called thermal (equilibrium) plasmas. Many laboratory plasmas however do not obey the conditions of LTE (neither CTE) since they have highly elevated electron temperature but low temperature of neutral species and ions, $T_e >> T_g \approx T_+$. We call them non-thermal (non-equilibrium) plasmas.

Traditionally, according to the temperature in LTE systems plasmas are divided to:

- High temperature plasmas with $T > 10^6$ K, these plasmas are strongly ionised (stars and thermo-nuclear fusion).
- Low temperature plasmas with $T < 10^6$ K (gas discharges, ionosphere, solar wind, etc.)

Yet, such a division is not very practical for people dealing with gas discharges and usual laboratory plasmas occurring at much lower temperatures. More commonly, *high temperature plasmas* are *thermal plasmas* (in LTE) characteristic of a relatively high temperature (e.g. arc discharges with T~10000 K). *Low temperature plasmas* are *non-thermal plasmas* with high T_e and approximately ambient T_g. We will deal in this work with non-thermal plasmas of this concept.

Various types of natural and artificial plasmas are classified according to the density and the kinetic energy of electrons, as shown in Figure 1.1.1 and Table 1.1.1.

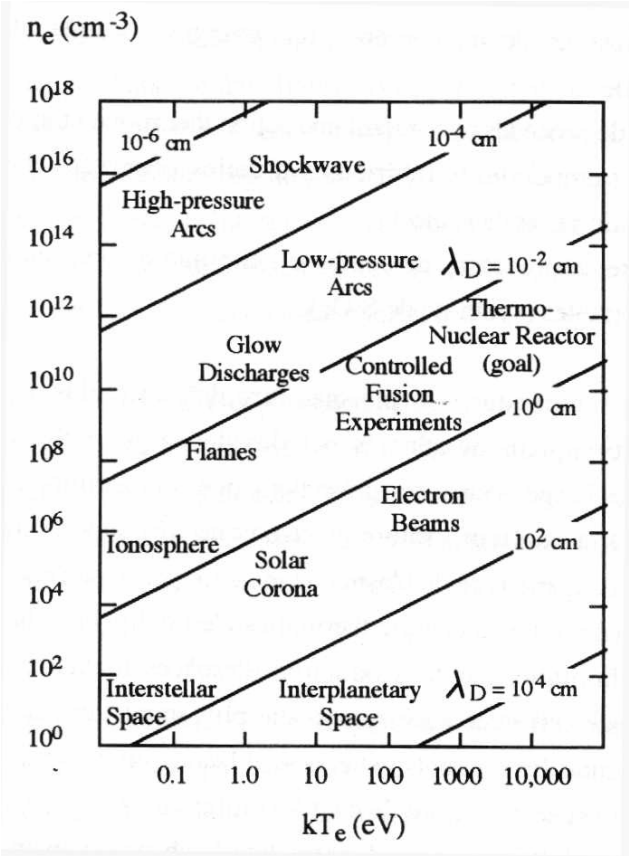

Figure 1.1.1 Classification of plasmas according to the electron density n_e, kinetic energy kT_e and the Debye length λ_D. **[Hll74]**

	Length scale (m)	Particle density (m^{-3})	Electron temperature (eV)	Magnetic field (T)
Interstellar gas	10^{16}	10^{6}	1	10^{-10}
Solar wind	10^{10}	10^{7}	10	10^{-8}
Van Allen belts	10^{6}	10^{9}	10^{2}	10^{-6}
Earth ionosphere	10^{5}	10^{11}	10^{-1}	3×10^{-5}
Solar corona	10^{8}	10^{13}	10^{2}	10^{-9}
Gas discharges	10^{-2}	10^{18}	2	—
Process plasmas	10^{-1}	10^{18}	10^{2}	10^{-1}
Fusion experiment	1	$10^{19}-10^{20}$	$10^{3}-10^{4}$	5
Fusion reactor	2	10^{20}	10^{4}	5

Table 1.1.1 Typical parameters of natural and laboratory plasmas **[Gls95]**

1.2 ELECTRIC DISCHARGES – A WAY OF PLASMA GENERATION

In general, plasmas can be generated by two basic approaches: thermal and electric. The thermal approach has been roughly illustrated in the introduction of this chapter - by a heating of the gas at a sufficiently high temperature we can ionise the gas atoms and molecules. Plasma generated by such a way is usually in the thermodynamic equilibrium state.

The electric approach uses an electric field capable, at certain conditions, to ionise the gas. Non-thermal as well as thermal plasmas may be then generated by this way. This is the principle of plasma generation by electric discharges.

Of course, there exist other approaches how to generate plasmas, e.g. ionisation of the gas induced by the UV irradiation, bombardment of the gas by highly energetic electrons (used in electron beams), etc.

We will deal here with the electric approach of plasma generation, i.e. electric discharges.

1.2.1 Townsend mechanism of discharge formation

1.2.1.1 Electron avalanches

Let us assume a gas in a region where exists an electric field, with at least one electron present. For example some charged particles appear from the cosmic radiation. Let us however allow an outer source of radiation (e.g. UV) inducing an emission of electrons from the cathode by the photoelectric effect (it occurs when the energy of radiation is higher than the work function of the electrode metal, $h\nu > \Phi$).

The electron is accelerated in the electric field. If the field is strong enough, the electron may get a kinetic energy higher than the ionisation potential ($kT_e > W_i$) of present neutral particles. As it collides with such a particle, this can be ionised and a new electron is released.

$e^- + A \rightarrow A^+ + 2e^-$ ionisation by electron impact

Now two electrons get the kinetic energy from the electric field and may initiate each two other ionisations resulting in 4 electrons and so on. The total number of electrons rises rapidly, that is why the process is called an electron avalanche.

The number of electrons formed in a layer dx along the x-axis going from the cathode to the anode is

$$\mathrm{d}n = \alpha\, n(x)\, \mathrm{d}x \qquad (1.2.1)$$

where $n(x)$ is the number of electrons at the place x. α [m^{-1}] is a number of ionisation collisions per a unit of length, it is called also the first Townsend coefficient. If relation (1.2.1) is integrated from 0 to d (the interelectrode distance), the number of electrons striking the anode at $x = d$ is $n_d = n_0 e^{\alpha d}$, n_0 being the initial number of electrons starting from the cathode. In the steady state, the external current i is equal to the sum of currents of electrons and positive ions, $i = i_e(x) + i_+(x)$ at each position x. If one puts $i_e(0) = i_0$ then, since no more positive ions are created at the anode, the external current is equal to the electron current movement at the anode. Thus

$$i = i_0 e^{\alpha d} \qquad (1.2.2)$$

Actually, i_0 is not entirely due to the electrons released at the cathode by the external UV beam. Indeed, positive ions are formed during the ionisation process as well as electrons. These positive ions drift slowly (since they are very heavy in comparison with electrons) to the cathode. As they reach the cathode, they are able to induce an emission of secondary electrons, by the phenomenon of potential emission (under the condition $W_i > 2\Phi$, W_i being the ionisation potential energy and Φ the work function of the cathode metal). The probability that one positive ion arriving to the cathode induces an emission of one electron is given by γ, so called the second Townsend coefficient.

Electrons, as they collide with gas particles, do not only ionise, but also excite the gas particles. These excited species consequently deexcite and the emitted photons may induce a secondary electron emission from the cathode by a photoelectric effect.

$e^- + A \rightarrow A^* + e^-$	excitation by electron impact
$A^* \rightarrow A + h\nu$	de-excitation

Fast neutral species, resulting from neutralising a positive ion by charge transfer, may also induce a secondary electron, as well as excited heavy species de-exciting at the cathode. It has been proved that all these processes of secondary electron generation are also included in the coefficient γ. Now the expression for the discharge current i (1.2.2) modifies to:

$$i = i_0 \frac{e^{\alpha d}}{1 - \gamma\,(e^{\alpha d} - 1)} \tag{1.2.3}$$

[LlJ56, Mrt95]

1.2.1.2 Condition of self-sustained discharge

The discharge is self-sustained if it exists even after stopping the production of cathode electrons by external means. Such condition is fulfilled only if the denominator of the expression (1.2.3) is zero:

$$\gamma\,(e^{\alpha d} - 1) = 1 \tag{1.2.4}$$

This condition is called the condition of self-sustained discharge. If it is not satisfied (i.e. if the field E gives to the coefficient α a too small value), the discharge is non-self-sustained and it vanishes as soon as the outer source of initial electrons (e.g. UV irradiation of the cathode) stops working. [Rai91, Ree78, Mrt95]

1.2.2 Modification due to the electron attachment - generalised Townsend theory of breakdown

The situation described in the above section is a little more complicated in electronegative gases, such as O_2 or air. Slow electrons may be attached to the electronegative gas molecules to form negative ions, some energy is released as a radiation or a kinetic energy of the third body.

$e^- + A \rightarrow A^- + h\nu$	radiative electron attachment
$e^- + A + M \rightarrow A^- + M$	three-body electron attachment

Electron attachment is characterised by the attachment coefficient η [m^{-1}], a number of attached electrons per a unit of length. Attachment is, of course, a process of electron vanishing which competes with the process of electron generation in ionisation. The equation (1.2.3) thus modifies to:

$$i = i_0 \frac{e^{(\alpha-\eta)d}}{1-\gamma\left(e^{(\alpha-\eta)d}-1\right)} \tag{1.2.5}$$

and the condition of the self-sustained discharge (1.2.4) modifies to

$$\gamma\left(e^{(\alpha-\eta)d}-1\right)=1 \tag{1.2.6}$$

Of course, many other elementary processes of electron generation and disappearing occurring in the volume and on the electrodes might be considered, hence modifying equations (1.2.3) and (1.2.4) by new coefficients leading to very complicated relations. This is the generalised Townsend theory of breakdown. [Wat78] Such processes are for example

volume photoionisation (direct of step-wise), ionisation by metastables (Penning's effect), electron detachment from negative ions, ion conversion processes, cathode electron emission by excited species, cathode field emission (autoemission), volume and surface recombination etc. Certainly some of them are negligible, other ones are important, it depends on the gas, pressure, electric field and other parameters. At high pressures (close to atmospheric) at which the electric discharges employed for pollution control usually work, the photoionisation is very important. [Ree78, Mrt95]

1.2.3 Reduced electric field and the Paschen law

Ionisation coefficient α is proportional to the ionisation cross section σ_i. It was found that the term α/N_g is a function of the term E/N_g, $N_g = N$ [m^{-3}] being the density of neutrals.

$$\frac{\alpha}{N} = f\left(\frac{E}{N}\right) \tag{1.2.7}$$

The parameter E/N is called the reduced electric field, it is a good characteristics of the discharge conditions uniting the electric (E) and the gas (N) properties. Its basic dimension is [$V.m^2$], but since it has very low values, the new unit named Townsend [Td] is introduced and widely used.

$$1\ \text{Td} = 10^{-21}\ \text{V.m}^2 = 10^{-17}\ \text{V.cm}^2$$

In older works we usually find E/p, p being the gas pressure, p and N are related through the state equation.

From the expression (1.2.7) we can get how E/N depends on α/N, using the electric potential (voltage) instead of the electric intensity ($U = E.d$) and find that the inception (breakdown) voltage U_i of the discharge depends on Nd value.

$$U_i = U_i\,(Nd) \qquad \text{or}$$
$$U_i = U_i\,(pd) \qquad \text{in } p\text{-representation.} \tag{1.2.8}$$

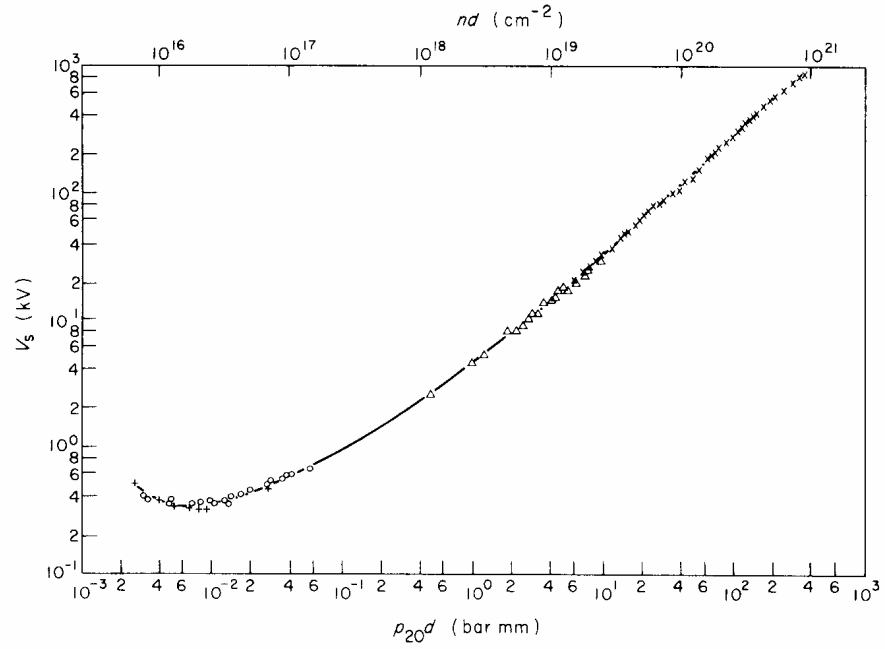

Figure 1.2.1 Breakdown voltages in atmospheric air. **[Bla78]**

The above dependence of the discharge breakdown voltage on the parameter *Nd* (*pd* respectively) is named the Paschen law. The Paschen law is usually represented by a curve characteristic for every gas and cathode material. Paschen curve allows to determine the inception voltage of the discharge in the interelectrode gap *d* and the gas with certain *N*. The inception voltage has a minimum at some $(Nd)_{min}$, $(pd)_{min}$ respectively.

The Paschen curve for atmospheric air is shown in Figure 1.2.1. [Rai91, Bla78, Mrt95]

1.2.4 Discharge mechanisms in the non-homogeneous electric field

1.2.4.1 Modified Townsend mechanism due to the non-homogeneous field

The Townsend mechanism of the discharge formation as introduced in section 1.2.1 assumed a homogeneous electric field, i.e. characterised by the intensity *E* independent from *x*. If the field is non-homogeneous, the number of newly generated electrons determined by the term $(\alpha-\eta)d$ (with electron attachment considered) in equations (1.2.5) and (1.2.6) has to be obtained by integration through *x*. The condition of self-sustained discharge then modifies to:

$$\gamma\left(e^{\int_0^d(\alpha-\eta)dx}-1\right)=1 \tag{1.2.9}$$

[Sig78]

1.2.4.2 Corona discharge

Corona discharge is a typical representative of a discharge occurring in the non-homogeneous electric field. Such field is obtained if one (or both) electrodes have a small radius of curvature (point, thin wire etc.). Typical configurations of corona reactors are point-to-plane (several points-to-plane, respectively) and coaxial (cylindrical). The spatial distribution of the field intensity E is given by the following equations:

$$E(x)=\frac{U}{\left(x+\frac{r}{2}\right)\ln\frac{2d+r}{r}} \tag{1.2.10}$$

for the hyperbolic point-to-plane geometry [Har64] and

$$E(r)=\frac{1}{r}\frac{U}{\ln\frac{R}{r_0}} \tag{1.2.11}$$

for the coaxial geometry.

According to the polarity of the voltage applied to the electrode with small radius of curvature one observes two types of corona discharge, respectively named:

- positive corona discharge (with positive voltage on this electrode)
- negative corona discharge (with negative voltage on this electrode)

When an a.c. voltage with low frequency (50 Hz) is applied, positive and negative corona are altered with this frequency.

Both types of corona have their specific regimes. The glow regime is the basic one, it is pulseless or with little pulses (bursts in positive corona, Trichel pulses in negative corona). Streamer corona regime easily develops as the applied voltage increases, streamer formation mechanisms will be explained in the next section.

The electric field is very strong in the very proximity of the curvatured electrode, so called ionisation region. It is responsible for the generation of energetic electrons by the process of avalanche ionisation. Other processes such as dissociations, excitations, formation of ions and radicals and secondary electron emission from the cathode (in negative corona) occur simultaneously in this active region.

A greater part of the discharge volume is represented by the drift (outer) region with electric field too weak for ionisations. Charged and neutral particles just drift and react in this region, and in electronegative gases (air, O_2), an electron attachment occurs. In some specific conditions, photoionisation can take place, which may lead to the formation of a filamentary discharge (streamer), commented in the next section. An important process is the electric wind - the drift of neutral particles towards the low voltage electrode (usually plane or cylinder) induced by the drift of charged particles. The electric wind helps to gas mixing which is important for the plasmochemical processes induced by corona discharge. [Sig78]

1.2.5 Streamer formation

1.2.5.1 Photoionisation process

The mechanisms of electron generation (ionisation by electron avalanches, secondary processes) and disappearing (arrival of electrons to the anode, electron attachment) run together. Of course, the excitation of atoms and molecules (mainly by electron impact) occurs simultaneously with the ionisation. These excited species de-excite (resonant-radiative excited state have lifetimes in the orders close to 10^{-8} s) releasing photons which propagate in all directions. If the energy of a de-excitation photon is higher than the ionisation potential of a gas particle ($h\nu > W_i$), this particle can be photoionised or photodissociated. As we have already noticed, the process of photoionisation becomes very important at high pressures (close to atmospheric). Schematically:

$e^- + A \rightarrow A^* + e^-$	excitation by electron impact
$A^* \rightarrow A + h\nu$	deexcitation
$h\nu + B \rightarrow B^+ + e^-$	photoionisation

1.2.5.2 Streamer - the filamentary discharge

Let us take a positive corona discharge with point anode and plane cathode. A cloud of slowly moving positive ions formed by electron avalanches modifies the outer electric field in the discharge volume by its space charge. This positive space charge prolonges the point anode. An advantage of the photoionisation process is that the electron-ion pairs quickly spread in volume, because their generation is induced by photons. Electrons generated by this way get the energy from the electric field modified by the space charge and may induce new avalanches at the places where they were generated, most importantly on the discharge axis, towards the plane cathode. These new avalanches located in a very small region where the space charge field is high, create a narrow ionising front called streamer. (Figure 1.2.2) The streamer leaves, behind its propagating path, a narrow ionised channel, referred to as a filamentary discharge or channel.

A rough, and simplified condition for the streamer propagation is that the electron avalanches at the discharge head (the streamer) must lead to the production of about 10^8 electrons. The space charge field thus becomes of the order of the outer Laplacian field. Drift velocity and ionisation nearly cease behind the streamer head, but increase in front of it. Behind the streamer front, almost field-free conditions leave electrons and positive ions intermixed in a filament of nearly neutral plasma. The electric potential distribution at the beginning of streamer formation and after some time of its propagation is sketched in Figure 1.2.4.

Photoionization ahead of the avalanche can increase the velocity of the streamer propagation to values greatly exceeding the electron drift velocity in the original field. Streamer propagation speed reaches 10^5-10^6 m/s.

Electron density in the streamer head is ~10^{15}-10^{16} cm^{-3}, potential fall along the ionising streamer of the order of ~kV. The temperature in the channel is of the order of 300 to 350 K. The mean electron energy in the streamer head is ~15 eV, while in the filamentary channel drops to 2-4 eV. As soon as the streamer reaches the opposite electrode (plane), it can vanish or initiate the secondary streamer propagating from the anode, but with no ionisation properties. The filamentary channel has a rotational symmetry, its diameter is equal to the diffusive radius of the avalanches, in the order of some 10s of μm. [Sig78, Sig94, Mar79, Mar93, Rea93]

An electric response on the streamer arrival to the opposite electrode (plane) is a fast growth of the discharge current due to the photoelectric emission of electrons from the plane.

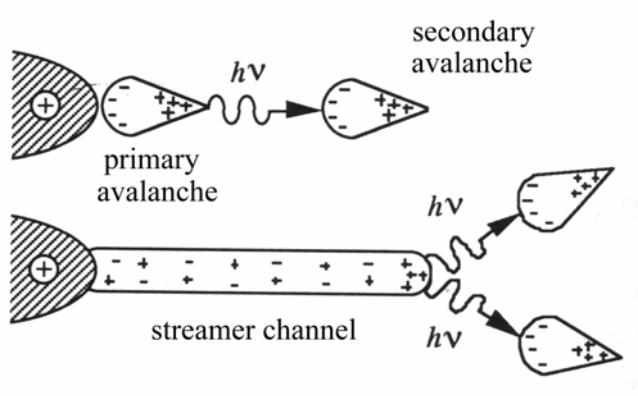

Figure 1.2.2 Photoionisation - mechanism of streamer propagation

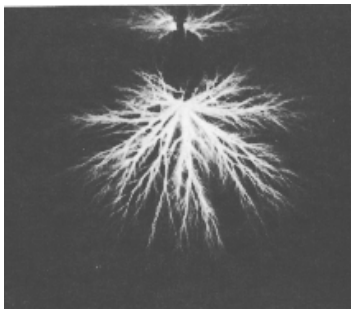

Figure 1.2.3 Streamer corona on a wire

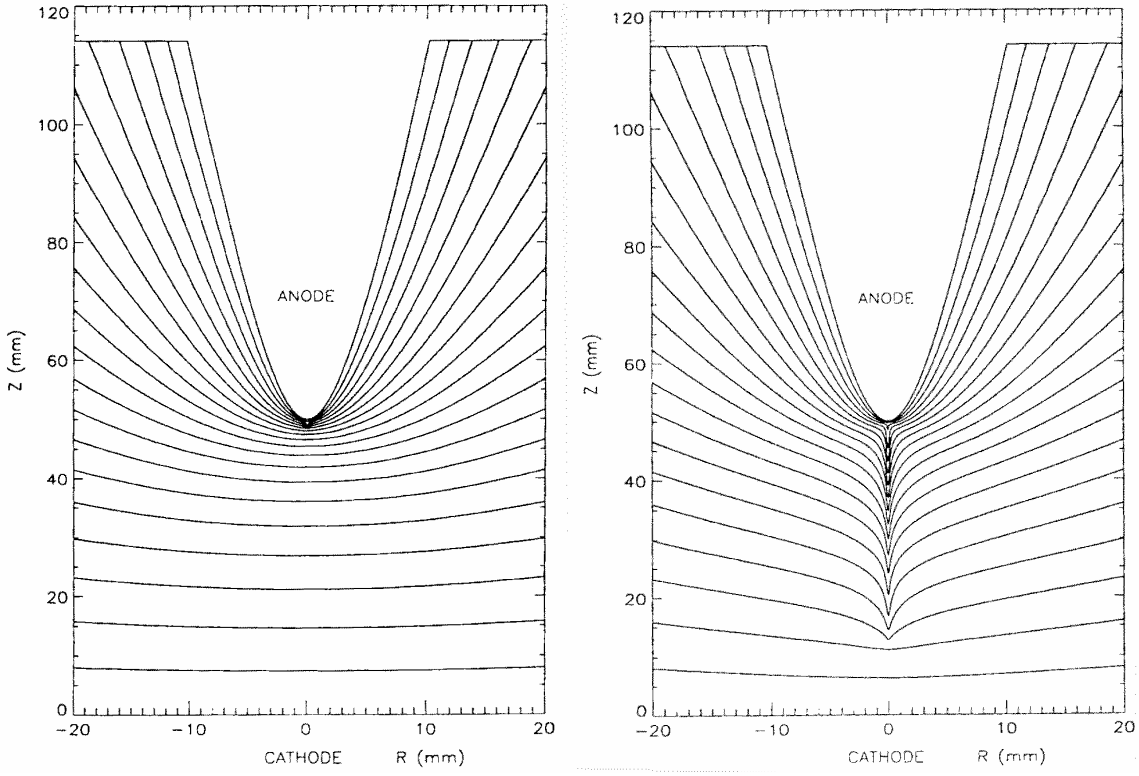

Figure 1.2.4 Electric potential distribution in the positive point-to-plane corona geometry showing the initial streamer formation (left) and its propagation (right) **[Mor97a]**

Brutal current growth is succeeded by its exponential decrease during the relaxation phase where recombination and electron attachment take place. (Figure 1.2.5) [Jaf95]

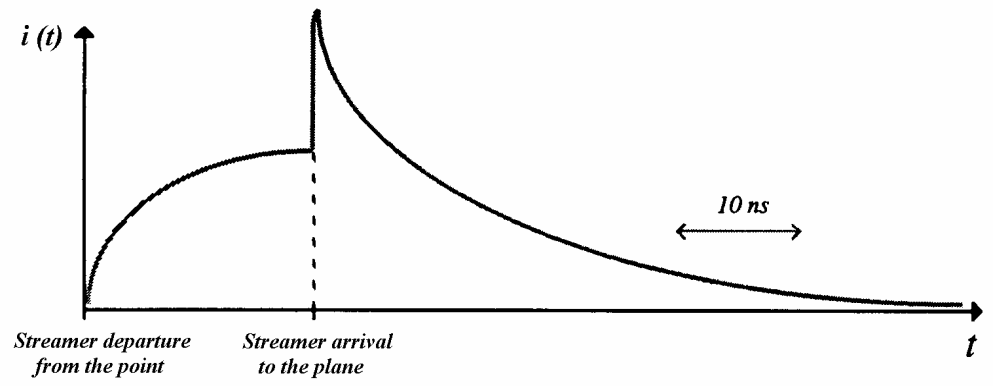

Figure 1.2.5 Current evolution during and after the streamer propagation. [Jaf95]

Streamer formation is a typical high pressure phenomenon. We have introduced the streamer formation in the case of non-homogeneous electric field (corona geometry, Figure 1.2.3), but streamers may also be formed also within the homogeneous electric field where they usually lead to the spark breakdown. Streamers in corona geometry develop whether the curvatured electrode is an anode or a cathode, however, the mechanisms of their formation are not the same (positive and negative streamers). [Sig78]

1.2.5.3 Transition to arc

At high values of the applied potential, the electrical energy released into the gas may lead to a thermal expansion of the discharge channel. It induces a decrease of the neutral density N, i.e. an increase of E/N. If E/N increases above the critical value corresponding to the equilibrium between ionisation and electron attachment, the ionisation starts up again, and leads to the formation of the spark breakdown. This mechanism will be described in chapter 4 dealing with Transient spark.

1.3 PHYSICO-CHEMICAL ASPECT OF THE PROCESSES IN PLASMAS

1.3.1 Collisions in plasma

Plasma is an ionised gas with a collective behaviour as we defined in section 1.1.2. The following types of particles are concerned:

Neutral particles:

- A, B, AB — neutral atoms and molecules
- A^*, AB^* — excited atoms and molecules (electronically, vibrationally, rotationally)

Charged particles:

- e^- — electrons
- A^+, B^-, AB^+, AB^- — positive and negative atomic and molecular ions

These particles collide due to their kinetic motion and outer fields (electric field). Each type of collision may be characterised by its mean cross section σ giving the probability of occurrence of this type of collision. The gas properties are characterised by the density of neutrals N. The mean free path λ is a macroscopic parameter representing the mean quantity of length that the particle is able to cross between two successive collisions.

$$\lambda = \frac{1}{\sigma N} \tag{1.3.1}$$

Most of the collisions occurring in non-thermal plasmas are elastic collisions with no change of the internal energy, just the kinetic energies of colliding particles are redistributed. The elastic collisions of electrons and heavy particles (atoms, molecules, ions) are the most frequent. Due to the great disproportion of masses of an electron and a heavy particle, the electron keeps practically the same kinetic energy after the collision. Elastic collisions, though very frequent, are unessential neither for the plasma generation processes such as electric discharges, nor for the desired purposes of plasma uses.

Inelastic collisions are characterised by an internal energy change of at least one of the colliding particles (obviously one in the case of electron impacts or photons absorption). These collisions are very important, because they are responsible for all elementary processes occurring in plasmas as well as for their physico-chemical effects.

1.3.1.1 The most important inelastic collisions in plasmas

The most important types of inelastic collisions and associated elementary processes have been already mentioned in the previous sections (ionisation and excitation by an electron

impact, de-excitation, photoionisation and photoexcitation, electron attachment and detachment). Let us remind them and mention also the following ones:

Ionisation:

$e^- + A \rightarrow A^+ + 2e^-$	by electron impact
$h\nu + B \rightarrow B^+ + e^-$	photoionisation
$A + B \rightarrow A^+ + B + e^-$	thermal

Excitation and de-excitation:

$e^- + A$ (or AB) $\rightarrow A^*$ (or AB^*) $+ e^-$	excitation by electron impact
$h\nu + A$ (or AB) $\rightarrow A^*$ (or AB^*)	photoexcitation
A^* (or AB^*) $\rightarrow A$ (or AB) $+ h\nu$	radiative de-excitation

Electron attachment:

$e^- + A \rightarrow A^- + h\nu$	radiative attachment
$e^- + A + M \rightarrow A^- + M$	three-body attachment

Dissociation of molecules (leads to the formation of radicals):

$e^- + AB \rightarrow A + B + e^-$ (or $A + B^* + e^-$)	by electron impact
$AB + C \rightarrow A + B + C$	thermal
$e^- + AB \rightarrow A + B^-$	dissociative electron attachment
$e^- + AB \rightarrow A + B^+ + 2e^-$	dissociative ionisation
$A^* + BC \rightarrow A + B + C$	dissociative de-excitation

Recombination of charged particles:

$e^- + AB^+ \rightarrow A + B^*$	dissociative recombination
$e^- + A^+ + M \rightarrow A^* + M$	with the third body (M)
$A^+ + B^- \rightarrow A + B + h\nu$	radiative ion-ion recombination

Ion-molecular reactions

$A + BC^+ \rightarrow AB^+ + C$	(or $AB + C^+$)	charge transfer with rearrangement
$A^+ + B + C \rightarrow AB^+ + C$		atom to molecule ion conversion

Chemical reactions (some involved species may be excited)

A + BC → AB + C change of bounds

A + B + C → AB + C synthesis

1.3.1.2 Rate coefficient of the reaction

Each type of collision is characterised by its mean microscopic cross section σ which determines its probability. Inelastic collisions leading to some state or structural changes of involved species are called (chemical) reactions. Reactions are more commonly characterised by the rate coefficient *k*, defined (for binary collisions) by:

$$k = \overline{\delta v_{rel}} \tag{1.3.2}$$

with v_{rel} being a relative velocity of colliding particles, i.e. $v_{rel} = v_1 - v_2$. Of course, the mean value has to be calculated by an integration of the distribution functions.

Let us take a representative reaction with two reactants:

A + B → AB

The rate coefficient *k* determines time changes of the concentration (density) of the reactant A (n_A [cm^{-3}]) dependent on the concentrations of both reactants A and B (n_A and n_B).

$$\frac{dn_A}{dt} = -kn_An_B \tag{1.3.3}$$

The unit of *k* of the reactions with two reactants (second order) is [cm^3s^{-1}]. In the reactions of three bodies (e.g. three body attachment or recombination) the concentration of the reactant A depends also on the concentration of the third body M. Schematically

A + B + M → AB + M $$\frac{dn_A}{dt} = -kn_An_Bn_M \tag{1.3.4}$$

then *k* is given in [cm^6s^{-1}].

In classical chemistry, the rate coefficients depend on temperature T according to the Arrhenius equation:

$$k = AT^i e^{-\frac{E_a}{RT}} \tag{1.3.5}$$

where A, E_a, i are specific for each chemical reaction (E_a being an activation energy of the reaction), R is a gas molar constant. In plasma chemistry, especially in plasmas generated by electric discharges, other parameters such as reduced electric field E/N influence the electron collisions and thus the associated rate coefficients. [Pol80]

1.3.2 Primary processes in non-thermal air plasmas at atmospheric pressure

In the following we will focus on the physico-chemical processes occurring in non-thermal plasmas in air at atmospheric pressure. Air at atmospheric pressure is an usual working environment of non-thermal plasma environmental applications. An ambient or a dry air, or a humid air are usual carrier gases of some pollutant, synthetic air (O_2+N_2) is sometimes used in laboratory conditions. In air plasmas, primary collisions occur dominantly between electrons and O_2 and N_2 molecules (normal air consists of approximately 21% O_2 and 78% N_2). Other air components (CO_2, Ar, H_2O etc.) also undergo collisions with electrons and other present species, H_2O is of greatest importance among them.

1.3.2.1 Electrons – the initiating factor

A formation of energetic electrons by avalanche ionisation is an essential process initiating all next elementary processes occurring in air non-thermal plasmas. Mean energy of electrons W_e rises with the reduced field intensity E/N. (Figure 1.3.1) Typical reduced field in gas discharges is about 150 Td which corresponds to W_e = 4 eV. Energetic electrons with energies over the ionisation potentials W_i and dissociation energies W_d of gas species (these values for air components are concluded in Table 1.3.1) are responsible for their ionisation and dissociation. Formation of excited species (atoms and molecules) is tightly associated with ionisations and dissociations.

Reduced field also influences the rate coefficients of the occurring plasmochemical reactions, see Figure 1.3.2 (G-values are defined later) and Figure 1.3.3.

The mean electron energy W_e determines what processes will dominate in air non-thermal plasmas. Vibrational excitation of N_2 molecules prevails at $W_e < 3$ eV, dissociation of O_2 molecules at 4 – 8 eV, dissociation of N_2 at $W_e > 8$ eV and ionisation of O_2, N_2 at $W_e > 12$ eV. Distribution of the input energy (power) to these processes depends on W_e (Figure 1.3.4). [Pen97a,b, Low95]

Air is an electronegative gas due to the high content of electronegative oxygen, thus an electron attachment as a main electron sink process competes with ionisation.

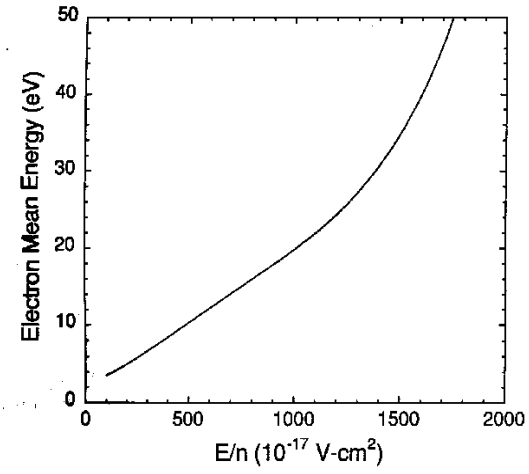

Figure 1.3.1 Average kinetic energy of electrons in an atmospheric pressure air discharges as a function of the reduced field intensity E/n. E/n in discharge reactors usually does not exceed 300×10^{-17} V.cm^2 (= 300 Td), the average electron kinetic energy is thus limited to values less than 10 eV. **[Pen97a]**

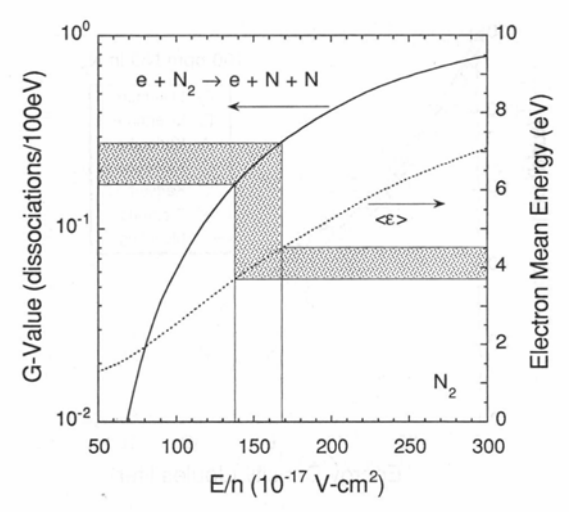

Figure 1.3.2 Calculated G-value for electron impact dissociation of N_2 and electron mean energy as functions of the reduced electric field. **[Pen97a]**

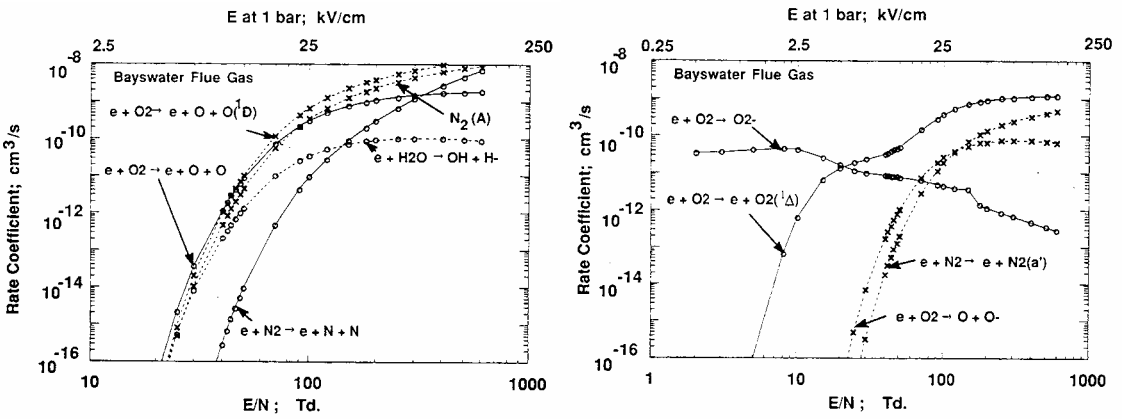

Figure 1.3.3 Rate coefficients for various reactions calculated from cross sections and solution of the Boltzmann equation. **[Low95]**

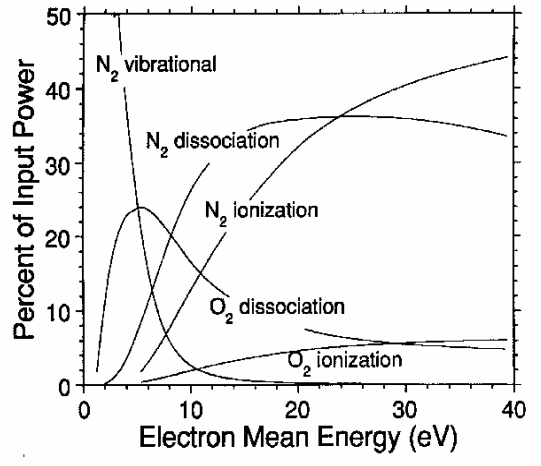

Figure 1.3.4 Power dissipation in an atmospheric pressure dry air discharge , showing the per cent of input power consumed in electron impact processes leading to vibrational excitation, dissociation and ionisation of N_2 and O_2. **[Pen97a]**

Atom or Molecule	Dissociation energy W_d [eV]	Ionisation energy W_i [eV]
N	-	14.51
N_2 (N≡N)	9.67-9.8	15.6
O	-	13.62
O_2 (O=O)	5.08-5.17	12.06
CO_2 (O=C=O)	4.4-8.29	13.8
H_2O (H-O-H)	4.44-8.6	12.61
OH	4.45	12.9

Table 1.3.1 Dissociation and ionisation energies of the most important air components. **[Atk94, Bro80, Loe65]**

1.3.2.2 Electron impact reactions in air

The most important primary processes occurring in air plasmas concern electrons and O_2 and N_2 molecules. They are viewed in the following table.

Reaction	Rate coefficient k [$cm^3.s^{-1}$]	Type of elementary process
$e^- + N_2 \rightarrow e^- + N(^4S) + N(^4S, ^2D, ^2P)$	9×10^{-11}	Dissociation
$e^- + N_2 \rightarrow 2e^- + N^+ + N(^4S, ^2D)$		dissociative ionisation
$e^- + N_2 \rightarrow N_2^+ + e^- + e^-$		ionisation leading to molecular ion
$e^- + N_2 \rightarrow e^- + N_2(A^3\Sigma_u^+)$	1.3×10^{-9}	excitation to metastable state
$e^- + N_2(A^3\Sigma_u^+) \rightarrow e^- + N_2$	1×10^{-8} (40 Td), 2.3×10^{-10} (70 Td)	deexcitation by electron impact (superelastic collision)
$e^- + O_2 \rightarrow O(^3P) + O(^3P) + e^-$	7.9×10^{-10}	dissociation
$e^- + O_2 \rightarrow O(^3P) + O(^1D) + e^-$	2.3×10^{-9}	dissociation
$e^- + O_2 \rightarrow O^- + O(^3P, ^1D)$	7.2×10^{-10}	dissociative attachment
$e^- + O_2 \rightarrow O_2(a^1\Delta_g) + e^-$	7.2×10^{-10}	excitation
$e^- + O_2 \rightarrow O_2^+ + 2e^-$	8×10^{-10}	ionisation leading to molecular ion
$e^- + O_2 + O_2 \rightarrow O_2^- + O_2$	2.5×10^{-30} cm^6s^{-1}	three-body electron attachment
$e^- + O_2 + N_2 \rightarrow O_2^- + N_2$	1.6×10^{-31} cm^6s^{-1}	three-body electron attachment
$e^- + O_2(a^1\Delta_g) \rightarrow e^- + O_2(X^3\Sigma_g^-)$	1×10^{-9}	deexcitation by electron impact (superelastic collision)
$e^- + O_2(a^1\Delta_g) \rightarrow O_2^+ + 2e^-$	8×10^{-10}	ionisation of excited molecule
$e^- + O_2^+ \rightarrow O_2$	2×10^{-7}	recombination

Table 1.3.2 View of the most important electron impact reactions occurring in air non-thermal plasmas. Rate coefficients at T=300 K and E/N=150 Td. **[Pen97a, Low95]**

1.3.2.3 G-value

B.M.Penetrante et al. define a so called G-value, the efficiency of a particular electron impact process:

$$G = 100\frac{k}{v_d\frac{E}{N}} \tag{1.3.6}$$

with reaction rate coefficient k [cm^3s^{-1}], electron drift velocity v_d and the reduced electric field E/N. G-value corresponds to the number of dissociation or ionisation reactions per 100 eV of input electron energy. The term kN represents the number of reactions per unit time and the quantity v_dE represents the amount of energy, in eV, expended by electrons per unit time. G-value is in fact an expression of the efficiency of energy transfer toward the specific process. Figure 1.3.5 shows calculated G-values of various electron impact ionisation and dissociations in dry air as a function of mean electron energy. [Pen95, Pen97a]

1.3.2.4 Additional electron impact reactions in humid air

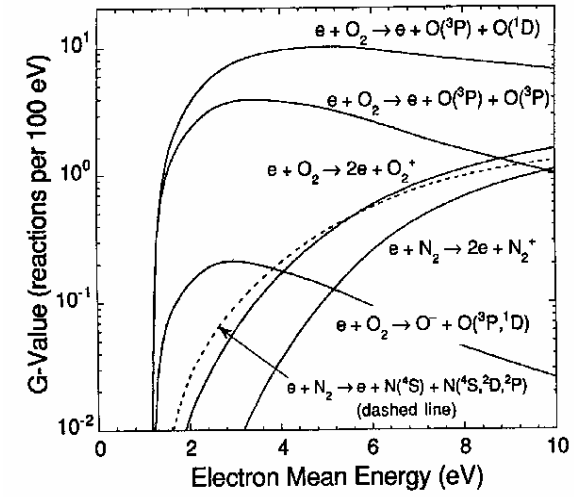

Figure 1.3.5 Calculated G-values for dissociation and ionisation processes in dry air as functions of electron mean energy in an atmospheric pressure discharge plasma. **[Pen97a]**

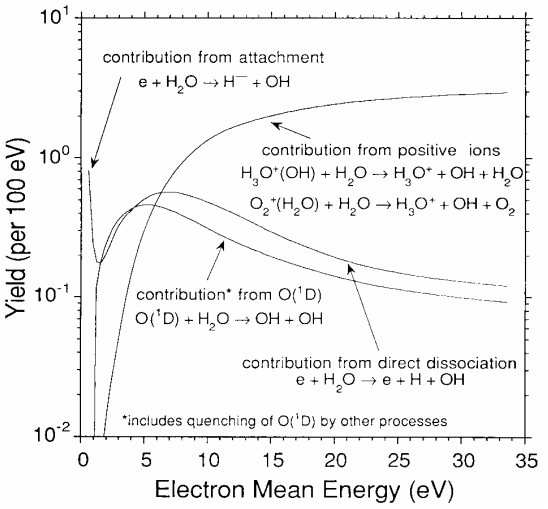

Figure 1.3.6 Contribution of various processes to the production of OH radical as functions of electron mean energy in an atmospheric pressure plasma for a gas mixture 5 % O_2, 10 % H_2O, 15 % CO_2 and 70 % N_2. **[Pen97a]**

When air contains a moisture, the electron impact of H_2O molecule is an important channel of the formation of highly reactive OH radicals [Low95]:

$e^- + H_2O \rightarrow H^- + OH$	$k = 7.2\times10^{-11}$ (300 K, 150 Td)	dissociative attachment
$e^- + H_2O \rightarrow e^- + H + OH$		dissociation

Another important channel of OH formation is by the collision of H_2O with the excited atomic oxygen $O(^1D)$ [Low95]:

$H_2O + O(^1D) \rightarrow 2OH$ $\quad k = 2.2\times10^{-10}$ (300 K) chemical reaction

G-values of various processes concerning H_2O and OH radicals as a function of mean electron energy are shown in Figure 1.3.6.

1.3.3 Secondary processes in atmospheric pressure air plasmas

1.3.3.1 Active intermediates

The above listed electron impact processes and many other processes occurring in air non-thermal plasmas lead to the formation of

atomic and molecular ions	O^+, N^+, O^-, O_2^+, N_2^+, O_2^-, O_3^-
excited atoms and molecules	$O^\bullet(^1D)$, $N(^2D, ^2P)$, $O_2(a^1\Delta_g)$, $N_2(A^3\Sigma_u^+)$
radicals	$N^\bullet(^4S, ^2D, ^2P)$, $O^\bullet(^3P, ^1D)$, $OH^\bullet$, $HO_2^\bullet$

Very reactive substances are formed from the originally neutral air. All these active species react together and with neutral air molecules to form secondary species, various radicals and intermediates which lead to the final products at the last stage.

1.3.3.2 Final gaseous species

Usual final gaseous species produced in non-thermal air plasmas are various nitrogen oxides (N_2O, NO, NO_2, N_2O_5), nitric and nitrous acid (HNO_3, HNO_2) and ozone (O_3). However, their formation is a result of very complicated mechanisms. A great number of reactions, bound together, competes for their generation and sink. We will not present a complete list of all possible reactions, it can be found elsewhere, e.g. [Bau82, Ati92, etc.] Moreover, all these processes depend on many parameters such as gas temperature and pressure, electric field and the type of the discharge, other species and impurities present in the gas (CO_2, H_2O, NO_x, organic compounds, etc.), material and surface properties of the plasmochemical reactor and many others.

The plasmochemical processes occurring in the non-thermal air plasmas leading to gaseous products can be roughly illustrated by the following scheme [Gol93]:

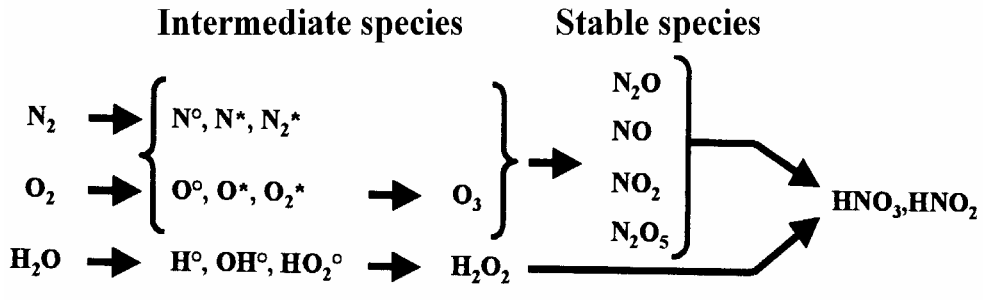

1.3.3.3 Formed particles

We have to note that the gaseous products sketched above are not the only final species produced in non-thermal air plasmas. Negative and positive ions generated in the primary processes are able to form clusters with water and other air impurities. They leave the active volume like small aerosol particles. The principal ion clusters formed in corona discharge in the ambient air (with CO_2 and H_2O present) are:

negative ion clusters	$O_3^-(H_2O)_n$, $O_2^-(H_2O)_n$, $CO_3^-(H_2O)_n$, $CO_4^-(H_2O)_n$, $NO_3^-(H_2O)_n$, $NO_2^-(H_2O)_n$
positive ion clusters	$H_3O^+(H_2O)_n$, $O_2^+(H_2O)_n$, $H_3O^+(OH)$

[Sha71, Bas75, Pen97a]

Some of the ion-water clusters contribute to the radical formation (particularly OH). G-values of corresponding reactions are shown in Figure 1.3.6.

The concentration of formed particles (clusters), as well as the concentration of newly formed gases, depends on a great variety of parameters, especially discharge type and temperature, it may reach 10^6 cm^{-3}. [Bor98]

1.3.3.4 Presence of other species in air

When a plasma is applied for the removal of some atmospheric pollutant (e.g. NO_x or VOC) is present in air, its decomposition is induced by the active intermediate species, but its presence on the other hand complicates and influences all running mechanisms in a plasma. Mechanisms of VOC decomposition will be discussed in chapter 2.5.

1.3.4 Plasmochemical reactor

The plasmochemical reactor is a device generating plasma where various chemical reactions take place. All physical processes of plasma generation (mechanisms of electric discharges) and all associated physico-chemical processes described in the previous sections have to run simultaneously in various regions of the reactor volume and surfaces.

Plasmochemical reactors are used for various purposes, practically everywhere where some physico-chemical effects of plasmas are helpful and can be employed for the desired purpose. Reactors for the pollution control, especially for the reduction of atmospheric pollutants work usually in air at atmospheric pressure and use non-thermal plasmas. A concept of primary and secondary processes described before is thus involved.

1.4 PLASMA TECHNIQUES FOR POLLUTION CONTROL AND OTHER ENVIRONMENTAL PLASMA APPLICATIONS

1.4.1 Introduction

Various elementary processes occurring in air plasmas make them a very active environment. The physico-chemical effects of such plasmas can be employed for various technical applications. Plasma applications for pollution control, especially for the reduction of various atmospheric pollutants will be here our special interest.

A lot of real situations of flue gas cleaning problems happens at the atmospheric pressure, thus almost all these plasma techniques run at atmospheric or close to atmospheric pressures. The mean free path of particles at such pressure is about 10 μm and the collisional frequency is high. Such conditions enable step-wise chemical changes of the targeted pollutants which is suitable from the energetic viewpoint and the viewpoint of reaction possibilities.

Plasma techniques for the removal of atmospheric pollutants can be roughly divided into two groups according to the plasma temperature:

- techniques using thermal plasmas where electronic temperature is in equilibrium with the temperature of bulk gas $T_e \approx T_g$ (condition of the local thermodynamic equilibrium is

fulfilled). Examples of thermal plasmas are *arc discharges, plasma torches - plasmatron,* some *ICP (inductively coupled plasma).*

- techniques using non-thermal plasmas where electronic temperature is not in equilibrium with the temperature of bulk gas, $T_e >> T_g$ (condition of the local thermodynamic equilibrium is not fulfilled). Typical examples are plasmas created by *electron beam* (non self-sustained case) and all commonly used electric discharges, e.g. *corona discharges (dc and pulsed), dielectric barrier (silent) discharges, surface discharges, discharges with ferroelectric packed bed, certain microwave and high frequency discharges, atmospheric pressure glow discharge, glidarc, prevented spark,* etc.

The advantage of non-thermal plasmas is that most of the electric energy delivered to the plasma from the outer generator is used for the formation of energetic electrons by the process of avalanche ionisation and that this energy is not lost into the thermal energy of heavy species. Energetic electrons enter to the excitation, ionisation and dissociation collisions with bulk gas particles, particles of targeted pollutant included. These collisions lead to the formation of reactive radicals, excited atoms and molecules, atomic and molecular ions; negative ions are formed mostly by the attachment of slow electrons. These active species take part in the plasmochemical reactions leading to the decomposition of the pollutants. Photons of UV and visible spectral region released by the deexcitation of the excited species often play an important role in photochemical processes.

On the other hand, techniques using plasma in LTE conditions (thermal plasma) are based on the high temperature of the whole bulk gas responsible for the thermal decomposition (thermodissociation, pyrolysis) of the targeted pollutant. Evidently, higher energy is necessary for the entire gas heating than that needed for gaining high energetic electrons only. This is why non-thermal plasma techniques are more studied and preferred.

However, when the thermal and non-thermal plasma techniques are compared, achieved decomposition rates, all energy and investment costs of the technique and formed products of the process have to be considered. A higher gas temperature often influences the chemical pathways. Regimes on the transition between non-thermal and thermal plasmas, i.e. non-thermal plasmas working at relatively high bulk gas temperatures, often give interesting results, e.g. prevented spark, glidarc and others. This is the reason why we studied new types of electric discharges generating such plasma conditions (high pressure glow discharge and transient spark).

1.4.2 Electron Beam (EB)

Electron beam is a basic non-discharge method of low temperature plasma generation. EB system contains the electron source and the high voltage device for the electron acceleration in the vacuum part. Electrons then penetrate through a thin foil working as the vacuum sealing to the atmospheric pressure part. High energy electrons (~125 keV) collide with neutral gas particles and initiate a formation of a large volume of plasma. [Pen97b] Secondary electrons with energies ~100 eV are created by the process of ionisation of neutral species. They initiate further collisions (excitations, ionisations, attachments and dissociations) and lead to the intense radical formation (especially OH a O).

High capital costs and the danger of X-ray irradiation (mainly at MeV accelerator types) make the EB technique disadvantageous in comparison with electric discharges, despite of the fact that EB is with no doubts the most effective way of radical production. Weaker types of electron accelerators (<200 keV) introduced recently are successfully applied in industry and some of them are already commercially accessible and used in pollution control applications. [Pen97b, Frk93, Pau93]

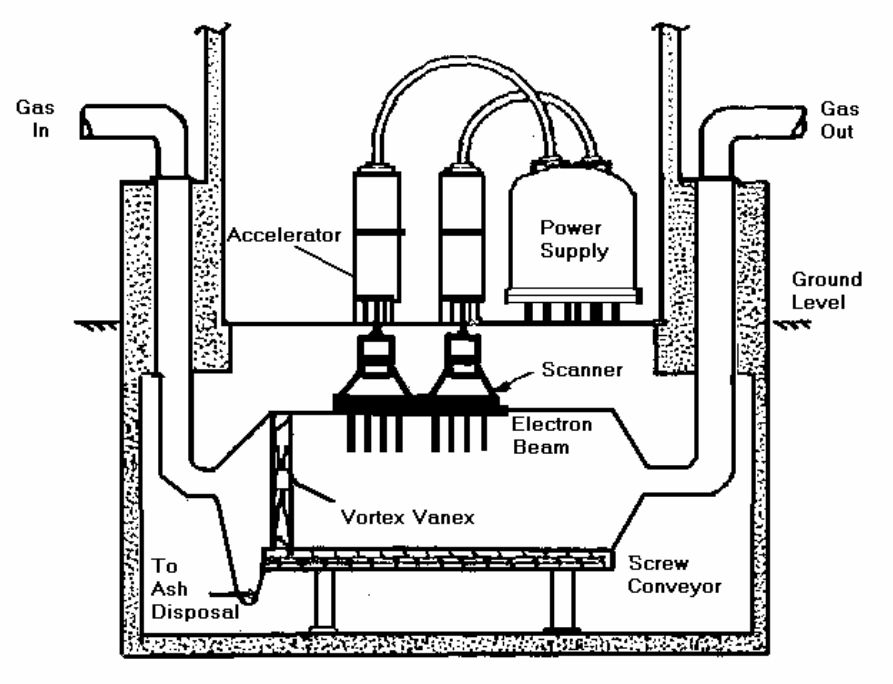

Figure 1.4.1 Pilot plant (5300 Nm^3/h) with electron beam processing (Research-Cottrell at TVA Shawnee Plant* [Frk93]*)

1.4.3 Corona Discharges (CD)

The principle of the corona discharge, as a representative discharge occurring in the non-homogeneous electric field and generating a typical non-thermal plasma, have already been described in section 1.2.4.2.

Various configurations of coronas find their applications in industry as well as in the pollution control. The typical one is a coaxial configuration, but point-to-plane and multipoint configurations are widely used as well. Corona discharges are historically the first plasmas applied for environmental protection. Nowadays they have a large variety of environmental applications such as electrostatic precipitation, exhaust gas treatment, generation of O_3 for water purification and sterilisation, ion sources, etc.).

1.4.3.1 Electrostatic precipitators

The principle of electrostatic precipitation is based on the corona discharge effects on neutral particles, namely their drift caused by the electric wind. Dust, aerosol and other particles of micrometric sizes can be separated from large volumes of industrial exhaust gases treated by corona. The electrostatic precipitators (Figure 1.4.2), devices where this process runs are widely used since the beginning of the 20th century (e.g. in power stations). They were, with no doubts, the first flue gas cleaning devices where an electric discharge was used.

1.4.3.2 Pulsed Corona Discharge (PCD)

D.c. coronas are a traditional and still used techniques of flue gas cleaning applicable for the removal of all types of pollutants. However, techniques using the pulsed corona discharge are preferred by many authors nowadays. (Figure 1.4.3)

Pulsed corona is characteristic by short pulses (<1 μs) of high amplitude (~30 kV). Streamers with short lifetime are generated due to the pulses, the electric energy can be thus more effectively transferred to electrons. Positive pulses are usually used, they are sometimes superposed on a d.c. bias voltage. The pulse rise time, peak value, frequency and many other parameters influence the efficiency of the process. [Don98, Pen97a, Low95]

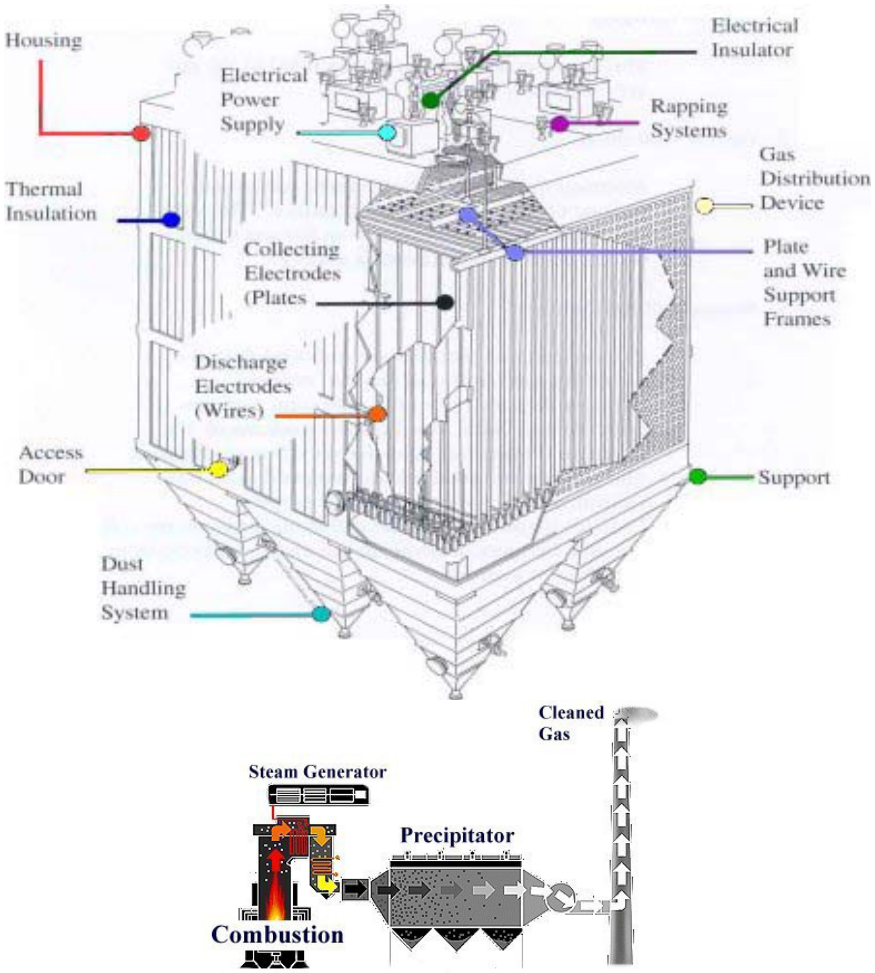

Figure 1.4.2 Electrostatic precipitator – scheme (up) and an example of its installation in the power station (down)

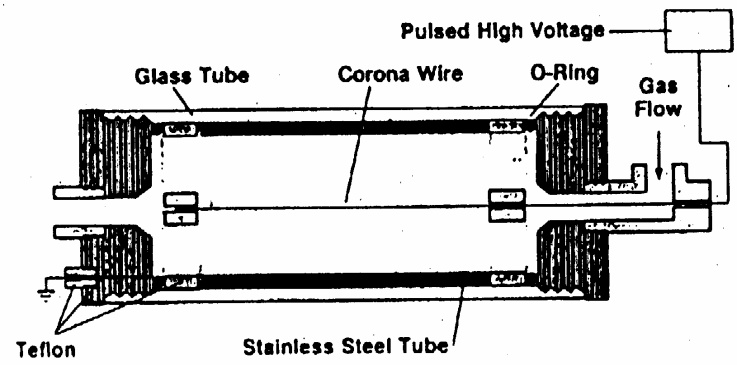

Figure 1.4.3 Coaxial pulsed corona reactor [Yam93]

1.4.4 Discharges with dielectrics

This name can be used for all discharges which contain a dielectric material somewhere in the interelectrode space. The presence of the dielectric material changes the electric field between the electrodes and implies using alternative applied potentials. Recently, discharges with dielectrics are more and more employed in many industrial applications, pollution control included.

1.4.4.1 Dielectric Barrier (Silent) Discharge (DBD)

DBD occurs when one or both electrodes are covered with a dielectric layer (e.g. glass or ceramics), or the dielectric material is inserted into the space between the electrodes. Usually, planar or cylinder electrode geometry is used. (Figure 1.4.4) Alternative or pulsed high voltage is applied to the electrodes. Charging of the dielectrics causes an intense enhancement of the electric field close to its surface. This strong field results in the initiation of a great number of microdischarges in the interelectrode space. The microdischarge is a transitory filamentary streamer with relatively high field intensity and short lifetime (~ns). Microdischarges are fed by the ionisation and electron detachment and stopped when the charge accumulated on the dielectric surface reduces the electric field between the electrodes and electron attachment starts to prevail. A non-equilibrium plasma is formed by this way, as well as in corona discharges. Typical microdischarge parameters are: current density ~10^3 A.cm^{-2}, density of electrons ~10^{14} cm^{-3}, reduced field ~100-200 Td, energy of electrons ~5 eV. Nowadays, DBD is routinely used for ozone and UV radiation generation. [Eli87, Ros93, Kog93]

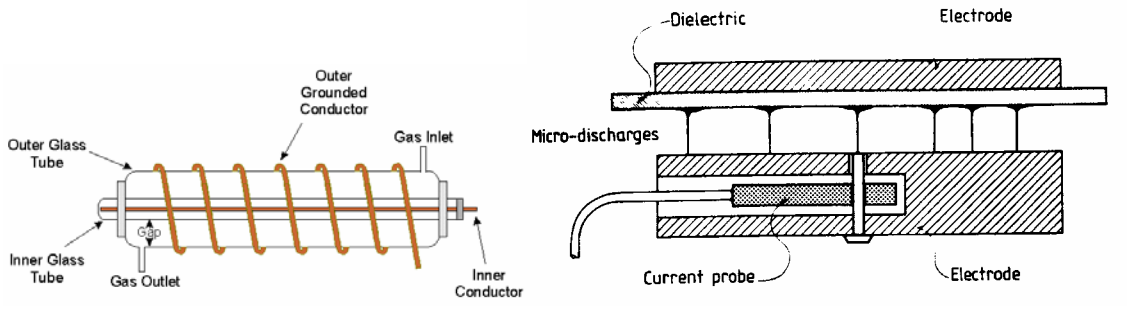

Figure 1.4.4 Coaxial (left) and planar (right) configurations of the dielectric barrier discharge reactor

1.4.4.2 Surface Discharge (SD)

This discharge type is formed on the dielectric surface and spreads just on its surface. A series of electrodes must be put in a special configuration, usually like thin metal stripes attached to the dielectric surface.

A high frequency voltage is applied to the strip electrodes. Surface discharge pulses propagate from edges of the strip electrodes over the dielectric surface, up to when the whole surface is covered by the discharge. In the flue gas cleaning and ozone generation applications, the treated gas flows through the region of generated non-thermal plasma, over the dielectric surface. SD is often combined with DBD; DBD acts in the interelectrode space and SD on the dielectric surface. Simultaneous effects of both these discharges result in greater efficiency of the process. [Msd93, Ito93]

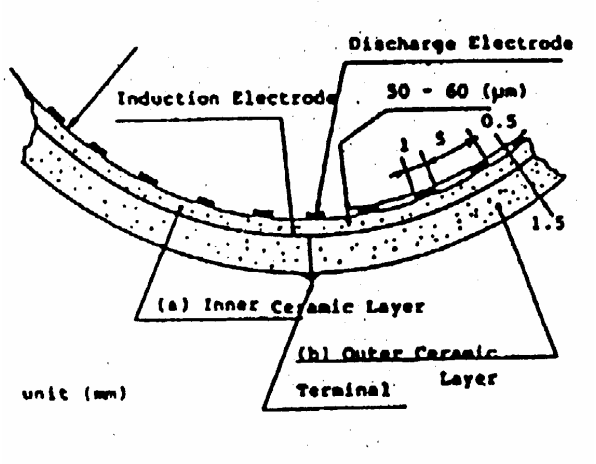

Figure 1.4.5 Scheme of the surface discharge plasma reactor

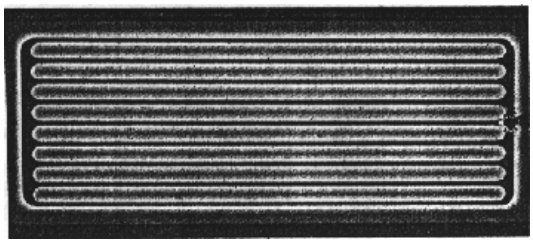

Figure 1.4.6 Performance of the surface discharge [Msd93]

1.4.4.3 Discharge in the ferroelectric pellet bed reactor

The principle of this discharge is very similar to the surface discharge. Pellets made of dielectric material with high permittivity (ferroelectrics) are put into the space between electrodes. These pellets are charged in the alternative outer electric field and enhance the field intensity in their close surroundings. The field is very intensive around their contact points and the discharges very similar to surface discharge are spread.

Reactor with the ferroelectric bed (Figure 1.4.7) uses an alternative high voltage, it is usually cylindric, pellets ($BaTiO_3$ and other materials) are separated in volume by metal grids. The type of generated plasma and its effects depend especially on the dielectric properties and dimensions of the pellets, the higher permittivity and smaller dimensions they have, the more

effective is plasma generation and its effects for treatment of pollutants. [SSz93, Yam93, Oga99]

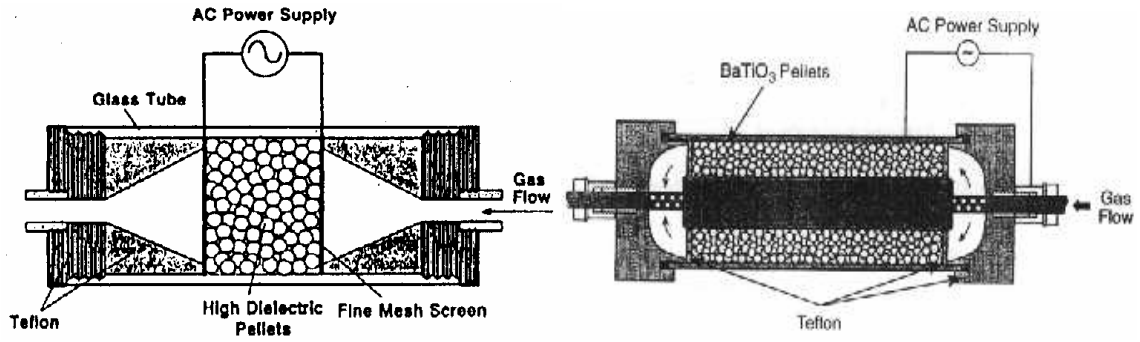

Figure 1.4.7 Reactors with ferroelectric pellet bed

1.4.5 High frequency discharges (microwave, radio-frequency)

High frequency discharges are well known mainly at low and medium pressures. They are applicable also to high pressures (close to atmospheric), the electromagnetic wave at high pressure is able to penetrate deeper into plasma. These discharges are generated by low and high power generators working at various frequencies, e.g. 13.56 MHz (radio-frequency discharge) or 2.45 GHz (microwave discharge). With respect to the input power, plasmas over a wide temperature interval are generated, from non-thermal plasmas at low powers up to plasmas close to LTE at high powers (HF plasma torches). The choice of the power generator is determined by the application purpose. (low and medium powers are suitable for flue gas cleaning or surface treatment, high powers for the pyrolisis, fullerene production etc.) [Kan98, Bra98, Mrc98]

High frequency discharge have many industrial applications due to the specific properties and a large variability of generated plasmas, large volume homogeneous plasmas can be generated by this way. However, examples of their environmental applications can be found relatively rarely.

1.4.6 Transition discharges

This section will deal with discharges generating plasmas which lay on the boundary between typical non-thermal plasmas with an ambient gas temperature T_g and a high electronic temperature T_e and thermal plasmas where these temperatures are equilibrated. By

other words, non-thermal plasmas with relatively high T_g, more or less approaching to LTE conditions are concerned. Such plasmas can be generated in the transition regimes of streamer-induced discharges. As already mentioned in the introduction to this chapter (section 1.4.1), these techniques often give interesting results comparable with typical non-thermal plasma techniques.

High pressure glow discharge (HPGD) and Transient spark (TS) applicable for VOC removal, the subject of the study presented in this work, belong to this category of non-thermal plasmas.

1.4.6.1 Prevented spark

Prevented spark developed by E.Marode is a representative of the transition discharges applicable for the reduction of atmospheric pollutants such as NO_x and SO_x. Its principle and mechanisms will be explained in chapter 4.1.1, since they are tightly bound to the transient spark, the discharge investigated in this work.

1.4.6.2 Gliding arc (glidarc)

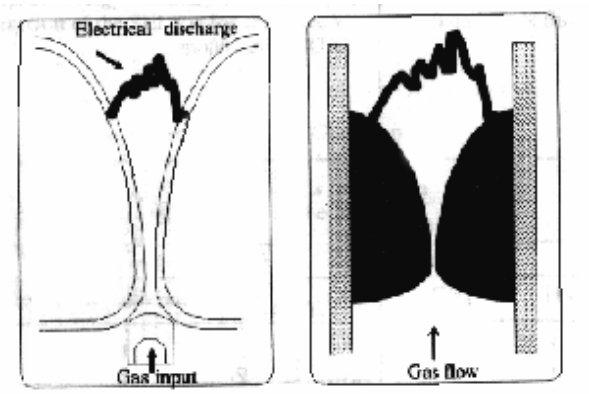

Figure 1.4.8 Diverging electrodes and glidarc formation **[Cze94]**

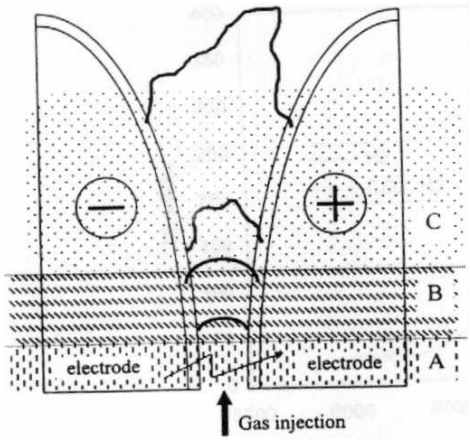

Figure 1.4.9 Phases of glidarc evolution: A - gas breakdown, B - equilibrium heating phase, C - non-equilibrium reacting phase **[Fri99]**

Glidarc developed by A.Czernichovski is a sort of arc occurring between two diverging metal electrodes at strong gas flow rates. (Figure 1.4.8) An arc is established in the place of the minimal interelectrode distance, but it quickly slides along the electrodes due to

the high gas flow. Glidarc can be supplied by either d.c. or a.c. high voltage (~20 kV), the currents reach 0.1-5 mA, it exists over a wide pressure range (3 kPa - 1 MPa). The first stage or arcing approaches LTE conditions with T~4000-6000 K, the second stage when it glides along the electrodes is further from LTE, T_e~10000 K but T_g~1000-3000 K. (Figure 1.4.9) [Cze98, Fri99]

Glidarc has been successfully used for flue gas cleaning from various kinds of pollutants.

1.4.7 Environmental applications of thermal plasmas

Thermal plasmas (plasmas in the local thermodynamic equilibrium or in the conditions close to LTE, i.e. with temperatures at least 5000 K) are broadly used in industry, e.g. for welding and cutting of metals, thermal synthesis of various materials etc. There are also some environmental applications of such plasmas, e.g. pyrolysis and thermal decomposition of wastes etc., but the treatment of atmospheric pollutants appear relatively seldom. [Huc98, Scl93, Huc00]

Typical procedures of thermal plasma generation are arc discharge and plasma torch. We will mention also the controlled thermonuclear fusion.

1.4.7.1 Arc discharge

Arcs exist over a wide pressure range (from 10^{-1} Pa to over 1 MPa), at low applied voltages (10-100 V), but reach high currents (10-100 A). The generated plasma is usually in LTE conditions, with T~5000-10000 K. Basic elementary processes supplying the arc by electrons are thermal volume ionisation and thermal electron emission from the cathode, for certain cathode materials autoemission (field emission) of electrons prevail. Arcs are characteristic by large current densities (10^4-10^7 A/cm^2). [Rai91, Mrt95]

1.4.7.2 Plasma torch

Classical plasma torch is a special modification of arc where a strong gas flow gets the plasma with T~8000 K out of the reactor. Plasma torch reactors are called plasmatrons. There exist also plasmatrons using radio frequency and microwave discharges. Plasmatrons have wide industrial applications, some of them touch the environment, e.g. pyrolysis of

hydrocarbons and wastes and production of iron from the fly ash emitted from electric power stations. [Rai91, Mrt95]

1.4.7.3 Controlled thermonuclear fusion

Controlled thermonuclear fusion works at very high temperature and strongly ionised plasmas ($T > 1$ MK). Such conditions are completely beyond the scope of this work oriented mainly to the low temperature gas discharge plasmas, however, it is worth to be mentioned as an environmental plasma application, because it is an adept to resolve the energy problem on Earth. From the environmental point of view, this technique of energy generation is excellent, almost unlimited supplies of deuterium used as a main fuel are present in oceans (heavy water D_2O represents about 0.013-0.018 % of all water on the Earth). Evidently, there are enormous technical and scientific problems how to store such hot plasma medium, how to make the thermonuclear fusion effective and many others. Magnetic holding of such plasmas is only possible (no material resists to T>1 MK), various toroidal configurations (tokamak, stellarator), magnetic mirrors or pinches are employed. New methods of high temperature plasma generation based on the laser induced supercompression are promissing.

Until now, the problems of controlled thermonuclear fusion have not been solved and are still under an intensive research. [Chn84]

2.

VOLATILE ORGANIC COMPOUNDS (VOC) AS ATMOSPHERIC POLLUTANTS AND THEIR REMOVAL

2.1 ATMOSPHERIC POLLUTION

2.1.1 Introduction - global and local environmental problems

Most of the eminent environmental problems facing the world today have risen due to the atmospheric pollution during the last century. Some of the problems seem to be more or less solved (e.g. acid rains caused by the sulphur dioxide (SO_2) and nitrogen oxides (NO_x) emissions have been reduced in many industrial countries), on the other hand, other problems became more significant, e.g. a photochemical pollution, but in particular an increasing greenhouse effect and a stratospheric ozone layer depletion.

In general, the environmental problems can be global or local. Global problems touch the whole Earth environment, although the emissions sources are localised, for example climate changes due to the enhanced greenhouse effect. They usually appear a long time after when the responsible compounds were emitted, because the transport times within atmosphere are quite long, especially between the troposphere and the stratosphere. On the other hand, these problems persist for a long time, they have a great inertia. An example is the ozone layer depletion induced by hard freons (CFC) which became serious 20 years after the conjunction of the hard freon utilisation, but is still actual despite of the stopping of the use of freons.

Local pollution problems touch just some localised region surrounding the emission sources. The intensity of their effects decreases as they spread to further regions. However, these problems may grow to very hazardous levels in the attacked regions. Fortunately, they persist for a relatively short time, determined by the lifetime of concerned compounds and the specific ventilation of the region. The polluted atmosphere relaxes to normal conditions within several hours-days as the emissions are stopped or decreased. A typical example is an atmosphere of large cities, emissions from concentrated industry and transport are responsible for increased ozone, NO_x and VOC concentrations leading to the smog formation, acid rains and almost unbreathable air under certain meteorologic conditions such as low clouds or inversion.

Some problems, however, can be classified as a transition between global and local problems, since they affect rather large regions, whole countries or continents. Examples are acid rains and photochemical pollution.

The most important atmospheric pollutants and the human activity sector of their origin are shown in Figure 2.1.1

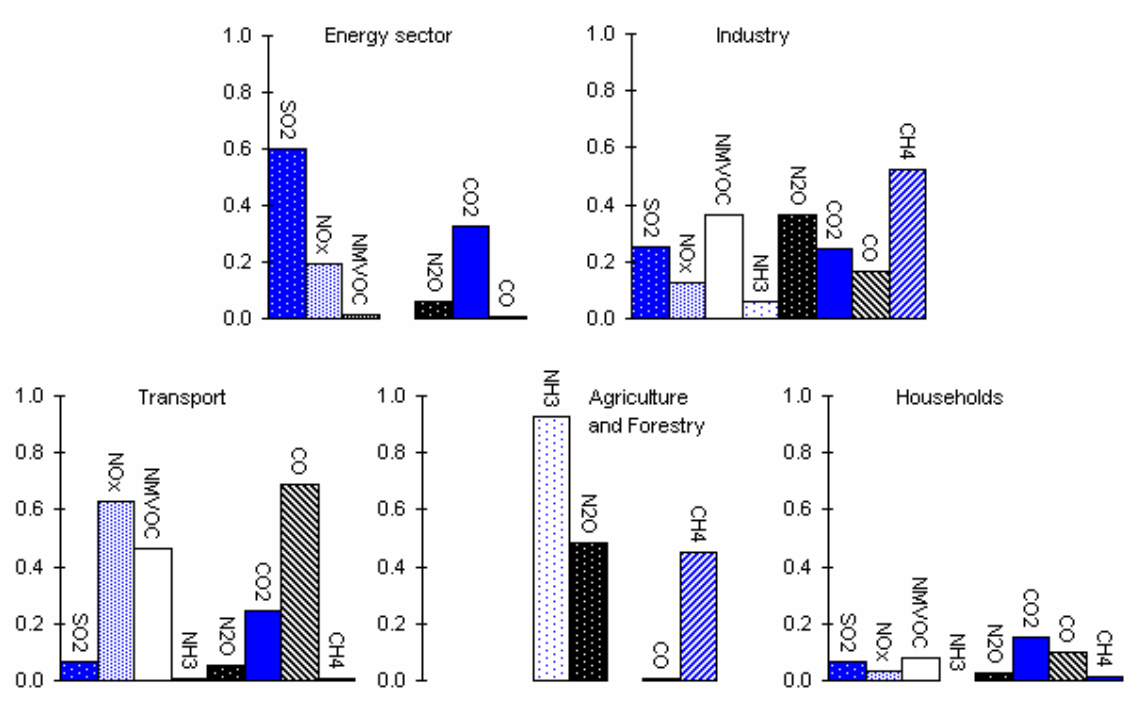

Figure 2.1.1 The most important atmospheric pollutants relative to the sector of their origin, total production of each compound by all sectors is 1. NMVOC means non-methane VOC. **[EEU99]**

In the next three sections we will discuss in more details the environmental problems which are fully or partially caused by atmospheric emissions of volatile organic compounds (VOC).

2.1.2 The role of VOC in the photochemical pollution

The photochemical pollution was firstly observed in the industrialised region of Los Angeles in 1940s. A special fog, called also a white (photochemical) smog (smog = smoke + fog) formed in low atmospheric layers during sunny days with a low air relative humidity. It reduced the visibility and behaved as an oxidising agent, aggressive for plants and human beings. It was found that the principal pollutant of the white smog is ozone formed in the reactions of NO_x and organic compounds (VOC) in a presence of the sunlight (UV B radiation in particular). Ozone then behaves as an oxidising agent, while other products, so called peroxy-acetyl-nitrates (PAN), participate to the smog aerosol formation.

Let us describe the mechanism of the photochemical smog formation in the troposphere. In a presence of NO_x and under sunlight the following reactions of ozone formation and decomposition occur (Chapman's cycle):

$NO_2 + h\nu \rightarrow NO + O(^3P)$ radiation with $\lambda < 398$ nm

$O(^3P) + O_2 + M \rightarrow \mathbf{O_3} + M$ M is a third body receiving energy (N_2 or O_2)

$NO + \mathbf{O_3} \rightarrow NO_2 + O_2$

These reactions are in equilibrium, formed O_3 is consequently destroyed.

However, this equilibrium is unbalanced when methane, CO or VOC are involved. They are responsible for the generation of hydroperoxyl (HO_2) and alkylperoxyl (RO_2) radicals. These are formed by various mechanisms, mainly by reactions with OH radicals and photodissociation of VOC fragments. We present some of them:

$CH_4 + OH^\bullet + O_2 + M \rightarrow CH_3O_2^\bullet + H_2O + M$

$CH_3O_2^\bullet + O_2 \rightarrow CH_2O + \mathbf{HO_2^\bullet}$

$CH_2O^\bullet + h\nu \rightarrow HCO^\bullet + H^\bullet$ (CO+ H_2 respectively)

$HCO^\bullet + H^\bullet + 2O_2 \rightarrow CO + 2\mathbf{HO_2^\bullet}$

$RH + OH^\bullet \rightarrow R^\bullet + H_2O$

$RCHO + h\nu \rightarrow R^\bullet + HCO^\bullet$

$R^\bullet + O_2 \rightarrow \mathbf{RO_2^\bullet}$

$HO_2^\bullet$ and $RO_2^\bullet$ are strong oxidants of NO, stronger than O_3.

$HO_2^\bullet + NO \rightarrow OH^\bullet + NO_2$

$RO_2^\bullet + NO \rightarrow RO^\bullet + NO_2$

The mechanism of O_3 consumption is weakened by the above reactions, O_3 formed by the photodissociation of NO_2 is thus saved and it accumulates in the troposphere. OH radicals initiating VOC and CH_4 decomposition may be generated by many ways, the most important ones are reactions of atomic oxygen with water vapour.

$O_3 + h\nu \rightarrow O_2 + O\ (^1D)$

$O\ (^1D) + H_2O \rightarrow 2\ OH^\bullet$

and a photodissociation of HONO (formed from NO_x)

$HONO + h\nu \rightarrow OH^\bullet + NO$

A part of NO_2 molecules reacts with OH and RO_2 radicals to form nitric acid and peroxy-acetyl-nitrates (PAN):

$NO_2 + OH^\bullet \rightarrow HNO_3$

$RCOO_2^\bullet + NO_2 \rightarrow RCOO_2NO_2$ (PAN)

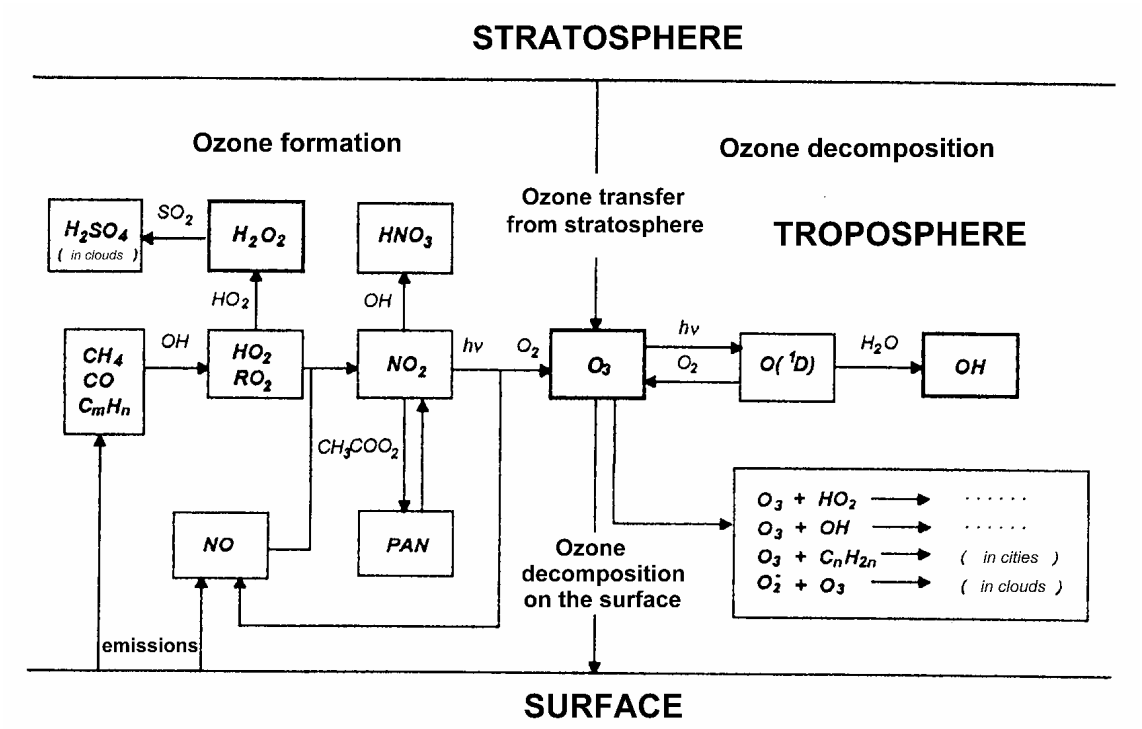

Figure 2.1.2 The most important processes of the tropospheric photochemistry [NCPSR]

PAN are preferentially formed from olefinic hydrocarbons emitted into the atmosphere. They are stable at low temperatures, able to associate metals and to form condensation nuclei for aerosols responsible for a white smog formation. At higher

temperatures, these reservoirs of radicals dissociate and release further ozone precursors. Both HNO_3 and PAN are aggressive for humans and materials.

In conclusion, VOC emissions into the troposphere influence the photochemical mechanisms involved and lead to the increase of the tropospheric O_3 and formation PAN responsible for photochemical smog. Of course, reaction schemes presented above are definitely not complete, the whole mechanism of the tropospheric photochemistry is much more complex, it is roughly sketched in Figure 2.1.2. Our aim was just to show the role of VOC in these mechanisms. [NCPSR]

2.1.3 CFC in the stratosphere and the ozone layer

Ozone, an aggressive oxidant and pollutant of the troposphere, is life important in the stratosphere, its layer protects the Earth from the solar UV radiation. The ozone equilibrium in the ozonosphere (part of stratosphere, altitude 25-40 km) is approximately described by the equations proposed by Chapman:

$O_2 + h\nu \rightarrow O + O$

$O + O_2 + M \rightarrow O_3 + M$ M - third body taking energy (usually N_2 or O_2)

$O_3 + h\nu \rightarrow O_2 + O$

$O_3 + O \rightarrow 2O_2$

The ozone concentration profile in the atmosphere is shown in Figure 2.1.3.

Some halogenated VOC, especially chloro-flouro-carbons (CFC) called also freons are responsible for O_3 decomposition and ozone layer reducing. CFC such as CF_2Cl_2 are non-toxic gases which were very widely used in industry of the 1970s-80s. They are chemically very stable, thus they rest in the atmosphere from tens to several tens of thousand years (e.g. CF_2Cl_2 has a lifetime 130 years, $CFCl_3$ 65 years and CF_4 50 000 years!). Due to their long lifetimes, CFC slowly penetrate to the stratosphere, they get to the high levels of the ozonosphere. The solar radiation in these altitudes contains wavelengths in UV A and UV B regions, since ozone layer absorbing these wavelengths is thinner. This UV radiation photodissociates CFC, and released Cl atoms consequently decompose ozone:

$CF_2Cl_2 + h\nu \rightarrow Cl + CF_2Cl$ $\lambda < 230$ nm

$Cl + O_3 \rightarrow ClO + O_2$

$ClO + O \rightarrow Cl + O_2$

The most disastrous effect of this mechanism is the catalytic effect of Cl which is not lost, being reproduced by the third reaction. Similar effects have NO_x in the stratosphere which also decompose O_3:

$NO + O_3 \rightarrow NO_2 + O_2$

$NO_2 + O \rightarrow NO + O_2$

These ozone destruction mechanisms can be only stopped by the reaction:

$ClO + NO_2 + M \rightarrow ClNO_3 + M$

$ClNO_3$ has a long lifetime in atmosphere. However, both mechanisms of O_3 destruction are very effective, especially those induced by CFC. This kind of compounds, although directly non-toxic, are very dangerous from the global point of view. Use of the hard freons (composed of C and halogens only) has been significantly reduced by many restrictions, just soft freons (containing hydrogen) are allowed now. [NCPSR]

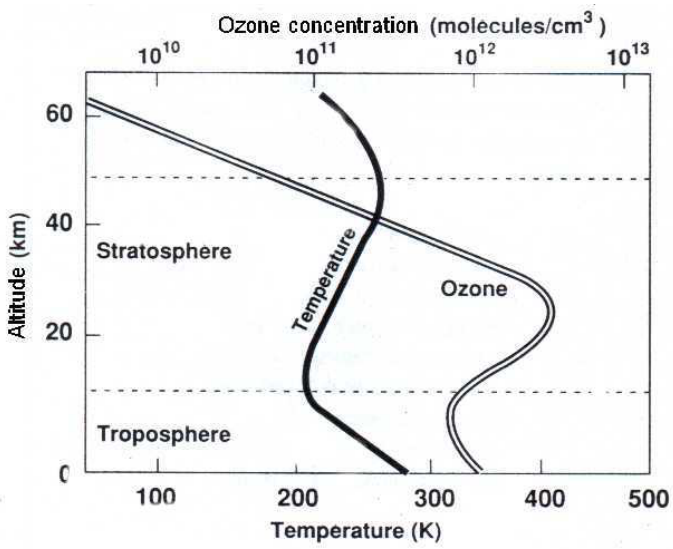

Figure 2.1.3 Ozone concentration profile in the atmosphere

2.1.4 Greenhouse effect

The natural Earth greenhouse effect rises the temperature of the planet by 33°C, thus making it habitable. In average, 343 W/m^2 of sunlight fall on the Earth, roughly 1/3 of which is reflected from the atmosphere back into space (Earth albedo). The other 2/3 reach the ground which re-radiates it as an infrared radiation of longer wavelengths. A part of this Earth radiation is absorbed by greenhouse gases, thereby warming the atmosphere. (Figure 2.1.4)

Natural greenhouse gases include water vapour (H_2O), carbon dioxide (CO_2), methane (CH_4) and nitrous oxide (N_2O). Any factor, which alters the amount of radiation received from the sun or lost to space, may influence the climate. Thus, any significant enhancement of the greenhouse effect is a cause for concern. Human activity is emitting extra amounts of greenhouse gases, which alter the amounts of radiation trapped by the atmosphere and so may have a climate effect. Carbon dioxide emissions are responsible for over 60% of the "enhanced" greenhouse effect [Por96].

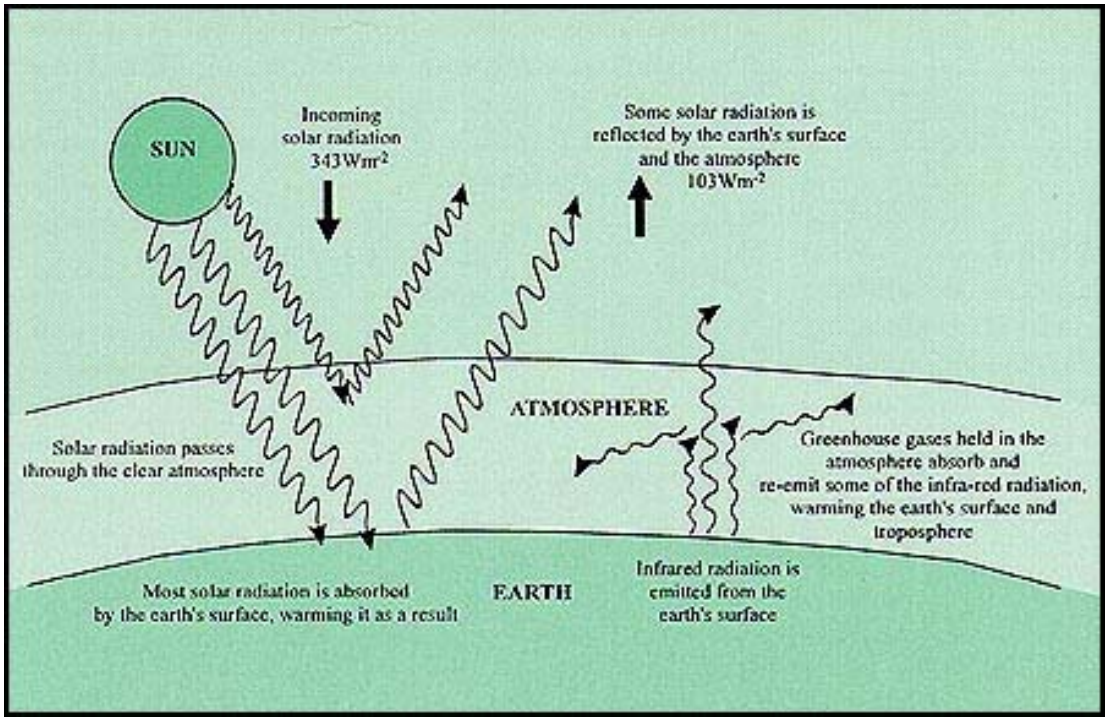

Figure 2.1.4 Greenhouse effect

The concentration of CO_2 in the atmosphere has increased from about 280 ppm, before the industrial revolution, to 358 ppm in 1994, 367 ppm now (2000) and this growth is

exponential! Its level is predicted to 540-970 ppm at the end of the 21st century. CO_2 has a long lifetime in the atmosphere, from 50 to 200 years (depending upon which sink mechanism is involved). Human activities are responsible for almost 30% of the free CO_2 levels, which continue to increase by almost 10 % every 20 years. [GHGT98, Wue93]

However, CO_2 is not the only factor responsible for the enhanced greenhouse effect, although the most important one. Other gases such as methane (CH_4), nitrous oxide (N_2O) and halogenated hydrocarbons have a significant part at this effect, although their concentrations in atmosphere are much lower than CO_2, see Figure 2.1.5. These compounds participate at the increasing greenhouse effect especially due to their high global warming potential (GWP), which is a rate of relative intensification of the greenhouse effect caused by the emission of 1 kg of the greenhouse gas, e.g. GWP(CO_2) = 1, GWP(CF_4)=12000. Table 2.1.1 provides some data on the most important antropogeneous greenhouse gases.

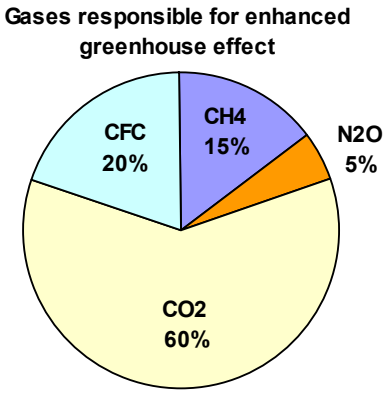

Figure 2.1.5 Approximative contributions of the most important gases responsible for the enhanced greenhouse effect. [IPCC]

The Intergovernmental Panel for Climate Change (IPCC) concluded that 'the balance of evidence suggests a discernible human influence on the global climate'. The IPCC has used emission scenarios and climate models to make projections about future climate change. Although uncertainties still remain in the climate modelling, a confidence in the models has increased in last years. The mean global surface temperature has risen by about 0.3 - 0.6 °C since the late 19th century - when the industrial record began - and by about 0.2 - 0.3 °C since 1955. Using the emission scenarios, the global mean temperature will increase by 1.5 - 6 °C in the year 2100, relative to 1990. The average rate of warming would probably be greater than any seen in the last 10000 years. [IPCC]

Greenhouse gas		CO_2 / ppm	CH_4 / ppb	N_2O / ppb	CFC–11 / ppt	CFC–12 / ppt
Tropospheric Concentration	years 1750-1800	280	700	275	0	0
	Recent	367	1720	312	268	484
Growth since pre-industrial era / %		28	145	7	-	-
Annual growth / %		0.4	0.6	0.25	-	-
Global annual antropogeneous emission / 10^9 kg		24 000 – 28 000	375	3 – 7	-	-
Residence time in the atmosphere / years		50 – 200	10	120	50	102
GWP		1	24.5	320	3500	7300

Table 2.1.1 The most important antropogeneous greenhouse gases and some their characteristics. GWP = global warming potential [IPCC]

Sea level rise is another important consequence of the climate change. Global sea level has risen by about 10-25 cm over the last 100 years. The temperature will continue to increase even after stabilisation of the greenhouse gas concentrations in the atmosphere, because of the thermal inertia of the oceans. Increased temperatures will cause some expansion of the sea water, and the retreat of glaciers and ice caps will also contribute to its increase. By 2100, sea level is projected to rise by 13-94 cm, with a mean value 47 cm (2-4 times more than the increase in the 20th century) due to the global melting of glaciers in Greenland and Antarctica [Hou94, IPCC].

There is also a possibility that unusual weather events, such as severe storms and hurricanes, may become more frequent. An altering in ocean circulation, such as in the Gulf Stream and El Niño, can also take place. Ecosystems, agriculture, forestry, and human health are sensitive to the climate. The range of diseases such as malaria could increase. Some ecosystems may be unable to adapt to the climate changes at an adequate rate. If the rate of climate changes could be limited to a low level, natural systems and humans will find it easier to adapt. A principal way to slow the rate of changes is to reduce emissions of greenhouse gases. [IPCC, UNFCCC, GHGT98]

2.2 VOLATILE ORGANIC COMPOUNDS (VOC) - GENERAL FACTS

Volatile Organic Compounds (abbreviation VOC will be used) are atmospheric pollutants of our special interest, possibilities of their removal are concerned in this work. Some general facts on VOC are provided in the following sections.

2.2.1 Definitions and classification of VOC

VOC are roughly thought to be hydrocarbons and their derivates which are liquid under normal conditions, but easily volatile. In a common life they are known as miscellaneous types of solvents, cleaning agents and fuels. However, several exact definitions of VOC have been proposed with respect to various criteria.

2.2.1.1 Definitions of VOC

According to their effects in the atmosphere, VOC are defined like a set of hydrocarbons of human origin, different from methane, capable to produce photochemical pollutants in the presence of nitrogen oxides and light.

According to their chemical composition the VOC definition includes all compounds composed of carbon C and hydrogen H, the latter (H) may be partially or totally substituted by other atoms (halogens, O, N, S, P etc), with an exception of methane, carbon oxides and carbonates. Compounds in gas or vapour state under working conditions are concerned.

Finally, the European directive project completes this definition with respect to the volatility and uses of these compounds: VOC are all organic compounds with saturated vapour pressure ≥ 0.01 kPa at 20 °C or having the same volatility in particular conditions of its uses. They are employed (pure or in a mixture not altering their properties) like cleaning agents, solvents, dispersion environments, viscosity adjusters, plastifiants or conservators. [RECOVI]

In this work we keep the last definition. VOC which we treated (cyclohexanone and toluene) satisfy the volatility condition, see Table 5.1.1 in chapter 5.

2.2.1.2 VOC classification according to their chemical composition

According to the chemical composition we can classify VOC by the following way:

- alifatic (e.g. ethylene, formaldehyde, acetone, methanol, ethanol)
- cyclic (e.g. cyclohexane, cyclohexanone)
- aromatic (e.g. benzene, toluene, xylene, ethyl benzene)
- polycyclic aromatic (abbreviated PAH, e.g. chryzene, pyrene, antracene)
- nitrogen containing (e.g. hydrogen cyanide, acetonitrile, peroxy-acetyl-nitrates)
- halogens containing, most important are chloro-fluoro-carbons CFC (freons, e.g. tetrachlormethane, trichlorethylene)

2.2.2 VOC effects on human organisms

Effects of VOC emissions in the atmosphere have already been mentioned at the beginning of this chapter. VOC vapours have many other effects, such as enhanced corrosion and degradation of some materials (especially plastics, e.g. cyclohexanone etches PVC) and the danger of inflammation when they are present within a certain concentration interval. However, the most abundant are their effects on living organisms, in particular human beings.

Most of VOC are characteristic by their smell, the threshold concentration limit for their nasal detection is individual and specific for each compound. Almost all VOC are toxic, i.e. they have some bad effects on humans and other living organisms. The type and rate of their toxicity depends mainly on the compound itself and its vapour concentration in air (which is given by its volatility), as well as the time of the dose, long doses of law concentration may be worse than short doses of high concentration. VOC vapours penetrate into the organisms especially by inhalation (breathing) and skin penetration.

The VOC toxicity in general may be chronic (long-lasting doses) and acute (short doses). Various VOC attack miscellaneous parts of the human body (as well as animals and other organisms), e.g. eyes, skin, blood and heart, bone marrow, respiratory system (lungs), digesting system, central nervous system, tissues and in particular liver and kidneys. Numerous VOC cause metabolism changes, many of them have narcotic, cancerogene (especially aromatic compounds and PAH - they attack RNA) and mutagene (attack of DNA) effects.

VOC concentration limits have to be respected in working environment (indoor) as well as in free atmosphere (outdoor) in order to avoid undesired VOC effects, most frequently

used limits are the mean maximum allowable concentrations during 15 minutes, 24 hours, 8 hours per day and 40 hours per week, etc. These limits are specific for each compound, they range at ppm levels. [Bro65, RECOVI, Poi97, Soo97]

2.2.3 VOC sources

VOC getting to the atmosphere are of natural as well as antropogeneous origin (from human activity). Natural sources represent about 90 % in the planetary scale, but they produce VOC in low concentrations and there are mechanisms of their natural degradation, so they do not unbalance the natural equilibrium. On the other hand, natural VOC sources become minor in industrialised regions where the antropogeneous sources produce high concentration of certain types of VOC and strongly unbalance the natural equilibrium.

Natural VOC sources are caused by living and decaying organisms (plants, animals and micro-organisms). Living organisms, particularly plants produce terpenes, acetone, methanol, ethanol, isoprene, pinene etc. in concentration of 10-100 ppb (sometimes up to 1000 ppb). Decaying organisms emit for example acetone and methanol, especially in a contact with water. [Lin98] A special VOC source is a biomass burning in tropical regions. It produces mainly CO_2 and CO, but also formaldehyde, acetaldehyde, acetone, propanol, methanol, cyanides (acetonitrile), aromatic compounds (benzene, toluene) in total concentrations up to 1000 ppm [Hlz98]. Acetone is especially important among these VOC, because it supports a formation of radicals HO_x in the atmosphere, thus a formation of PAN which work like a reservoir of NO_x and lead to the photochemical smog. [War98] [Lin96] Another important natural VOC source is a volcanic activity and deposits of raw oil, natural gas and organic sediments (black slates containing resins).

VOC are present also in the human breath (methanol, ethanol, acetone, isoprene; about 100-1000 ppb), this can be considered as an antropogeneous source, although of minimal importance in comparison with other antropogeneous sources.

An important antropogeneous source of VOC is industry, heavy as well as light, namely oil mining and petrochemistry, chemical industry, production and treatment of gum, plastic materials and fats, paper industry, cosmetics and pharmaceutical industry, production and treatment of paints and lacquers, treatment and conservation of wood, energetic industry.

Recently, road transport became the greatest VOC source in industrial countries in recent years. Especially diesel engines are responsible for this growth, because almost all

petrol engines use catalysts. Concentration of aromatic compounds, such as toluene, xylene and benzene, in the city atmospheres at traffic hours reach 10-100 ppb [Jor96].

Agriculture, especially animal production such as broiler chicken farms, also contributes to the VOC emissions. Finally we have to mention communal sources such as combustion of communal refuse, decaying and vaporising of wastes, etc.

Indoor sources, such as gas cookers and smoking, contribute to the indoor VOC emissions.

Miscellaneous types of VOC (alifatic, cyclic, aromatic, halogenated, polycyclic) get into the atmosphere by these ways, in concentrations from 1 ppb up to several %.

Rates of VOC emissions by various sectors are shown in Figure 2.2.1. VOC emissions relative to other pollutants by sectors are shown also in Figure 2.1.1 in chapter 2.1.

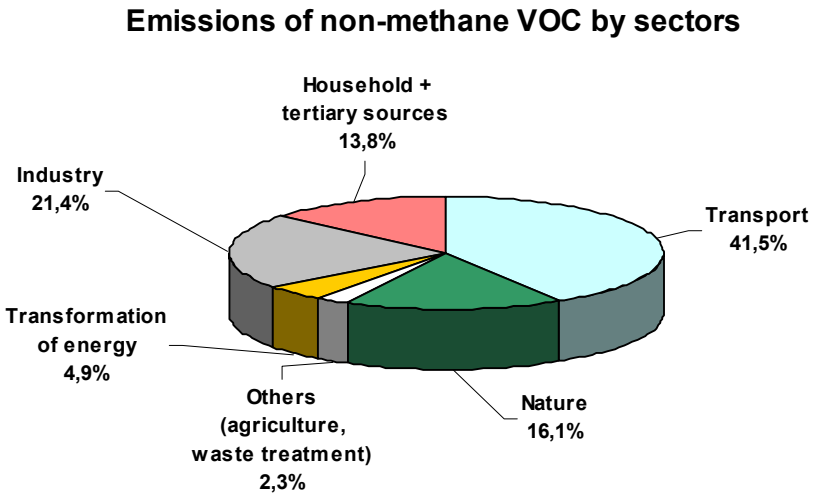

Figure 2.2.1 VOC emissions by various sectors of the human activity in France in 1990. **[RECOVI]**

2.3 “CLASSICAL” TECHNIQUES OF VOC EMISSIONS ABATEMENT

This chapter will be concentrated on the conventional or “classical” techniques of VOC atmospheric emissions abatement, i.e. methods which are well known, understood and widely used in industry and other sectors of a human activity. Although many of these

techniques are relatively old, they still undergo a development and improvement. They can be divided into two basic groups:

1. Recuperative techniques that allow recovery of VOC
2. Destructive techniques that destroy VOC and covert them into other products

2.3.1 Selection criteria

Selection and uses of the VOC removal techniques depends on the number of factors which have to be taken into account. The most important criteria are:

2.3.1.1 Physico-chemical parameters

- gas flow rate and its variations (during daily/weekly operation, etc.)
- VOC concentration and its variations
- composition of the exhaust (single compounds or mixtures) and its variations
- non-VOC admixtures (e.g. water, ammonia, halogens, SO_x and NO_x, dust particles)
- temperature and its variations
- down and up limits of inflammability and explosivity of the treated VOC

[vBe92, Rdd93]

2.3.1.2 Technical criteria

- required reduction in emissions
- nature of installation site (available space, utilities such as steam, liquid N_2 etc.)
- maintenance possibilities (materials, staff, safety aspect etc.)

[vBe92]

2.3.1.3 Economic factors

- investment costs
- maintenance (operation) costs

2.3.2 Recuperative VOC abatement techniques

These techniques remove VOC from the emitted air streams and allow their recovery which is an advantage in comparison with destructive techniques.

2.3.2.1 Absorption (scrubbers)

Old and quite simple absorption methods are based on the absorption (dissolving) of VOC from polluted gas in a convenient liquid medium (or foam). The name *“wet washing”* is also used. The main task is a choice of the absorption medium which has to well dissolve the treated VOC and not to be volatile, inflammable, toxic and expensive. (Figure 2.3.1)

High recovery yields are possible (95-98 %), operating costs can be low and recovered solvent can have a high purity. Scrubbers are suitable for air streams with temperatures not far above ambient and for relatively high concentrations (> 50 g/Nm^3), they are not applicable for all types of VOC. [RECOVI, vBe92]

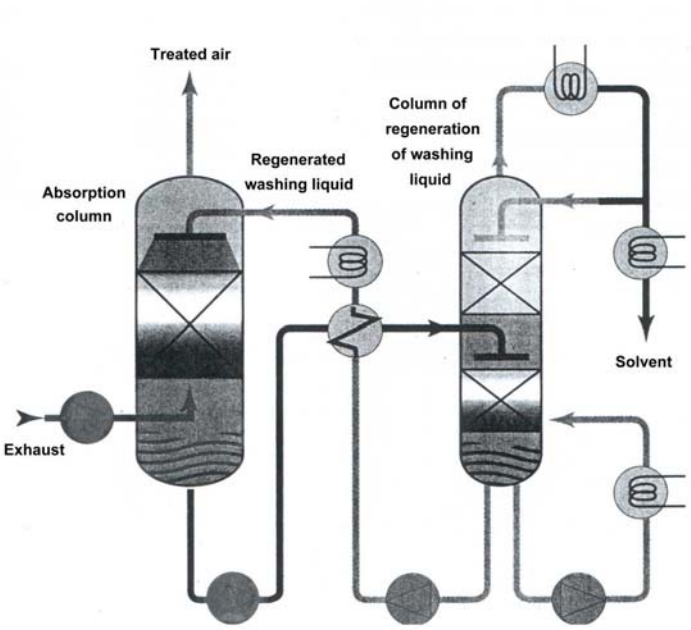

Figure 2.3.1 Scheme of the absorption scrubber (wet washing) with regeneration of the washing liquid. **[RECOVI]**

2.3.2.2 Adsorption

The technique is based on the physical property of certain solid media such as activated carbon, molecular sieves, clays, zeolites etc. to fix VOC (and other) molecules reversibly by van der Waals forces. Reliable operation demands a frequent change of the adsorption medium, because its capacity is limited (it saturates). (Figure 2.3.2)

The technique can provide high recovery yields (90-98 %) and is suitable for air streams with low or medium VOC concentrations (< 50 g/Nm^3). It is applicable for a large

range of flow rates. Requirements for air stream temperature, humidity and dust content put certain limitations to its applicability, for example it is not very convenient for highly toxic and cancerogene VOC. [Met84, ChD89, RECOVI, vBe92]

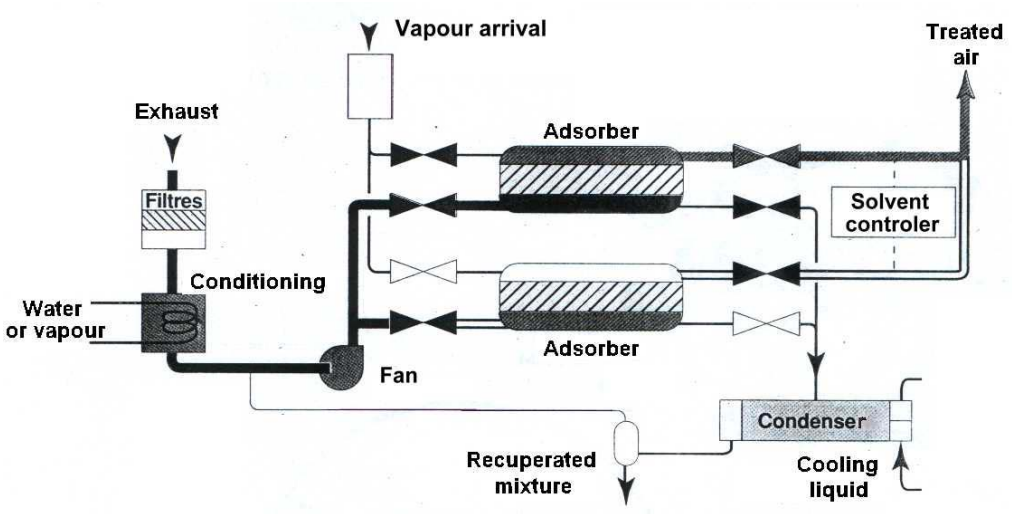

Figure 2.3.2 Scheme of the adsorption technique **[RECOVI]**

2.3.2.3 Condensation

Condensation of VOC vapours from the exhaust gas works on the principle of temperature lowering which decreases the saturated vapour pressure of the treated compound, under its partial pressure. The technique is not selective, the condensation systems are usually made in several stages, water is separated first and a concentrated VOC condensate at the end. A part of cool VOC condensate can be employed for further treatment of the same, still not condensed, VOC. [RECOVI] (Figure 2.3.3)

This technique is convenient just for high VOC concentrations (> 10 g/Nm^3) and low flow rates (< 3000 Nm^3/h). Efficiencies are as high as 50-90 %. Using cryocondensation (liquid N_2) almost 100 % recovery yields can be reached. However, such method is rather expensive and sensitive to the presence of moisture. Condensation techniques are often combined with adsorption. [vBe92, AMTS97]

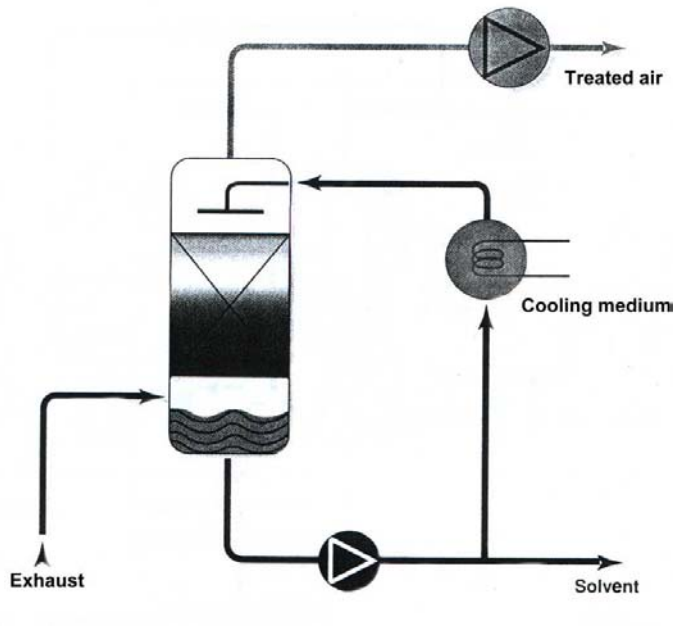

Figure 2.3.3 Scheme of the direct contact condensation technique **[RECOVI]**

2.3.2.4 Membrane gas separation

This is a fairly new technique offering an additional advantage of solvent recovery in cases where other techniques are not suitable. Treated exhaust is exposed to a contact with the semi-permeable polymer membrane which is under reduced pressure from the opposite side. The pressure difference and the membrane properties drive the VOC molecules through the membrane while smaller molecules cannot penetrate. Separated VOC on the opposite side of the membrane are recovered by condensation. (Figure 2.3.4)

Membrane separation is particularly suitable for mixtures of solvents when emitted in small volumes (600-6000 Nm^3/h) at high concentration. The best recovery yields are however limited to 90 %, therefore in most cases the remaining air stream needs further treatment. [vBe92, RECOVI, AMTS97]

2.3.2.5 Other techniques of VOC recovery

The above basic methods of VOC recovery can be combined or variously modified, for example oil absorption-desorption, oil absorption - membrane separation, nanoporous filters with cyclic work, etc. Distillation and other techniques are sometimes used as well. A simple example of fuel (gasoline) recovery by condensation are hermetic nozzles at fuel stations. [Pnn84, AMTS97]

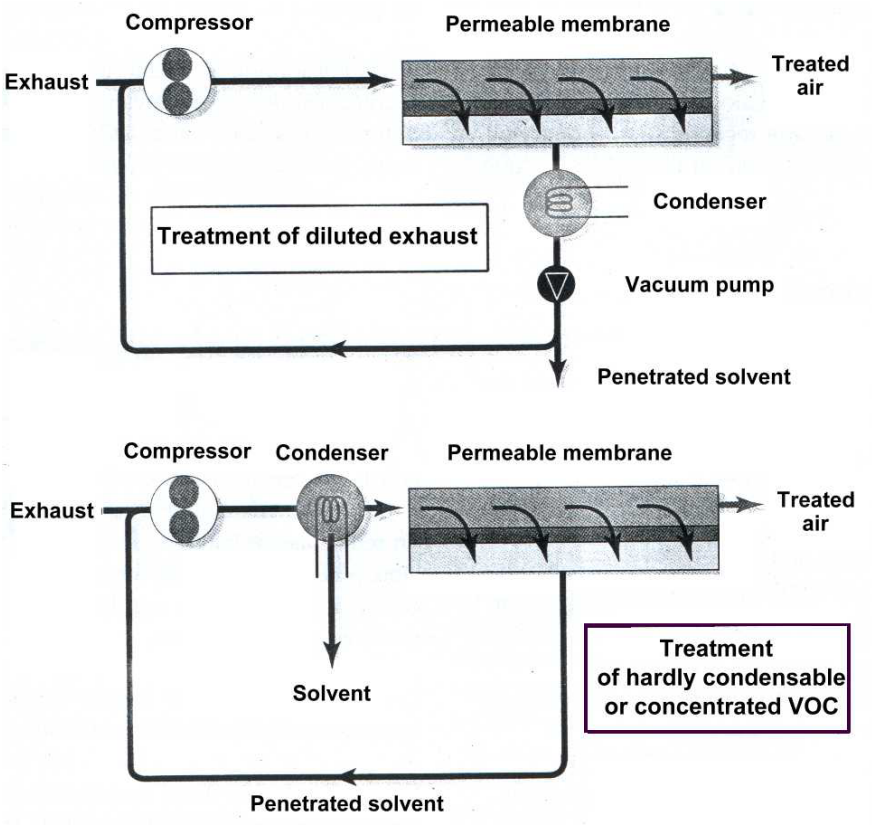

Figure 2.3.4 Scheme of two types of the membrane gas separation technique **[RECOVI]**

2.3.3 Destructive VOC abatement techniques

These techniques treat VOC emissions by a destructive manner. Firstly, VOC are not recovered, thus cannot be reused, and secondly, some by-products of this process are evidently formed. The products have to be attentively analysed and all their effects considered (e.g. toxicity, effects in atmosphere, etc), especially when they get out with treated gas streams. From these two reasons, destructive techniques are generally worse than recuperative ones, but sometimes there is no possibility to use recovery techniques. Moreover, after consideration of all criteria, use of the destructive techniques may be better.

2.3.3.1 Thermal oxidation (combustion, incineration)

Complete oxidation of VOC to CO_2 and H_2O requires conditions such as high temperature (over 750 °C), optimal oxygen content, sufficient residence time and optimised

turbulences in the combustion reactor. If these conditions are not fulfilled, oxidation is incomplete and can produce dangerous gases (CO, NO_x).

The thermal incinerator consists of the combustion chamber with a burner fuelled usually by the treated gas, and the system of thermal energy exchanges. The thermal energy given to the treated gas is either reused for the gas preheating in recuperative incinerators (Figure 2.3.5) or stored in ceramic beds in regenerative ones (Figure 2.3.6).

Thermal incineration is convenient for VOC at medium and high concentrations (over 5 g/m^3) and a vast range of flow rates (1000-300 000 Nm^3/h), up to 99.9 % of VOC reduction can be reached. At low VOC concentrations the exhaust can not be directly incinerated, large amounts of supporting fuel make the technique too expensive. However, from the point of view of global ecology, all combustion processes are undesired, because they produce CO_2, the main contributor of the enhanced greenhouse effect and the precursor of the Earth climate changes. [Mur84, RECOVI]

Thermal VOC destruction is also a technique where a high temperature is used, it is applicable especially for off-gases with low O_2 content where oxidation processes cannot take place (e.g. combustion exhausts enriched by VOC).

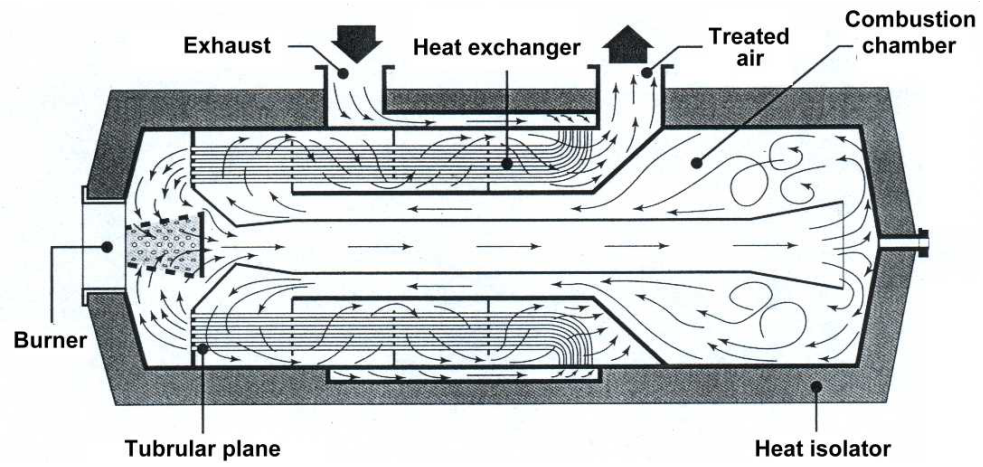

Figure 2.3.5 Scheme of the recuperative thermal incinerator (with heat exchangers inside). **[RECOVI]**

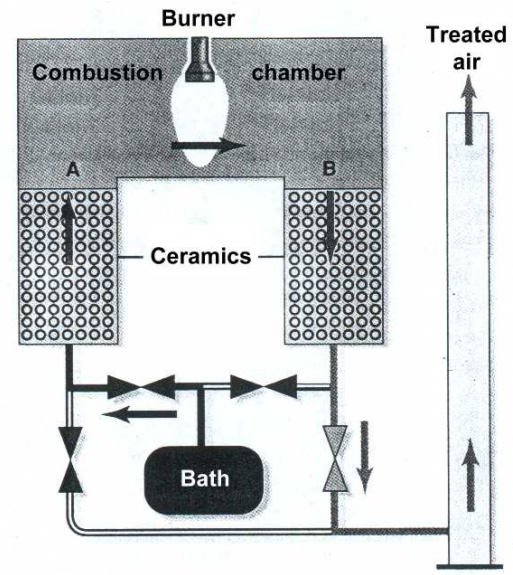

Figure 2.3.6 Scheme of the regenerative thermal incinerator (heat storage in two ceramic beds). **[RECOVI]**

2.3.3.2 Catalytic oxidation (catalytic combustion, incineration)

VOC oxidation supported by catalysts (noble metals, metal oxides) does not require such high temperatures as the thermal incineration, 200-500 °C are sufficient (it depends on the catalyst type). Moreover, emissions with lower VOC concentration (< 12 g/Nm_3) can be effectively treated.

The catalytic oxidation process occurs on the heated catalyst surface. (Figure 2.3.7) The catalyst's lifetime is 1-2 years, then it must be regenerated. The energy, investment and operation demands of the catalytic oxidation are high, the technique is very sensitive to the catalyst modifications caused by chemical poisoning, masking of active sites, mass losses, etc. It is applicable for medium gas flow rates (1000-30000 Nm^3/h) and reaches 99 % of VOC destruction.

The catalytic incinerators use the same heat recovery systems as the thermal ones. Heated ceramic beds of the regenerative system are used as the catalyst supports which enables the system to work at lower temperatures (200 °C) [Bak84, AMTS97, RECOVI]

Photocatalytic destruction is a special modification of the catalytic VOC destruction method. It is based on the photocatalysis of the matrix covered by TiO_2 which produces large amounts of OH radicals. These radicals then attack and decompose the treated VOC. [AMTS97]

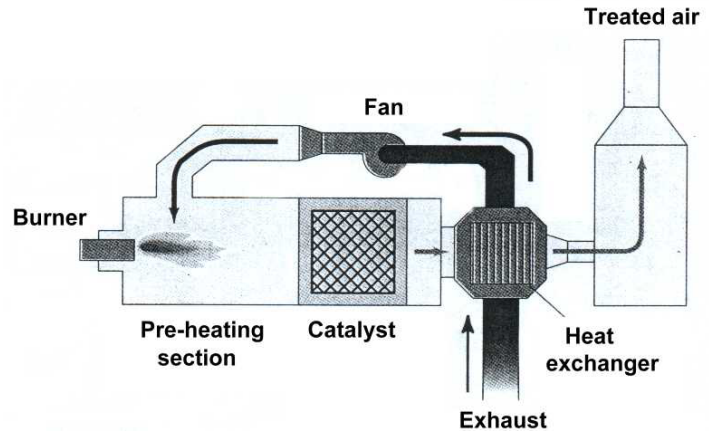

Figure 2.3.7 Scheme of the catalytic oxidation technique with heat exchangers **[RECOVI]**

2.3.3.3 Biological treatment

Some micro-organisms are able to degrade VOC usually to CO_2 a H_2O by an aerobe process (in the presence of O_2). Biological treatment techniques based on this effect use reactors (biofilters) filled with solid natural material (soil, compost, etc.) containing the biolayer with various bacteria or other micro-organisms. (Figure 2.3.8) The technique is particularly suitable for moist air streams of any flow rates containing low concentrations of biodegradable VOC, especially soluble in water (e.g. smelling and humic acids) and it is not expensive. The removal efficiencies reach 90 %. On the other hand, it is very sensitive on the variations in the gas composition and VOC concentration, as well as temperature range (it works best within 20-40 °C interval).

Anaerobe bioreactors use micro-organisms which decompose VOC by anaerobe processes (without a presence O_2). This method is suitable for higher VOC concentrations.

VOC well soluble in water can be treated in bioscrubbers with fluid reactor where their water solution serves as the living environment for involved micro-organisms. This technique, practically modified wet washing, is effective with cheap operation.

Another modification of biological filters is the formation of the catalytic slash (e.g. rutil containing) which is activated by UV radiation. The VOC are absorbed and partially decomposed in the slash. [Smi96, AMTS97, RECOVI]

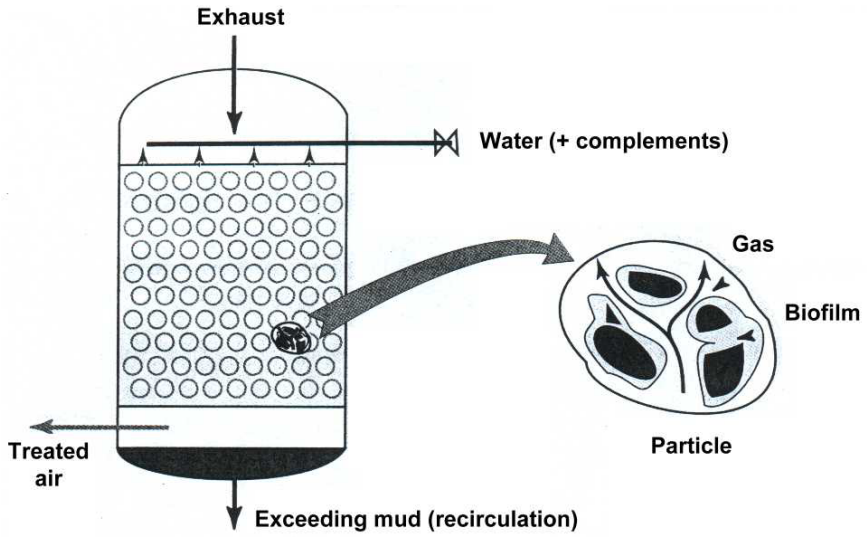

Figure 2.3.8 Scheme of the biofilter **[RECOVI]**

2.3.4 Overall comparison and some remarks

Figure 2.3.9 provides a good overall comparison of classical VOC removal techniques from the viewpoint of physical parameters - gas flow rate and VOC concentration. Reached VOC removal efficiencies vary from 80 to almost 100 %. Investment and operation costs of each technique can be estimated just roughly, because they vary from case to case. However, there is much more parameters and factors (described in section 2.3.1) influencing the technique selection which have to be taken into account.

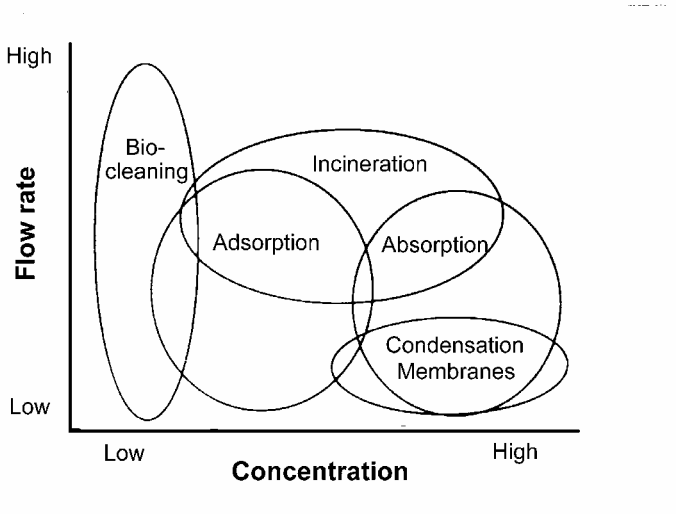

Figure 2.3.9 Overall view of the applicability of the classical VOC abatement techniques **[vBe92]**

In general, solving the complex problems related to the VOC abatement in exhaust gases, requires an attentive and judicious approach based on a large overview of all available techniques, their principles and other possibilities. It is often necessary to combine various techniques, or to adapt them to the specific conditions, in order to gain optimal effects at reasonable costs. All environmental aspects of the technique have to be considered, especially at destructive methods producing by-products which may be noxious. Certainly, it would be ridiculous to remove VOC and create even worse pollutants during the process.

2.4 PLASMA APPLIED FOR VOC REMOVAL

The conventional techniques for VOC abatement described in the previous chapter are widely accepted and well understood. However, with respect to some parameters, such as concentration and compounds treated, cost and energy requirements, these techniques have certain practical limitations. [Yam93] The field of VOC emissions control is thus open for developing alternative techniques. This trend is even enhanced by more and more pronounced environmental problems and by the environmental policy which becomes more severe.

Plasma techniques belong to this novel and promising approach, their results are not only comparable with results of conventional techniques but often better from various points of view.

2.4.1 Basic parameters characterising the VOC removal process

VOC removal process (abbreviated to deVOC in the following, "de" a prefix which indicates removal) induced by plasma can be characterised by various parameters, the most frequent and practical ones will be introduced now. Removal processes of other gaseous pollutants, like NO_x, can be characterised by the same way.

2.4.1.1 Removal efficiency

The basic parameter is the VOC removal efficiency η (relative removal rate, chemical efficiency) which tells what relative amount of the treated VOC was removed. It is usually given in %.

$$\eta = 1 - \frac{c}{c_0} \tag{2.4.1}$$

with initial VOC concentration c_0 and final VOC concentration c, they can be expressed in arbitrary but uniform units (ppm, g/m^3, mol/m^3). An ideal process with no VOC outlet (i.e. c = 0) is characterised by η = 100 %. Removal efficiency is used also in conventional techniques.

2.4.1.2 Energy density

The second parameter general for plasma processes is the specific input energy density R_V. It tells what amount of energy is delivered into the treated gas per unit volume:

$$R_V = \frac{E}{V} = \frac{P}{Q} \qquad \left[\frac{\mathrm{J}}{\mathrm{l}}\right] \tag{2.4.2}$$

where E is the energy dissipated in the treated volume V, P is the power and Q is the gas flow rate. J/l is a usual unit of R_V, other units such as kWh/m^3 are also possible.

2.4.1.3 Energy costs

The energy input density R_V does not give any information on the effectivity of the process, it is independent from the VOC removal itself. Therefore, another energetic parameter is necessary, taking the process efficiency into account. We define the energy costs (energetic efficiency) R_m usually given in [kWh/kg] or R_{mol} given in [eV/molecule] by:

$$R_m = \frac{E}{m} = \frac{E}{(c_0 - c)V} = \frac{P}{Q}\frac{1}{\eta c_0} = \frac{1}{\eta c_0} R_V \qquad \left[\frac{\mathrm{kWh}}{\mathrm{kg}}\right] \tag{2.4.3}$$

$$R_{mol} = \frac{E}{N} = \frac{M_m}{N_A}\frac{E}{m} = \frac{M_m}{N_A} R_m = \frac{M_m}{N_A}\frac{1}{\eta c_0} R_V \qquad \left[\frac{\mathrm{eV}}{\mathrm{molecule}}\right] \tag{2.4.4}$$

where E is the energy dissipated in the treated volume V, m is the total mass of the removed VOC, N is the total number of molecules in the treated volume V, M_m [g/mol] is the specific molar mass of the concerned compound and $N_A = 6.023\times10^{23}$ mol^{-1} is the Avogadro's

number. Initial and final VOC concentrations c_0 and c must be expressed in the mass concentration units [g/m^3] (see conversion equations in Appendix 1) and a factor of 100 has to be considered if η is expressed in [%]. Certainly right conversions of energy units [J, kWh, eV] and gas flow units [l/min, l/s etc.] has to be done to get [kWh/kg] and [eV/molecule]. R_{mol} is practically R_m multiplied by a constant specific for the treated compound, both represent the same parameter. Energy costs represented by this way include the removal efficiency and the energy density at the same time, they indicate the energy necessary to destroy one kg (R_m) or one molecule (R_{mol}) of the treated VOC. It seems that it is the best parameter characterising the deVOC process. Of course, the purpose is to reach as low R_m (R_{mol} respectively) as possible.

However, the problem is raised by the initial VOC concentration c_0. Equations (2.4.3) and (2.4.4) show evidently that R_m (R_{mol} respectively) will decrease with rising ηc_0, they are inversionally proportional. Let us consider that the removal efficiency η is fairly dependent (independent, respectively) on c_0, which was our case (will be shown in chapter 5). By other words, the higher is the initial concentration of the treated VOC, the lower are the energy costs R_{mol} and the process seems better, despite of a low efficiency η, for example. Therefore, although the energy costs are the best parameter of the deVOC process, it cannot be used as the only and general parameter. Initial VOC concentration c_0 has to be always indicated, as well as the removal efficiency η (relative removal rate).

Remark: Most of works dealing with deVOC plasma processes reach lower energy costs at higher initial VOC concentration which is in agreement with equations (2.4.3) and (2.4.4). In spite of the evident inversion proportion of R_{mol} and c_0, there appeared some works claiming an opposite phenomenon – energy costs have risen with increasing c_0 (silent discharge plasma was used). [And99, Oga99] It can only be explained by a brutal decrease of the removal efficiency η with rising c_0 in their specific case (η is also inversionally proportional to R_m), so brutal that ηc_0 decreased even with rising c_0.

2.4.1.4 Products

Since all plasma techniques of removal of gaseous pollutants are destructive, some by-products are always formed. The character and amounts of all formed by-products are very important parameters characterising the process itself, unfortunately often neglected or

omitted. However, a reasonable and "environmental" approach to the problems of pollution control demands to take all parameters into account, products included.

The most typical products of plasma deVOC processes appear in the gas phase, namely CO_2, CO, H_2O, NO_x, other VOC, O_3, HNO_3, sometimes NH_3, HCN, etc.; Cl_2, HCl, HF, $COCl_2$ etc. if halogenated VOC were processed. Gaseous products are often very noxious gases (e.g. CO, NO_x, HCN, $COCl_2$), thus it must be really carefully considered if the process is optimal. An effective technique reducing some toxic VOC, but producing toxic by-products in higher total concentrations will not obviously be a solution for VOC emissions control. Even CO_2 which is generally considered to be an ideal gaseous product of deVOC, is a greenhouse gas strongly participating at the increased greenhouse effect and consequent climate changes on Earth. In that case however, global comparison should be done between the gain in obtaining the VOC abatement (the VOC may be a strong greenhouse gas too!) and the bad effect due to the emitted CO_2 release.

The production of by-products in other phases (liquid, solid) often accompanies the deVOC processes. Some of these products get out of the reactor in a form of aerosol, another part remains in the reactor and the gas leading system. In general, these products make anxious many people dealing with the deVOC, especially due to technical difficulties in the reactor systems that they cause (deposits on electrodes, etc.). An usual trend in plasma deVOC processes is to minimise this kind of products. However, these products are often not toxic and their formation is accompanied by lower emissions of noxious gaseous products, which is advantageous. Thus, it might be worth to try to resolve technical problems associated with solid and liquid by-products and to regulate the process in order to enhance their formation and to decrease the emissions of noxious gases at the same time. Even toxic solid products may be regarded as better than toxic gases emitted to the atmosphere, because the toxic material is separated and concentrated at one place which makes its further processing easier. However, this is a completely new approach to the plasma deVOC research.

Some other parameters can be derived from the produced concentrations of the gaseous and other phase products, e.g. CO to CO_2 ratio determining the perfection of the combustion process, total carbon balance indicating the distribution of carbon present in treated VOC to gaseous and other products and many others. Parameters of this kind that were surveyed in this work will be defined later.

2.4.2 Results obtained by plasma VOC removal techniques

Various plasma techniques having some environmental applications, in particular to the pollution control, have already been described in chapter 1.4. These techniques can be generally applied for the abatement of VOC emissions as well. Non-thermal plasmas are most frequently employed for this purpose (especially pulsed corona and dielectric barrier discharges, electron beam), although deVOC processes in transition plasma regimes (non equilibrium plasmas with relatively high temperature, described in section 1.4.6) are also interesting (e.g. prevented spark, glidarc, some microwave discharges). It is not the case of NO_x removal, where plasmas with higher temperature are used very seldom.

The following Table 2.4.1 presents a large comparison of various plasma techniques of VOC removal with corresponding results as they were reported in accessible literature sources during approximately the last 10 years. Almost all types of VOC (alifatic, olefinic, aromatic, halogenated) in a wide range of concentrations (from some ppm to more than 10 %) and a variety of plasma techniques are mentioned. Plasma deVOC techniques have been sometimes combined with other techniques in order to obtain better efficiency of the process, e.g. catalysis [Frc98, Rud00], UV irradiation [Shv98] or active carbon adsorption [Ans97].

Most authors have used ambient, dry or humid air as the carrier gas, some of them have worked in other atmospheres (N_2, Ar, Ar + O_2, combustion exhaust). Many of them report better efficiency of the process in the humid air.

Listed authors have usually worked at ambient temperature and atmospheric pressure, but some of them report different conditions, e.g. lowered pressure (necessary for some discharges, [Tep95, McC99]) or increased temperature. According to some of them, an increased temperature often improves the deVOC process. Yet, it is not evident if they included the energy spent for gas heating into the energy requirements of the process! [And99, Hsi95, Aki96, Frc98, vHe98, ChM97, Sny98, HsL98, Kud00]

Various diagnostic techniques were applied for the detection of the treated compounds and formed products. The most frequent are IR absorption spectroscopy (usually Fourier transform - FTIR), gas chromatography (GC) often combined with mass spectroscopy (MS), flame ionisation detectors (FID), NO_x and O_3 analysers, etc. Unfortunately, many authors are still not aware of an importance of the precise product analysis and they do not indicate what products they made, or they produce very hazardous species!

Most of presented experiments have been performed in laboratories. Some authors have resolved a difficult task of scaling and adapted their technique to the pilot-scale which applies to much larger gas flow rates and much greater technical difficulties. [Smu98, vHe98, Cze96, Cze98, Shv98]

Removal efficiency (removal rate) is usually given as the main parameter of the process, some authors also indicate specific energy density and energy costs. However, very few works provide all these parameters, so it is rather difficult to compare the techniques.

Plasma technique [authors]	Treated compound	Initial concentration c_0 [ppm]	Gas (ambient air if not specified)	Flow Rate Q [l/min]	Energy density R_v [J/l]	Removal Efficiency η [%]	Energy costs R_m [kWh/kg]	Products
Electron beam								
[Pen95, Pen97a,b]	CH_3OH CH_2Cl_2, TCE CCl_4				50 50	98 98		$COCl_2$, Cl_2, HCl
[Pau93] (pilot scale)	butyl acetate ketones toluene,xylene benzene, mesithylene	~ 400		> 1000 Nm^3/h		60 – 90 (alif.) 60 – 80 (arom.) 20 – 40 (benzene)	total 40, related to C 25 – 100 71 – 111 55 – 167	aerosols (52%) CO_2 (20-10%) CO (10%) VOC (24%)
[Sch93]	TCE					99		$COCl_2$ dichloroacetyl chlorid
[Ans97] (+ adsorption on active C)	chlorinated VOC	50-1000		(pilot scale)				
d.c. Corona Discharge								
[Mrv93]	styrene					82 – 99 (- polarity) 60 (+ polarity)		copolymers
[Bai92]	CFC-113, TCE acetone ethyl acetate cyclohexene					80		
[Mra96]	CCl_4 aromatic							CO_2, Cl_2
[Ska93]	CCl_2F_2					> 90 (-)		
[Jaw96]	mixture-petrol	3500				80 – 90		CO_2, H_2O, CO, NO_x
[Huc00]	benzene		air N_2 Ar	20 20 12		64 (+), 77 (-) 18 (+), 5 (-) 100 (+), 87 (-)	44 (+); 19.5 (-) 12.4 (+); 1.3 (-) 52 (+); 4.7 (-)	condensate of amino acids
Pulsed Corona Discharge								
[Fil98]	Ethylene			5 – 10	56	64 – 74		HCOH, CH_4
[Hsi95]	methanol TCE	400 160	dry air 120°C dry air 120°C dry air 300°C		180 60 140	50; max. 95 50 80; max 90		CO, CO_2 (methanol) $COCl_2$, HCl, CO_x dichloroacetyl chlorid

Plasma technique [authors]	Treated compound	Initial concentration c_0 [ppm]	Gas (ambient air if not specified)	Flow Rate Q [l/min]	Energy density R_v [J/l]	Removal Efficiency η [%]	Energy costs R_m [kWh/kg]	Products
[Pen95]	CCl_4	100			50	25		CO_2, CO, Cl_2
[Yam93]	toluene CH_3Cl CFC-113		air, N_2			100 95 67		solid product
[Don98]	chlorinated hydrocarbons	100 – 500	dry & humid air					CO_2, Cl_2, $COCl_2$
[vHe98] (pilot scale)	biogas-toluene, styrene, …	125 – 450 (tol) 30 – 190 (sty) 80-1000 (others)	dry air 850°C	1667	147	90	40	CO, particles tars
[Frc98] (+ catalysis)	butyl acetate, …	< 100	air 30 – 400°C		36 – 54	99		CO_2, H_2O, organic acids aldehydes
[Smu98] (pilot scale)	styrene, toluene,… propane, butane TCE	50 – 2000	ambient air	500				
[Kor98]	toluene CH_3Cl CCl_2F_2	~330	dry & humid air (various RH)	45	120-175 810 840	90 60 30	~29.3 ~1020 eV/molec ~2000 eV/molec	CO_2, O_3, particles, ?
[Shv98] (+ UV irradiation)	TCE PCE	20-200	air, CO_2	1-12		80 (95 with UV) 65 (90 with UV)		solid product, ?
Dielectric barrier discharge (silent discharge)								
[ChM97]	toluene MEK	50 – 400	dry & humid air (25-100°C)	3 – 4		65 – 75 45 – 80	196 625	CO_2, CO, NOx HCHO, C, H_2, solid product
[Kra96]	toluene	100	dry air	5.3		98	77	CO_2, CO, particles
[Par99, Odi98] [Odi99]	toluene isopropanol	1000 – 2400	dry air	2.5 – 5		80 – 91 99	46 – 106 169	CO_2, CO, NO_2, NO particles, acetone
[And99]	styrene	5370 1000	Ar / O_2 (8 %) (90°C) (300°C)	1 – 20	750 – 2060 0 – 900		31 – 44	solid product (polystyrene or poly acrylic acid) CO_2, CO, H_2O, other VOC

Plasma technique [authors]	Treated compound	Initial concentration c_0 [ppm]	Gas (ambient air if not specified)	Flow Rate Q [l/min]	Energy density R_v [J/l]	Removal Efficiency η [%]	Energy costs R_m [kWh/kg]	Products
[Fal99]	toluene TCE	100	air with 0 – 20% O_2 Ar, N_2		 15			
[Nee93]	HCOH, HCN benzene							
[New94]	TCE	1800-18000	humid air	0.1-1	210-2100	99.9		CO_2, Cl_2, HOCl condensate
[Krw98]	CCl_4	11%	Ar, Ar + O_2, O_2	0.08-0.12				
[Gau98]	TCE	450	dry air humid air	< 0.15		97	4.1 – 32.6 4.1 – 8.2	CO_2, CO, HCl, $COCl_2$
[Bug96]	CH_4	54%	CH_4 (natural gas) +O_2 (0°C)	1.67	480	57	15-20 (condensate) 30 (HCOOH)	condensate of H_2O (53%) HCOOH (27%) CH_3OH, CH_3COOH, $HCOOCH_3$, C_2H_5OH...
[Hsi95]	TCE CH_3OH	160 400	dry air (120°C,300°C) dry air 120°C 300°C 300°C		10-60 230 60 150	50 50 50 80		
[Rud00] (DBD + catalysts)	ethyl acetate	10-100	dry & humid air		72			
[ChM95]	HCOH	100	dry & humid synt. air		600	97		
[Sny98]	chlorobenzene	250-1000	air, Ar + O_2 160°C various O_2 contents		1500-2000 500-1000 300	90-99 (air) >99 (Ar + O_2) 99 (Ar + 2.7% O_2)		CO, CO_2 (CO/CO_2 = 1-3)
Surface Discharge & Ferroelectric packed bed								
[Msd93] (surface)	CFC-113	100-1000						
[Yam92] (packed bed)	toluene	229	dry air	0.8		95	44	CO, CO_2, O_3, NO_x, particles
[Yam93] (packed bed)	toluene CH_3Cl CFC-113					up to 100		

Plasma technique [authors]	Treated compound	Initial concentration c_0 [ppm]	Gas (ambient air if not specified)	Flow Rate Q [l/min]	Energy density R_v [J/l]	Removal Efficiency η [%]	Energy costs R_m [kWh/kg]	Products
[Ura97] (packed bed)	toluene	2000	dry air	1		75	39	CO_2, particles
[Ler95] (DBD + packed bed)	TCE	300 – 1100	air, N_2		200	90-95		
[Oga99] (packed bed)	benzene	< 50 – 200	synthetic air	0.2	3000	100		O_3, NO_x, CO_2, CO
[Fut98] (packed bed)	benzene toluene cyclohexene		dry & humid air, N_2	0.5-3	20000 5000 18000 5000	75 65 90 80		CO_2, CO in N_2: cyclohexanone cyclohexene oxide cyclopentyl aldehyde
Microwave and Radio-frequency (RF) discharge								
[HsL98]	CH_3Cl	3, 5, 10%	O_2, Ar (also heated to 440°C)	0.1	60000	99.99		CH_4, $COCl_2$, soot
[Gri98]	freons (CCl_4, CCl_3F, CCl_2F_2, $CClF_3$, CF_4							
[Jas00] (microwave torch)	$C_2H_2F_4$ CCl_2F_2	2 – 8 %	synthetic air	1 – 2	2520-6120	90-100 78-91	4	COF_2, CO, CO_2, NO_x COF_2, CO, CO_2, $COCl_2$, Cl_2, NOx
[Kud00]	Pentane hexane heptane octane cyclohexane		O_2 (120, 20°C)	0.06	10656		284 93 74 63 45	alcohols, ketones, H_2O, other, H_2O_2
[Tep95] (RF, 500 W)	toluene n-heptane		He + O_2 (25-70 kPa)	0.15 – 0.4		99.9		CO_2, H_2O, carbon black
DC glow discharge								
[Aki96]	toluene	10 – 15	dry & humid air (66°C)	25		90		
[ChJ93b]	CH_4		Ar			90		
[McC99] (low pressure)	CH_2Cl_2 benzene	300 – 400	He, Ne, Ar (2-22 Torr)	1	300 250 – 300 50	80 – 100 (Ar) 60 – 70 60 (pulsed discharge)		

Plasma technique [authors]	Treated compound	Initial concentration c_0 [ppm]	Gas (ambient air if not specified)	Flow Rate Q [l/min]	Energy density R_v [J/l]	Removal Efficiency η [%]	Energy costs R_m [kWh/kg]	Products
Gliding Arc								
[Cze98] (pilot scale)	H_2S CH_3SH	10 – 10000			50-200	4 – 39 7 – 69	9 - 3300 130 - 840	SO_2, CO_2, CO
[Les94]	CH_4				3000			CO_2, CO, H_2O
[Cze94]	$CHCl_3$	1 – 20 %				94	5 – 30	HCl, CO_2, CO, CCl_4, C_2Cl_4
[Cze96] (laboratory and pilot scale)	xylene (pilot) heptane toluene MEK TCE, …	200 2200 1800 2000 500	ambient air?	2000 30 33.3 53.3 31.7		75 100 92 66 100	80 (all related to C) 60 60 100 900	CO_2, CO, ?
[Opa00]	hexane toluene ethyl acetate	200 – 600	dry & humid air	58 – 66	< 1620	51 46 60		
Other plasmas								
[ChJ97] (corona torch)	CCl_4	445-8720		0.5-5			11-111 0.25-10	CO_2, H_2O, Cl_2, HCl
[Koh98] (capillary discharge)	toluene TCE, EGM	50-2300	dry air	<<1-6		< 85 40	200-500	CO_2, CO, H_2O, NO_2, HNO_3, aerosol
[Huc00] (atmospheric pressure glow discharge with dielectrics)	benzene		He, He + H_2, He + C_2H_2	0.15				CH_4

Table 2.4.1 Overall view of the results of deVOC processes in various plasma techniques. Blank cells mean that the data were not available. TCE = C_2HCl_3, PCE = C_2Cl_4, CFC-113 = $C_2Cl_3F_3$, MEK = methyl-ethyl ketone, EGM = ethylene glycol mono-ethyl ether

2.5 CHEMICAL ASPECTS OF THE PLASMA INDUCED VOC DESTRUCTION PROCESS

Detailed understanding of the plasmochemical processes associated with the decomposition of every treated compound in every type of plasma is practically impossible. Firstly, exact time and space characteristics of the electric field and other physical features of the environment such as temperature, density of neutral and charged species, etc. is not clearly known for each discharge type. Secondly, there exists a great variety of possible chemical reactions among the components of the treated gas (usually a small concentration of some VOC or a mixture of several VOC in ambient air, often humidified) and produced reaction intermediates. Moreover, preferred reaction channels depend strongly on the above mentioned physical properties of the working environment. And finally, heterogeneous reaction on the electrode surfaces and reactor walls influence the overall plasmochemical mechanisms.

Despite these problems, even a partial understanding of the VOC decomposition processes and all involved mechanisms gives a rough but useful approach.

2.5.1 Bonds and their energy

Each organic compound contains some characteristic structural groups composed of atoms bound together. Binding energies of the most frequent bonds between atoms and functional groups in organic compounds are given in Table 2.5.1.

Theoretically, the energy at least of the value of the binding energy of the specific bond is necessary to break it ($E \geq W_b$). However, T.Yamamoto has found out that each VOC molecule has its characteristic vibrations corresponding to some frequencies f_0. If the plasma is able to vibrate the molecule with the frequency $f \approx f_0$, the resonance occurs and the molecule (its specific bond) may break, although the energy delivered from plasma is below the binding energy of the bond ($E < W_b$), it is theoretically insufficient to break the bond. [Yam97]

This is an important fact worth of consideration in plasma induced deVOC processes. If we want to make the deVOC process more efficient, it is sometimes sufficient to increase the residence time of the treated VOC in the reactor volume in order to enhance the interaction of active substance formed by plasma with treated VOC, rather than increasing

just the input energy. Moreover, such conditions change all involved plasmochemical mechanisms, the forming intermediates have greater chance to interact, which often leads to different final products.

Bond	Binding energy W_b [eV]	Bond	Binding energy W_b [eV]
C–H	3.5 – 4.5	**C–O**	11.2
C–C	3.6 – 6.3	**O=C=O**	5.5
C–C (benzene)	5.4	**H_2C=O**	3.8 – 7.7
C_6H_5–CH_3	4.3	**H–O**	4.4 – 5.11
C_6H_5–H	4.8	**C–Cl**	3.5-4
CH_2=CH_2	7.45	**C–F**	5.7
C≡C	10		

Table 2.5.1 Binding energies of some bonds present in VOC **[ChM95, Mra96, Yam97, Fut97, HCP]**

2.5.2 Primary reactions of VOC decomposition

In chapter 1.3 we dealt with the physico-chemical processes in non-thermal atmospheric pressure air plasmas. Such plasma conditions are used in the most of plasma induced deVOC techniques.

Let us remind briefly the primary and the secondary processes running in such plasmas. First, energetic electrons induce the formation of active ions, radicals and excited species by the mechanisms of ionisation, dissociation, and electron attachment. In the second stage, these active species react together and with all other gas components forming further intermediates leading to final products.

VOC usually enter to the plasmochemical reactions in the second stage described above, when all active species formed, due to the electron induced primary processes, start to act. Direct electron impact on VOC molecules occurs rarely, because VOC are usually present in low concentrations, from about 10 ppm to 1%. Therefore, dominant electron collisions occur with O_2 a N_2 molecules as described in chapter 1.3.

VOC molecules are with much greater probability attacked by highly reactive radicals, ions and excited species. Certain bonds in their molecules are consequently broken and new

VOC radicals and fragments are formed. This is the primary process of VOC decomposition, in fact corresponding to the second stage of processes occurring in plasma.

The most important primary mechanisms of VOC decomposition will be noticed in the following sections. Rate coefficients k of the reactions are given for T = 298 K.

2.5.2.1 Oxidation by O• radicals

O• radicals (atomic oxygen) are formed by the dissociation of O_2, mainly by electron impact or dissociative electron attachment, see Table 1.3.1. Both basic O(^{3}P) and excited O(^{1}D) states of O• are formed. [Low95]

O(^{1}D) is more reactive, e.g. oxidation of HCHO by this state releases more energy than by O(^{1}D)

$O(^1D) + HCHO \rightarrow HCOOH$ $\quad \Delta H$=-408.2 kJ/mol

$O(^3P) + HCHO \rightarrow HCOOH$ $\quad \Delta H$=-125 kJ/mol [Nee89]

Oxidation by O• radicals is, according to many authors, the most important channel of the decomposition of many VOC, for example toluene [ChM97], HCHO [ChM95], CH_4 [Bug96], C_2H_4 [Fil98], CCl_4 [Pen95], TCE [Ler95], combustion exhaust [Glb95], other VOC [Par98].

2.5.2.2 Oxidation by OH• radicals

Hydroxyl radical OH• is considered to be the most reactive radical. It is formed e.g. by a reaction of O_2 and H• radical (scattered from a VOC):

$H + O_2 \rightarrow OH + O$ $\quad k = 1.6\times10^{-10}$

However its formation by an electron or O(^{1}D) impact of H_2O (present in humid or ambient air) is more important, see section 1.3.2.4. [Low95, Kon97]

Reactions with OH• are dominant channels of the destruction of almost all VOC, they usually have high rate coefficients ($k \sim 10^{-11}$-10^{-12}). It is the reason why many people working with plasma deVOC techniques support its formation by adding H_2O (vapour or droplets) into the reaction volume. [ChM97, ChM95, New94, Mra96, Kal96, Par98,

Don98, Gau98, Pen97a, Emd92, etc.] On the other hand, according to some others it is not convenient to add water at low VOC concentration (<10 ppm), because it supports electron attachment and lowers the process effectivity. [Pen97b]

2.5.2.3 Oxidation by $HO_2^\bullet$ radicals

Hydro-peroxyl radical belongs among the most reactive. It may be formed by a variety of channels, usually in the reactions with involved $OH^\bullet$ radical. $HO_2^\bullet$ together with $OH^\bullet$ play an important role in the tropospheric chemistry (formation of the tropospherical smog, remind chapter 2.1.2). In the deVOC processes, it takes part e.g. in the reaction with HCHO.

$$CHO + HO_2^\bullet \rightarrow OH^\bullet + H^\bullet + CO_2 \qquad k = 1.5\times10^{-11} \qquad \text{[ChM95, Glb95]}$$

2.5.2.4 Oxidation by molecular oxygen - O_2 and O_2^+ ion

Non-dissociated O_2 (ground or excited state) is an important oxidant of combustion exhaust, toluene, CCl_4, etc.

$$CCl_3 + O_2 + M \rightarrow CCl_3O_2 + M \qquad k = 1.4\times10^{-9} \times T^{-1.1} \qquad \text{[Pen95, Emd92, Glb95]}$$

Molecular ion O_2^+ formed by an electron impact of O_2 enters to some deVOC reactions and assists at OH radical formation. [Low95]

2.5.2.5 Oxidation by ozone O_3

Ozone O_3 is formed by a direct or three body reaction of O and O_2. It has strong oxidising effects used especially for sterilisation. O_3 is capable to destruct unsaturated hydrocarbon bonds, it is thus helpful in the decomposition of aromatic compounds or C_2H_4.

$$O + O_2 \rightarrow O_3 \qquad k = 1\times10^{-14};\ 8.5\times10^{-15}$$

$$O + O_2 + M \rightarrow O_3 + M \qquad k = 6.2\times10^{-34} - 1.5\times10^{-33} \text{ (depends on M type)} \qquad \text{[Low95, Mar98]}$$

$$O_3 + C_2H_4 \rightarrow \text{products} \qquad k = 1.2\times10^{-14}\times\exp(-2630/T) \qquad \text{[Fil98]}$$

2.5.2.6 Reaction with $N^{\bullet}$ radicals

Atomic nitrogen radical is formed particularly by an electron impact of N_2 (tab Table 1.3.1) It is important especially in the tertiary processes under lack of oxygen, but primary reactions of $N^{\bullet}$ with some VOC (CCl_4, CH_2Cl_2) have high rate constants and may prevail over oxidations induced by O-containing radicals.

$N^{\bullet} + CH_2Cl_2 \rightarrow$ products $\qquad k=1.5\times10^{-12}$ [Pen95, Pen97b]

In N_2 atmosphere these radicals are the most important participating at primary VOC decomposition. [Ler95]

2.5.2.7 Reaction with molecular nitrogen - N_2^* and N_2^+ ions

Molecular nitrogen ions are formed mainly by electron impact of N_2 (Table 1.3.1). They take part in the decomposition mechanisms of some VOC.

$N_2^+ + CH_3OH \rightarrow CH_3^+ + OH + N_2 \qquad k = 10^{-7}$
[Pen97b]

Various excited states of N_2 generated by an electron impact (Table 1.3.1) and radiative transitions from one state to another are very numerous in air plasmas. For instance, the radiation emitted from $C^3\Pi_u - B^3\Pi_g$ transition is responsible for a typical violet colour of discharges in air and enables to explore such discharges by means of emission spectroscopy which was widely used in this work.

Long living metastable $A^3\Sigma_u^+$ state is found to have the greatest population among all other active species in air streamer-induced discharges [Fil00]. Its role in the VOC decomposition process is not very explored, but M.Morvová, F.Hanic et al. invoke its great importance in the plasmochemical processes of the CO_2 and CO depletion and suspect it to influence also deVOC and deNO_x processes. [Mrv98a, Mrv99a, Mrv00, Han00] This aspect will be of our special interest later.

2.5.2.8 Direct electron attack

As we already mentioned, the probability of the direct electron attack of treated VOC is low since VOC are usually present in a low concentration, much lower in comparison with O_2 and N_2. Therefore, this mechanism is important only if the rate coefficient of such a reaction is several orders of magnitude higher than that of the electron impact of O_2 and N_2.

An example of such situation is a direct electron attack of HCHO or CCl_4 which dominates even over the reaction with OH radicals.

$$e^- + CCl_4 \rightarrow Cl^- + CCl_3 \qquad k = 4\times10^{-7} \qquad \text{[ChM95, Pen97b]}$$

2.5.3 Secondary reactions of VOC decomposition

Primary reactions of VOC decomposition (mostly oxidations) lead to the formation of further radicals and active intermediates. These species react with each other, as well as with primary active species created by plasma.

Many parameters determine the reaction channels between these intermediates, e.g. the residence time in the reactor volume, dissipated energy, gas temperature etc. At higher temperatures, the hydrocarbon residues are broken to small fragments C_1 (CH_x) and C_2 (CH_xCH_y), at lower temperatures these residues tend to agglomerate to large complexes (clusters).

Electric field also influences the reactions, we have already mentioned its influences to the rate coefficients (chapter 1.3.2). It affects especially reactions of the polar compounds, since they are polarised in the field, some reaction channels than prevail, other are suppressed. Such phenomena do not occur in classical chemistry. An example of the importance of stereochemistry is the reaction of HCOH with O radical. Reaction type and products depend on that from which side of HCOH molecule $O^\bullet$ approaches. [Nee89]

The possible reactions of NO_x, ozone and other products formed in non-thermal air plasmas (remind chapter 1.3.3.2) with VOC residues have to be taken into account.

There exist a great variety of VOC fragments and radicals entering to the plasmochemical processes. We will note just some important reactions of radicals $H^\bullet$, $CH_x^\bullet$, $HCO^\bullet$, $NCO^\bullet$.

2.5.3.1 Reactions with $H^{\bullet}$ radicals

Hydrogen radical is either released when VOC is broken or is formed by the dissociation of water. It is strongly reactive, its importance at VOC decomposition is described in several works. [Bug96, Emd92]. As an example we present its reaction with toluene.

$C_6H_5CH_3 + H \rightarrow C_6H_5CH_2 + H_2$ $\quad k=1.2\times10^{14}\times\exp(-8235/RT)$

2.5.3.2 Reactions with $CH_x^{\bullet}$ radicals

Radicals $CH_x^{\bullet}$ (x=1-3) are formed when VOC is broken as well as $H^{\bullet}$ radicals, the whole group is scattered. Naturally, they tend to bind to other radicals and hydrocarbon fragments. [Bug96, Kal96, ChJ93b]

Reactivity of other hydrocarbon radicals of types C_2 (ethyl), C_3 (propyl), C_6 (phenyl) is decreased due to their size. They break or agglomerate, according to the temperatures and the presence of other radicals.

2.5.3.3 Reactions with $NCO^{\bullet}$ radical

These radicals are important intermediates in combustion processes, in particular in the conversion of fuel nitrogen into nitrogen oxides and in the so-called "prompt" NO formation process. [Mll89]. $^{\bullet}N=C=O$ radical is formed mainly in the presence of N-containing compounds (HCN, C_2N_2, pyridine, amines) e.g. by their oxidation with O or radical reactions of $CN^{\bullet}$ with $OH^{\bullet}$ and O_2.

$HCN + O^{\bullet} \rightarrow NCO^{\bullet} + H^{\bullet}$

$CN^{\bullet} + O_2$ (or $OH^{\bullet}$) $\rightarrow NCO^{\bullet} + O^{\bullet}$ ($NCO^{\bullet} + H^{\bullet}$ respectively) [Per85]

In the discharges and combustion exhausts it is preferentially formed by the reaction of excited N^* (NO_x respectively) with CO_x. [Per85] Once formed, it strongly influences the plasmochemical mechanisms due to its very long lifetime, up to 24 h. [Cop92] It plays a role also in the removal of VOC and combustion exhaust where N incorporates, especially in the hetero-phase reactions leading to amides and amino acids. [Kur97, Mrv98a,b]

$CO_2 + N^* \rightarrow NCO + O$

2.5.4 Tertiary reactions of VOC decomposition

As primary reactions of VOC decomposition we understood those, where original VOC molecules were attacked, secondary were reactions among various intermediates. As tertiary reactions we understand those leading to final products. Since they determine the result of the whole plasmochemical process of deVOC (of course with regard to primary and secondary reactions), it is worth to know and try to control them.

The character of these reactions, hence also final products, is strongly influenced by the residence time of the treated gas in the reactor. These reactions run often slowly, at too short residence times they cannot terminate or they statistically relax outside of the reactor volume where is no electric field.

When the deVOC process is run in an oxygen rich environment and a sufficient energy delivery into the reactor volume, oxidations prevail in all stages of the process and the final products of VOC removal are CO_2 and H_2O (ideally). Such plasma induced deVOC process is similar to the classical combustion from the point of view of products, although it has run under non-thermal conditions.

When the delivered energy is not high enough or not completely oxidised VOC fragments get to colder places of the reactor (walls), condensation leading to liquid or solid products may take place. Electrodes may also influence the products, the intermediates can form dimmers, trimmers up to polymers, the electric field plays a role in these processes. The appearance of condensate or solid products was observed by many authors, see Table 2.4.1.

A specific situation occurs when the gas is characterised by the lack of oxygen (from the beginning or when it has been consumed in oxidations). In high energy plasmas (arcs, torches) the treated VOC are carbonised. Various modifications of carbon (graphite, fullerenes) and soots are formed. [Huc98] In low energy discharges, atomic nitrogen can incorporate into the VOC fragments and form organic-nitrogen complex. [Ler95] Excited N_2 ($A^3\Sigma_u^+$) under some specific conditions can do so as well, such a process may lead to the formation of amino acids or their polymers. [Mrv98a,b, Mac98a, Mrv99b, Mrv00, Han00]

Finally, it is to note the radiation emitted from the discharge which can influence the mechanisms of VOC primary decomposition as well as those of final product formation. However, up to now this field stays rather unexplored.

3

GLOW DISCHARGE AT HIGH (ATMOSPHERIC) PRESSURE

3.1 INTRODUCTION

The glow discharge induced between two metal electrodes is a well known discharge state, fairly well understood at low pressures. However, it is not very known at pressures close to the atmospheric since the discharge dimensions become very small (in the micrometer range). In this chapter we have studied a specific discharge regime, identified as a pulseless continuous glow discharge at atmospheric pressure, occurring in a non-homogeneous electric field gap, namely a point-to-plane geometry. This regime is obtained using a specific external electric circuit and will be referred as High Pressure Glow Discharge (HPGD) in the following. The HPGD may be established both polarities with a d.c. high voltage applied on the point. Positive and negative HPGD have many similarities, but there are also some differences, because the electrodes have different shapes and are made of different materials. Some preliminary studies of the HPGD have already been presented in [Mac98b].

To avoid any terminology confusion we must underscore that the presented high pressure glow discharge is, as will be shown, a specific discharge regime. It should neither be identified as a corona discharge in its glow regime [Sig78, Mor97b] frequently used for flue gas cleaning and sterilisation, nor as the so called "atmospheric pressure glow discharge" which is a special modification of the dielectric barrier discharge (it uses dielectric layers) [Oka93, Mas98, Sho97, Ghe98]. The latter is usually used for polymer treatment.

A similar glow discharge between two metal electrodes has been studied in pure gases (O_2, N_2) by Nicolas et al, in a point-to-plane geometry and a pressure ranging within 50-760 Torr. While a pulseless glow regime has been observed in N_2, streamer-like pulse regime has been observed in O_2. [Nic94] Mezei et al studied a glow discharge in air and He in the same pressure range and a special discharge cell with either Cu or electrolyte cathode. [Mez98] D.c. glow discharge in air at 1-2 atmospheres in point-to-plane geometry (point cathode) was studied by Akishev et al. (employed for NO_x treatment). They measured a reduced electric field of 80-100 Td, current densities of about 10 mA.cm^{-2} and found a positive (rising) current-voltage characteristics of the discharge. [Aki93]

The high pressure glow discharge in both polarities has already been successfully applied to the flue gas cleaning: removal of some VOC, e.g. aromatic hydrocarbons (toluene, ethyl benzene, xylene) and cyclohexanone [Mac98a,c]. This application is

much more advanced here. An experimental study of the properties of this discharge helps to understand the mechanisms involved in the pollutant removal process.

3.1.1 Some remarks on the glow discharge

The glow discharge is a self-sustaining discharge usually running at low pressures between two planar metal electrodes with a d.c. high voltage applied. Two most important elementary processes occurring in the discharge are electron impact ionisations and secondary electron emission from the cathode surface, due to the cathode bombardment by secondary species produced by the electrons during their way to the anode (mostly positive ions). We observe several regions in the discharge channel which differ in the nature of the emitted light and other physical properties. Figure 3.1.1.

The discharge is maintained by the ionisation occurring close to the cathode in the regions called the Aston dark space, the cathode glow and the cathode dark space. These form the cathode layer with a large positive space charge where electronic avalanches dominate.

The absolute value of the intensity of the electric field E falls linearly from a value E_0 at the cathode to almost 0 at a distance d_c towards the anode (the end of the cathode dark space). Consequently, the potential rises along this distance d_c from 0 to a large value V_c (100-400 V or more) [Rai91, Fra56]

This value V_c is called the potential cathode fall, it depends on the gas nature and the cathode material. It has been shown that it has something to do with the minimum of the Paschen curve (breakdown potential as a function of the pd value) at pd_c. [Mou92] Figure 3.1.2, Figure 1.2.1. The intensity of the electric field on the cathode is given by:

$$E_c = \frac{2V_c}{d_c} \tag{3.1.1}$$

The next regions in the glow discharge are: the negative glow with E near 0, the Faraday dark space with slightly rising E and the positive column with a fairly constant E. The positive column is a region of charge collection and plasma maintenance. Close to the anode we observe the anode layer where E rises again.

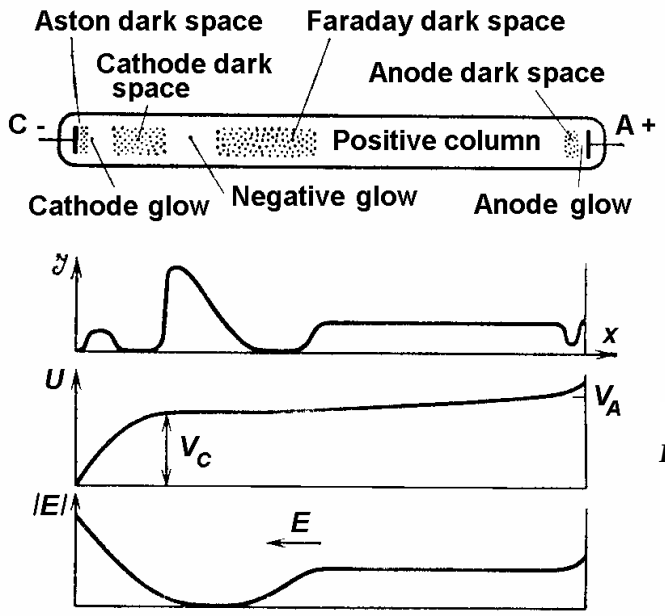

Figure 3.1.1 Scheme of the glow discharge in the glass tube with plane electrodes. Axial profiles of the light intensity I, electric potential U and the absolute value of the intensity of electric field E. **[Rai91, Fra56]**

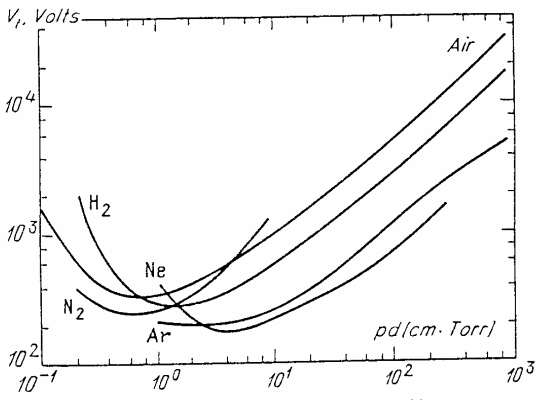

Figure 3.1.2 Paschen curves for various gases over a wide range of pd values. **[Rai91]**

If the interelectode distance is decreased the positive column first shortens, later disappears completely, then the same happens with the Faraday dark space and the negative light. The applied voltage decreases during this process. As we reach d_c, the voltage begins to rise again, we have moved from the Paschen minimum on the left side of the curve (lower *pd*). As the gas pressure rises, the cathode layer thickness d_c shortens which is evident from the Paschen law. Moreover, the discharge channel constricts. The collisions of electrons with neutral particles become more frequent. In electronegative gases, such as air, the process of electron attachment competing with the ionisation has to be taken into consideration.

The glow discharge is typically characterised by its cathode fall V_c, the cathode layer thickness pd_c and the value of the reduced current density j/p^2 (j/p^2=const), the latter for normal glow discharge only. For our purpose, let us recall that these characteristics for the glow discharge in air with a copper cathode are viewed in Table 3.1.1.

Cu cathode, air	V_c [V]	pd_c [Torr.cm]	j/p^2 [μA.Torr^{-2}.cm^{-2}]
	370	0.23	240

Table 3.1.1 Characteristics of the normal glow discharge in air with Cu cathode. **[Rai91]**

3.1.2 Discharge temperatures

The temperature of heavy species (neutrals and ions) belongs to the most important discharge parameters. One of the usual techniques of its determination is a UV-VIS emission spectroscopy, whenever the discharge emits light. Here, air has been used in most of the experiments. Thus, the major and the most radiative species in the UV-VIS region are the N_2 molecules. Consequently, the bulk gas temperature is determined by the rotational temperature of N_2.

The rotational temperature of excited N_2 molecules is determined by a technique which compare experimental spectra with simulated ones. It concerns the second positive system of N_2 (corresponding to the $C^3\Pi_u$-$B^3\Pi_g$ electronic transition) like in [Che94a]. (Figure 3.1.3, determination of these temperatures from the emission spectra are generally explained in Appendix 2) At high pressures (e.g. atmospheric) the rotational temperature T_r tends to equilibrate with the kinetic temperature of heavy species (in our case N_2), i.e. with the gas temperature ($T_r = T$).

The method of evaluating the vibrational temperature T_v is to measure the distribution of intensity of the second positive N_2 band heads, and to infer the vibrational temperature of the ground state by using the Frank-Condon factors (which govern the upper vibrational states distribution when they are produced by electron impact from the ground state) [Che94b]. Collisions with electrons are a key mechanism generating excited (upper) N_2 states (mainly $C^3\Pi_u$), hence measured T_v should have some relation with the electronic temperature T_e. However, the situation is more complicated due to the quenching mechanisms of the upper states - numerous collisions with heavy species occurring at high pressure. Actually, the measured T_v is only indicative (apparent) as we will discuss later, while the rotational temperature T_r can be more surely taken as the local gas temperature T.

If the generated plasma is in the local thermodynamic equilibrium the gas temperature should be equal to the electronic temperature, and then $T_e = T_r = T_v$. But here, in the HPGD case, the plasma seems to be in a non-equilibrium state. We obtain $T_r \neq T_v$.

Emission spectroscopy of the discharge also enables to measure the intensity of light emitted from the discharge. Changes of the light intensity emitted from various places in the discharge channel indicate different regions in the discharge and different processes occurring in them.

Analysis of the metal electrode surfaces, treated by the HPGD, gives also an additional information to the overall understanding of the HPGD.

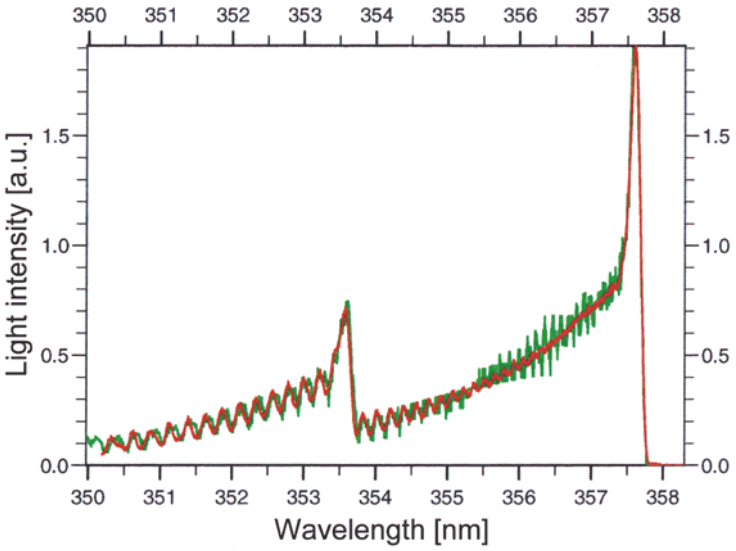

Figure 3.1.3 Experimental (red) and simulated (green) spectrum of N_2 (2^{nd} positive system) used for the determination of the rotational temperature.

3.2 THE EXPERIMENTAL STUDY OF THE HIGH PRESSURE GLOW DISCHARGE

The experimental set-up used for the study of the HPGD is presented in Figure 3.2.1. In most of the experiments the discharge operates in a closed chamber, in dry air at the atmospheric pressure. There was a constant weak air flow not affecting the discharge, in order to ensure always the same environment in the chamber. Rhodium (Rh) point and copper (Cu) plane as electrodes formed a non-homogeneous electric field with a changeable interelectrode distance *d*, usually set to 7 mm.

The point is submitted to either positive or negative high voltage, while the plane is grounded. High voltage generator DEL RHVS Series (max. 60 kV, 5 mA) with a possibility of current stabilisation was used. The external resistance *R* has a stabilising and protection function. Its value has been changed in order to minimize energy losses and, at the same time, to keep the discharge regime unchanged (values from 1270 to 80 kΩ have been used). The discharge current and voltage were detected by the 400 MHz digital oscilloscope Tektronix DSA 602 connected to a PC.

The discharge chamber is attached to an acquisition system of emission spectroscopy. The light emitted from the discharge channel is focused on the entrance slit of the Jobin Yvon monochromator, type HR 640 (200-700 nm, resolution 0.1 Angstrom) controlled by the OMA (Optical Multichannel Analyser). Parallely, the emitted light is acquired through the photomultiplier Hamamatsu C 659 S whose electric signal feeds an oscilloscope. The filamentary discharge is focalised perpendicularly to the entrance slit of the monochromator. Since the system permits to move the whole discharge chamber, it allows to acquire the emission spectra from a small part of the discharge channel, whose size is determined by the width of the entrance slit (usually 100 μm). It was applied for the determination of temperature and light intensity profiles.

Several additional measurements of the discharge properties in different environments have been done aimed towards a better understanding of the VOC (Volatile Organic Compounds) removal process by discharge mechanisms. We have used the same experimental set-up as in the case of air. Explored environments are: humid air (100% relative humidity), dry air + VOC (2000 ppm of cyclohexanone or toluene), humid air + VOC, pure N_2, N_2 + VOC, N_2 + H_2O (100% humidified N_2), N_2+H_2O+VOC and pure O_2.

Another discharge tube has been used additionally consisting of a glass tube with the discharge operating in the radial direction. (Figure 3.2.2) This tube was adapted to study the influence of the gas flow on the discharge behaviour, but it was not used for the emission spectroscopy.

To derive rotational temperatures, the 0-1 and 1-2 vibrational transitions of the second positive system of N_2 have been used. It allows to obtain T_r with an accuracy of about 20 K. Several bands of the same system have been taken to determine vibrational temperatures in the discharge with accuracy 100 K (explained in Appendix 2).

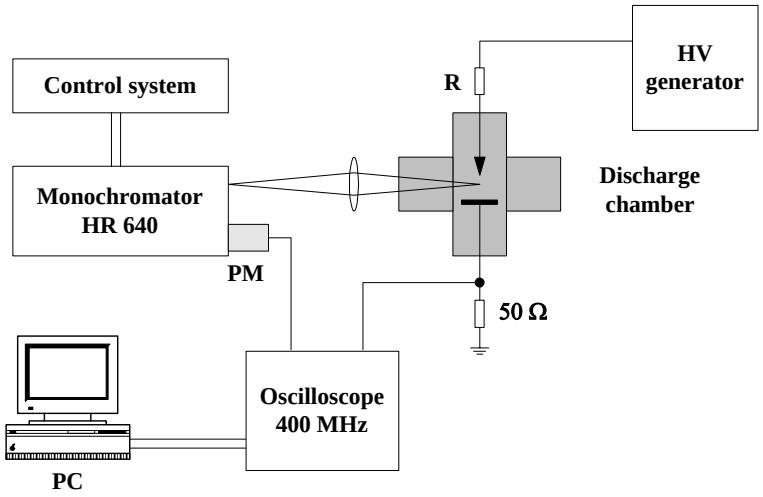

Figure 3.2.1 Experimental set-up used for the emission spectroscopy

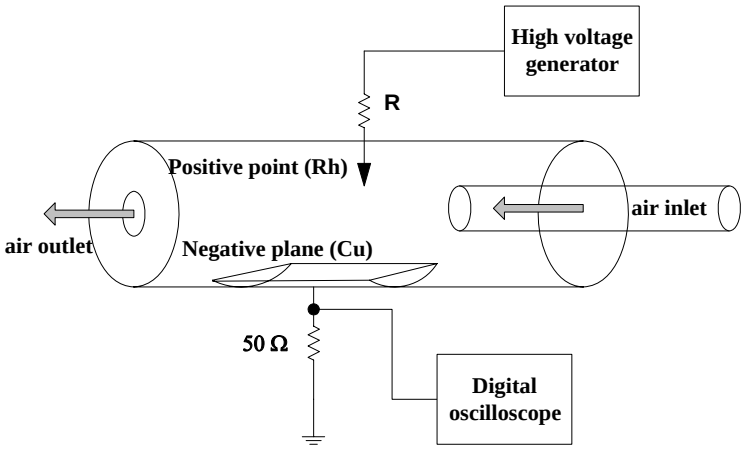

Figure 3.2.2 Discharge tube used for the study of the gas flow influence

Changes of the surfaces of the plane, as well as the point electrodes are studied using optical microscope Reichert Austria Me F2 (maximum magnification 1000) and scanning electron microscope Jeol JSM-840 equipped with the Kevex superdry X-ray detector for microanalysis of elements. Additionally, for the analysis of treated electrodes we use the infrared absorption spectroscopy, the dispersive spectrometer SPECORD M 80 working in the middle and far infrared region (4000-200 cm^{-1}) equipped with the reflection device.

3.3 RESULTS AND OBSERVATIONS

3.3.1 The way leading to the HPGD establishment

When a dc voltage applied to a non-uniform gap (positive point to plane gap in this case) is increased above a given threshold, a discharge regime consisting of repetitive individual streamer discharges establishes. The voltage is actually applied through a ballast resistor which limits the current delivered by the generator to a maximum value I_g. The discharge current then consist of a succession of streamer pulses with maximum current I_d, largely above this limitation. The maximum current I_d can thus only be supplied by the stray capacitance of the gap. Since the needed streamer energy is quite small, this stray capacity, delivers easily this amount of streamer current limited in time, without supporting a large potential fall.

However, when the voltage is increased, one of those streamer discharges establishes a more conductive discharge channel, and a spark establishes. The discharge current becomes then much more stronger, discharging dramatically the stray capacity. If the I_g is small enough the discharge extinguishes and the stray capacity recharges slowly through the ballast resistor. If, however, I_g is large enough (when the ballast resistance R is relatively low, 100-1000 kΩ), the discharge, in spite of extinguishing, enters a state of permanent conduction, controlled by the value of I_g. This state is precisely what we call the high pressure glow discharge HPGD. It is initiated by a streamer discharge, but is not a spark, being sustained by the current I_g largely lower than a spark current. This point is confirmed by the spectroscopic analysis presented in the following pages.

The HPGD properties correspond to the well known glow discharge as will be shown later. This type of discharge state has been discovered studying the prevented spark regime [Mar93, Mar98].

3.3.2 Electrical properties of the HPGD

As already mentioned above, the discharge is pulseless, its voltage U_d ranges from 1.6 to 3 kV (for interelectrode distance d = 7mm and maximum I = 5 mA). Fluctuations in the current and voltage waveforms are caused by noise. (Figure 3.3.1) The discharge current I is in the range 1-10 mA, below 1 mA this type of the discharge has not been observed. The

current as a function of the voltage (VA characteristics) is negative (decreasing). (Figure 3.3.2) Negative HPGD (with negative high voltage applied on the point) has the same current and voltage waveforms and VA characteristics.

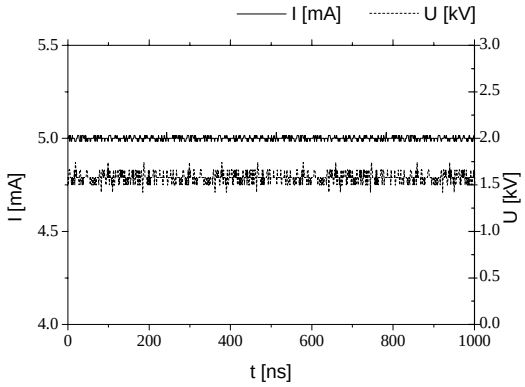

Figure 3.3.1 Current and voltage waveforms for the positive HPGD, d = 7 mm; U_d = 1.6 kV, I = 5 mA, R = 500 kΩ

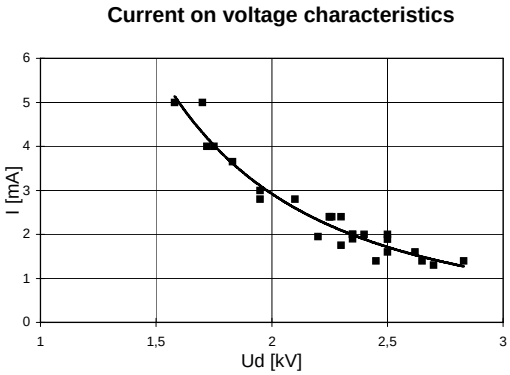

Figure 3.3.2 VA characteristics of the positive HPGD, d = 7 mm

The value of the external resistance *R* is important for the existence of HPGD. It also influences the behaviour of the discharge, the greater is *R* the more stable is the discharge and lower current can be obtained. On the other hand, the greater is *R*, the greater are energy losses.

3.3.2.1 Power measurement

Measurement of the discharge power P_d, respectively total power *P* spent by the whole circuit, is necessary to evaluate the energy costs of the discharge applied for some gas treatment. This evaluation is very simple in the case of the HPGD because the discharge is pulseless with continuous current *I* and voltage U_d. We can simply take

$$P_d = U_d I \tag{3.3.1}$$

$$P = U_g I \tag{3.3.2}$$

where U_g is the generator voltage.

3.3.3 Visual observations of the discharge behaviour

The first visual impression of HPGD in air is a luminous constricted channel of not varying violet colour, in the negative polarity of violet-rose colour. Its spatial movements depend mainly on the point polarity, the plane surface state and the gas flow rate. At lower currents (1-3 mA) we observed a light intensity decrease (darker place) close to the cathode.

In the positive point polarity the discharge takes root at the very top of the point. The channel moves a lot on a virgin well polished plane surface, it “dances” on the surface. After several minutes of the discharge operation, the plane surface covers by a thin layer of the deposition and then the discharge finds its favourite place and stays fixed there.

In the negative point polarity the channel does not necessarily rise from the point top, it often burns from its side. No favourite place fixes the channel on the positively charged plane, even after several minute of operation. The channel slides on the plane surface, despite of the formation of the deposit.

3.3.4 Influence of the gas flow and other conditions

The gas flow through the discharge influences its stability. For a given value of the flow rate, i.e. for a specific flowing velocity $v_{stab,}$, the discharge is stabilised. At this velocity the discharge channel does almost not move and lower currents can be obtained. We have found that v_{stab} = 0.14-0.42 m/s. This result is important from the point of view of the adaptation of the discharge parameters to the flue gas cleaning. The gas flow is limited by a certain v_{max} > 1-1.4 m/s, above which the discharge is no more pulseless, its regime transfers to some other one (d.c. corona or a pulse regime similar to the prevented spark).

The d.c. glow discharge in the negative point-to-plane geometry (operated in air at atmospheric pressure) presented by Akishev et al. resists to much higher gas flowing velocity (70-200 ms^{-1}). Such velocities, on the other hand, induce a spatial diffusion of the discharge. [Aki93]

No influence of other parameters such as open or closed system, glass or metal discharge chamber, curvature radius of the point etc. has been observed.

3.3.5 Emission spectroscopy of the HPGD

3.3.5.1 Whole spectrum in the 200-700 nm region

The whole emission spectrum of HPGD has been acquired in the range allowed by the monochromator (200-700 nm). In dry air and both polarities of HPGD two principal systems of bands have been observed:

1) The 2nd positive system of N_2 in the violet region corresponding to the transition $C^3\Pi_u$-$B^3\Pi_g$ of N_2 excited states. (Figure A.2.5, Table A.2.1 in Appendix 2) This is the most significant radiative system in the whole scanned spectrum, it was used for the determination of the discharge temperatures.
2) The 1st positive system of N_2 in the orange-red region corresponding to the transition $B^3\Pi_g$ - $A^3\Sigma_u^+$ ($A^3\Sigma_u^+$ being a metastable state of N_2, see Table A.2.1 in Appendix 2) This system has a much weaker intensity compared with the 2nd positive system.

3.3.5.2 Temperature determination

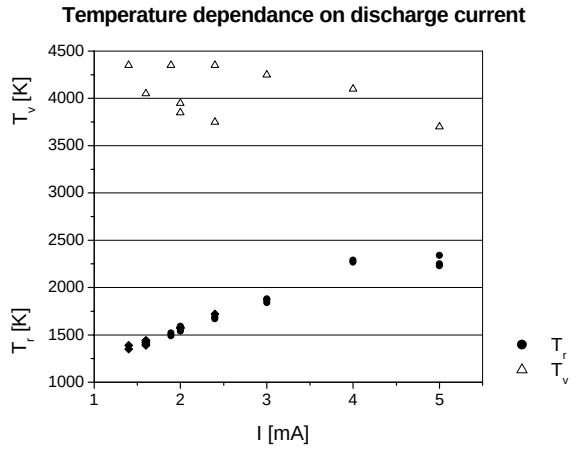

Figure 3.3.3 Temperature dependence on discharge current, positive HPGD, d=7 mm

The profiles of the rotational temperature T_r (corresponding to the gas temperature) and apparent vibrational temperature T_v along the axis of the discharge channel at I = 2 mA for both polarities are shown in Figure 3.3.4. T_r ranges from 1400 to 1800 K in the positive polarity and from 900 to 2000 K in the negative polarity.

The temperature dependence on the discharge current for the positive polarity is presented in Figure 3.3.3. T_r measured always at the same place in the channel (exact x) rises almost linearly with rising I, for I = 5 mA it reaches 2200-2300 K. This dependence is very similar in the negative polarity.

The vibrational temperature T_v in $T_v(I)$ and $T_v(x)$ graphs (Figure 3.3.3 and Figure 3.3.4) is clearly much higher than T_r; T_v ranges around 3400-4000 K in the positive polarity and 4000-6500 in the negative one. T_r and T_v tend to approach with rising current I.

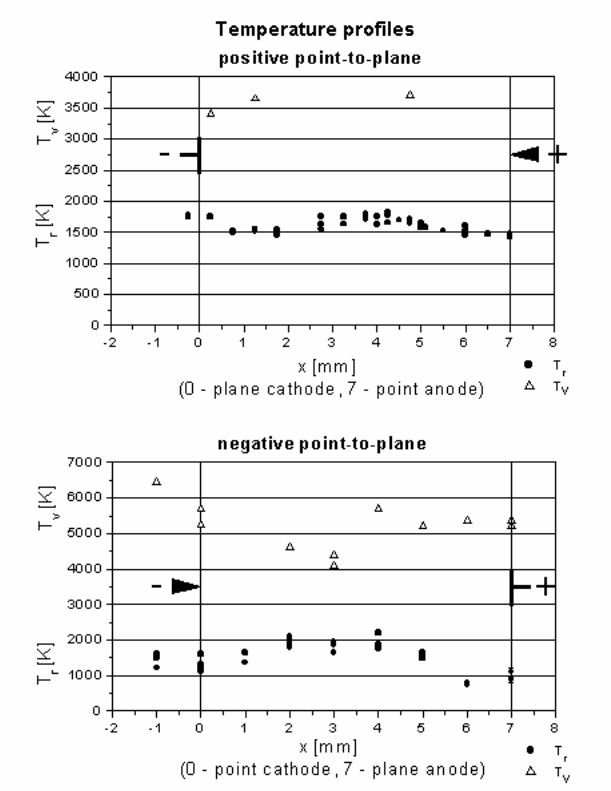

Figure 3.3.4 Rotational and vibrational temperature profiles along the discharge channel at I = 2 mA. Up - positive point-to-plane, down - negative point-to-plane

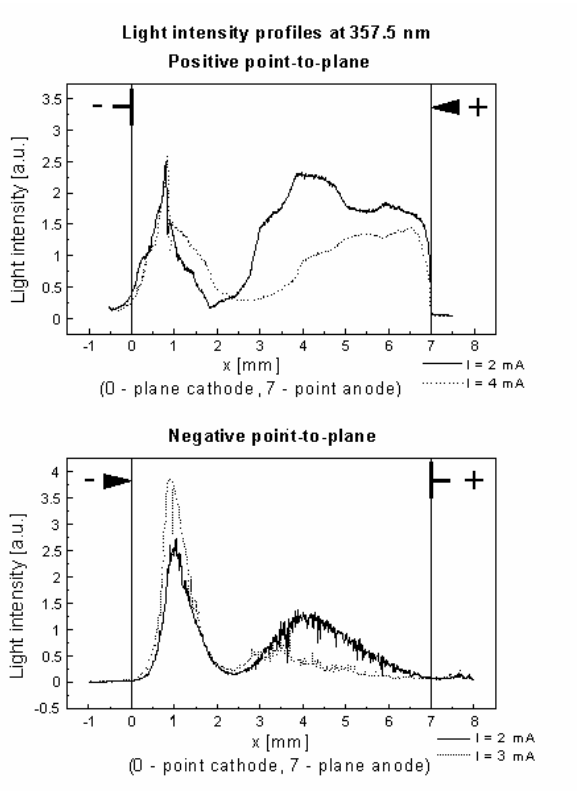

Figure 3.3.5 Light intensity profiles along the discharge channel at 357.5 nm for various currents. Up - positive point-to-plane, down - negative point-to-plane

3.3.5.3 Light intensities

The light intensity measured along the discharge channel (x-axis, x = 0 mm cathode, x = 7 mm anode) at various wavelengths (bands of N_2+ system) gives qualitatively the same profile. Profiles at 357.5 nm (peak of 0-1 transition) for both polarities are shown in Figure 3.3.5. The light intensity changes with I, but the parts close to the cathode (x = 0 mm) stay unchanged. The intensity decrease around x = 2.5 mm is visually observable like a darker place, especially at low currents. A sharp peak at x = 1 mm for all I is very remarkable. T_r profile agrees with the light intensity profile (compare Figure 3.3.4 and Figure 3.3.5)

To confirm that HPGD is a glow discharge, we have tried to change the interelectrode distance *d*. When prolonging *d*, the light intensity maximum close to the cathode at x = 1 mm and the minimum at x = 2.5 mm remain unchanged, only a luminous part from x = 3 mm prolonged to the anode. When shortening *d*, this part shortened and finally disappeared, then the dark place disappeared. At d < 1 mm, a sparking occurred, because the electric field was too strong.

3.3.6 Cathodes

In the positive HPGD the cathode was a copper plane, while in the negative HPGD it was a rhodium point. Although these two types of cathodes differ in their material and shape, which results different electric fields close to them, there are many similarities.

3.3.6.1 Cu plane cathode - positive HPGD

A thin film of the black-grey deposit has formed on the surface of the Cu plane cathode in the positive HPGD after several hours of the discharge duration. Observations under the optical and electronic microscopes have shown deep holes with relatively regular size and round shape in the rough cathode surface. (Figure 3.3.6) The diameter of the holes is approximately 250-300 μm. They deepen with an increasing time of the discharge operation, we have measured the depths up to 60 μm. Their shape is like a volcano, the central part deepens by melting of the Cu surface [*] and the borders grow with the growth of the deposit.

A crystalline structure of the deposit around and between the holes is evident from the electronic microscope photos. (Figure 3.3.7)

The X-ray element analysis of the crystalline deposit has shown a presence of Cu and O and traces of Si from the dust impurities. The analyser did not demonstrate the presence of C.

The infrared spectroscopic analysis has given the following results: The deposit consist of the mixture of CuO and Cu_2O with a possible presence of a non-stoichiometric Cu_xO_y, the central part of the plane where the discharge channel arrived contained a

[*] Local melting of Cu surface is due to the high discharge temperature (melting point of Cu is 1357 K). This process probably competes with the heat transfer through the electrode, Cu is a good heat conductor (heat conductivity λ = 400 $Wm^{-1}K^{-1}$).

majority of CuO while further parts of the deposit were composed mainly of Cu_2O. Traces of hydrocarbons and amide groups have been found in the infrared absorption spectra.

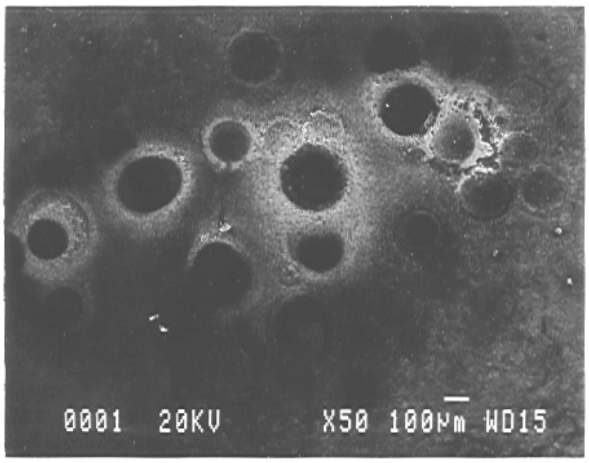

Figure 3.3.6 Electronic microscope photograph of the Cu cathode surface of the positive HPGD – round holes formed by the discharge, magnification 50

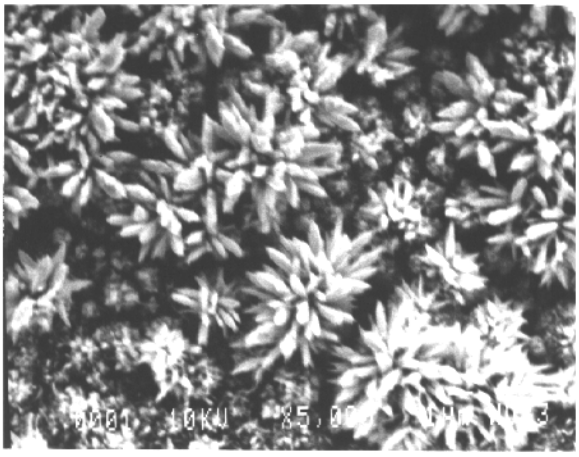

Figure 3.3.7 Electronic microscope photograph of the crystalline deposit on the Cu cathode surface of the positive HPGD, magnification 5000

3.3.6.2 Rh point cathode - negative HPGD

In the negative HPGD the shape of the Rh point cathode has been significantly changed in the discharge. (Figure 3.3.8). We observed craters in the Rh surface, although their form and size are not so regular like of holes in the planar Cu cathode, an approximate diameter of a crater in the point is of the hole size.

A very interesting observation is that the craters are not only on the top of the point, but also at its sides. This agrees with the visual observation that the negative discharge does not always rise from the point top. It shows that the discharge does not necessarily need an electric field enhanced by the point-to-plane geometry.

A cauliflower-like structure of a deposit has been observed around the craters. (Figure 3.3.9) It is probably a rhodium oxide Rh_2O_3. Rh is inert at ambient temperature and does not form oxides. There are two possible reasons why the deposit has formed on the Rh cathode surface: a high temperature and a strong electric field. An analysis of this deposit and its structure needs further investigation.

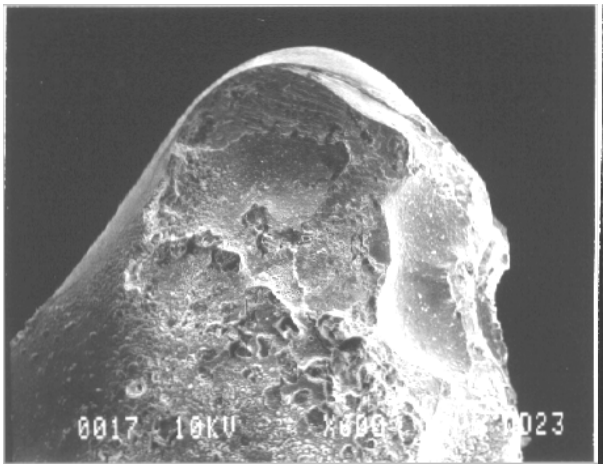

Figure 3.3.8 Electronic microscope photograph of the Rh point cathode of the negative HPGD – craters formed by the discharge, magnification 600

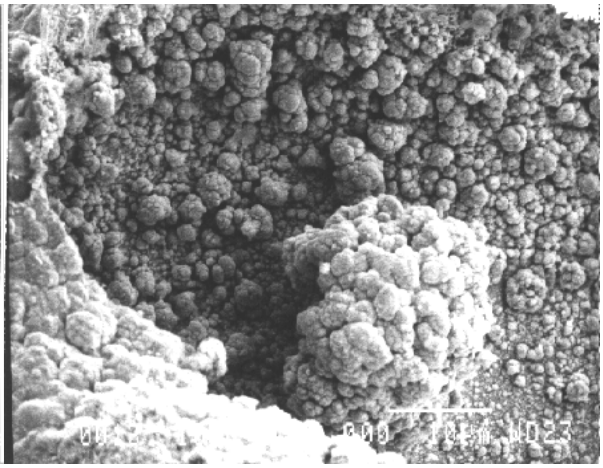

Figure 3.3.9 Electronic microscope photograph of the "cauliflower" deposit formed on the Rh point cathode of the negative HPGD, magnification 5000

3.3.7 Anodes

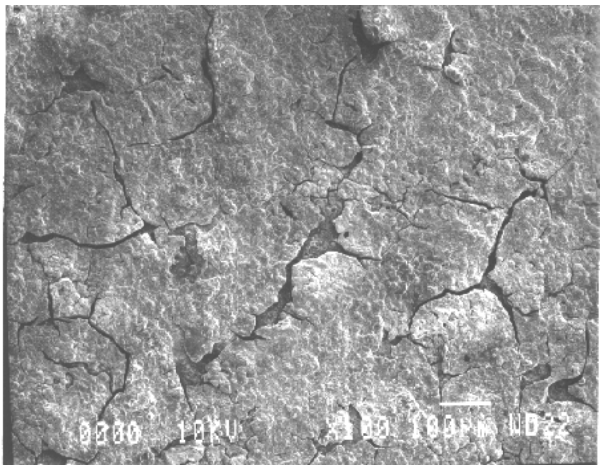

Figure 3.3.10 Electronic microscope photograph of the Cu anode surface of the negative HPGD, deposit layer forms cracks, magnification 100

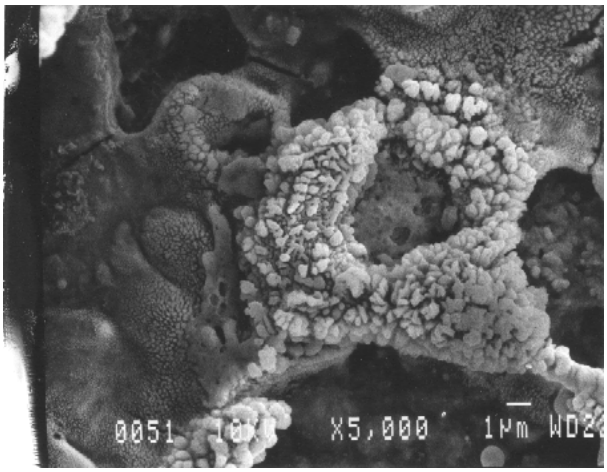

Figure 3.3.11 Electronic microscope photograph of the Cu anode surface of the negative HPGD, detail inside of the crack, magnification 5000

In the positive HPGD an anode was a Rh point. No changes have been observed on the point after the discharge operation.

In the negative HPGD an anode was a Cu plane. After the discharge operation it was covered by a rough black-grey deposit, similarly to the Cu cathode after positive HPGD, but

no special regular holes have been observed. (Figure 3.3.10) Infrared absorption analysis showed the same chemical composition of the deposit: CuO dominant in the region where the discharge arrived and Cu_2O in further parts. However, the structure is different from that of the Cu cathode, no significant crystals are visible. Various irregular micrometric craters with some origins of crystals are visible at higher magnification. (Figure 3.3.11)

3.3.8 Effects of environments

3.3.8.1 Humid air, air + VOC, humid air + VOC

When HPGD of both polarities was applied to the VOC removal, the carrier air was charged by various concentrations of VOC (toluene and cyclohexanone), most typically 2000 ppm. We studied also the effect of moisture to the VOC removal process. A question appears: do these admixtures influence the features and behaviour of the discharge itself? By other words, are the discharge properties measured for HPGD in dry air changed when HPGD is applied for VOC removal?

The answer is fortunately negative, the admixtures of H_2O in air (relative humidity close to 100%, ambient working temperature), VOC (about 2000 ppm) in air and both H_2O and VOC in air (the same concentrations) do not influence the discharge properties. The electric properties (current and voltage, VA characteristics) of both - positive and negative HPGD are the same like in air. The discharge behaves by the same manner, with the same emission spectra, strong bands of the 2^{nd} and weak bands of the 1^{st} positive system of N_2, the same light intensity profiles and approximately the same profiles of T_r.

The only difference is a little lower rotational temperature at the cathode T_c (x = 0 mm). For I = 2mA and d = 7 mm:

- in air T_c = 1700 K,
- in air+VOC and air+VOC+H_2O T_c = 1500 K,
- in air+H_2O T_c = 1200 K.

Deposits formed on the electrodes were analysed after an application of HPGD to the VOC removal process, this will be discussed later (chapter 5.3.5).

3.3.8.2 Nitrogen

We studied the HPGD in pure N_2 in order to better understand the mechanisms of its existence and to compare its features in electronegative air with some electropositive gas. There are many differences in comparison with air.

From the viewpoint of electrical parameters, the discharge in N_2 is pulseless with constant current I and voltage U_d and negative VA characteristics like in air. Nevertheless, a continuous and stable discharge exists at lower currents I (from 0.6 mA) than in air and for a given I requires a little lower voltage U_d (U_d =1.8 kV for I=2 mA). Furthermore, it is much more stable than in air.

Visually, the discharge colour was orange-yellow and not violet like in air. This is surprising, because gas discharges in N_2 usually emit violet light. In fact, there is a strong emission of the 1st positive N_2 system in orange-red which accompany the 2nd positive system emitting in violet. Both these systems were observed in air too, but the 1st positive system was much weaker than the 2nd one, while in N_2 these two systems are of comparable intensity. The orange-yellow colour is a result of the mixture of these two systems.

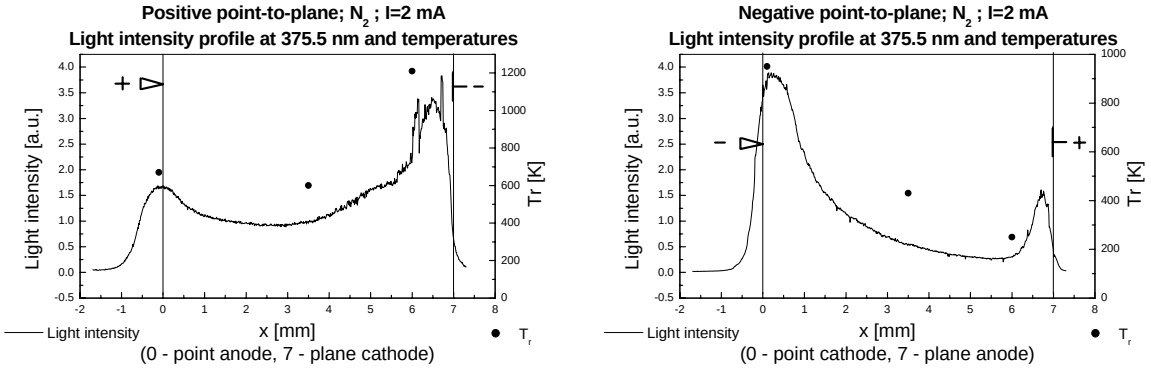

Figure 3.3.12 Light intensity profiles and rotational temperatures measured at three places in the discharge channel for positive (left) and negative (right) HPGD in N_2. I = 2 mA, d = 7 mm.

Rotational temperatures of positive and negative HPGD in N_2 (I = 2 mA and d = 7 mm) were measured at three fixed places: close to the cathode (x = 0 mm), in the middle of the channel (x = 3.5 mm) and close to the anode (x = 6 mm). (Figure 3.3.12) The discharge temperature is the highest at the cathode in both polarities (1000 – 1200 K), then drops to the anode (250 – 600 K), in negative HPGD the temperatures are lower. In comparison with air, the discharge is generally colder. Higher temperatures were obtained in the positive HPGD, while in air it was in the negative one.

The light intensity profiles of HPGD in N_2 (I=2 mA and d=7 mm) are also different from those ones in air. (Figure 3.3.12) Emission maxima close to the electrodes are observed, the stronger maximum being close to the cathode in both discharge polarities.

3.3.8.3 N_2 + VOC

When dry or humid air was charged by VOC vapours no significant changes of the HPGD features were observed. On the contrary, when VOC (2000 ppm of toluene or cyclohexanone) were added into N_2, the features of HPGD changed incredibly.

The discharge is much less stable, and it is only in the range of 3-4 mA that a pulseless regime may be obtained. For a given I it requires a higher voltage than in N_2 and even in air. Its stability is poor, especially in the negative polarity where it spontaneously oscillates between pulseless and pulsed regime.

The emitted light is of blue colour and a very strong intensity, several times stronger than in N_2. In the whole spectrum (200-700 nm), bands belonging to the 2^{nd} positive system of N_2 and CN violet system are observed (with the strongest band at 388.3 nm). There appeared many other unidentified bands below 300 nm and in 500-700 nm region, their identification requires further work. The UV bands at approximately 213, 232 and 250 nm might be assigned to the emission of toluene. [Pea50]

The discharge temperature (i.e. T_r) has been measured in the middle of the discharge channel (x = 3 mm). Its determination from the measured spectra was very difficult, because other bands overlapped with the bands of $N_2(2S^+)$ system. The only reliable results are (with uncertainty 100 K):

- positive HPGD, I = 3 mA — T = 1800 K
- negative HPGD, I = 5 mA — T = 2100 K

These temperatures are much higher than in N_2, they are approximately in the same range like in air for the same currents.

A typical feature of HPGD burning in N_2+VOC atmosphere is a fast growth of a black deposit on both electrodes. The deposit has a porous structure as it grows on the electrodes, after a gentle knocking on the discharge chamber it falls down as a fine powder. A thin black layer of probably amorphous structure stays fixed to the electrodes. The same deposit was formed in the multipoint reactor used for VOC removal in N_2 atmosphere (chapter 5.4.1).

Infrared absorption analysis showed no bands in 4000-600 cm^{-1} region. It gives rise to a hypothesis that the deposit could be a soot of pure carbon, probably of amorphous structure (symmetric C-C groups are inactive in IR). It is possible that this carbon might have properties of active carbon due to its porous structure. Certainly, it needs further investigation.

The growth speed of the deposit was about 0.5 mm/min, a rather fast rate. It caused difficulties when scanning the emission spectrum of the discharge, because the interelectrode distance decreased during a spectrum acquisition. This changed some discharge properties (one spectrum 3500-3585 Å with typical resolution 0.05 Å was scanned in 8.5 min, with lower resolution 0.1 Å in 4.25 min).

As a consequence, the light intensity profiles of HPGD in N_2+VOC mixture have not been detected due to the instability of the discharge and quickly shortening interelectrode distance.

3.3.8.4 $N_2 + H_2O$, $N_2 + H_2O + VOC$

To enlarge the HPGD analysis in various environments, we examined some discharge properties also in the humid nitrogen (100% relative humidity at ambient working temperature) and a mixture of the humid N_2 charged with VOC (2000 ppm of toluene). This mixture will be used later to study the VOC removal in such atmosphere (chapter 5.4.1).

The properties of the HPGD of both polarities are approximately the same in N_2 + H_2O and in N_2 + H_2O + VOC. In both atmospheres they are very similar to air: violet luminous channel, electrical parameters, stability and emission spectra. Evidently, this is due to the presence of water vapour, in pure N_2 and N_2 + VOC the discharge behaved differently.

3.3.8.5 Oxygen

We have already investigated the HPGD in air containing as main components N_2 and O_2, in air with some admixtures, and finally in electropositive N_2 and N_2 with admixtures. In order to complete this research, we have also examined the discharge in pure O_2 which is an electronegative component of air.

However, the HPGD as a pulseless discharge with its typical features observed in other environments could not be established in O_2. We just found a pulse regime, similar to a

streamer regime, even when a value of external resistance *R* used for the pulseless regime was changed. This result is in accordance with [Nic94] (see chapter 3.1 Introduction).

The discharge in oxygen emits a pale blue light with low intensity constant along the whole discharge gap. There are no spectral lines or systems of bands in 200-700 nm region of the emission spectrum. Due to this fact the discharge temperature could not be measured.

3.4 DISCUSSION

3.4.1 Existence of the HPGD regime

The high pressure glow discharge in air is obtained after a spark transition. During the spark phase, the temperature within the discharge channel is high. The electron attaching particles are not allowed to form inside the channel due to this increased temperature. Particle concentration *N* is decreased, which strengthens the reduced electric field *E*/*N* in the channel and the ionisation coefficient α prevails over the electron attachment coefficient η.

During the high spark current falling towards 0, the temperature decreases, the *E*/*N* and α decrease and the electron attaching particles may appear again with the increase of η. When $\alpha < \eta$ the discharge scavenges. However, there exists an equilibrium state when $\alpha = \eta$, it corresponds to some critical value of the reduced field $(E/N)_{crit}$. This is probably a state which gives rise to the formation of the HPGD regime, ensured by the condition of equilibrium between ionisation and electron attachment ($\alpha = \eta$).

The value of the critical reduced field in air is approximately:

$(E/N)_{crit} = 100 \text{ Td} = 10^{-15} \text{ V.cm}^{-2}$ [Ree65, Dut63]

Anyway, let us remind that the temperature within the stable HPGD channel is relatively high (1500-2000 K). Since the discharge is continuous, a pressure equilibrium between the discharge channel and the surrounding gas occurs. The heat accumulated in the channel spreads around by the process of thermal transfer. To keep the constant temperature in the channel, there must exist mechanisms of the transfer of electric energy to heat, generating neutral species of such high temperatures. Under atmospheric pressure conditions where the collisional frequency is high, this can be hardly explained by the collisions of

electrons and neutral heavy species. Positive ions formed in ionisation collisions have to be considered. The energy transfer occurs more probably between electrons and ions due to their Coulombian interactions and later between ions and neutral species, which are of about the same mass. The essential sink process of the charged particles at such conditions seems to be the electron-ion recombination, probably with the assistance of the third body. However, the electron attachment may have some role as well, especially in air containing electronegative O_2.

In general terms, let α comprise all electron producing mechanisms, i.e. ionisation in the HPGD case, and η all mechanisms of electron disappearing (recombination and attachment). The HPGD regime is stable when $\alpha = \eta$.

3.4.2 External resistance and the discharge stability

In the previous chapter (3.4.1) we tried to explain the existence of the HPGD from the point of view of elementary processes. Now we will try to explain the stability of the HPGD from the viewpoint of electrical circuit of the discharge, especially the external resistance *R*.

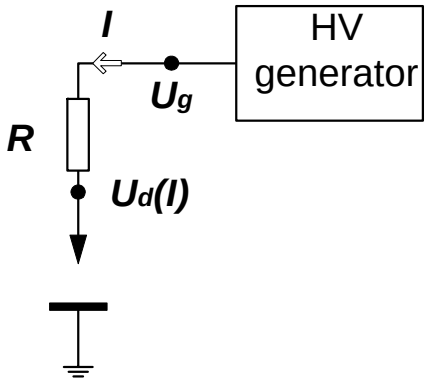

Figure 3.4.1 Model circuit of the HPGD in the point-to-plane geometry

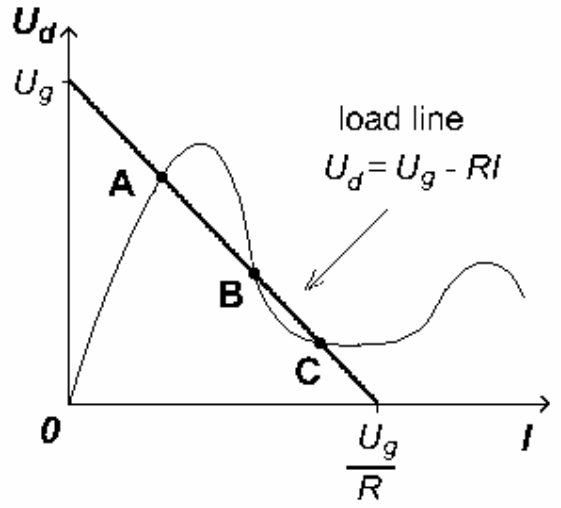

Figure 3.4.2 Some VA characteristics of discharges with a load line

Let us have a simple circuit with a point-to-plane discharge gap fed trough a resistance *R*. (Figure 3.4.1) When a current *I* passes through the discharge gap characterised by the discharge voltage $U_d(I)$, the generator voltage U_g is given by the following relation:

$$U_g = RI + U_d(I) \tag{3.4.1}$$

This is an ideal case when electric resistance only is considered, in reality there is an impedance with an inductive and a capacitive component which appears when either the current or the potential is time dependant. Let us assume that the self inductance *L*, in series with *R*, is the main reactive component. Then the relation (3.4.1) must be modified as follows - the current *I* being now a function of time.

$$U_g = RI + U_d(I) + L\frac{dI}{dt} \tag{3.4.2}$$

We can divide $I(t)$ into two components: a time constant I_0 and a little time dependent variation δi around I_0.

$$I = I_0 + \delta i$$

thus

$$\frac{dI}{dt} = \frac{dI_0}{dt} + \frac{d(\delta i)}{dt} = \frac{d(\delta i)}{dt}$$

These modifications entered to the formula for U_g (3.4.2) give:

$$U_g = R[I_0 + \delta i] + U_d(I_0 + \delta i) + L\frac{d(\delta i)}{dt}$$

$$U_g = RI_0 + R\delta i + U_d(I_0) + \frac{dU_d}{dI}\delta i + L\frac{d(\delta i)}{dt} \tag{3.4.3}$$

The difference between equation (3.4.3) and (3.4.1), the latter for the time constant case ($I = I_0$), gives:

$$0 = R\delta i + \frac{dU_d}{dI}\delta i + L\frac{d(\delta i)}{dt}$$

or

$$\frac{d(\delta i)}{dt} + \frac{R + \frac{dU_d}{dI}}{L}\delta i = 0$$

which is a differential equation with an exponential solution

$$\delta i = (\delta i)_0 \, e^{-\frac{R+\frac{dU_d}{dI}}{L}t} \tag{3.4.4}$$

The discharge is stable when the current variation $\delta i \rightarrow 0$. As a consequence of (3.4.4), this state occurs when

$$\frac{R+\frac{dU_d}{dI}}{L} > 0 \tag{3.4.5}$$

Since the self-inductance L is always positive, the condition (3.4.5) is only fulfilled when

$$R > -\frac{dU_d}{dI} \tag{3.4.6}$$

For better understanding of this condition (3.4.6) let us look at some VA- (or $U_d(I)$)-characteristics of gas discharges at high pressures (see for example [Bad65]), (Figure 3.4.2). The figure plots the gap voltage U_d as a function of I given by

$$U_d = U_g - RI \tag{3.4.7}$$

(derived from (3.4.1)). It appears as a descending straight line with the slope $-R$ and a maximum U_g for $I = 0$ which is called a load line [Rai91]. Several intersection points of this load line with a curve of general VA-characteristics, for the same R and U_g, are possible. At these points the equation (1.4.7) and the $U_d(I)$ characteristic are satisfied. But all these points do not correspond to stable discharge states since the condition (3.4.6) for the discharge stability has to be considered.

a) If the VA-characteristics is ascending (positive) or constant, i.e. $dU_d/dI \geq 0$, the condition (3.4.6) is fulfilled for every R, because $R > 0 > -dU_d/dI$. Hence, if the intersection point appears in the ascending or constant part of the curve we can say that it corresponds to a stable discharge state. An example is the point A in Figure 3.4.2. However, the point A being before the self sustained discharge, i.e. the current is maintained by some external mean, it cannot be considered as stable.

b) The situation is more complicated if the VA-characteristics is descending (negative), i.e. $dU_d/dI < 0$, the condition (3.4.6) is fulfilled when $|R| > |dU_d/dI|$ only. Hence, if the intersection point appears in the descending part of the curve we can establish such type of the discharge only if the line descends steeper than the curve. Otherwise the discharge will not be stable. Examples are the point B (unstable) and C (stable) in Figure 3.4.2.

The b) case is precisely a HPGD case since its VA-characteristics is negative. We can obtain a stable discharge by a suitable choice of R which fulfils the condition $|R| > |dU_d/dI|$. Point C in the Figure 3.4.2 represents the HPGD.

To conclude this consideration, we can say that a suitable value of the external resistance R is essential for maintaining of the HPGD.

3.4.3 HPGD in air is a glow discharge

The glow discharge is normally characterised by its cathode fall V_c, the width of the cathode fall pd_c and the normal glow discharge also by the value of the reduced current density j/p^2. Generally, the reduced electric field in gas discharges is given by E/p. All these characteristics suppose that the gas temperature is ambient. But at high pressures, the temperature of neutral species in the discharge is often elevated. To take it into consideration it is better to express these characteristics using the density (concentration) of the neutral species N instead of the pressure p. At high pressures it is common to express the reduced electric field in terms of E/N instead of E/p. Similarly, the new glow discharge characteristics will be : Nd_c and j/N^2. The pressure p, temperature T and particle concentration N are joined by the state equation:

$$p = NkT \tag{3.4.8}$$

where k is the Boltzmann constant.

3.4.3.1 The light intensity profiles

The experimental light intensity profiles of the positive and negative HPGD in air (Figure 3.3.5) are very similar to the profile of a classical glow discharge (Figure 3.1.1). In the experimental profile we find regions which are similar to the positive column, the Faraday dark space and the negative glow of the glow discharge. When the interelectrode distance d decreased, the suggested positive column has been shortening and finally disappeared. When

d increased, the positive column reappears and is further prolonged. The other parts near to the cathode could not have been distinguished since they are too short at atmospheric pressure.

3.4.3.2 The cathode fall

Let us derive the width of the cathode fall of the glow discharge in air with Cu cathode in terms of Nd_c. At ambient temperature:

pd_c = 0.23 Torr.cm.

At a pressure of 1 Torr d_c = 0.23 cm. At this pressure and T_0 = 273 K, the density of neutral species is:

$N_L = 3.54\times10^{16}$ cm^{-3} (Lochsmidt number), and

$$N_L d_c = 8.13\times10^{15} \text{ cm}^{-2} = Nd_c \qquad (3.4.9)$$

This is a general characteristic of the glow discharge in air with Cu cathode valid for any value of the density of neutrals *N*.

Now we can try to apply this Nd_c to the studied HPGD. For a typical current *I* = 2 mA and an interelectrode distance of 7 mm, the temperature measured close to the cathode is T_c =1700 K (for both polarities). The working pressure is atmospheric (760 Torr), the discharge is continuous, without pulses, we can suppose that the pressure equilibrium is reached everywhere so that the atmospheric pressure is also inside the discharge channel. Thus we can express the density of the neutral species in the discharge channel close to the cathode from the state equation (3.4.8). We thus get:

$N_c = 4.3\times10^{18}$ cm^{-3}.

Then putting this N_c into (3.4.9) we obtain the width of the cathode fall of HPGD:

$d_c = 19\times10^{-6}$ m = 19 μm.

It is really too short distance to be distinguished by an eye or by a monochromator whose entrance slit is of the order 100 μm. In addition, the cathode layer is usually hidden inside a hole formed in the cathode deposit (maximal measured depth of a hole was 60 μm).

The cathode fall for the glow discharge in air with Cu cathode is [Rai91]:

V_c = 370 V

From the equation (3.1.1) and calculated d_c we can express the field intensity at the cathode:

$E_c = 3.9\times10^7$ V/m = 390 kV/cm,

The reduced field for N_c corresponding to T_c = 1700 K at the cathode is then given by:

E_c/N_c = 8950 Td

This reduced electric field at the cathode is rather high, but still not enough to induce a field emission of electrons. Probably a process of the secondary electron emission induced by positive ions coming to the cathode occurs, like in the glow discharge at low pressure.

On the other hand, a rather high electric field on the cathode possibly enhances a formation of CuO crystals. This oxide is amorphous at normal conditions, but forms crystals on the Cu cathode surface, as shown by means of the electronic microscopy.

In the case of the negative HPGD, the cathode was a rhodium (Rh) point. Its shape even enhances the electric field around it. However, this field enhancement is probably not necessary for the discharge existence, we often observed that the discharge burned from the side of the point. The high temperature, as well as the elevated electric field, possibly support a growth of the Rh_2O_3 deposit on the point, with a special structure.

3.4.3.3 The positive column

In the classical glow discharge the electric field intensity E is near 0 within the negative glow and increases slightly in the Faraday dark space until reaching a fairly constant

value E_+ in the positive column. If we consider HPGD to be a glow discharge we can evaluate the reduced field E/N in its positive column.

For a typical HPGD with I = 2 mA, d = 7 mm and U_d = 2 kV (U_d is the potential difference between electrodes) we estimate the length of the positive column d_+ = 4 mm from the light intensity profiles The measured temperature in the positive column varied around 1650 K in the positive HPGD. Thus, the density of neutral particles in its positive column is

$N_+ = 4.45\times10^{18}$ cm^{-3}

A constant E_+ in the positive column is given by:

$$E_+ = \frac{U_d - V_c}{d_+} \tag{3.4.10}$$

where V_c is the cathode fall and d_+ is the length of the positive column. This gives the reduced field in the positive column:

$(E_+/N_+)_{pos}$ = 92 Td (± 20 %)

The uncertainty comes from the uncertainties of measurements of T and U_d, but especially from the approximate measurement of d_+. The calculated value of E_+/N_+ is very close to the critical value in air $(E/N)_{crit}$ = 100 Td corresponding to the equilibrium between ionisation and electron attachment ($\alpha=\eta$). This experimental result indicates an important role of the electron attachment among the processes maintaining the discharge stable.

In the negative HPGD of the same parameters (I = 2 mA, d = 7 mm, U_d = 2 kV and d_+ = 4 mm) the mean temperature in the positive column is a little higher than in the positive one: T_+ = 1900 K. It slightly changes N_+ and consequently the reduced field:

$(E_+/N_+)_{neg}$ = 106 Td (± 20 %)

This is also a value very close to the $(E/N)_{crit}$. We took V_c for Cu cathode supposing a close value also for the Rh cathode.

Yu.S.Akishev et al. in their d.c. glow discharge in air and the negative point-to-plane configuration measured the reduced field in the same range (80-100 Td). [Aki93]

3.4.3.4 Reduced current density

Another characteristics of the normal glow discharge is a reduced current density j/p^2. At high pressure and elevated temperature it is clearer to take j/N^2 instead. For air and Cu cathode:

$j/p^2 = 240\ \mu A.cm^{-2}.Torr^{-2}$ [Rai91]

which corresponds to

$$j_0/N_0^2 = 1.92\times10^{-37}\ A.cm^4 = j/N^2 \qquad (3.4.11)$$

for every j and N.

Let us consider HPGD to be close to a normal glow discharge. Then taking the N_+ value in the positive column and assuming constant j/N^2 (3.4.11), for typical I = 2 mA and d = 7 mm, T = 1650 K, we obtain the current density:

$j = 3.79\ A.cm^{-2}$

This value is much greater than the current density measured in the glow discharge of Akishev (10 $mA.cm^{-2}$), but HPGD is a constricted discharge, while their discharge was diffuse due to the high flowing velocity of the gas [Aki93].

Taking the calculated value of the current density j, the cross section of the discharge channel should be then:

$S = I/j = 5.28\times10^{-8}\ m^2$,

which gives a discharge channel diameter of:

D = 259 μm.

This D agrees perfectly with the measured diameter of holes formed in the Cu cathode surface by a positive HPGD (250-300 μm). Under the assumption that the discharge channel is everywhere uniformly thick, this says that HPGD is a glow discharge in its normal regime.

3.4.4 HPGD in other environments

In the previous chapters (3.4.1, 3.4.3) we have presented a consistent theory of the positive and negative high pressure glow discharge in air. Results of studies of this discharge in other environments show additional information on the discharge mechanisms.

3.4.4.1 Air with admixtures

The HPGD properties do not change when air is humidified or charged by VOC or both. This tells that the main species involved in the mechanisms maintaining the discharge are N_2 and O_2 and the admixtures have a minor role. Even more likely, the most important species is electronegative O_2, its concentration determines the process of electron attachment characterised by a coefficient η.

3.4.4.2 Nitrogen

There is no electron attachment in electropositive N_2. The principal mechanism of electron disappearing is the recombination competing with the ionisation.

We can estimate the E/N value in HPGD in N_2 by the same way like in air (chapter 3.4.3.3). Unfortunately, the measured light intensity profiles of HPGD in N_2 (Figure 3.3.12) do not correspond so well to the typical profile of a glow discharge, thus we cannot learn the length of the positive column where E = const from these profiles. We can obtain a brief approximation of E/N supposing E = const on the whole length of the discharge channel except the cathode layer, $d_+ = d - d_c$. The cathode layer thickness d_c can be calculated like in air (chapter 3.4.3.2).

For a discharge with I = 2 mA, d = 7 mm, voltage U_d = 1.8 kV and d_+ = 7 mm the measured temperatures in the middle of the channel T_+ and at the cathode T_c were:

T_{+pos} = 600 K and $T_{c\,pos}$ = 1210 K	positive HPGD,
T_{+neg} = 420 K and $T_{c\,neg}$ = 950 K	negative HPGD.

The density of neutral particles in the middle of the discharge channel N_+ and at the cathode N_c is then

$N_{+pos} = 1.22\times10^{19}$ cm^{-3} and $N_{c\,pos} = 6.06\times10^{18}$ cm^{-3} positive HPGD,
$N_{+neg} = 1.75\times10^{19}$ cm^{-3} and $N_{c\,pos} = 7.72\times10^{18}$ cm^{-3} negative HPGD.

For the glow discharge in N_2 with Cu cathode the cathode fall V_c and pd_c value are[1]:

$V_c = 208$ V
$pd_c = 0.31$ Torr.cm

When pd_c is expressed in terms of Nd_c due to the increased temperature at the cathode, we obtain the following cathode layer thickness:

$d_{c\,pos} = 18$ μm positive HPGD,
$d_{c\,neg} = 14$ μm negative HPGD.

Then the electric field at the cathode E_c calculated from equation (3.1.1) is:

$E_{c\,pos} = 231$ kV/cm positive HPGD,
$E_{c\,neg} = 297$ kV/cm negative HPGD

and the reduced electric field at the cathode is:

$E_{c\,pos}/N_{c\,pos} = 3812$ Td positive HPGD,
$E_{c\,neg}/N_{c\,neg} = 3849$ Td negative HPGD.

If we compare these results with those obtained in the HPGD in air ($d_c = 19$ μm, $E_c = 390$ kV/cm, $E_c/N_c = 8950$ Td) we can see that the cathode layer thickness is approximately the same, but the electric field and the reduced field at the cathode are lower in

[1] pd_c was only available for Al cathode, it will not be very different for Cu. We suppose close V_c and pd_c values also for the cathode of Rh, these data were not available.

N_2 than in air. Lower cathode electric field is needed to maintain the discharge in N_2, it is associated with lower electron losses due to no attachment.

Supposed constant E in the discharge channel given by equation (3.4.10) gives

E_+ = 2.27 kV/cm

in both polarities.

This E_+ gives the following reduced electric field in the positive and negative HPGD (positive column):

$(E_+/N_+)_{pos}$ = 19 Td (± 30%)	positive HPGD
$(E_+/N_+)_{neg}$ = 13 Td (± 30%)	negative HPGD

Again, the reduced electric field in the positive column of the HPGD in N_2 is considerably lower than in air. The discharge in N_2 is maintained stable thanks to the equilibrium between ionisation and recombination (represented in this case by η). The stability is achieved at lower E/N due to no attachment. The uncertainty of calculated (E_+/N_+) is greater than in air, because d_+ was estimated very approximately.

3.4.4.3 Oxygen

On the contrary to HPGD in N_2, the electron attachment coefficient η and $(E/N)_{crit}$ are very high in electronegative O_2. Such a high E/N cannot be obtained without passing into a spark. At usual applied voltages determining certain $E/N < (E/N)_{crit}$ the discharge remains in the low temperature streamer regime. Formed negative ions are probably O_2^-.

3.4.4.4 Nitrogen with admixtures

When various admixtures (H_2O, VOC and H_2O + VOC) were added into N_2, we observed different discharge properties if compared with pure N_2, such as higher discharge voltage at a given current, higher minimal current, lower stability, different emission spectra and higher temperatures. From the point of view of the critical reduced electric field corresponding to the equilibrium between electron producing and electron consuming mechanisms ($\alpha=\eta$, remind chapter 3.4.1), it seems that the admixtures in N_2 increase the

attachment coefficient η, which causes higher $(E/N)_{crit}$. The substituents are probably electronegative. We suppose a formation of negative ions, such as CN^- in N_2+VOC mixture and OH^- in N_2+H_2O and N_2+H_2O+VOC mixtures. These negative ions play a similar role like O_2^- in the discharge in air.

However, such an interpretation is not the only possible, the admixtures may enhance other electron sink mechanisms (e.g. recombination) as well.

3.4.5 The plasma generated by the HPGD

The rotational and vibrational temperatures T_r and T_v in the discharge channel have been determined by a technique of emission spectroscopy in UV-VIS region. Let us first discuss the question of these temperatures for the neutral N_2 molecules under the condition of the studied discharge. We assume that the main mechanism of excitation of N_2 molecules are collisions with electrons.

The question is, how the energy stored in the rotational and vibrational levels of excited states of N_2 will react with collisions among heavy species? Such collisions are very numerous at atmospheric pressure. Since the energies between rotation levels are of the same order of magnitude as the energy corresponding to the neutral speed, a quick relaxation of the rotational energy towards a thermal equilibrium with the neutral species will happen. Thus the rotational temperature of the ground state should quickly relax to the gas temperature T, and the intensity distribution of the rotational components into a molecular band may be used to derive T_r [Che94b].

This is however not the case with the level of vibrations. Since the energy between two consecutive vibration levels (for low value of v however) are much larger than the thermal energy, the v-t collisions (i.e. vibration to translation transfer) are very small and rather the v-v (vibration to vibration) dominates. When the electrons excite a population of nitrogen molecules with its specific vibrational distribution towards the C states, it will reflect somehow the distribution of the ground state. Somehow only, since the excitation will follow the various values of the Frank-Condon factors (which are v=0 to v'=0 / 0.54, 0 to 1 / 0.3, 0 to 2 / 0.107, 1 to 0 / 0.347, 0 to 2 / 0.267, 0 to 3 / 0.18, 0 to 4 / 0.08; the transition not listed being negligible) [Ncl62]. Due to this non-uniform Frank-Condon factors the upper distribution in the C state of vibration level does not have the same shape as the ground state. If the upper state vibrational distribution is not perturbed by heavy species collisions, it is

possible to infer the initial ground state vibrational distribution i.e. T_v. However, at atmospheric pressure, the collisions between heavy species are numerous and quenching of the upper $C^3\Pi_u$ state happens. Do these collisions drastically change the distribution of the vibrational states not destroyed by the quenching? The question appeals three remarks.

Firstly (1), following the studies on C state extinction by quenching effect [Alb71], it is mainly due to O_2 collisions. The pressure quenching for the v'=0 and the v'=1 of the C state are respectively p_0=3.57 Torr and p_1=2.67 Torr. While depletion of the v'=1 state should be more important, it however does not change drastically the upper v' distribution.

Secondly (2) the derivation of T_v from the upper state assumes implicitly that these upper states are populated due to the collisions of electrons with the ground state. This assumption is probably not completely correct, since a non-negligible fraction of the upper state production may come from the A or B nitrogen states.

Finally (3), N_2(X) colliding with N_2(C, v'≠0) may end with N_2(C, v'=0), overpopulating the v'=0 state. [Alb71] Changes of the distribution of the v' states may happen, but this last effect can only lead to a lowering of the value of the apparent T_v.

Therefore, the measured values of T_v in the HPGD should be taken as an "apparent" vibrational temperature, the real T_v (at least for the distribution in the first v levels) should not be to far from this order of magnitude. Rotational temperature T_r corresponds well to the temperature T of neutral species (bulk gas).

In thermal plasma, i.e. plasma in the local thermodynamic equilibrium (LTE), these two temperatures are equal, i.e. $T_r = T_v$. Experimental results demonstrate that in HPGD $T_r \neq T_v$ in the measured range of currents (1-5 mA) which means that the plasma generated by the HPGD of both polarities is out of the LTE. The difference between T_r and T_v is less significant as the discharge current rises, at higher currents (5 mA and more) the plasma tends to approach LTE conditions (Figure 3.3.3).

In spite of the non-equilibrium conditions, the temperature of neutral particles in the discharge is rather high (900-2300 K), it depends on the current and the location within the discharge channel. It is higher than in typical non-thermal plasmas which operate at high electronic temperature and ambient gas temperature. This fact predetermines the HPGD used for the pollution control applications to treat the pollutants by two main effects:

1. their thermal decomposition which probably occurs in the close surroundings of the discharge channel due to a high temperature

2. volume reactions induced by radicals occurring in further and cooler parts of the reactor

Both these effects cooperate and lead to the removal of the pollutants as will be shown later (in chapter 5 dealing with VOC removal). Application of this type of the discharge for the pollution control is neither a typical non-thermal plasma application, nor a fully thermal plasma process, it is something between them.

Finally, let us mention a long living metastable state $A^3\Sigma_u^+$ of N_2 molecule (lifetime τ=1.3-1.9 s [Lof77, She69, Mag92]) which is probably important in plasmochemical processes involved in VOC removal and in the formation of some solid products, because it can serve as a reservoir of energy. [Han00, Mrv00] It will be discussed in more details later (section 5.3.4.3). Observation of the 1st positive system of N_2 ($B^3\Pi_g$ - $A^3\Sigma_u^+$ transition) confirms that HPGD in air, and especially in pure N_2, generates N_2 molecules in this state.

3.5 CONCLUSION

We have studied a streamer-induced pulseless discharge between two metal electrodes of the point-to-plane geometry in air and some other environments at atmospheric pressure. The features of this discharge correspond to the normal glow discharge, regardless to the polarity of the point electrode. It is maintained pulseless even at the atmospheric pressure thanks to the equilibrium between ionisation, recombination and electron attachment, and the pressure equilibrium of the discharge channel with the surrounding gas. This condition is guaranteed by the external electric circuit, especially by a suitable choice of the series resistance.

The gas temperature in the discharge is relatively high (900-2300 K), but still lower than in arc discharges with T > 5000 K. It rises with rising discharge current and changes along the discharge channel. A generated plasma is out of the local thermodynamic equilibrium in the studied range of currents (1-5 mA). This fact and a simplicity of the system to obtain and maintain the HPGD predetermine it to be used as a special non-thermal plasma application where medium temperatures are needed.

New information obtained from the study of the high pressure glow discharge, especially measured temperatures and surface changes are important from the point of view of the fundamental, as well as the applied research.

4.
TRANSIENT SPARK

4.1 INTRODUCTION

A new type of a streamer-induced discharge named the “transient spark” or “spontaneously pulsing transition discharge” was applied to CO_2 and CO depletion [Mrv98b, Mrv99a, Mrv00] and to the VOC removal [Mac00]. Interesting results obtained in these applications became a motive to study the properties of this discharge in more details.

The transient spark (TS) is a discharge of a streamer-to-spark transition type supplied by a d.c. high voltage of both polarities. It is initiated by a streamer transforming to a spark, the spark phase being too short to develop into an arc and to reach conditions of the local thermodynamic equilibrium (LTE). That is why we named it the transient spark. It is able to generate a non-thermal plasma, as resolved from its rotational and vibrational temperatures determined by means of UV-VIS emission spectroscopy. Measurement of rotational and vibrational temperatures of a discharge has already been introduced in chapter 3.1, we used the same technique like for the high pressure glow discharge (HPGD). Metal electrode surfaces treated by TS were analysed additionally to get more information on the properties of TS and its surface effects.

The formation of the ‘classical’ spark is believed to follow the mechanism outlined by Rogoff, Marode and Sigmond. [Rog72, Mar79, Sig84] The main process leading to the final breakdown of the gap is attributed to the gradual increase of the reduced electric field *E/N*. It is caused by a decrease of the gas density *N* in the filamentary streamer-induced channel. Indeed, a weak pressure expansion of this channel due to the heating by the discharge current occurs and leads to a decrease of the density *N*. In air, the initial value of the *E/N* ratio inside the discharge channel gives an attachment greater than the ionisation, and the current decreases. However, as the density *N* decreases, the reduced field becomes high enough to reverse the situation and the ionisation starts to dominate over the electron attachment. This leads to the spark formation.

All applications of non-thermal plasma for flue-gas cleaning are based on the ability of high pressure gas discharges to induce chemical activities within the gas volume and to convert the gaseous pollutants into somewhat non-hazardous. An attempt to promote a special type of the streamer-induced discharge called “prevented spark” has been suggested some years ago. [Mar93, Haf95] Its nature is similar to the transient spark presented in this work.

4.1.1 Prevented spark

Prevented spark belongs to the family of filamentary discharges induced by a streamer. The filamentary discharge structure is due to a tube of positive ions which results from the streamer trail along its way from the positive anode to the negative cathode. The ions keep all the electrons inside their tube and render a filamentary current distribution. As the streamer reaches the cathode, a conductive plasma bridges the electrodes and a spark may occur within this bridge.

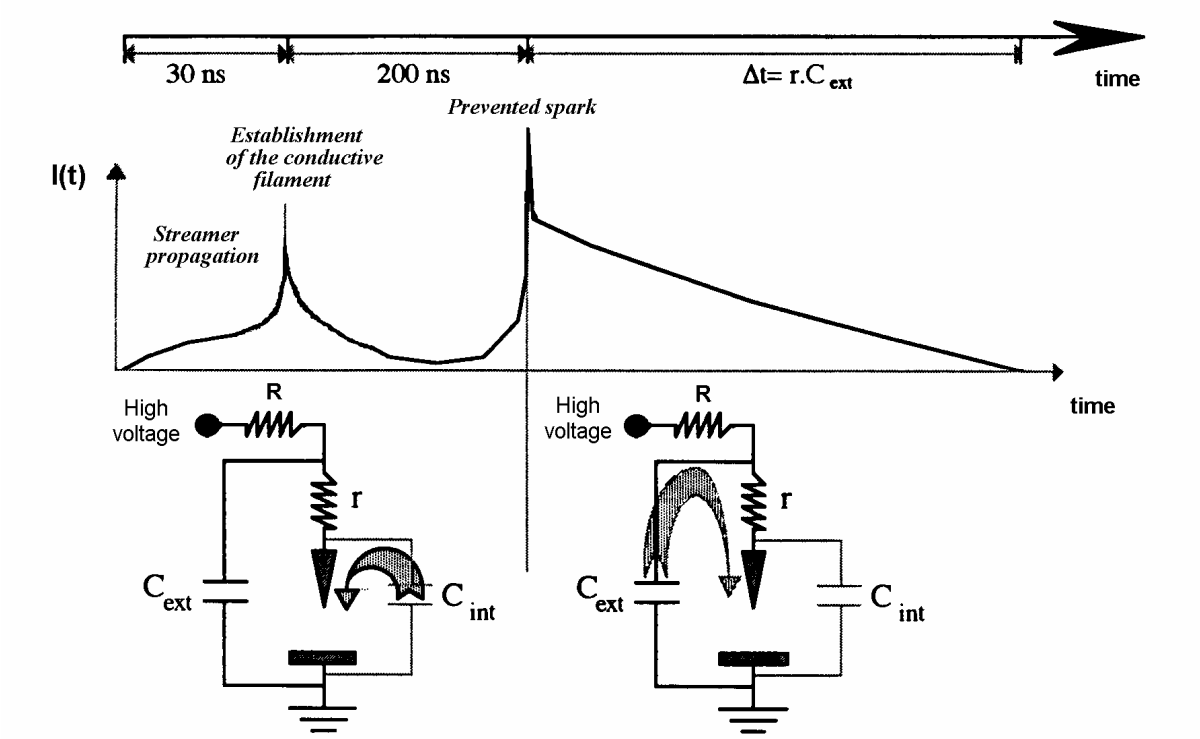

Figure 4.1.1 Prevented spark. Electric circuit and time development of the current. **[Jaf95]**

Figure 4.1.1 shows a typical discharge circuit for prevented spark and the time development of the current in various phases of the discharge. It also indicates a principle of the prevented spark formation. [Jaf95] C_{int} is an internal capacity of the discharge gap. Corona electrode geometry of is used, since the discharge is initiated by a streamer corona well controlled by such geometry.

For an applied potential U_g under the spark threshold value, repetitive streamers appear in the discharge gap. They have typical current pulses and induce a small voltage fall. These individual discharges vanish regularly due to the electron attachment (typical repetitive rate 30 kHz, discharge duration of some 200 ns). With rising voltage, the streamer pulse is

followed by the spark pulse inducing a strong potential fall. The spark intensity depends on the value of impedances *R, r, C_{ext}, C_{int}*. If the internal gap capacity C_{int} is small (some pF) then the available energy in this capacity is too small to sustain a spark phase. In such case, after the transient spark occurrence which practically discharges C_{int}, a current phase is maintained by the external capacity C_{ext} which discharges through the remaining filamentary bridge of the transient spark phase.

However, the energy stored in C_{ext} has to be delivered into the gap through the control resistance *r*. Sometimes, as soon as the current rises strongly towards the spark, the capacity C_{int} too small for sustaining even the transient spark, is helped by C_{ext}. In such case, however, *r* drops the discharge voltage without allowing the spark itself to be formed. In fact, *r* prevents the spark to develop or maintain the decreasing state of a transient spark. This is the way of controlling the discharge nature by an external circuit which allows to form the non-thermal prevented spark plasma. The relaxation time, during which the prevented spark phase exist, is controlled by the relaxation time of C_{ext} discharge through *r*, i.e. rC_{ext}. The product RC_{ext}, in turn, controls the recharge of the capacities and the whole process repeats. [Mar93, Mar98]

4.2 EXPERIMENTAL SET-UP FOR THE STUDY OF THE TRANSIENT SPARK

We used two electrode configurations for the application of the transient spark for VOC treatment. The first was a typical point-to-plane configuration with Rh point and Cu plane and a usual interelectrode distance d = 7 mm. Mainly this configuration was used for the experimental study of the TS properties. (Figure 4.2.1)

The second was a special modification of a coaxial configuration: a rod with a thread (stud) M6 (diameter 6 mm) as a high voltage electrode inside the cylinder electrode. Both rod and cylinder are made of copper, inner diameter of the cylinder is 21 mm, d = 7.5 mm, length of the discharge tube is 50 cm. (Figure 4.2.2) This configuration was used mainly for the tests of VOC removal process induced by TS.

The point and threaded rod were supplied by a high voltage of both polarities from the high voltage generators DEL RHVS Series (max. 60 kV, 5 mA, with a possibility of current

stabilization) or Universal Voltronics Mintrol (max. 30 kV, 150 mA; used mainly for the discharge tube with the rod). Opposite electrodes were grounded. The electric circuit for the transient spark in point-to-plane geometry (Figure 4.2.1) is a little different from the circuit of the prevented spark (Figure 4.1.1). There is no resistance *r* dividing the external capacity C_{ext} from the discharge gap like in prevented spark circuit, there is only a protection resistance *R* put behind the generator. It means that C_{ext} and the internal capacity of the gap C_{int} represent one resulting capacity $C = C_{ext} + C_{int}$.

In the threaded rod-cylinder discharge chamber (Figure 4.2.2), there is no *r* as well, but usually we did not use any C_{ext}, just the internal capacity C_{int}. C_{ext} is not necessary, because the capacity $C=C_{int}$=30 pF in this discharge chamber is high enough to sustain the spark pulses.

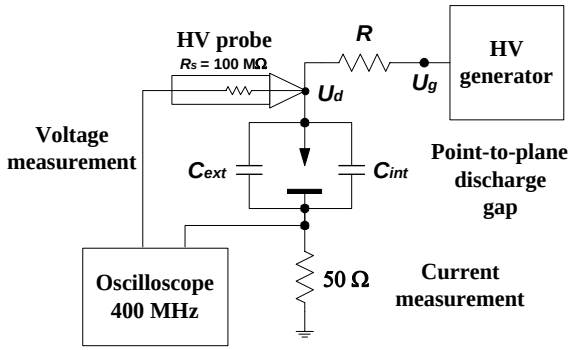

Figure 4.2.1 Point-to-plane experimental set-up used for TS

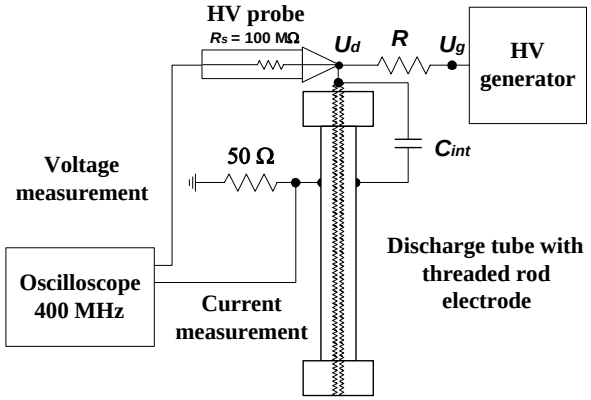

Figure 4.2.2 Set-up with discharge tube with threaded rod used for TS

To control the TS we used a higher range of values of the external resistance *R* than in HPGD: from 2 to 7 MΩ. In the point-to-plane geometry C_{int}=3-5 pF for a typical gap length *d*=7 mm (higher limit in the closed metal discharge chamber used for emission spectroscopy). To sustain a stable TS, a total capacity *C* at least of 20 pF is needed, thus we used external capacitors with C_{ext} in the range of 15-45 pF.

The discharge current pulses were detected by the 400 MHz digital oscilloscope Tektronix DSA 602 or the 500 MHz oscilloscope Tektronix TDS 544 A. The discharge voltage was measured by the high voltage probe Tektronix T6015 A (1000 ×, 3 pF, 100 MΩ) leading the signal to the same oscilloscopes. The oscilloscopes allowed to evaluate various

functions of the signals, e.g. a power $P=UI$ or an energy $E=\int UI\mathrm{d}t$. The mean values of the generator voltage and the total current were measured by d.c. meters comprised in the generator. Use of the signal attenuator was often necessary for the oscilloscopic detection of current pulses, because the pulses were often too intense, over the range of oscilloscope.

To study the physical properties of the transient spark, especially for the spectroscopic study of its emission, we used the same experimental set-up with the point-to-plane electrode discharge chamber, and the same experimental conditions as for the study of the HPGD. (Chapter 3.2, Figure 3.2.1). Cylindrical discharge chamber was not used for the acquisition of emission spectra.

Similarly like in the HPGD study, we used the additional glass discharge tube where the discharge operated in the radial tube direction, in order to study the influence of the gas flow on the TS behaviour. (Chapter 3.2, Figure 3.2.2).

The study of the physical properties of TS was primarily effectuated in dry air. We explored also the influence of some admixtures in dry air such as H_2O, VOC and H_2O with VOC, because it corresponds to the situation of VOC removal. With the aim of a better understanding of TS-induced VOC removal process in the reducing N_2 atmosphere (which has given interesting results, see chapter 5.4.1) we have done some additional measurements in the atmosphere of N_2 charged by VOC (2000 ppm of toluene).

Emission spectra of the TS were used for the determination of rotational and vibrational temperatures like in HPGD. Unfortunately, the accuracy was worse than in HPGD (50-100 K) due to the higher noise caused by this pulsed discharge.

We applied also the same analysis techniques for the electrodes treated by TS like in HPGD (optical microscopy, scanning electron microscopy with element microanalysis and infrared absorption spectroscopy)

4.3 RESULTS AND DISCUSSION

4.3.1 Mechanisms and electrical parameters of the transient spark

The transient spark (TS) is a filamentary discharge induced by a streamer. The mechanism of its function is similar to the prevented spark, but the prevention is here done by the small energy stored in the capacity C rather than by the resistance limiting the current

value in the prevented spark case. At lower applied voltages we observe regularly vanishing streamers. As the applied voltage is increased, the small capacity C (order of 10s pF; $C=C_{ext}+C_{int}$ in the point-to-plane configuration, Figure 4.2.1; $C=C_{int}$ in the threaded rod tube, Figure 4.2.2) is charged during the post-streamer relaxation phase. The energy stored in it is delivered to the discharge gap which forms a spark pulse with a current maximum. The intensity of this pulse is defined by the amount of energy stored in C. Since C is low, this energy is not sufficient for the spark development. Once C is discharged very quickly, the high spark current I falls to 0 due to the capacity voltage fall.

Although the spark current maximum is not controlled by the resistance r (like in the prevented spark), the spark is quenched very quickly, before it can develop to LTE state. It thus does not have properties of a typical spark discharge, as will be shown in the following. That is why we named it the transient spark.

During the quenched phase with no conductive discharge current, the discharge capacity C is recharged, and the potential U on the stressed electrode (point or rod) grows in time t according to the following equation:

$$U(t) = U_g \left(1 - e^{-\frac{t}{RC}}\right) \tag{4.3.1}$$

with the generator voltage U_g, the external resistance R and the total capacity C.

Usually, during this relaxation phase when the gap potential crosses a specific threshold, there appears a corona discharge in its glow regime, i.e. a discharge sticking around the point electrode, and some pre-breakdown streamers, extending through the whole gap. As soon as C is again sufficiently charged, it feeds a new streamer process enough strong to induce the transition towards the transient spark. It occurs in the time $t = T$, at the threshold voltage U_{TS} which is given according to the (4.3.1) by:

$$U_{TS} = U_g \left(1 - e^{-\frac{T}{RC}}\right) \tag{4.3.2}$$

Dividing this equation by U_g and taking the natural logarithm we get the characteristic frequency f of the process:

$$f = \frac{1}{T} = \frac{1}{RC \ln\left(\frac{U_g}{U_g - U_{TS}}\right)} \qquad (4.3.3)$$

Indeed, the measured values of the repetitive frequency of pulses *f* are well coherent with the values calculated according to (4.3.3). For typical $R \sim 5$ MΩ and $C \sim 30$ pF, the frequency *f* is in the order of several kHz, so that the discharge makes a characteristic noise.

However, the measured frequency is not absolutely regular, we often observe fluctuations and a fairly rising trend with the increasing total time of the discharge operation.

This effect may be explained by this way: The TS threshold potential U_{TS} may also depend on the frequency *f*. The interelectrode gap may remain pre-ionised, especially at higher *f*, thus the next TS breakdown occurs at lower U_{TS}. Lower U_{TS} consequently increases *f*, as evident from their relation (4.3.3).

On the contrary, another effect may reduce the temporal frequency growth of the TS: a formation of the deposit layer on the electrodes. This layer may change the electric parameters of the discharge circuit, especially by increasing the internal capacity C_{int}, thus lowering the resulting frequency. The dielectric properties of the deposit layer certainly depend on its thickness and its chemical composition. We can thus say, that the discharge is in a certain way influenced and controlled by the time of its operation and the involved plasma chemistry.

The capacity *C* used in the TS has rather small values (tens of pF), the series resistance *R* must thus have rather high values (order of MHz), otherwise the repetition frequency would be too high, which would cause an insufficient relaxation time between two consecutive pulses and a development of an arc or another discharge form (when *R* is in the order of 100s of kHz HPGD regime is often established). This result is principally in accordance with the result of Larsson who found that a high value of the series resistance prolongs the streamer-to-spark transition time, but does not inhibit the disruptive discharge, neither changes the energy injected into the discharge gap during the streamer-to-spark transition. [Lar98] However, a high series resistance *R* is indispensable for maintaining the regime of the transient spark.

In our paper accepted for publication [Mac00] describing an application of this discharge to the cyclohexanone removal, and in some other publications of Morvová et al. [Mrv98b, Mrv99a,b, Mrv00] the name "spontaneously pulsing transition discharge" (SPTD) has been used for the same discharge. It fits probably better than the name "transient spark" (TS), because it comprises the pre-streamers occurring before the spark pulse and a certain spontaneous behaviour of the discharge, its dependence on the time of operation and

involved plasmochemical mechanisms. However, in the following we will keep the name "transient spark" (TS).

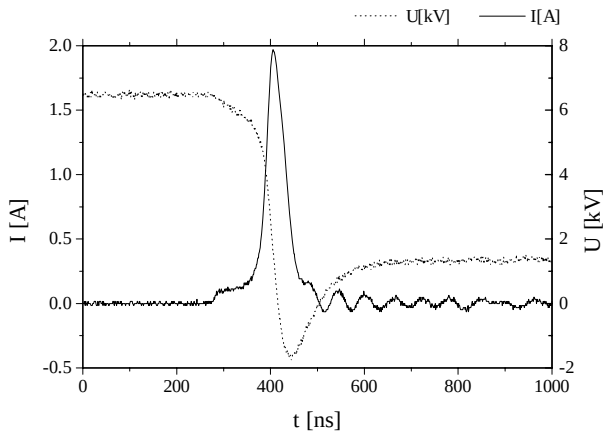

Figure 4.3.1 Transient spark in positive point-to-plane configuration, gap 7 mm; Voltage and current waveforms for short time scale, U_g=9.3 kV, $I_{average}$=0.73 mA, C=25 pF, R=5 MΩ

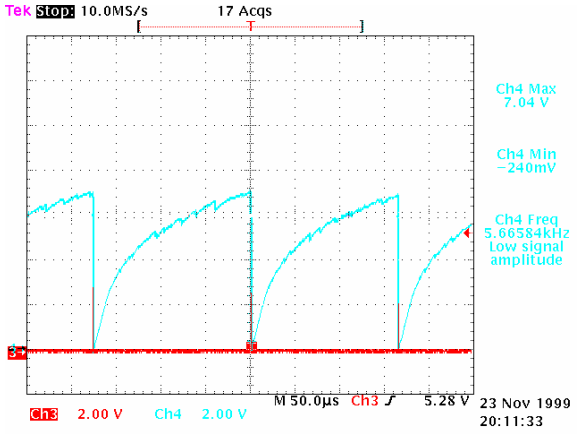

Figure 4.3.2 Oscillogram of TS in positive point-to-plane, discharge voltage (Ch2-blue) and current (Ch3-red) waveforms at large time scale, U_g=8.4 kV, R=5 MΩ, C=15 pF, f=5.67 kHz

Typical oscilloscopic waveforms of the TS potential and current in a short time scale (1 μs) are shown in Figure 4.3.1. The current waveform demonstrates an initiating streamer (t=300ns) and its transition to the typical transient spark pulse (t = 380 ns). Discharge voltage drops brutally as the current rises. Figure 4.3.2 shows *U*- and *I*-waveforms in the large time scale (500 μs). *I*-pulses are not well resolved, but *U*-waveform is remarkable: steep drops as *C* is discharged and exponential growths as *C* is recharged. Notice that the streamer-to spark phase of the process is 3 orders of magnitudes shorter than the post-spark relaxation phase.

4.3.2 Problems of power measurement

The measurement of the discharge power P_d, respectively total power P spent by the whole circuit, is necessary to evaluate the energy costs of the discharge applied for some gas treatment. In the HPGD it was very simple, because the discharge is pulseless with continuous current and voltage. We took simply $P_d=U_dI$, respectively $P=U_gI$ (equations (3.3.1) and (3.3.2), section 3.3.2.1).

4.3.2.1 Total power measurement

Current and voltage of the transient spark have a form of more or less regular pulses. However, total power taken from the generator can be simply calculated from the generator voltage U_g and the mean value of outgoing current I.

$$P = U_g \bar{I} \tag{4.3.4}$$

U_g and the mean value of I can be measured simply by a d.c. voltmeter and ampermeter (these d.c. meters were a part of the generator).

Another way for measuring the total P is based on the measurement of the mean value of the discharge voltage U_d . The total current I going from the generator is given by:

$$I = \frac{U_g - \overline{U_d}}{R} \tag{4.3.5}$$

Putting I (4.3.5) into the formula for P (4.3.4) we obtain:

$$P = U_g \frac{U_g - \overline{U_d}}{R} \tag{4.3.6}$$

The discharge voltage U_d can be measured by the high voltage probe leading the signal to the oscilloscope able to evaluate its mean value.

4.3.2.2 Discharge power measurement - Method of UI integration

A rather simple and more correct method for the discharge power measurement is to integrate the product of $U_d(t)I(t)$ in a certain time t to obtain the energy dissipated in the discharge during this time t (in order to measure correctly, t has to be much longer than the repetitive period of pulses, $t > T$).

$$W_d = \int_0^t U_d I dt \tag{4.3.7}$$

If the pulses are regular, i.e. with a constant frequency, we obtain the discharge power by:

$$P_d = fW_d = f\int_0^t U_d I dt \tag{4.3.8}$$

An example of an oscillogram of measured U_d, I and W_d calculated from U_dI (equation(4.3.7)) is shown in Figure 4.3.3.

However, there appear several problems with such method of power measurement:

1) The *I*-pulse of TS is often high, over the range of oscilloscope. This can be solved by using the signal attenuator.
2) The *I*-pulse in TS is very short (some 20-50 ns). Hence, this way of power measurement is correct only if *I*- and *U*-pulse are detected synchronously on the oscilloscope, the delay between these two signals in the coaxial cables (respectively in HV probe and coaxial cable for *U*-signal) must be the same.
3) The sampling rate of the oscilloscope must be sufficient to detect correctly *I*- and *U*-pulse (at least 500 MSamples/s = 1 Sample per 2 ns) which is possible only at short time scaling (10-50 ns/division). On the other hand, at such time scaling, the frequency of repetitive pulses cannot be measured, because the scaling time of the oscilloscope must be changed to some 50-100 μs/division for its measurement. Yet, the sampling rate at this time scaling is too low to detect correctly the *I*-pulse (5-10 MSamples/s = 5-10 Samples/μs). Thus, the energy from one pulse and the pulse frequency must be measured at different time scalings. Being aware of this fact, a regular frequency of pulses is even more required. However, it was not experimentally confirmed, there are always some frequency fluctuations in the TS.
4) The most important problem is hidden in the measured discharge current *I* which enters to the calculation of P_d. As explained in chapter 4.3.1, the spark current pulse is caused by discharging of the capacity *C* which is composed of external capacity C_{ext} parallel with the discharge gap and the internal capacity of the gap C_{int} (for the point-to-plane set-up). The current which passes through the 50 Ω resistance and is detected by the oscilloscope is just the current from discharging of C_{ext}. There is a part of the discharge current associated with discharging of C_{int} which is not detectable by the oscilloscope, this current passes only within the gap. Therefore, the real energy dissipated in the discharge, and the discharge power are not correctly calculated from (4.3.7). This

problem is essential especially in the threaded rod discharge tube, where usually no external capacity is present, i.e. $C = C_{int}$.

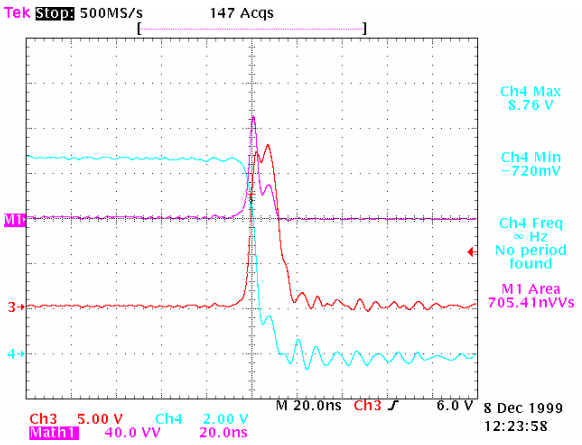

Figure 4.3.3 Oscillogram of TS in positive point-to-plane. Measured waveforms of U_d (Ch4 -blue), I (Ch3-red) and U_dI (M1-pink), W_d calculated from time integration of U_dI (M1-Area). U_g=9.8 kV, R=5 MΩ, C=15 pF

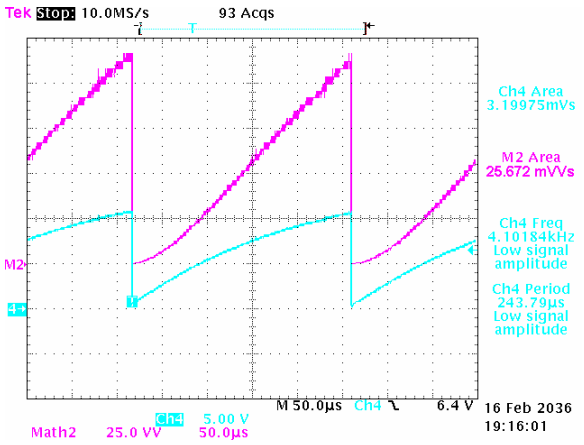

Figure 4.3.4 Oscillogram of TS in positive threaded rod-cylinder. Measured waveforms of U_d (Ch4 -blue), and U_d^2 (M2-pink), and their calculated time integrals (Ch4-Area, M2-Area). U_g=16 kV, R=5 MΩ, C=40 pF

4.3.2.3 Discharge power measurement - Method based on the discharging capacity

In order to verify P measured by the previous method we can use another one. It is based on the principle of the TS - the spark pulse is formed due to the discharging of the capacity C, $C=C_{ext}+C_{int}$. The voltage on this capacity (equal to the discharge voltage) drops from some U_{up} to some U_{down}. The energy stored in C before and after the pulse can be expressed like:

$$W_{C_{up}} = \frac{1}{2} C U_{up}^2$$

$$W_{C_{down}} = \frac{1}{2} C U_{down}^2$$

The difference of these energies gives the energy delivered to the discharge from C:

$$W_C = W_{C_{up}} - W_{C_{down}} = \frac{1}{2} C (U_{up}^2 - U_{down}^2) \tag{4.3.9}$$

Thus:

$$W_C = W_d \tag{4.3.10}$$

The discharge power will be again given by the discharge energy multiplied by the frequency, compare with (4.3.8):

$$P_d = fW_d = \frac{1}{2} fC(U_{up}^2 - U_{down}^2) \tag{4.3.11}$$

To evaluate P_d we need to know C and to measure U_{up}, U_{down} and f which is rather simple from the oscilloscopic U-waveform (see Figure 4.3.2). This technique is also sensitive on regular frequency like the previous one. And the hardest task is an exact measurement of the capacity $C = C_{ext} + C_{int}$ which is in the order of some pF.

4.3.2.4 Discharge power measurement - Method of total energy balance considering the high voltage probe in the circuit

Results of measurements of the TS power by the method of *UI* integration and of discharging capacity show some discrepancy, even when C_{ext} and C_{int} are considered in the sense described above. There is another problem in the circuit: some current escapes through the high voltage probe. The used HV probe has its characteristic resistance R_s=100 MΩ. This resistance is very high if compared with the resistance of the discharge gap during the spark pulse when the gap is bridged by the conductive plasma. Nevertheless, it is higher or comparable with the gap resistance during the relaxation time without spark pulse. During this time when C is charged there appears a current which escapes through R_s.

In order to consider this escaping probe current, and to avoid at the same time problems described in previous two methods, we found a new way of P_d measurement based on total energy balance of the circuit.

Let us come from some equations describing the total energy balance of the circuit. (The circuit scheme is in Figure 4.2.1.)

Total current I going from the generator is given by the formula (4.3.5). The probe current I_s can be expressed like:

$$I_s = \frac{U_d}{R_s} \tag{4.3.12}$$

The total energy delivered from the generator to the circuit is:

$$W = \int_0^t U_g I dt = \int_0^t U_g \frac{U_g - U_d}{R} dt \tag{4.3.13}$$

Energy lost in the resistance R:

$$W_R = \int_0^t \frac{(U_g - U_d)^2}{R} dt \tag{4.3.14}$$

and energy lost in the probe due to the probe current I_s

$$W_s = \int_0^t \frac{U_d^2(t)}{R_s} dt \tag{4.3.15}$$

Energy dissipated in the discharge is then given by

$$W_d = W - W_R - W_s \tag{4.3.16}$$

After inserting terms W, W_R, W_s and simplification (4.3.16) resolves in the following expression:

$$W_d = \int_0^t U_d \left(\frac{U_g}{R} - \frac{R_s + R}{R_s R} U_d \right) dt \tag{4.3.17}$$

Formula (4.3.17) shows that for calculation of W_d we need to know the exact values of R and R_s, in order to measure $U_d(t)$ and $U_d^2(t)$ and to evaluate their time integral. An example of such an oscillogram is shown in Figure 4.3.4. The discharge power will be obtained by the same way like in the previous methods (4.3.8):

$$P_d = f W_d \tag{4.3.18}$$

which means that we need to measure f too. This method, as well as the previous ones, is sensitive to the regular frequency of TS pulses.

Anyhow, it is the best method for the measurement of TS discharge power that we found. It can be used for all configurations of electrodes, whether there is some external capacity in the circuit or not. There is no problem of undetectable current caused by discharging of the internal gap capacity like in *UI*-integration method, because we do not need to measure $I(t)$. Furthermore, there is no problem of exact measurements of C_{ext} and C_{int}. The only problem is the above mentioned regularity of pulses.

On the base of all these reasons, the method of total energy balance described here has been used for discharge power measurement of TS applied for VOC removal. (Chapter 5.3.3)

4.3.3 Visual observations of the TS behaviour and the gas flow influence

A visual impression given by the transient spark in air is a brush composed of the strongly shining white-blue channels. This brush may be more or less “dense” with thick or thin channels, it depends on the parameters of the circuit. The higher is *C* the thicker are the channels and the brush is less dense.

This behaviour can be simply explained by the property of a human eye capable of about 0.1 s resolution of consecutive visual images. In the kHz frequency range we can see several hundreds of discharge channels at the same moment. Higher *C* lowers the frequency, thus the brush seems less dense, on the other hand, higher *C* stores more energy inducing stronger current pulses, hence the channels are more intense and seem thicker.

The discharge brush moves on the plane electrode of the point-to-plane configuration. A gas flow does not significantly influence its behaviour and properties, higher flows (flowing velocity over 2 m/s) have an effect of frequency lowering. Higher breakdown voltage for TS ignition is necessary at high gas flows.

In the discharge tube with threaded rod electrode the discharge brush may migrate along the rod, or turn around it, or the luminous channels may distribute radially around the rod, or even other spectacular behaviours of the discharge may occur. We can see several discharge brushes at the same time. The axial migration of the discharge is enhanced with the gas flow. At high flows it moves quickly in the flow direction, at the end of the tube it vanishes and a new running brush appears immediately at the tube beginning.

We did not observe very special effects of the polarity on the discharge behaviour what was the case in HPGD. The only effects were higher frequency in the negative polarity, thus denser discharge brushes, and lower generator voltage.

4.3.4 Emission spectroscopy

4.3.4.1 Whole spectrum in the 200-700 nm region

The whole emission spectrum of TS has been acquired in the range allowed by the monochromator (200-700 nm). In dry air and both polarities of TS two principal systems of bands have been observed like in HPGD:

1) 2nd positive system of N_2 ($C^3\Pi_u$-$B^3\Pi_g$ transition) was the most significant radiative system in the whole scanned spectrum. It was used for the determination of the discharge temperatures. (Figure A.2.5, Table A.2.1 in Appendix 2)
2) 1st positive system of N_2 ($B^3\Pi_g$ - $A^3\Sigma_u^+$ transition) with bands of very weak intensity in comparison with the 2nd positive system. (Table A.2.1 in Appendix 2)

Many other unidentified bands have been observed in the spectrum (344, 501, 518, 567, 618, 649, 657, 661 nm etc.). They may belong to the metal (Rh, Cu) bands and/or to various atomic spectra of N, O, etc. Their interpretation needs further investigation.

4.3.4.2 Temperature determination

The profile of the rotational temperature T_r (corresponding to the gas temperature) along the axis of the TS discharge channel $T_r(x)$ at average I=1.5 mA for positive polarity is shown in Figure 4.3.5. Although the T_r values are rather dispersed, we can see that T_r rises from about 500 K at the point anode to about 1500-1700 K close to the plane cathode. The dispersion is due to the uncertainty of T_r measurement which is about 50-100 K (more than in HPGD). It is due to the higher noise caused by TS and probably also due to the low regularity of this discharge, each experimental point in the emission spectrum was acquired from a different pulse.

$T_r(x)$ profile of the negative TS could not have been acquired, because the negative TS in point-to-plane geometry is even more irregular, the spark channels arriving to the plane anode have a large spatial dispersion (they form a “shower”), which causes such a noise that the spectra could not have been evaluated. The only successfully measured T_r values were close to the point cathode where the discharge channels forming a “shower” were not too dispersed. We have measured T_r = 600-800 K at the point cathode (x = 0) of negative TS. It is about twice lower than close to the plane cathode of the positive TS. We suspect the temperature profile to be similar to the positive TS, T_r rising from the point to the plane, regardless to the polarity of electrodes. Such behaviour is different from the HPGD where the

temperature profile was approximately similar from the cathode to the anode, the electrode form did not play a too significant role. (see chapter 3.3.5.2, Figure 3.3.4)

Vibrational temperature T_v in the TS was determined only with great difficulties. The reason is again the noise, as well as the discharge irregularity which caused an extreme uncertainty of T_v (more than 1000 K). Indeed, the intensities of several spectral bands of the 2nd positive N_2 system are needed for T_v determination, but each spectral band was induced by the emitted light of different pulses, rather distant in time. However, measured values of T_v in both polarities of TS are clearly much higher than T_r; T_v was about 8000 K.

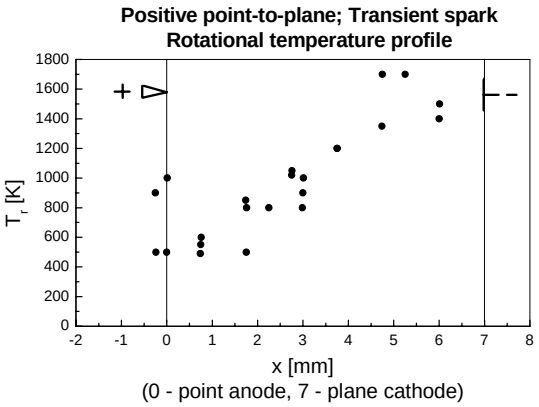

Figure 4.3.5 Rotational temperature profile along the TS discharge channel in positive point-to-plane, average I = 1 - 1.5 mA, f ~ 2 kHz

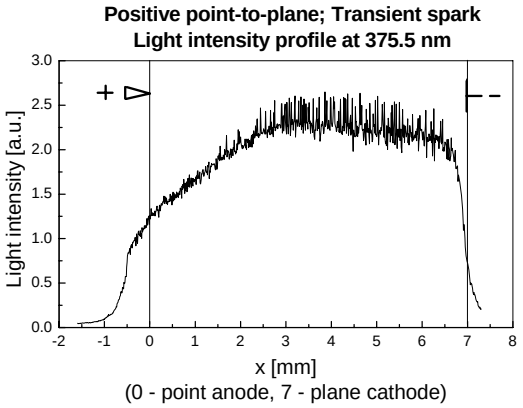

Figure 4.3.6 Light intensity profile along the TS discharge channel in positive point-to-plane scanned at λ=357.5 nm, average I = 1.5 mA, f ~ 2 kHz

4.3.4.3 Light intensity

The profile of the intensity of light emitted from TS was measured along the TS channel (*x*-axis) at 357.5 nm wavelength (peak of 0-1 transition of 2nd positive system of N_2), in the positive TS. (Figure 4.3.6) We observe that the light intensity rises from the point to about x = 2.5 mm, then stays approximately constant and drops at the plane. There is some light emitted even behind the point top. Measured T_r profile agrees roughly with the light intensity profile (see Figure 4.3.5 and Figure 4.3.6)

Change of the interelectrode distance d does not qualitatively influence the light intensity profile.

The measured light intensity profile shows that the TS channel is formed at the point where the electric field is high and propagates to the plane approximately homogeneously.

4.3.5 Plasma generated by the transient spark

Before evaluating the results of the measured values of rotational and vibrational temperatures of the neutral N_2 molecules in the TS, let us discuss the applicability of this spectroscopic approach under the condition of the studied TS discharge.

As mentioned in section 4.3.1, the TS is preceded, some hundred nanoseconds before, by a preconditioned situation established by a streamer discharge. In such condition, Tholl has shown that the transient plasma temperature may reach several tens of thousand degrees. [Tho70] The streamer begins to produce a plasma bridge between cathode and anode due to the crossing of the streamer ionisation wave. The plasma bridge is a cold cylindrical plasma, whose neutral temperature T_g remains during this transition at about 350 to 400 K. The electrons running through this plasma filament have, however, an electron temperature well above the neutral one. Their mean energy reaches 1 to 2 eV, i.e. 7000 to 15000 K (on the basis of a temperature conversion given by $3/2kT_e$). [Mar75] Due to this high mean electron energy, the electrons in the tail of the distribution electron distribution function ionise and excite the molecules, and namely, excite various levels of rotations and vibrations. The large value of the electron energy is due to the small electron energy loss during elastic collisions. The electron energy is mainly consumed by inelastic collisions. Moreover, in air, 90 % of their energy goes towards vibrational excitations, increasing drastically the vibrational temperature of N_2 [Gal79]. Indeed, the number of collision undergone by each electron with neutrals at atmospheric pressure is in the order of 3.10^3 collisions during 10 nanoseconds (on the basis of a mean collision cross section in the order of 1.10^{-15} cm^{-2} and 2 eV). Without collisions between heavy species, the distribution of rotation and vibration levels of the molecules inside the cold plasma column would thus reflect the electron energy distribution, rather than the neutral temperature distribution. Before the transient spark appears, at least some hundreds of nanoseconds, this cold plasma channel prepares the gas inside the path of the transient spark.

The question is now the same as that we raised in the case of HPGD, how this energy stored in the rotational and vibrational levels will react with collisions between heavy species? Since the energies between rotation levels are of the same order of magnitude as the energy corresponding to the neutral speed, a quick relaxation of the rotational energy towards a thermal equilibrium with the neutral species will happen. Thus the rotational temperature of the ground state should quickly relax to the gas temperature $T_g = T$, and the intensity

distribution of the rotational components into a molecular band may be used to derive T_r. [Che94b]

This is however not the case with the level of vibrations. Since the energy between two consecutive vibration levels (for low value of v however) are much larger than the thermal energy, the v-t collisions (i.e. vibration to translation transfer) are very small and rather the v-v (vibration to vibration) dominates. It has been shown that such a situation, where a group of molecules excited vibrationally share their energy through v-v transition (with $\Delta v = +1$ or -1), leads to a vibration distribution of the Treanor type. [Mar86] This distribution is somewhat different from the Boltzmann distribution for high v levels, but is near a Boltzmann distribution for small v levels. In pure nitrogen, the relaxation of vibrational levels at atmospheric pressure requires some hundred of microseconds. With the presence of oxygen, this figure should change only a little (it is mainly with the presence of CO_2, used as pump of $N_2(v)$ in the CO_2 laser, that the vibration of N_2 are quickly destroyed which is not the case here).

The several hundreds of nanoseconds of the filamentary cold plasma existence before the transient spark is thus largely insufficient to allow a relaxation of the vibrational distribution towards T, and thus T_v (determined from low values of v), may be much larger just before the transient spark arise. At high pressure, within the filamentary "pretransient spark" state, the rotational temperature T_r should be near T while the vibrational temperature T_v should be in-between T and T_e.

The vibrational distribution in the excited C states of N_2 molecules will reflect the distribution of the ground state according to the various values of the Frank-Condon factors (given in chapter 3.4.5 Plasma generated by the HPGD). [Ncl62] These factors are non-uniform, thus the upper distribution in the $C^3\Pi_u$ will not have the same shape as the ground state. Furthermore, quenching mechanisms due to the numerous collisions with heavy species will influence the distribution of the vibrational states. The question if these collisions change this distribution drastically and if it is possible to infer the initial ground state vibrational distribution, i.e. T_v, have already been discussed for HPGD (chapter 3.4.5). The same three remarks are applicable for TS. Briefly, (1) quenching effect is mainly due to O_2 collisions which do not drastically change the upper v' distribution [Alb71], (2) the upper state may be produced also from the A or B nitrogen states and (3) overpopulating of the v'=0 state may change the distribution of the v' states which can only lead to a lowering of the value of the apparent T_v [Alb71].

In conclusion, while the value of 8000 K given for T_v in the SPTD case should be taken as an "apparent" vibrational temperature, the real T_v (at least for the distribution in the first v levels) should not be to far from this order of magnitude.

Now we can evaluate correctly the measured rotational and apparent vibrational temperatures T_r and T_v in the TS discharge channel. Experimental results show that $T_r < T_v$ for used parameters of TS (R, C, I) which means that the plasma generated by the TS of both polarities is out of the local thermodynamic equilibrium (LTE). This result might seem surprising, one would expect that the spark-like discharge generates a thermal plasma. However, it is not the case in the transient spark.

To provide a possible explanation of this effect, let us emphasise that the duration of one high current pulse of TS lies into the tens of nanosecond range (max. 100 ns), the spark cannot fully develop as explained in chapter 4.3.1. A created plasma can hardly reach LTE conditions in such a short time. Moreover, the TS discharge works with frequency 1-10 kHz which corresponds to 0.1-1 ms of the relaxation time without the current. There is no thermal source during this "dead" time between two pulses which is 1000-10000 times longer than the spark pulse duration. A corona discharge in its glow regime which is possibly present in the gap as the voltage rises during the relaxation time, even some pre-streamers not leading to the spark pulse are too weak thermal sources to increase the gas temperature.

A comparison of the results of emission spectroscopy from the HPGD and TS demonstrates that the plasma formed in HPGD is more thermal (closer to the LTE) than the TS plasma. It is surprising, but explainable, the HPGD burns continuously with a temperature of ~2000 K in the channel, there is no relaxation time without thermal source. This feature will be shown even later, from the point of view of the plasmochemistry induced by these two types of discharges.

Although the TS generates a non-thermal plasma, the temperature of the neutral particles in the discharge is relatively high (500-1700 K). It is lower than in HPGD, but higher than in typical non-thermal plasmas which operate at high electronic temperature and ambient gas temperature. When TS is applied for the pollution control, the same two basic effects of pollutant treatment probably occur, like in the HPGD (described in chapter 3.4.5 Plasma generated by the HPGD). So, the TS applied for the flue gas cleaning is not a typical non-thermal plasma application, because the thermal effect of generated plasma is also important, it accompanies the effect of electrons and radicals.

The main objective of the spectroscopic measurements, being aimed towards revealing the non-equilibrium plasma state within the TS stage, may be considered as fulfilled.

Finally, let us notice that like in HPGD, we have observed the 1st positive system of N_2 ($B^3\Pi_g$ - $A^3\Sigma_u^+$ transition) in the emission spectrum of TS, though in very low intensity. It confirms that TS generates N_2 molecules in this state. Long living metastable state $A^3\Sigma_u^+$ of N_2 molecule (τ = 1.3-1.9 s [Lof77, She69, Mag92]) is probably important in plasmochemical processes involved in VOC removal, because it can serve as a reservoir of energy. [Han00, Mrv00]. It will be discussed in more details later (chapter 5.3.4.3).

4.3.6 Electrodes treated by the TS

Rhodium point and copper plane as electrodes from the point-to-plane set-up were analysed after the TS treatment by means of optical and scanning electronic microscopy. An interesting result is that there is almost no difference between points, respectively planes, treated either by positive or by negative TS, although they worked either as a cathode or as an anode. We did not observe such effect in HPGD where, on the contrary, regardless to the shape of the electrode, it was treated according to its polarity in the discharge (chapters 3.3.6, 3.3.7). In TS, the electrode polarity is not important, just its shape and probably material. This chapter will be thus divided into two following parts:

4.3.6.1 Rhodium points

The shape of the Rh point electrode has been significantly changed in the TS of both polarities as seen comparing a virgin point (Figure 4.3.7) and the point treated by TS (Figure 4.3.8). The top of the point was “eaten” by the discharge, the longer the discharge operated, the more. Zoomed detail of the point surface shows that it has a rough aspect. Element microanalysis of the point surface confirmed a pure Rh, without any other elements. The point top was cleaned by the discharge. It is probably due to scattering of particles from the point surface caused by electron and ion impact. Electrons or ions (it depends on the point polarity) are accelerated in the high electric field around the most curvatured top of the point. Reduced electric field *E/N* and the flux of charged particles are high in the whole discharge channel during the transient spark phase, also close to the point.

Another possible explanation of the point top sputtering is the temperature effect. Although the discharge temperature at the point was rather low (~ 500 K), it might have been lowered due to the latent heat of metal evaporation from the electrode.

We found a deposit composed of Rh, Cu, O and Si on the side of the point. Si may come from the dust impurities caught on the deposit, but Cu comes from the opposite electrode. It must have been scattered by the discharge or evaporated due to the increased discharge temperature close to the plane (1500-1700 K), and then deposited, respectively condensed (desublimated) on the point side. O is incorporated from air.

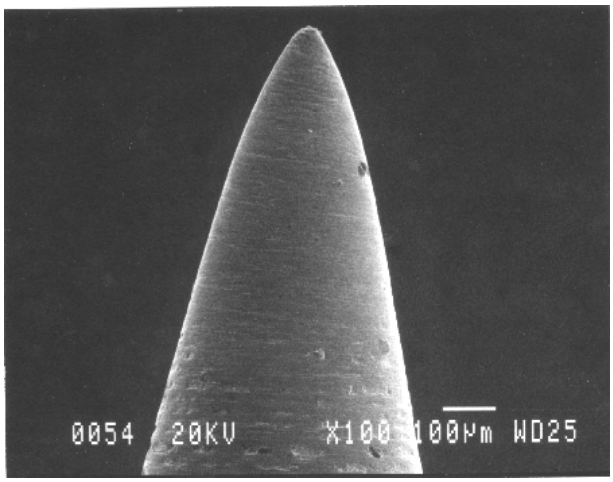

Figure 4.3.7 Electronic microscope photograph of the virgin Rh point, magnification 100

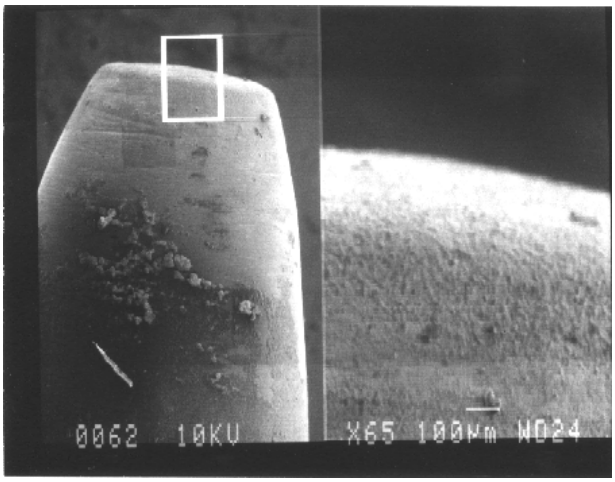

Figure 4.3.8 Electronic microscope photograph of the Rh point treated by positive TS, magnification 65, part in the frame zoomed in the right

4.3.6.2 Copper planes

A thin film of the black-grey deposit has been formed on the surface of the Cu plane electrode in the TS after several minutes of the discharge duration. Microscopic observations show deep craters of irregular shapes in the rough Cu surface with the diameters varying from 30 to 60 μm and depths up to 20 μm. (Figure 4.3.9, Figure 4.3.10)

The deposit around and between the craters has a crystalline structure. Its composition is similar to the deposit formed on the Cu cathode in the positive HPGD, but crystals are not so well developed. The element analysis of the deposit has shown a presence of Cu and O and traces of Si and Rh. Si probably comes from the dust impurities, and Rh from the sputtered point.

The infrared spectroscopic analysis has confirmed the same deposit composition like in HPGD: a mixture of CuO and Cu_2O with a possible presence of a non-stoichiometric Cu_xO_y, the central part of the plane where the discharge channel arrived contained a majority of CuO while further parts of the deposit were composed mainly of Cu_2O. High discharge

temperature close to the plane and electric field are probably responsible for its crystalline structure.

The deposit composition is much more complicated when the TS operates in the atmosphere enriched by some hydrocarbon vapours, there are various organic compounds present. This is in more details discussed in chapters 5.3.5, 5.3.6.

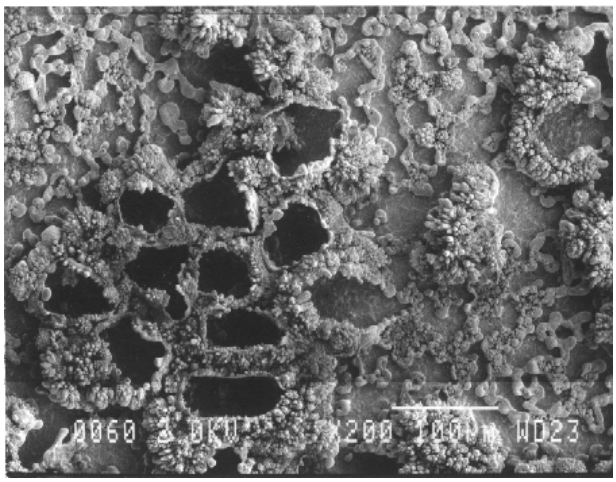

Figure 4.3.9 Electronic microscope photograph of the Cu plane cathode of the positive TS – irregular craters formed by the discharge, magnification 200

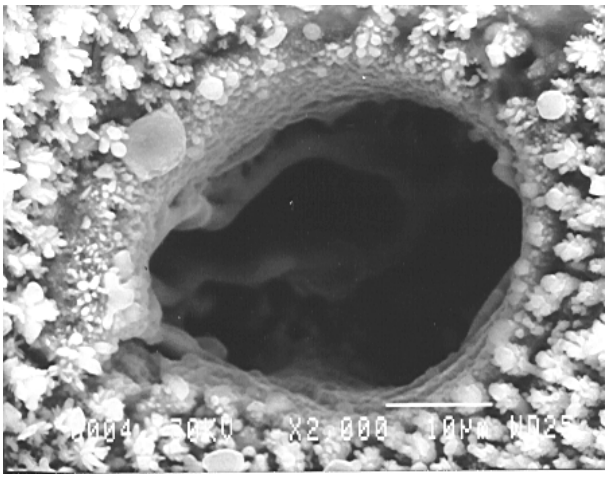

Figure 4.3.10 Electronic microscope photograph of the Cu plane cathode in the positive TS, detail of one crater and crystals formed around, magnification 2000

4.3.7 Transient spark in other environments

4.3.7.1 Humid air, air + VOC, humid air + VOC

When TS of both polarities was applied to the VOC removal, the carrier dry air was charged by various concentrations of VOC (toluene and cyclohexanone), most typically 2000 ppm. We studied also the effect of moisture to the VOC removal process. We ask the same question like in HPGD: do these admixtures influence the features and behaviour of the discharge itself?

The answer is the same like in HPGD, the admixtures of H_2O in air (100% relative humidity, ambient working temperature), VOC (2000 ppm) in air and H_2O and VOC in air (the same concentrations) do not importantly influence the discharge properties of TS. The electric parameters (current and voltage, VA characteristics), as well as the emission spectra

of TS are almost like in air. There is just a small difference in the onset voltage of TS, it is little lower in humid air than in dry air. A presence of VOC also lowers the onset voltage.

Anyway, the TS properties almost did not change when air was humidified or charged by VOC or both. This tells that N_2 and O_2 are the main species playing role in the mechanisms maintaining the discharge, the admixtures have just a minor role. Even more likely, the most important species is electronegative O_2, its concentration determines the process of electron attachment which is responsible for scavenging of the spark pulse.

Deposits formed on the electrodes are the result of the TS-induced plasmochemistry of the VOC removal process, this will be discussed later (chapters 5.3.5, 5.3.6).

4.3.7.2 N_2 + VOC

With regard to interesting results obtained in TS treatment of VOC in the reducing N_2 atmosphere (chapter 5.4.1), and to the results of emission spectroscopy of HPGD in the N_2+VOC mixture (chapter 3.3.8.3), we explored basic electric parameters and emission spectra of TS in the environment of N_2 with 2000 ppm of toluene.

The discharge is less stable, it requires higher onset and operation voltage than in air. Emitted light is of blue colour and very strong intensity, much stronger than in air. In the whole emission spectrum (200-700 nm) we observe bands belonging to the 2^{nd} positive system of N_2 and very strong CN violet system (with the strongest band at 388.3 nm). [Pea50] There are many other bands in the emission spectrum, the same ones like in the spectrum of TS in air and some new ones too. Their identification needs further investigations.

We tried to measure the discharge temperature, but it was not possible, because other bands, especially of CN violet system, overlapped with the bands of N2+ system and changed the background of the N2+ bands.

A black powder deposit grows quickly on both electrodes when TS burns in N_2+VOC atmosphere. The deposit has the same structure and properties as the deposit formed in HPGD in such an atmosphere (chapter 3.3.8.3). This fact implies that the discharge type is not so important in the plasmochemical process of the deposit formation, the discharge probably serves just as a thermal source in it. Such a deposit was formed also in the cylindrical discharge tube used for VOC removal in N_2 atmosphere. (chapter 5.4.1.3)

4.4 CONCLUSIONS

We investigated the transient spark, a new type of a streamer-induced discharge working in the regime of streamer-to-spark transition. It was operated between two metal electrodes of the point-to-plane geometry supplied by a d.c. high voltage in air and some other environments at atmospheric pressure. This discharge has some specific features, mainly short pulses of limited energy, its regime is found somewhere between a non-thermal streamer corona discharge and a thermal arc discharge.

The gas temperature in the discharge channel measured by means of emission spectroscopy is in between 500 to 1700 K, much lower than in arc discharges with $T > 5000$ K, but higher than in a streamer corona. It rises almost linearly from the point to the plane, regardless to the electrode polarity. The generated plasma is out of the local thermodynamic equilibrium. The electric parameters of the circuit, especially the low capacity which is discharged through the discharge gap, are responsible for the transient character of the spark pulse. It results that TS does not develop into an arc and does not reach LTE conditions.

In comparison with the high pressure glow discharge, TS with suitable electric parameters generates colder plasma (further from the LTE) than the HPGD. As well as the HPGD it can be used as a special non-thermal plasma application where medium temperatures are needed, but the plasmochemical processes induced by the TS are different than those induced by the HPGD.

The information obtained from the study of the transient spark, especially the measured temperatures are important from the point of view of the basic approach, as well we the applied research.

5.

APPLICATION OF THE HIGH PRESSURE GLOW DISCHARGE AND THE TRANSIENT SPARK TO THE VOC REMOVAL – LABORATORY APPROACH

5.1 INTRODUCTION

In the two previous chapters we studied the properties of two new types of streamer-induced electric discharges operating in the non-uniform electric field at atmospheric pressure and generating the non-thermal plasma: the high pressure glow discharge (HPGD) and the transient spark (TS). In this chapter we will describe the applications of these two discharges to the removal of VOC. The aim is a basic laboratory research of finding the new methods of VOC removal. We investigated the effects of these discharges in various discharge systems (reactors) and varying many parameters, such as discharge properties, gas flow and gas composition conditions, etc. This large comparative study tends to identify the optimal systems and regimes for the VOC decomposition processes in the frame of various viewpoints (e.g. removal efficiency, energy costs, products). Another important aim of this research was to demonstrate that, under some conditions, the use of these two transition-type discharges is a promising method for flue gas cleaning.

HPGD and TS have until now never been used for the VOC removal, except our preliminary and recent studies. [Mac98a,b,c, Mrv99b, Mac00] The discharge regime close to TS was used for CO_2 and CO depletion by M.Morvová et al. [Mrv98a,b, Mrv99a, Han00] Other similar approaches may however be quoted such as a pulseless atmospheric pressure glow discharge in the capillary reactor used for the dissociation of methane [ChJ93a] and a DC glow discharge at atmospheric pressure in the multipoint reactor applied to the removal of toluene [Aki96]. These two discharges are similar to the HPGD. A pulsed discharge operated in the capillary tube reactor which is electrically similar to the TS was used for the destruction of several VOC (toluene, TCE, etc.) [Koh98].

5.1.1 Types of considered VOC

We used two different organic compounds as VOC representatives in this work: cyclohexanone and toluene. The plasma-induced decomposition of cyclohexanone has not ever been reported. Toluene, on the contrary, is a common VOC representative in plasma applications. Hence, the choice of these two compounds enables to compare obtained results with other techniques (toluene) and to explore unexplored research areas (cyclohexanone). We can also learn if the decomposition processes of these two compounds differ in

macroscopic (result removal efficiency, energy costs, formed products) as well as microscopic level (decomposition reaction pathways, intermediates). This comparison may indicate if the technique is generally applicable for any compound or specific conditions for the treatment each compound must be found out.

5.1.1.1 Cyclohexanone

Cyclohexanone ($C_6H_{10}O$) is a 6-membered cyclic ketone with the cycle in trans-configuration, its chemical structure being shown in Figure 5.1.1 and physical properties viewed in Table 5.1.1. In normal conditions it is a colourless, volatile, unpleasantly smelling liquid.

Cyclohexanone was chosen as a VOC representative from the following three reasons:

1) It is widely used in industry, e.g. for the production of adipic acid, polyamides 6 and 6.6, amino acid lysine and as a solvent for various materials, such as cellulose and its acetates and nitrates, PVC, paints, waxes, fats and lubricants, for the production of glues for PVC, etc. [Bro65] Due to its wide industrial use it often becomes a non-desired indoor and outdoor air pollutant.
2) It is toxic for living organisms, vapours of cyclohexanone cause eye, throat and nose irritation, in higher concentrations it attacks human skin and liver. [Bro65]
3) It has a cyclic but non-aromatic structure. Very few organic compounds of such structure have been investigated in plasma-induced flue gas cleaning treatment. The plasma treatment of cyclohexanone opens a relatively unexplored area of a scientific research. Its behaviour in electric discharges may differ from the aromatic (e.g. toluene, benzene) and the aliphatic (e.g. formaldehyde, acetates, alcohols, aliphatic ketones) VOC which are usually tested in plasma treatment.

As already mentioned, the treatment of cyclohexanone in plasma applications of VOC removal has not been published yet, except our preliminary and recent studies [Mac98c, Mac00]. The only reported similar cyclic non-aromatic VOC treated by plasma are cyclohexene and cyclohexane. Futamura et al. [Fut98] reported cyclohexene destruction in the ferroelectric packed bed reactor with efficiencies up to 80-90 % (increasing with specific energy density, cyclohexanone was present among the by-products in wet N_2). Bailey et al. [Bai92] used a d.c. corona discharge to decompose up to 80 % of cyclohexene and other VOC. Cyclohexane in the mixture with other hydrocarbons comprised in the extracted petrol

was removed up to 80-90 % in the d.c. corona combined with dielectric barrier discharge, reported by Jaworek et al. [Jaw96].

From other ketones, 45-80 % decomposition of aliphatic methyl-ethyl-ketone (MEK) in the silent discharge plasma has been reported by M.B.Chang et al. [ChM97]

Figure 5.1.1 Structural formulae of cyclohexanone and toluene

5.1.1.2 Toluene

Toluene (C_7H_8) is a mono-substituted aromatic hydrocarbon. In normal conditions it is a colourless, volatile liquid with a benzenelike smell. It is insoluble in water but soluble in ethanol, ether, acetone, benzene. Its physical properties are viewed in Table 5.1.1.

Toluene is very widely used in industry, it belongs to the top 50 industrial chemicals. It is prepared by the catalytic reforming of petroleum. It is used above all for the production of benzene, phenol, benzoic acid, then the production of high octane number gasoline, explosive tri-nitro-toluene (TNT) and other compounds. It is used as a solvent for polymers, gums, fats and resins. Toluene together with other aromatic compounds is a typical emission gas from the semiconductor and paint industries too. [ChR88, Bro65]

Due to the wide industry use of toluene many papers deal with its plasma induced destruction. Typically used are techniques with silent discharge plasmas (dielectric barrier discharges). They were successfully applied to the removal of toluene at low input concentrations: 99 % removal at 100 ppm [Fal99], 75 % removal at 300 ppm and energy costs 196 kWh/kg [ChM97], as well as higher concentrations (~2000 ppm): removal efficiencies up to 99 % at various energy densities and energy costs from 158 eV/molecule (46 kWh/kg). [Odi98, Odi99, Par98, Par99]. Pulsed corona discharge and reactors with ferroelectric packed beds were successfully applied for toluene destruction as well. [Yam93, Smu98] DC glow discharge which is not a typical technique used for VOC removal was also tested for toluene with 90 % removal. [Aki96] The electron beam irradiation of various VOC including toluene in the pilot scale lead to 95% removal for single compounds at low concentrations 20-40 mg/m^3 (5-10 ppm). [Pau93]

compound	M_m g.mol^{-1}	T_{boil} °C	p_s (at T) kPa (°C)	ΔH_c kJ.mol^{-1}	ΔH_c eV/molec	W_i eV	MAC ppm	X
cyclohexanone	98.14	155.6	0.6 (25)	-3517.6	-36.3	9.18	50	4.02
toluene	92.14	110.6	2.78 (20) 3.56 (25)	-3910.9	-40.4	8.82	100	3.76

Table 5.1.1 Some physical properties of cyclohexanone and toluene. M_m - molar mass, T_{boil} - boiling point, p_s - saturated vapour pressure at certain temperature T, ΔH_c - enthalpy of combustion (negative values signify exothermic reactions - released heat), W_i - ionisation energy (to form a simple positive ion), MAC - maximum allowable concentration (8 hours per day), X - factor of conversion from ppm to mg.m^{-3} (1 ppm = X mg.m^{-3}, conversion of these units is explained in Appendix 1) **[Bro65, Tim50, Wol72, Lou76, Coo46, Lu92, HCP]**

5.1.2 Characteristics of the VOC removal process

We always used several parameters characterising the VOC removal process (deVOC process) induced by the studied electric discharges: the removal efficiency η, the specific energy density R_V and the energy costs R_m (respectively R_{mol}). Their formulae and the reasons of necessity of their use were already given in chapter 2.4.1. Energetic quantities (R_V, R_m, R_{mol}) can be expressed taking the total energy spent by the whole system or just the energy spent really in the discharges. The first gives a valuable information on the overall energy costs of the technique (we marked R_{Vtot}, R_{mtot}, R_{moltot}), the second one characterises the involved plasmochemical processes induced by the discharges (we marked R_{Vdis}, R_{mdis}, R_{moldis}). The removal efficiency η and energy costs R_m (respectively R_{mol}) were usually referred to the specific energy density R_V, sometimes to the discharge power P_d, gas flow Q, residence time in the discharge chamber τ or initial VOC concentration c_0.

Another important parameter of the deVOC process are formed products in all phases Gaseous products and a part of aerosols get out of the reactor, while liquid and solid products usually rest in the reactor and its pathways. Special chapters will be dedicated to the products in all phases.

5.2 EXPERIMENTAL SET-UPS AND DESCRIPTION OF THE EXPERIMENTS

5.2.1 Discharge chambers and their electric circuits

Two basic and some additional discharge chambers (reactors) have been used for VOC removal process. All of them use a corona geometry with one electrode of small radius of curvature, represented usually by a point. This geometry is necessary for both used discharges: high pressure glow discharge and transient spark.

5.2.1.1 Glass tube reactor with 5 parallel points

A glass tube reactor with 5 parallel Rh points and a common plane Cu electrode (Figure 5.2.1) was a basic reactor for the study of HPGD influences on VOC. It allows to operate from 0 to 5 parallel discharges. The length of the glass tube is 21 cm, its inner diameter 11 mm, the active length (length of the plane electrode) is 14 cm. The points are fixed in teflon buttons, 3 cm distant one from another. Each point is equipped with its own series resistance R (usually 500 kΩ, but also 1.16 MΩ for high gas flow rates), all of them are supplied by one high voltage generator (Universal Voltronics Mintrol, max. 30 kV, 150 mA). The construction allows to change the interelectrode distance for each point.

Total current from all operated discharges was measured by an oscilloscope (500 MHz Tektronix TDS 544 A) on a 50 Ω resistance. The discharge voltage was measured by the HV probe Tektronix T6015 A (1/1000, 3 pF, 100 MΩ) leading the signal to the same oscilloscope. It allowed to evaluate various functions of signals lead to their channels, e.g. a power $P=UI$ or energy $E=\int UI\mathrm{d}t$. The mean values of the generator voltage and the total current were measured by d.c. meters comprised in the generator.

The internal capacity of the 5-parallel-points glass tube reactor is about 3 pF. Such small capacity is not able to sustain the transient spark, thus when we operated the TS in this reactor, additional external capacitors with C_{ext}=15 pF were added to each point. The electric scheme of such set-up of this reactor is analogous to the one point reactor used for emission spectroscopy, see chapter 4.2, Figure 4.2.1. Use of the signal attenuator was often necessary for the oscilloscopic detection of TS current pulses which were too intense, over the range of the oscilloscope.

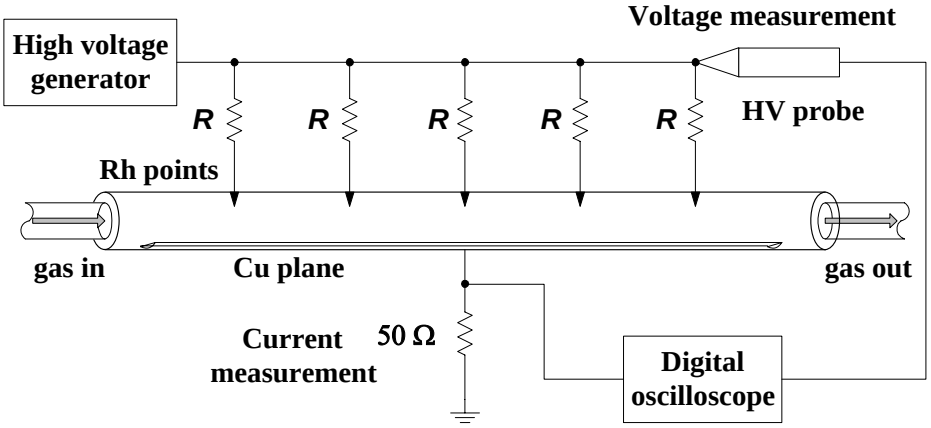

Figure 5.2.1 Glass tube reactor with 5 parallel points and its electric circuit

5.2.1.2 Copper tube with threaded rod electrode

This discharge chamber is a special modification of a coaxial corona configuration: a rod with a thread M6 (diameter 6 mm) as a high voltage electrode inside the cylinder electrode. Both rod and cylinder are made of Cu, inner diameter of the cylinder is 21 mm, interelectrode distance d = 7.5 mm, active length (length of the Cu tube) of the discharge tube is 50 cm. The ends of the tube are equipped with teflon cylinders with holes for gas inlet and outlet. The internal capacity of the tube is approximately C_{int} = 30 pF, usually we did not use any additional external capacity. This discharge chamber has already been described in chapter 4.2, Figure 4.2.2, it was developed in Bratislava but its copy was used also in Gif sur Yvette.

The Cu-tube reactor was supplied by a d.c. HV generator (Universal Voltronics Mintrol, max. 30 kV, 150 mA or DEL RHVS Series, max 60 kV, 5 mA, used in Gif sur Yvette; or Baur PGK 70, max 60 kV, 20 mA, used in Bratislava). We used the external resistance R ranging from 2 to 7 MΩ. Total current from the discharge was measured oscilloscopically (500 MHz oscilloscope Tektronix TDS 544 A) on the 50 Ω resistance. The discharge voltage was measured by the HV probe Tektronix T6015 A (1/1000, 3 pF, 100 MΩ). The mean values of the generator voltage and the total current were measured by d.c. meters comprised in the generator. It was often necessary to use the signal attenuator for the oscilloscopic detection of TS current pulses, because the pulses were sometimes too intense, over the range of the oscilloscope.

5.2.1.3 Additional discharge systems

Some additional discharge systems were used in the experiments aimed at VOC removal.

- Two 5-parallel-points glass tube reactors in series were used for operating more than 5 discharges (HPGD), usually 10. A function of 1, 2, 5 or 10 discharges and their influences to the plasmochemical process of VOC removal were compared. Two glass tube reactors were identical, put in series, i.e. the treated gas was lead from the outlet of the first one to the inlet of the second one. They were supplied from one HV generator (Universal Voltronics Mintrol, max. 30 kV, 150 mA), each point had its own resistance *R*. The discharge current and voltage were measured by the same way like in the case of one glass tube reactor.

- Glass tube reactor with 5 serial points was developed for HPGD, in order to decrease energy losses in the resistances *R* of each point. Its scheme is shown in Figure 5.2.2. The principle of its function are very simple: the applied potential drops at one point-to-plane with the formation of the HPGD in this gap, while the other receive the remaining potential, i.e. an increased potential which forces the other gap to pass, successively in the HPGD phase. Each plane (except the last one) is connected with the next point so that we have just one simple circuit with one series resistance *R* (usually 530 kΩ). In other words, the discharge gaps are put in series. Our system is constructed with 5 serial discharges. Energy losses in such a system are 5 times lower than in the reactor with 5 parallel points. We operate 5 discharges at the same time, either positive or negative HPGD, according to the polarity of the voltage applied on the first point.

  There is another advantage of this system, the middle ”point-planes” (electrodes on the floating potential) can be turned inside the tube in various directions, forming a ”star section”. Though the interelectrode distances are a little decreased by this way, the gas passing through the reactor is better treated, the molecules have greater chance to pass through the discharge channel. This was not possible in the tube with 5 parallel points and one common plane where all discharges were in one plane.

  A disadvantage of this system is that it requires rather high applied voltage, especially for the first breakdown leading to the ignition of discharges (more than 40 kV when gap distance is set to 7 mm). We had to use the high voltage generator DEL RHVS Series giving up to 60 kV, but maximal current 5 mA. The discharge current and

voltage were measured by the same way like in the glass tube reactor with 5 parallel points.

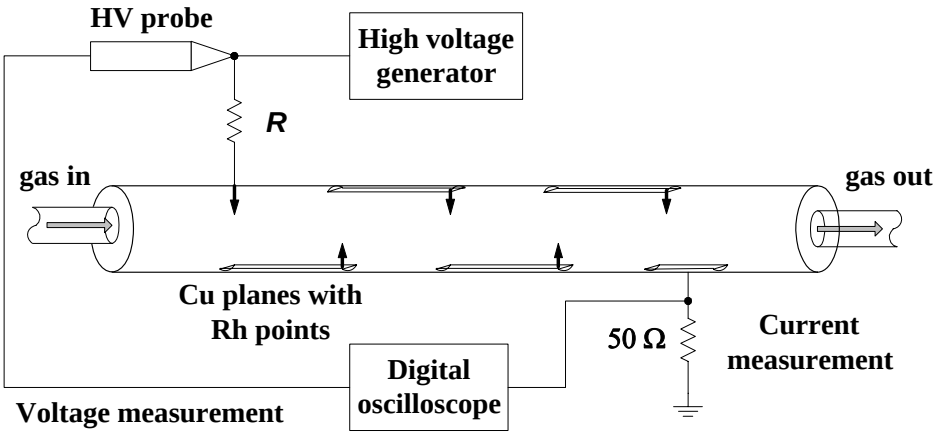

Figure 5.2.2 Glass tube reactor with 5 points in series developed for the lowering of energy losses in HPGD.

- Transparent discharge chamber with threaded rod electrode is a special modification of the Cu tube with threaded rod electrode (diameter 6 mm) which is adapted for operating of HPGD. It is and made of Plexiglas with rectangular cross section (2 × 3.5 cm). The advantage of this discharge chamber is that the front walls are transparent which enables visual observation of the discharge, rather important for HPGD. Two copper planes as low voltage electrodes are fixed on the side walls (inside of the chamber), they are grounded. The interelectrode distance is 7 mm (from rod to each plane). Total length of the chamber is 80 cm, active length 50 cm. The value of external resistance R = 300 kΩ was usually used for HPGD.

5.2.2 Gas flow system, gas composition and setting of VOC concentrations

Experiments aimed at VOC destruction were carried out in the flowing regime, Figure 5.2.3. A dry air was used as a carrying gas in most of experiments. The air flux was divided into two or three branches controlled by the flowmeters with different ranges. We used flowmeters Sho RATE Brooks in France, types Carboloy R2 15B (0.5-6 l/min), Tantale R2 15 AA (0-0.5 l/min), Glass R2 15 AAA (0-3.3 l/h) and ELMES Rožnov in Slovakia (ranges 0-1, 0.2-2, 4-21, 10-85 l/min).

One branch controlled by a flowmeter with a small range passes through a bubbler with a liquid VOC. The air passing here is enriched by VOC vapours at their saturated vapour

pressure. Another branch can optionally pass through the bubbler with water. It enriches the passing air with water vapours at their saturated pressure. The adjustment of the flowmeters enables to change the resulting VOC and H_2O concentration in the gas. Usually, when we worked with humid air we let all the carrying air enrich by H_2O vapours, except the part passing through the VOC, the relative humidity of air was close to 100 % at given temperature.

The three branches are rejoined in the mixing chamber before passing to the discharge reactor. The total gas flow value can be varied as well.

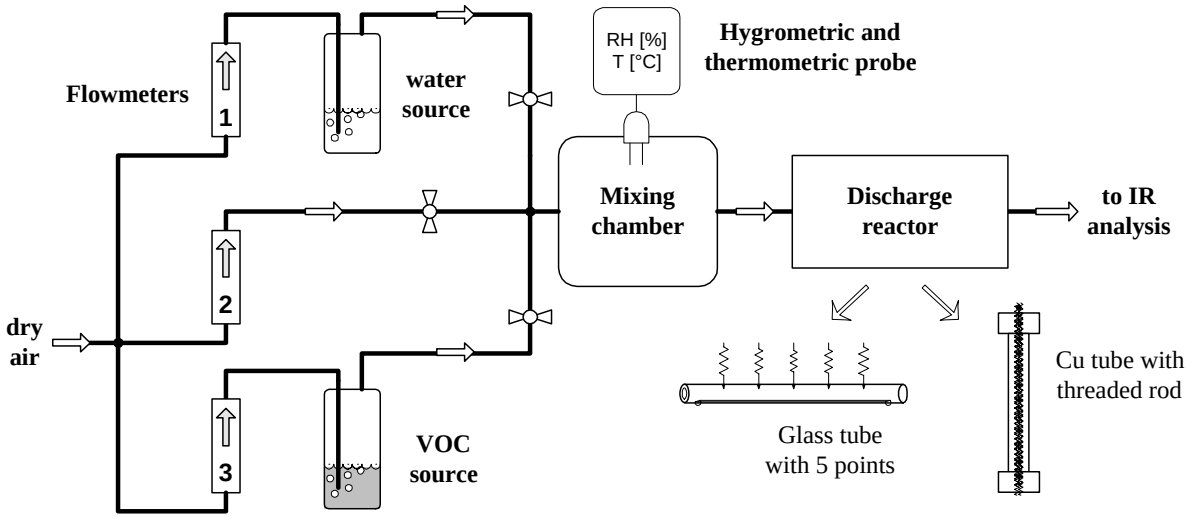

Figure 5.2.3 Gas flow system for flowing regime. Usual ranges of flowmeters: No 1,2 - 0.5-6 l/min, No 3 - 0-0.5 l/min. Additional discharge reactors were used as well.

Again, as already said, we used two VOC components: toluene and cyclohexanone. The concentration of VOC has been calculated from the absorbance of certain calibrated characteristic bands in their IR spectra (explained in section 5.2.5.1). The calibration was based on the saturated vapour pressure of VOC (toluene: 2780 Pa at 20 °C and 3560 Pa at 25 °C, cyclohexanone: 599 Pa at 25 °C). The maximal obtainable concentration at room temperature (25 °C) is approximately 35000 ppm for toluene and 6000 ppm for cyclohexanone. Typical used VOC concentrations were from 500 to 6000 ppm. The temperature *T* and the relative humidity (*RH*) were measured in the mixing chamber by a capacitive hygroscopic and thermometric probe Hanna HI 8564 (± 0.4 % in the *T* range of 0-100 °C; ± 2% between *RH* = 5-95 %).

The IR absorption spectrometer used in France and its gas cell were adapted for dynamic analysis of the gas flowing through the cell. (Figure 5.2.3) In Slovakia, we used two gas cells collecting samples of the non-treated gas in front of and treated gas behind the discharge chamber. Such a sample acquisition was chosen to profit of the double-beam spectrometer allowing measurements of real concentrations (scanned spectrum was referred to the reference spectrum specific for each measurement, no to the background spectrum acquired before the experiment itself). Another reason was the spectrometer sensitivity - high noise caused by the discharge when the spectrometer worked at the same time.

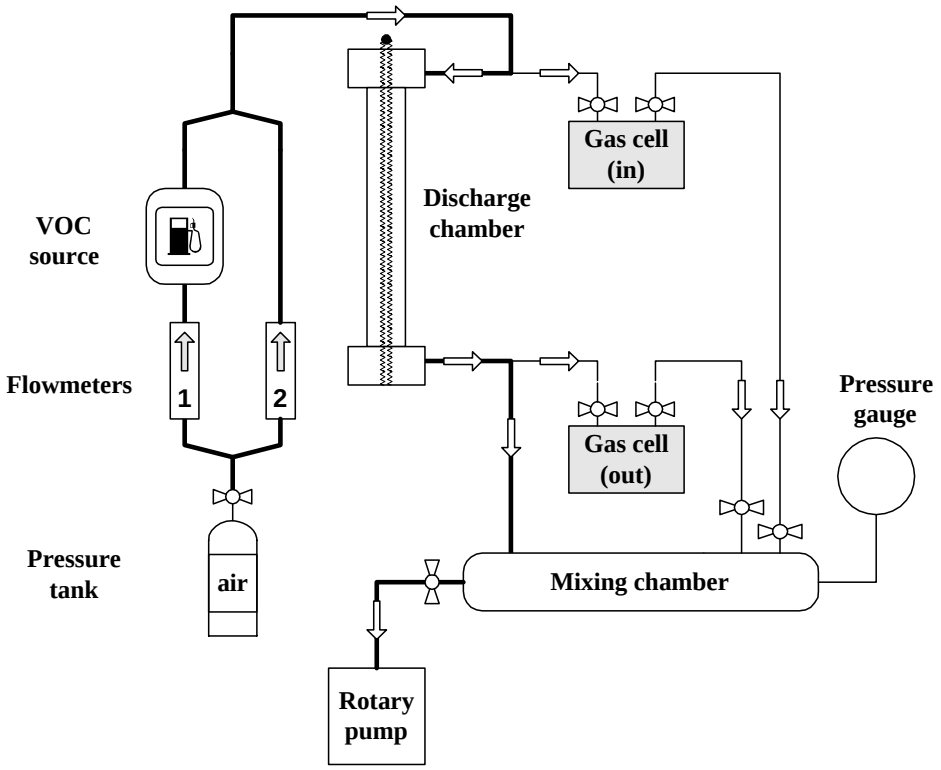

Figure 5.2.4 Gas flow system adapted for the isokinetic sample acquisition

Anyhow, simple putting of the gas cells in front of and behind the reactor causes some gradients of the pressure in the whole flowing system, especially during their closing as samples are acquired. This is significant in particular for high gas flow rates, the overpressure in the parts before the gas cells can change the gas flow rates and cause other problems, e.g. leakage. Therefore we applied an isokinetic acquisition of samples, i.e. the ”in” and ”out” gas cells were on two by-passes linked to the main flow system including the discharge chamber. (Figure 5.2.4) The gas flow through the by-passes is many times lower than in the main system, keeping the same flowing speed everywhere, therefore closing of the gas cell valves

does not affect the flowing parameters of the main system. The whole system is pumped by the rotary pump in order to control the atmospheric pressure everywhere. Furthermore, the isokinetic sample acquisition is the only which is recognised by the law and the environmental policy.

5.2.2.1 Other environments - oxygen rich and oxygen poor atmospheres

Most of the measurements aimed at VOC removal in electric discharges were primarily effectuated in dry or humid air charged by various concentrations of VOC. In normal air the nitrogen to oxygen ratio is approximately $N_2/O_2 = 78/21$. With the aim directed towards a better understanding of the role of oxygen and oxidising reactions in the VOC removal process, especially of the processes occurring in reducing atmosphere, we have done some additional measurements in the atmosphere of N_2 and O_2 with the following ratios: $N_2/O_2 = 70/30$ (oxygen rich), 95/5 (oxygen poor) and 100/0 (pure N_2). These gas mixtures were charged by VOC (2000 ppm of toluene) and sometimes also by moisture (100% relative humidity).

N_2 and O_2 were taken from the pressure tanks, their ratios were set by the adjustment of the flowmeters. We used the same gas flow system and dynamic analysis like in the experiments performed in air.

5.2.3 Diagnostics

5.2.3.1 Infrared absorption spectroscopy

The infrared (IR) absorption spectroscopy was used as a main diagnostic method. Its general theoretical bases are described in Appendix 3.

In France we used one-beam Fourier transform infrared spectrometer (FTIR) Bruker IFS 45 working in the middle infrared region (4000-600 cm^{-1}, best resolution 0.5 cm^{-1}) controlled by a PC (software OPUS). A 10 cm long gas cell made of brass with KBr or CaF_2 windows or the long-path gas cell made of boro-silicate glass with adjustable optical length 0.8-8 m, gold mirrors and ZnSe windows were used for the gas phase analysis. The long path cell (Figure 5.2.5) allows to detect very low concentrations of gas-phase by-products. Each measured IR spectrum was a difference spectrum referred to the background acquired before, in the gas cell filled with dry (humid respectively) air. The spectrometer was equipped with the infrared microscope able to work in transmission or reflection regime. It allowed to

analyse samples in the solid or liquid phase and the surfaces, especially deposits formed in the deVOC process and surfaces of treated electrodes.

In Slovakia we used double-beam dispersive spectrometer SPECORD M 80 Carl Zeiss Jena working in the middle and far infrared region (4000-200 cm^{-1}, usual resolution 1-2 cm^{-1} depending on the wavenumber) with the beam polarizator (0.1°) and the attenuator of the reference beam (precision 0.01 %). Its basic function is an analysis of gas samples in the 10 cm gas cells with windows of various available materials (KBr, CaF_2, KRS-5, CsI, polyethylene, etc.). It is also equipped by many additional devices which enlarge its functions to the complete analysis in all phases, namely:

- liquid cells using CaF_2, KRS-5, CsI and polyethylene windows for the analysis of liquids,
- device and crystals (KRS-5, Ge) for attenuated total reflectance (ATR) technique (angles of incidence 45° and 60°) used for the analysis of liquids, Figure 5.2.6
- device (pellet press) and accessories for KBr pellet technique used for the analysis of solids,
- device for the technique of reflection spectroscopy used for the analysis of surfaces. Figure 5.2.7.

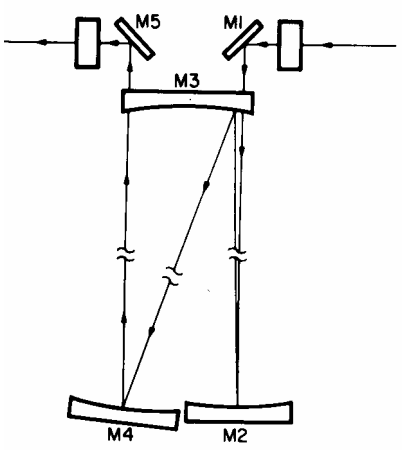

Figure 5.2.5 Scheme of a long path gas cell. M1, M2, M3 and M5 are fixed mirrors, M4 is an adjustable mirror. Its position determines the number of reflections, hence the optical length of the cell.

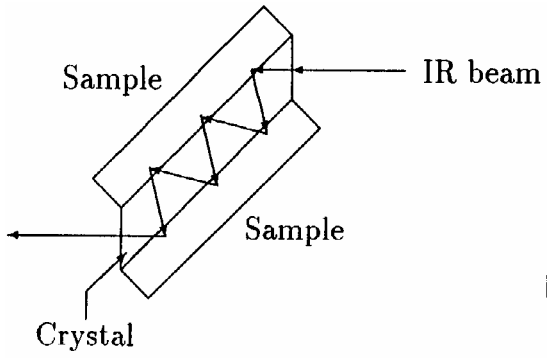

Figure 5.2.6 Scheme of the attenuated total reflectance (ATR) device. Multiple total reflectance occurs in the crystal with high refraction index, the penetration of the beam into the sample is in the order of the radiation wavelength **[Hol75].**

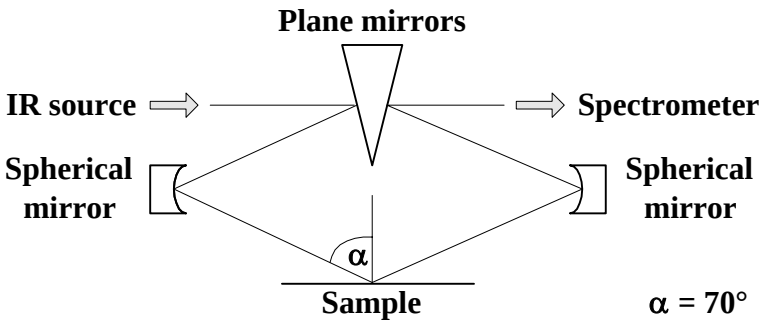

Figure 5.2.7 Scheme of the device for reflection spectroscopy with 70° angle of incidence.

The advantage of a double-beam spectrometer (e.g. Specord M 80 used in Slovakia) is that the scanned spectrum is always compared to the reference one, while in one-beam spectrometers (e.g. Bruker IFS 48 used in France) we scan the reference spectrum before the measurements. If the one-beam spectrometer is not hermetically closed (which is a usual case) we often observe fluctuations of the concentration of some gases, e.g. CO_2 and H_2O. These concentrations change with a number and a position of persons breathing in the laboratory. This occurs even when the spectrometer is purged by dry air or N_2. Another advantage of Specord M 80 was its wavenumber range enlarged to the deformation region (700-200 cm^{-1}), thus more information obtained from the spectra. Also we had greater choice of window materials and better possibilities for complex analysis in all phases.

On the other hand FTIR Bruker IFS 48 is much faster, one spectrum acquisition takes about 45 s, while on Specord M 80 it takes about 23 min (due to this long acquisition time we had to modify the gas-flow system used in Slovakia, remind chapter 5.2.2). It has a better spectral resolution too, to improve the resolution on Specord M 80, the acquisition time had to be even increased. The long path cell available in France is a great advantage for gas-phase analysis as well. And finally, the work on Bruker IFS 48 is much more comfortable because it is controlled by a PC and the spectra are directly PC-processed.

5.2.3.2 Microscopic techniques

The electrodes treated by discharges and the deposits formed on them were analysed also by microscopic techniques. We applied optical microscopy (optical microscope Reichert Austria Me F2 with maximum magnification 1000) and scanning electron microscopy (SEM) with X-ray element microanalysis (scanning electron microscope Jeol JSM-840 equipped with the Kevex superdry X-ray detector). The electronic microscope allowed to obtain also

the image formed by the backscattered electrons (BE) which gives additional information to basic scanning electron (SE) image. BE image gives a valuable information on relative proportions of atomic number *Z* in the sample, lighter places indicate higher *Z* and darker ones indicate lower *Z*.

5.2.4 Some experimental problems and tricks in infrared analysis

IR absorption spectroscopy is a diagnostic method which covers a large variety of analysed samples practically in all phases, the more equipment is available the larger are possibilities. However, besides the knowledge of chemistry and the theory of molecular vibrations, it requires a lot of experience with interpretation of spectra, as well as certain experimental skills. In the following we will note some experimental problems that we met in the experiments and some methods of their solution and other tricks.

5.2.4.1 Choice of windows used in gas-phase analysis

Good choice of IR transmission windows for gas cells is needed to analyse correctly the gas samples. Possible interactions of analysed gases with the window material must be kept in mind. For example, KBr windows, which are very common in IR spectroscopy and have low absorption within the wide wavenumber range (4000-400 cm^{-1}). They are hygroscopic, i.e. they are not suitable for samples where water vapours are present. Another inconvenience is that KBr reacts with NO_2 or HNO_3 to form KNO_3 on the window surface, as reported by Hensel et al. [Hen96]. We have observed a formation of this deposit with a characteristic broad band at 1360 cm^{-1} which arised in the IR spectrum. Its formation decreases the concentration of the really produced NO_2 so that the new IR band deforms, respectively covers other important bands in the spectrum.

H_2O and NO_2 are often present among the gas products in the deVOC processes. Furthermore, we performed many experiments in the humid air. Hence, since KBr windows were not suitable for gas-phase analysis, we preferred CaF_2 windows. However, CaF_2 have a narrower range of transmissivity in IR (4000-1000 cm^{-1}) and we lose the part of the spectrum below 1000 cm^{-1} which can include several important bands facilitating the analysis. Due to this reason we used KRS 5 windows (TlI/TlBr) in experiments performed in Slovakia (they were not available in France). These windows are chemically inert and have a larger range of transimssivity in IR (4000-200 cm^{-1}). Their inconvenience is that they have relatively high

absorption of the transmitted radiation which decreases the background and increases the noise. To eliminate this effect as far as possible we used the reference beam attenuator.

5.2.4.2 Use of the long path cell

The long path gas cell with adjustable length (0.8-8 m) was used with Bruker IFS 48 spectrometer in some of the experiments performed in France. We can detect gas species in several times lower concentrations than in usual 10 cm gas cell. Although it seems much better than a 10 cm gas cell, there are some disadvantages.

Firstly, opening and cleaning of the interior of this cell is an extremely complicated and expensive operation, thus all liquid or condensed phase deposits inside the cell have to be avoided. The cell itself has to be equipped with an effective purge system and purged after every measurement.

Secondly, to analyse correctly the gas composition we have to let pass such a volume of the gas which is about 10 times bigger than the volume of the cell, in order to achieve an equilibrium state. The total volume of the used long path cell (3 1) is much greater than the volume of the used 10 cm gas cell (31 ml). In consequence, at low gas flow rates it takes a long time to achieve an equilibrium in the long path cell (e.g. for Q = 0.5 l/min it takes 1 h!). Too long ”equilibration time” increases the total time of an experiment which is rather disadvantegeous.

Due to these reasons we used the usual 10 cm gas cell in most of the experiments of VOC removal, the long path cell was applied just to verify the gas by-products appearing in trace amounts.

5.2.4.3 Analysis of the solid and liquid products

We used some experimental tricks to analyse the deposits formed on the electrodes and inside the reactor and leading pipes. The plane electrodes have been analysed directly by a reflection spectroscopy using IR microscope or the reflection device. One way to analyse deposits was to put clean metal planes behind the reactor, the deposit was caught on them and than easily analysed by the reflection spectroscopy.

Other deposits on the reactor walls or in the pipes were dissolved in acetone, ethanol or water. This solution was then dropped either onto the cleaned KBr window (when dissolved in acetone) or Al mirror (when dissolved in ethanol or water) and let to evaporate.

The deposit which rested on the window (mirror respectively), was then analysed in transmission (reflection respectively).

Another way of the deposit analysis was to drop its solution into the Petri dish, evaporate the solvent, mix the deposit with dried KBr powder, prepare a KBr pellet in the special press and to analyse this pellet in transmission. A direct liquid-phase analysis of the solution by ATR technique is always possible, but it requires subtracting the solvent from the spectrum. Pure spectrum of exactly the same amount of the solvent has to be acquired before.

The solid product analysis was more complicated when we used Cu discharge tube, we could not analyse the electrode surface directly. The method of the deposit dissolving was applied, but in order to verify if we did not lose any component of the product possibly attached to the electrode surface we fixed a piece of an adhesive Cu tape in several places inside the tube electrode. This tape was then analysed in reflection.

A special care is required for the analysis of the deposits, especially when various solvents are used. In order to exclude possible interactions of the product with the solvent we performed the analysis of the same sample by several methods and the results were compared.

5.2.5 Calibration of some infrared bands

Infrared absorption spectroscopy was used as the only and sufficient gas-phase diagnostic technique in all experiments aimed at VOC removal in electric discharge. A calibration of infrared (IR) bands of all concerned species was therefore indispensable. Whenever an IR band of a certain compound is calibrated, in most of cases we can determine the extinction coefficient ε specific for this band and then calculate the concentration of the compound using Lambert-Beer law (Appendix 3 Formula A.3.12). Some cases where Lambert-Beer law is not valid may appear (e.g. CO_2 at high concentration), but they are rather rare.

5.2.5.1 Calibration of IR bands of VOC

Examples of calibration IR spectra of studied VOC, i.e. toluene and cyclohexanone, are shown in Figure 5.2.8, Figure 5.2.9. The most important spectral bands of these two compounds and their interpretation are shown in Table 5.2.1.

The VOC concentration was calculated from the absorbance of certain characteristic IR bands using Lambert-Beer law. For toluene we have done a calibration of ν CH band at

3040 cm^{-1} with exact concentrations of toluene (based on exact temperature measurement and calculation of saturated vapour pressure at various gas flow rates) resulting in determination of the extinction coefficient. This coefficient differs from one spectrometer to another, mainly due to their different resolutions. The efficiency η of toluene removal was checked in every case from the decrease of the bands and ν_{as}, ν_s CH_3 at 2950 and 2880 cm^{-1} and the skeletal ring bands ν_{ring} at 1610 cm^{-1} and 1500 cm^{-1}.

The same procedure of calibration was applied to cyclohexanone, we have calibrated the most intense bands in its IR spectrum, ν_{as} CH_2 at 2940 cm^{-1} and ν C=O at 1740 cm^{-1}. The efficiency η of cyclohexanone removal was additionally checked from the decrease of the bands γ CH_2 band at 1224 cm^{-1} and the band of the skeletal vibration of cyclohexanone cycle ν_{cycle} at 1125 cm^{-1}.

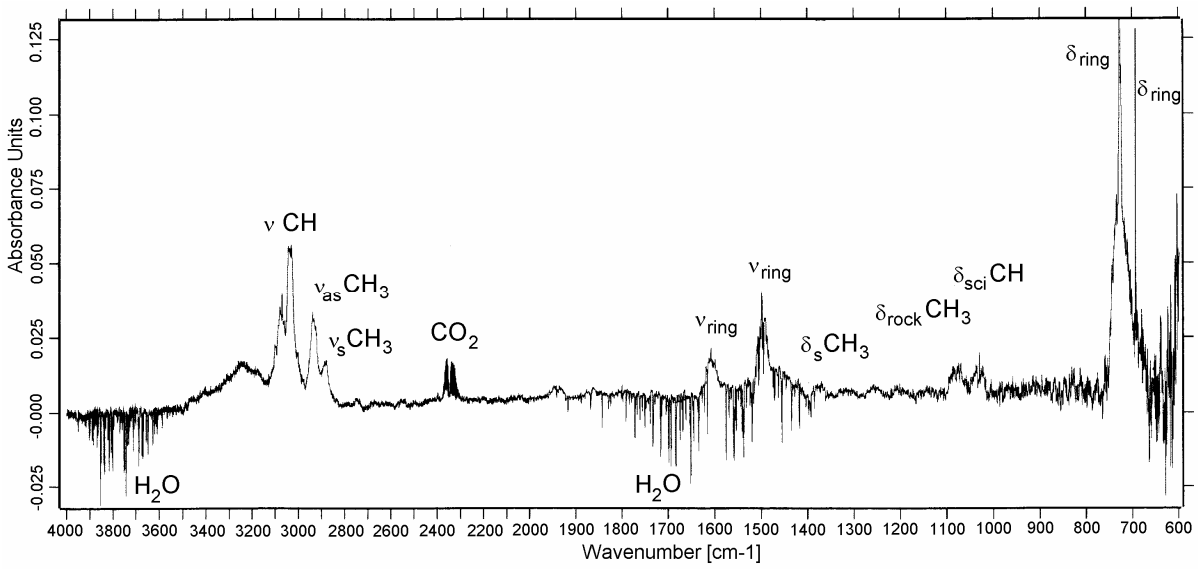

Figure 5.2.8 Toluene (~2000 ppm) in dry air. Absorbance spectrum scanned on Bruker IFS 48 spectrometer with interpretation of the bands. CO_2 and negative H_2O bands appeared due to the difference with the reference spectrum.

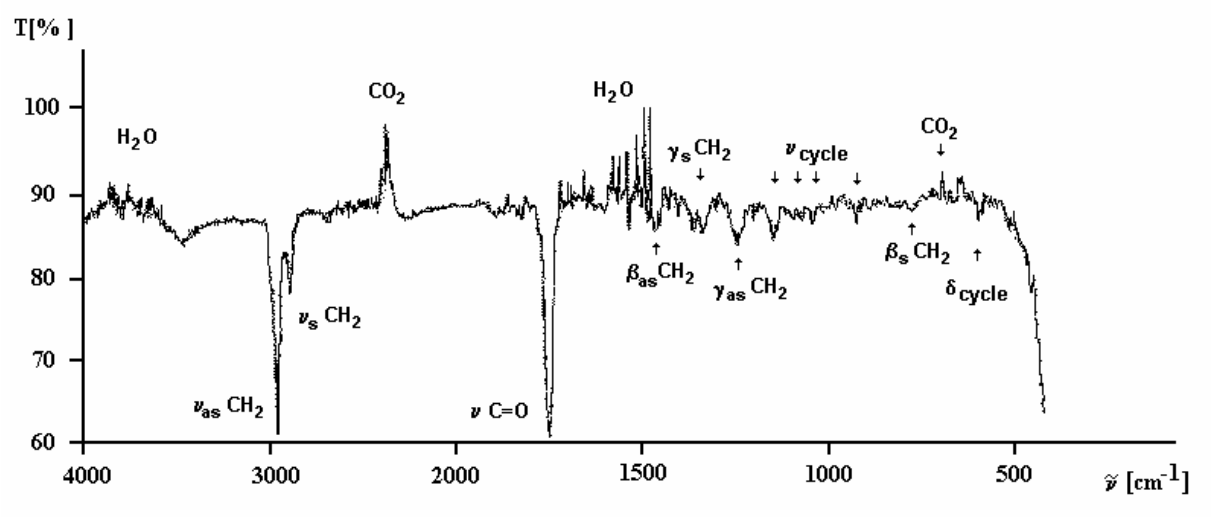

Figure 5.2.9 Cyclohexanone (~6000 ppm) in ambient air. Transmittance spectrum scanned on Specord M 80 spectrometer with interpretation of the bands. Negative CO_2 and H_2O bands appeared because their concentrations were lower than in the reference beam.

TOLUENE			CYCLOHEXANONE		
ν [cm^{-1}]	Intensity	Group vibration	ν [cm^{-1}]	Intensity	Group vibration
3040	vs	ν (C_{arom}-H)	2950-2930	vs	ν_{as} (CH_2)
2940	s	ν_{as} (CH_3)	2880-2860	s	ν_s (CH_2)
2885	m	ν_s (CH_3)	1745-1710	vs	ν (C=O)
1604	s	ν_{ring} Kekule	1450-1425	m	δ_{sci} (CH_2)
1500	s	ν_{ring} Kekule	1340-1309	m	δ_{wag} (CH_2)
1379	m	δ_s (CH_3) umbrella bend	1221-1220	m	δ_{twi} (CH_2)
1081	m	δ_{sci} (C_{arom}-H)	1118-1115	m	ν_{cycle}
1030	m	δ_{rock} (CH_3), δ_{sci}(C_{arom}-H)	908	w	ν_{cycle}
728	vs	δ_{wag} (C_{arom}-H)	750	w	δ_{rock} (CH_2)
694	s	δ_{ring}	490	w	δ_{cycle}
464	m-s	δ_{ring}			

Table 5.2.1 Characteristic IR bands for toluene (left) and cyclohexanone (right). Typical intensities and corresponding group vibrations.

Determined extinction coefficients ε characteristic for spectrometers Bruker IFS 48 (France) and Specord M 80 (Slovakia) are given in Table 5.2.2.

5.2.5.2 Calibration of IR bands of other gases

The procedure of calibration of IR bands was applied also to other gases which often appear as products of VOC decomposition process (CO_2, CO, H_2O vapours, NO_2, NO, N_2O,

HNO_2, HNO_3, O_3, HCN, HCHO, C_2H_2). For some of these gases we have used the extinction coefficients characteristic for the same Bruker IFS 48 spectrometer (France) given by E.Odic and L.Parissi [Odi98, Par99]. We had to make ourselves the calibration of the species on Specord M 80 spectrometer (Slovakia) and the calibration of some of them on Bruker IFS 48 as well (HCN, C_2H_2, and especially CO_2, the next chapter (5.2.5.3) is dedicated to the CO_2 calibration). All result extinction coefficients obtained on both spectrometers are listed in Table 5.2.2.

Spectrometer	Bruker IFS 48			Specord M 80		
molecule, band	$\nu = 1/\lambda$ [cm^{-1}]	ε [cm^{-1}]	Detection limit [ppm]	$\nu = 1/\lambda$ [cm^{-1}]	ε [cm^{-1}]	Detection limit [ppm]
toluene ν CH	3040	1.915 *	60	3040	0.85	150
cyclohexanone ν_{as} CH_2	2945	8.6	10	2940	3.24	50
cyclohexanone ν C=O	1745	8.79	10	1740	3.4	50
CO_2	2360	30 **	4	2360	23.6	10
CO	2170	5.1 *	20	2170	2.1	50
H_2O	3853	5	20			
NO_2	1630	20.58 *	5	1650	27	10
NO	1900	2.77 *	40	1920	1.4	100
N_2O	2235	17.8 *	7			
HNO_2	1263	53 *	2			
HNO_3	1325	13.4 *	8			
HCHO	2778	4.3 *	20			
O_3	1050	4.66 *	25			
HCN	3331	4.7	25			
acethylene	3320	8	10			

Table 5.2.2 Calibration of characteristic IR bands on two spectrometers (Bruker IFS 48 used in France and Specord M 80 used in Slovakia). Characteristics band wavenumbers ν, extinction (absorption) coefficients ε and detection limits (in 10 cm gas cell) for certain species in gas phase.

****Extinction coefficient taken from [Odi98, Par99]***

*****Extinction coefficient for CO_2 valid for concentrations below 5000 ppm only, explained in chapter 5.2.5.3.***

5.2.5.3 Calibration of the CO_2 bands

The concentration of produced CO_2 was rather high (more than 10000 ppm) in some experiments with high VOC concentrations treated by discharges with high energy density. The CO_2 bands in IR spectra detected on Bruker IFS 48 spectrometer behaved strangely at such high concentrations of CO_2. It seemed that the Lambert-Beer law was not obeyed. This was the reason to redo an exact calibration of all CO_2 bands in 4000-1000 cm^{-1} region, i.e. the

main doublet band (ν CO_2) at 2350 cm^{-1} (2360 and 2340 cm^{-1}), its shoulder at 2270 cm^{-1} and two overtone doublets at 3727 and 3625 cm^{-1}. Concerned CO_2 bands are shown in Figure 5.2.10. The region below 1000 cm^{-1} (with important triplet band δ CO_2 at 667 cm^{-1}) was omitted, because we were obliged to use CaF_2 windows not transparent below 1000 cm^{-1} due to high concentrations of NO_x produced together with CO_2 at high energy densities of discharges (explained in chapter 5.2.4.1).

The results of this calibration are shown in Figure 5.2.11. The dependence of the absorbance *A* on the CO_2 concentration is almost linear up to approximately 5000 ppm for all bands. The less intense auxiliary bands (2270, 3727 and 3625 cm^{-1}) show a linearity up to about 10000 ppm (=1 %). In the linear region, the Lambert-Beer law is obeyed and we can calculate the extinction coefficients ε characteristic for each band, ε for the main band at 2360 cm^{-1} is given in Table 5.2.2. In the interval of concentrations 5000-10000 ppm we can eventually use auxiliary bands with lower intensity. However, this is not always easy, because 3727 and 3625 cm^{-1} bands often overlap with the bands of water.

The situation is more complicated at higher concentrations (above 5000 ppm for 2350 cm^{-1} doublet and 10000 ppm for less intense bands) where we observe a saturation effect of the absorbance as a function of CO_2 concentration. The Lambert-Beer law is valid just within a certain concentration range, specific for each absorption band. [Hol75] Too high CO_2 concentration are beyond the range of its validity, thus we cannot determine the extinction coefficient because it is not constant. The way to learn the CO_2 concentration from the measured absorbance is to calculate it from the equation determining the polynomial curve interpolating the calibration results. This curve and its equation are specific for each band. However, we cannot use this interpolation curve for low concentrations, the concentration *c* calculated form the curve is negative when the absorbance *A*=0, which has no sense. The interpolation curve can be applied just for high concentrations of CO_2 (over 5000 ppm), the calculated extinction coefficient from the linear *A*(*c*) curve has to be used for low concentrations.

The conclusion of the results of the CO_2 calibration is that a special care has to be paid to the IR measurements of the CO_2 concentration in every performed experiment. We were always obliged to investigate several CO_2 IR bands. Concentrations below 5000 ppm were determined from the calculated extinction coefficient, while for higher concentration interpolation curves had to be used.

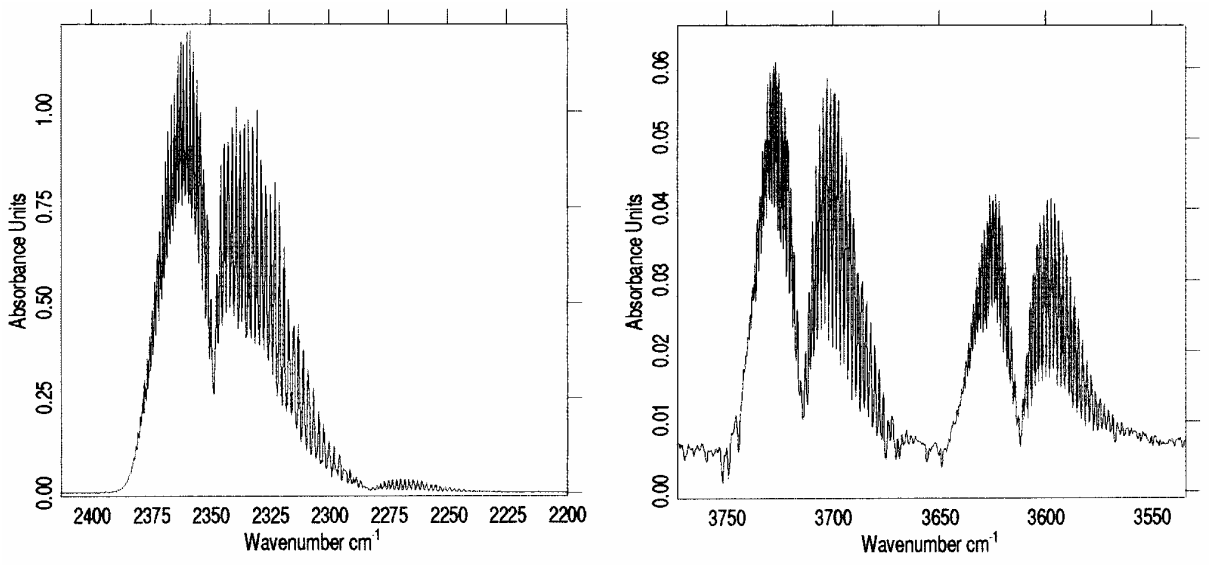

Figure 5.2.10 IR bands of CO_2 (concentration 1 % in N_2) on spectrometer Bruker IFS 48. Main doublet band at 2350 cm^{-1} (left) and weak overtones in 3750-3550 region (right). The intensity of the shoulder of the main band at 2270 cm^{-1} is about the same as the intensity of the band at 3625 cm^{-1}.

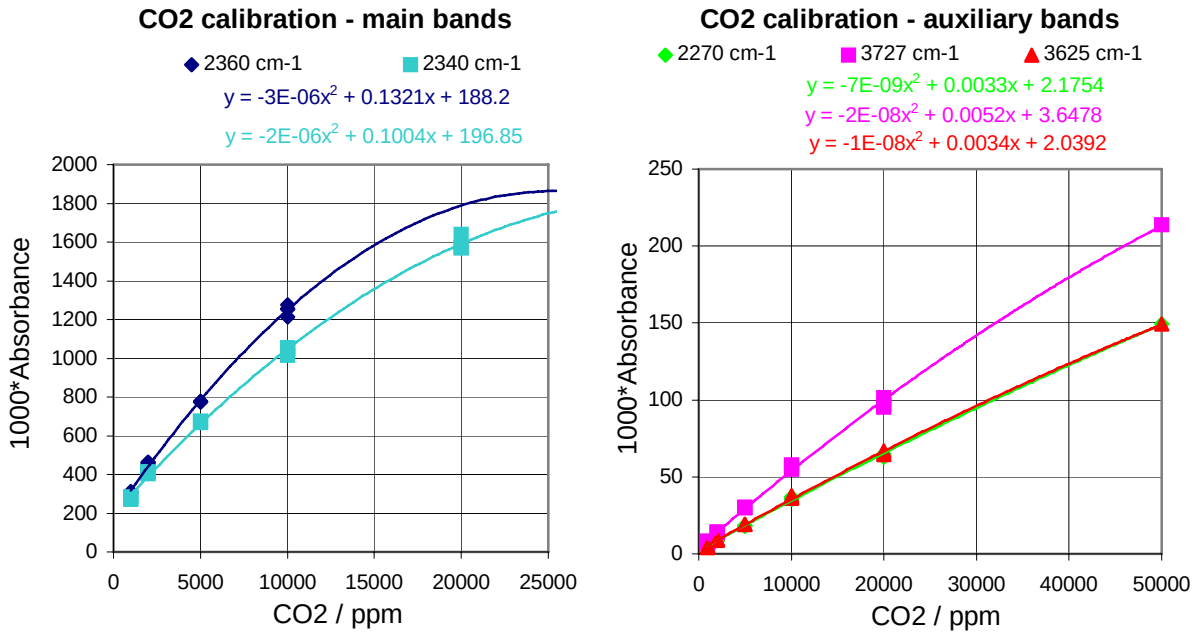

Figure 5.2.11 Calibration of CO_2 main (left) and auxiliary (right) bands on IR spectrometer Bruker IFS 48

5.3 VOC REMOVAL PROCESS IN AIR - RESULTS AND DISCUSSION

Air is typically used as a carrying gas in most of VOC removal techniques. In our experiments directed to the VOC removal by HPGD and TS we used mainly dry or humid air as well.

5.3.1 VOC removal by HPGD in the glass tube reactors

High pressure glow discharge of both polarities was applied to the treatment of dry or humid (close to 100% relative humidity) air charged by various concentrations of cyclohexanone or toluene. These experiments were performed mainly in the glass tube reactor with 5 parallel points and common Cu plane (described in section 5.2.1.1) operating 5 discharges. Additional measurements were performed operating just 1 discharge in the 5-point reactor, then in the system of two such reactors operating 10 parallel discharges and two distant discharges, and finally in the reactor with 5 serial discharges (described in section 5.2.1.3).

The most important results of the VOC removal process in HPGD of both polarities in dry and humid air (which makes four different cases) will be presented in graphs which correspond to the treatment of cyclohexanone in the basic reactor with 5 parallel discharges. The same graphs have been traced for cyclohexanone treated by HPGD in other reactors and for toluene, but will not be presented here to avoid a confusion of the reader by a flood of graphs and information. Their results will be noticed only if they are significantly different from those on the presented graphs.

5.3.1.1 Influence of the initial VOC concentration

We have observed almost no influence of the initial concentration c_0 of both concerned compounds to the removal efficiency η, as evident from dispersed result values on Figure 5.3.1 (left). Achieved removal efficiencies vary from 30 to 96 % in cyclohexanone and from 13 to 77 % in toluene treatment, depending especially on the energy density.

Total energy costs R_{moltot} decrease with rising c_0 as shown in Figure 5.3.1 (right). This trend logically results from the definition formula for R_{mol} (2.4.4). R_{moltot} in cyclohexanone

ranges from 50 eV/molecule which is a rather low value, to 5000 eV/molecule which is extremely high, in toluene within 150 - 3500 eV/molecule. Here we reveal a problematic point when the removal process is characterised only by its energy costs - it might seem excellent if the input pollutant concentration is high, although in reality it is poor. The best is to characterise the process by more parameters (c_0, η, R_V, R_{mol}).

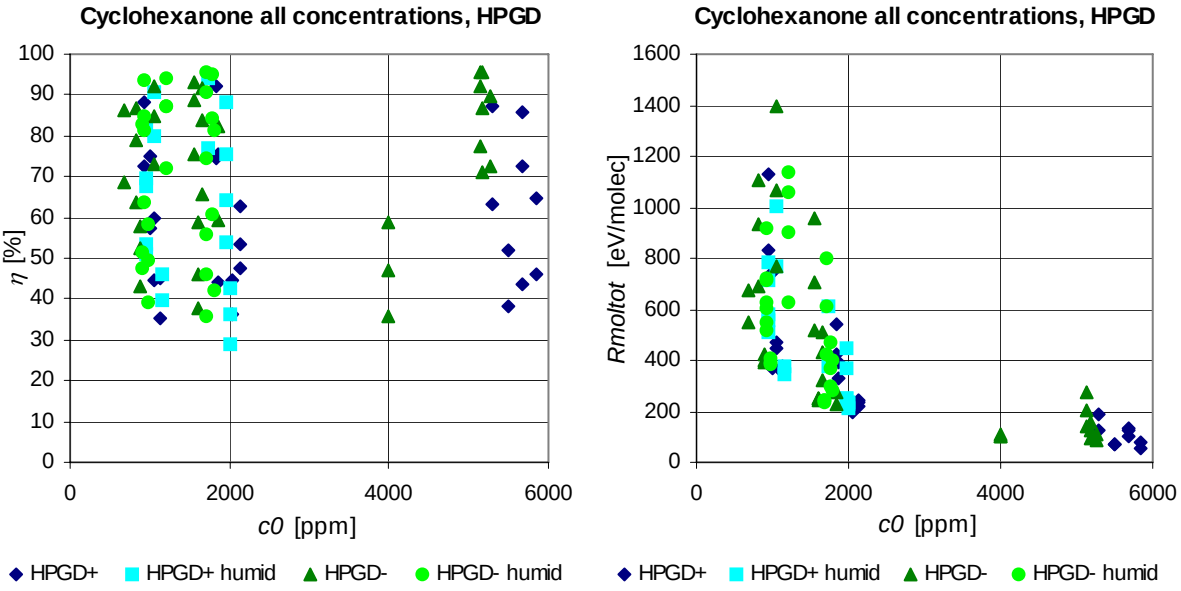

Figure 5.3.1 Removal efficiency η (left) and total energy costs R_{moltot} (right) as functions of the initial cyclohexanone concentration c_0. Both polarities of HPGD in the 5-points glass tube reactor in dry and humid air.

5.3.1.2 Influence of the discharge energy density

The discharge energy density R_{Vdis} (= R_V) is a good characteristics of the discharge because it concludes the power injected into the discharge zone and the residence time of the treated species in the active zone (via the gas flow) according to the formula 2.4.2. Thus, in the following we will refer to the two basic characteristics of the VOC removal process: the removal efficiency η and the energy costs R_{mol}, as functions of the discharge energy density R_V.

The resulting trend of the $\eta(R_V)$ curve is logarithmic for both studied compounds in any concentration in dry as well as humid air, Figure 5.3.2 (left). This is in accordance with results of many other authors [Jaw96, Smu98, Odi98, Odi99, Par99, Fut98, McC99, Sny98, Fal99, ChM97, etc.]. It implies that to obtain higher removal

efficiency we have to increase the energy density, but a linear increase of R_V does not result in the linear increase of η. An effect of non-linearity (saturation) occurs. It is easy to achieve e.g. 60 % removal rate (of cyclohexanone), but doubling of the energy costs yields just 20 % more in efficiency so that the energy is used less effectively. This is a rather discouraging result, but also challenging to find out the best systems of VOC removal and their most convenient parameters.

Figure 5.3.2 also shows that there are little differences between the effects of positive or negative discharge polarity and the presence or not of moisture. The weak polarity effect will be obvious also in the next graphs. This result was expected since the properties of positive and negative HPGD are very similar. However, the humid air and the negative discharge polarity yield a little higher efficiency for the same R_V.

Discharge energy costs R_{mol} as a function of the discharge energy density R_V for cyclohexanone treatment in all four cases are shown in Figure 5.3.2 (right). The saturation effect of the $\eta(R_V)$ dependence is reflected into this one though formulas 2.4.3 and 2.4.4. In both compounds we observe that R_{mol} rises with R_V exponentially, first fairly, than rapidly. Thus, to decrease the energy costs of the process it is better to work at low energy costs, but we pay by the lower removal efficiency η.

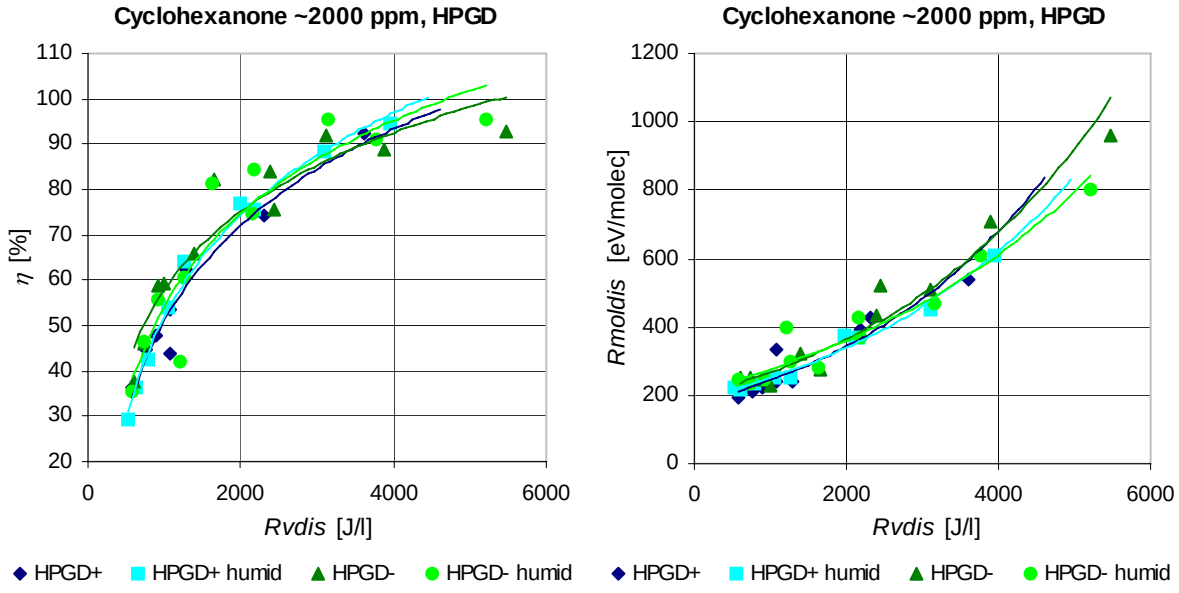

Figure 5.3.2 Removal efficiency η (left) and discharge energy costs R_{moldis} (right) as functions of the discharge energy density R_{Vdis}. Both polarities of HPGD in the 5-points glass tube reactor in dry and humid air.

We observed again that humid air gives slightly better results (lower R_{mol}) for both compounds, especially in the negative polarity. It is probably caused by the formation of highly reactive OH radicals.

5.3.1.3 Effect of non-linearity - glass tube reactors with 1, 2, 5 and 10 discharges

We have studied in more details the effect of non-linearity described previously (section 5.3.1.2), i.e. the fact that the removal efficiency η does not rise linearly with rising energy density R_V. This effect gave rise to an idea that the first discharge is responsible of the maximum of work and every next one is less and less effective. In order to verify this phenomenon and to find out optimal parameters for VOC removal (number of discharges, their power and gas flow) we compared the effects of 1 discharge (HPGD) in the 5-point reactor, 10 parallel discharges in two 5-point reactors put in series and 2 distant discharges (each one operated in one 5-point reactor, they were joined in series by a hose of 2 m long) with results of 5 parallel discharges (chapter 5.3.1). This comparison was effectuated for all four typical cases (positive and negative HPGD, dry and humid air) at about 2000 ppm of cyclohexanone, we will present results of the negative HPGD in humid air only, other three cases are qualitatively the same.

The result $\eta(R_V)$ curves are shown in Figure 5.3.3. We observe that the saturation effect is present in all cases, even when just one discharge was operated. On the contrary to what we suspected, the achieved efficiency is higher at the same energy density when working with more discharges, except the case of 10 discharges, which are not more effective than 5 discharges. Hence, to increase the efficiency it is better to work with about 5 discharges, each at low energy density, than with few more energetic discharges.

In general, values of the discharge energy density $R_V = R_{Vdis}$ delivered into the treated bulk gas can be changed by three ways - either by a change of the discharge power P_d or by a change of the gas flow Q or by a change of the number of working discharges. In order to simplify the comparison of the effect of 1, 2, 5 or 10 discharges, we took a fixed gas flow Q = 1 l/min, R_{Vdis} then represents just the discharge power P_d. $\eta(R_V)$ curves (from the left graph in Figure 5.3.3) are by this way simplified to a form shown in the right graph of the same figure. We can observe that the use of two distant discharges at about twice P_d gives approximately twice greater efficiency than one unique discharge. This linearity is not followed when going from 2 to 5 and from 5 to 10 working discharges. Anyhow, it is clear that working with 10 discharges is not effective.

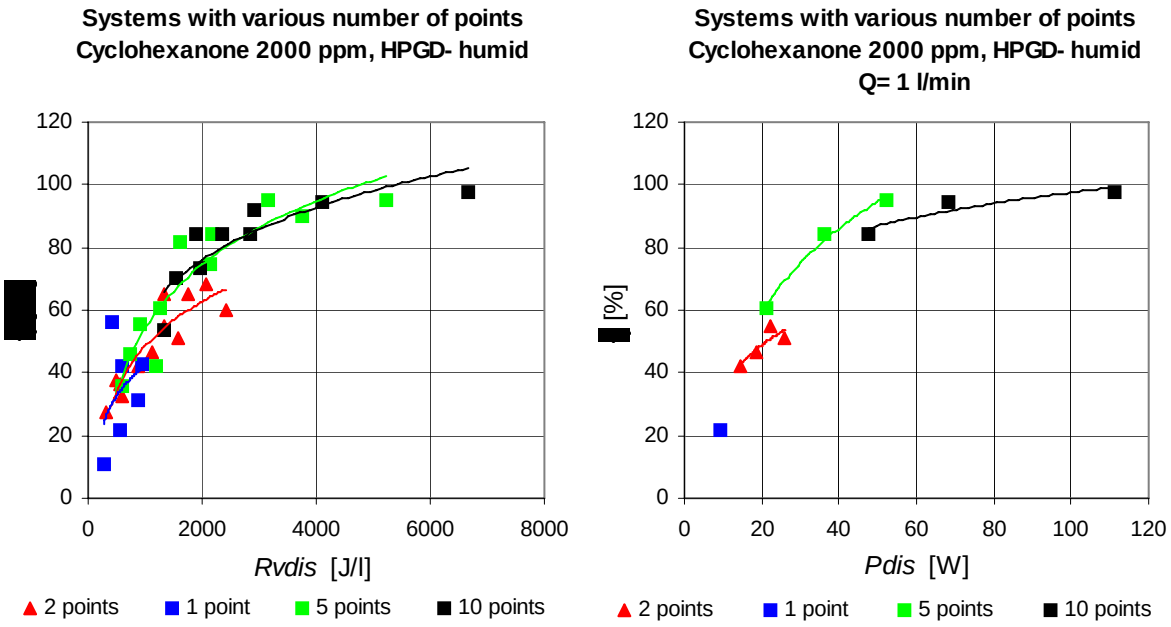

Figure 5.3.3 Removal efficiency η as a function of the discharge energy density R_{Vdis} (left) and of the discharge power P_{dis} at the fixed gas flow Q=1 l/min (right). Systems with 1, 5, 10 discharges and 2 distant discharges (negative HPGD, humid air) in the glass tube reactors.

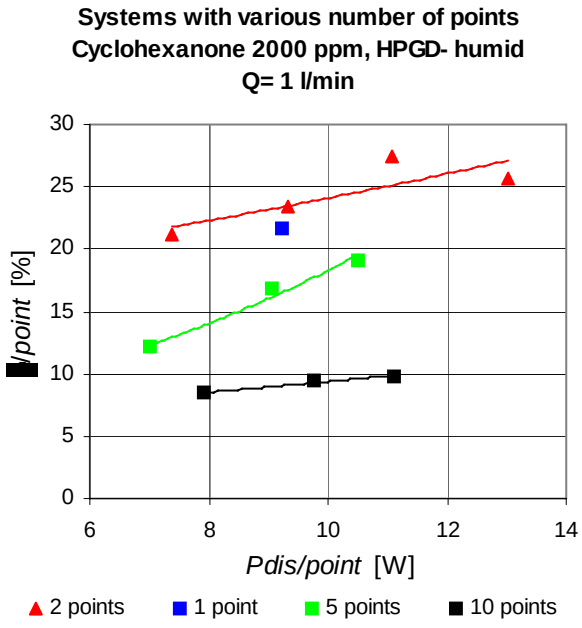

Figure 5.3.4 Removal efficiency η as a function of the discharge power P_{dis} at fixed gas flow Q=1 l/min normalised to the number of working discharges. Systems with 1, 5, 10 discharges and 2 distant discharges (negative HPGD, humid air) in the glass tube reactors.

Let us "normalise" the $\eta(P_d)$ curves from the right graph of Figure 5.3.3 by the number of working discharges (η and P_d were divided by the number of discharges), Figure

5.3.4. This graph shows the efficiency of each used discharge. We can see that the efficiency per one discharge is the highest in the case of 2 distant discharges and the lowest when 10 discharge were used. Moreover, the efficiency per discharge for 2 distant discharges is greater than for a unique discharge. However, the total efficiency (not divided by number of discharge) is rather low in the system with 2 discharges. The optimal number of discharges to obtain the highest efficiency and not to lose too much energy is 5.

Anyway, surprising results obtained in the system of two distant discharges open a hypothesis that it is better to work with several low-energetic discharges which are rather distant one from another. A possible explanation is the following: each discharge has a thermal decomposition effect to the treated VOC and creates reactive radicals. While the thermal effect occurs just within a small volume close to the discharge channel where the gas temperature is high (~2000 K), formed radicals are active in further parts of the reactor volume. It seems better to enlarge this post-discharge space in order to utilise the work done by these radicals in maximum. This new information shows a novel way how to construct the discharge reactor for HPGD applied to VOC removal: to operate about 5 discharges which are ”distant” one from another (”distant” in a sense of volume, not necessarily length).

5.3.1.4 Lowering of the total energy costs of HPGD - reactor with serial points

A special reactor with 5 discharges fed in series (described in section 5.2.1.3) was developed with the aim of lowering of the total energy costs of the VOC removal process. The energy losses are minimised in comparison with the typical reactor fed in parallel with 5 discharges, because all 5 discharges are here controlled just by one series resistance. Typical P_d/P ratio (P_d is the power spent in the discharge, P is the total spent power) determining the energy distribution in the circuit is about 0.7-0.8 in the serial reactor which means that 70-80 % of the energy is spent effectively in the discharge. In the reactor with parallel discharges where each discharge is controlled by its own resistance, typical P_d/P=0.3-0.5, i.e. at least half of the energy is lost in the resistances.

Greater effectivity of the serial reactor is evident from Figure 5.3.5 which compares the cyclohexanone removal in these two reactors, namely dependencies of the removal efficiency η and total energy costs R_{moltot} on the total energy density R_{vtot} (calculated from the total spent power P). Yet, the effectivity of the serial reactor is not twice better than in the parallel reactor, what could be expected according to almost twice better P_d/P ratio. Not very significant difference between the effects of these two reactors is probably due to the greater

cross section of the glass tube of serial reactor (see Figure 5.2.1 and Figure 5.2.2). Thus, a greater amount of the gas passes through the reactor without direct contact with the discharges. In spite of this effect, the comparison of serial and parallel reactors confirms that better properties of the reactor with discharges in series are to be expected.

Considering this result and the result of the comparison of 1, 2, 5 and 10 parallel discharges (previous section 5.3.1.3), we can suggest a new type of the deVOC reactor based on HPGD – a reactor with several discharges electrically in series but with long pathways leading the treated gas from one discharge to another.

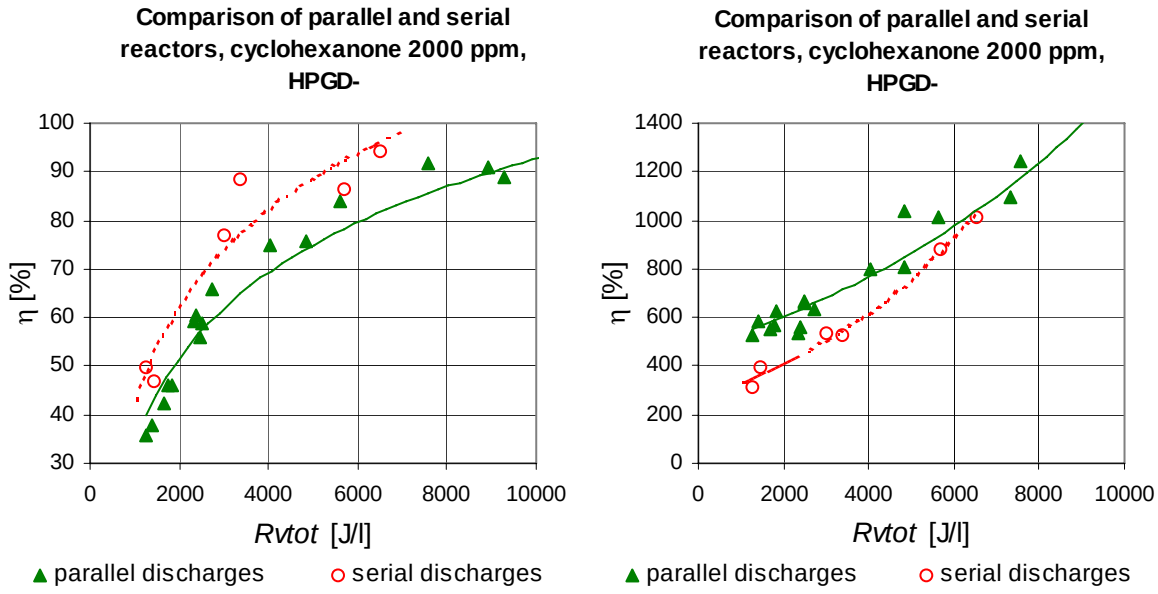

Figure 5.3.5 Comparison of effects of serial and parallel reactors with 5 discharges. Removal efficiency η (left) and total energy costs R_{moltot} (right) as functions of the total energy density R_{Vtot} , cyclohexanone removal in negative HPGD.

5.3.2 Gaseous products of the VOC removal process in HPGD in glass tube point-to-plane reactors

VOC vapours treated by HPGD operated in the glass tube reactors were converted to some gaseous and some condensed products. Their character and created concentrations depend on the discharge polarity, presence of moisture in the carrying air, VOC type and its initial concentration and especially the energy density dissipated in the reactor. The most typical gaseous products of the HPGD for both cyclohexanone and toluene removal are: carbon dioxide (CO_2), carbon monoxide (CO), water (H_2O), nitrogen dioxide (NO_2) and nitrogen oxide (NO). In trace amounts we often found formaldehyde (HCHO) and nitrous acid (HNO_2), in humid air sometimes nitric acid (HNO_3). Very seldom we found some traces of nitrous oxide (N_2O) and alcohols (methanol, ethanol).

A representative IR spectrum of cyclohexanone before and after the negative HPGD treatment in the 5-point reactor and humid air is shown in Figure 5.3.6.

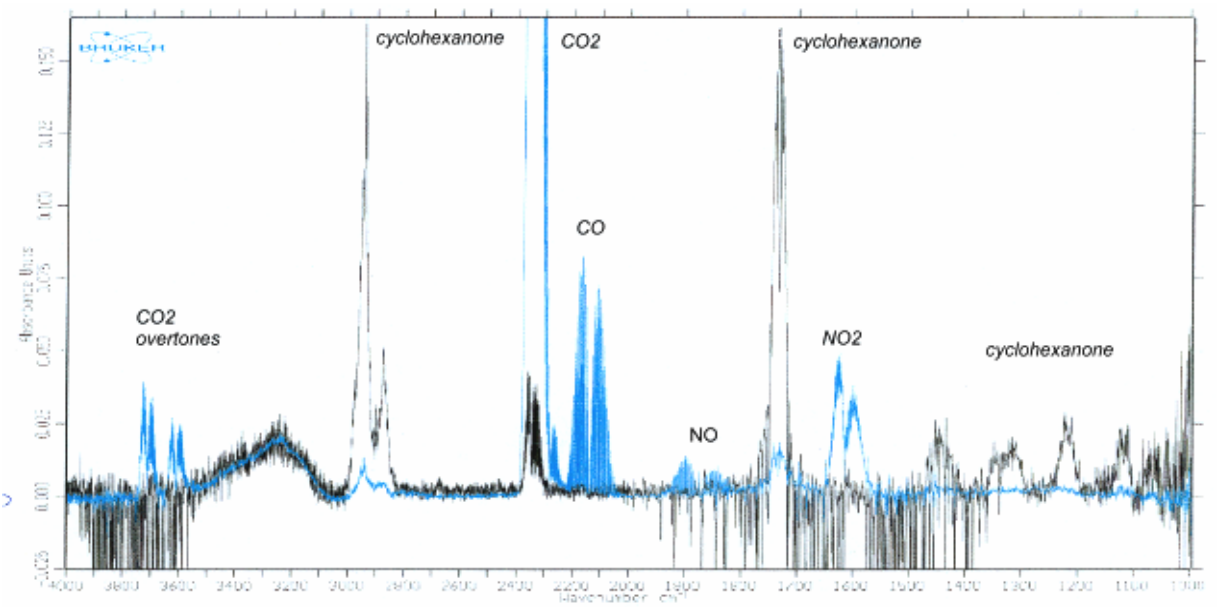

Figure 5.3.6 Infrared spectrum of cyclohexanone (2000 ppm) before (black) and after (blue) negative HPGD treatment in the 5-point reactor and humid air with identification of the most important gaseous products.

Graphs showing formed concentration of the typical gaseous products as a function of discharge energy density R_V=R_{Vdis} of the positive and negative HPGD and both dry and humid air (four cases) applied to the removal of about 2000 ppm of cyclohexanone in the reactor

with 5 parallel discharges are in Figures 5.3.8, 5.3.12, 5.3.13. The same graphs have been traced for cyclohexanone treated by HPGD in other reactors and for toluene treated in the 5-point reactor, but will not be presented here. Results of these experiments will be given whenever they are significantly different from those appearing on the presented graphs, in order to show specific effects of various reactors and VOC types.

5.3.2.1 Effects of HPGD on dry and humid air without and with VOC

Before starting the process of VOC removal by the high pressure glow discharge we will examine how the discharge acts in dry and humid air, without the presence of VOC. Physical properties of HPGD in air have already been studied in chapter 3, now we refer to the changes in air composition induced by the HPGD of both polarities. We will use the 5-point reactor with just one discharge operated. Then we will charge air by about 1400 ppm of a VOC (cyclohexanone) and investigate how it influences the gaseous products, especially the NO_x formation, in the same system with one discharge.

Generally, HPGD of both polarities in air (dry and humid) forms nitrogen oxides (NO_x), especially NO and NO_2, in trace amounts also N_2O and HNO_2. NO_x formation (Figure 5.3.7, open points, dashed lines) increases exponentially with the discharge energy density, especially due to the increasing discharge and bulk gas temperature. However, NO_x formation is not the same when we use positive or negative HPGD, it is lower in the negative polarity, though the discharge temperature is a little higher in the negative HPGD (remind chapter 3, sections 3.3.5.2, 3.3.8.1). A presence of moisture in air significantly reduces NO_x formation in spite of the fact that it does not decrease the discharge temperature in comparison with dry air. It implies that the formation of NO_x in HPGD is not purely dependent on the discharge temperature, but is a result of the involved radical-induced plasmochemistry.

When an organic compound (cyclohexanone) enters to this system, it becomes even more complicated. The NO_2 formation was enhanced and the NO production was reduced in all four studied cases (HPGD in both polarities in both dry and humid air), see Figure 5.3.7, full points, solid lines. The rate of the NO_x formation in four cases remains in the same order, i.e. maximum for positive HPGD in dry air, then negative HPGD in dry air, then positive HPGD in humid air and the minimum for negative HPGD in humid air. Trends of $NO_2(R_V)$ curves changed from exponential-like to the logarithmic-like, an effect of saturation of NO_2 formation occurs when VOC is present. This effect does not happen in NO formation.

When a VOC is present in the discharge system, we often observe a formation of a white aerosol (fog) in the reactor. This aerosol can be assigned to be a photochemical smog based on peroxy-acetyl-nitrates (PAN) which forms in the reactor by the mechanism similar to the photochemical smog formation in the atmosphere (explained in chapter 2.1.2). Indeed, all components necessary for PAN formation, such as hydrocarbon-, peroxyl- and OH-radicals, as well as nitrogen oxides are present in the system. PAN were found also in the gas-phase IR spectra according to their characteristic bands of carbonyl (C=O at 1700-1800 cm^{-1}) and nitrate group (-NO_2 superposed on the doublet band of gaseous NO_2 at 1630 cm^{-1}). The superposition of the nitrate group on the gaseous NO_2 band increases the intensity of this band, generally used to determine NO_2 concentration. Therefore, in reality, the measured NO_2 concentration includes gaseous NO_2 and NO_2 attached in PAN. By this way we can explain a rise of NO_2 production when VOC was added into the discharge system. A rise of gaseous NO_2 production in reality need not occur, mainly the formation of PAN with attached NO_2 group is enhanced. Unfortunately, the PAN formation brings an uncertainty (estimated to 10-20 %) into a precise measurement of formed gaseous NO_2 concentration in the deVOC process. What we in reality measure is the sum of gaseous and aerosol (PAN) NO_2.

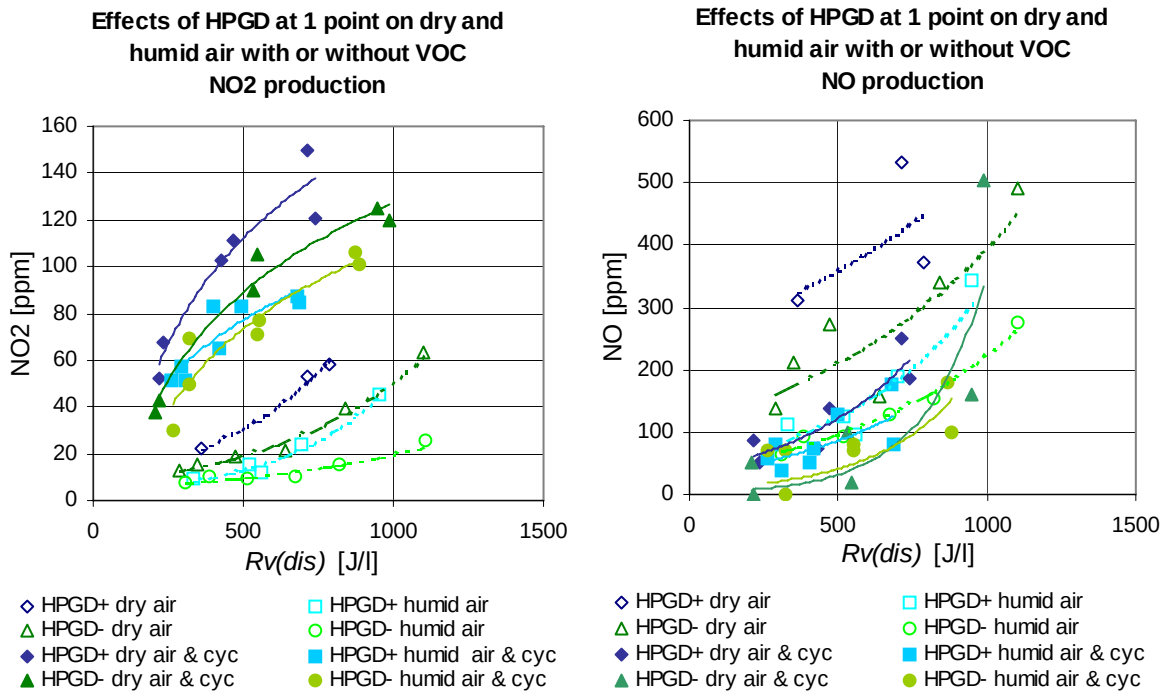

Figure 5.3.7 NO_2 (left) and NO (right) production by HPGD at 1 point in dry and humid air with (full points, solid lines) or without (open points, dashed lines) VOC (cyclohexanone ~1400 ppm) as a function of the discharge energy density R_{Vdis}.

The chemical effects of HPGD on air change significantly when an organic compound is added, even in relatively low concentration (1400 ppm). It occurs despite of no effect of the organic admixture to the discharge properties, especially its temperature (observed in chapter 3, section 3.3.8.1). This result demonstrates again that the discharge temperature is not the only factor influencing the chemical processes induced by the HPGD.

5.3.2.2 CO_2, CO and their ratio

Formation of CO_2 as a function of the discharge energy density R_V (Figure 5.3.8, left) has qualitatively the same logarithmic trend (a little steeper) as $\eta(R_V)$ dependence (Figure 5.3.2, left). It shows that CO_2 is a main gaseous product of the removal process, its concentration corresponds to the amount of the destroyed VOC. Produced CO_2 concentrations for treated 2000 ppm of cyclohexanone are from 600 to 6000 ppm, higher when humid air was used, little lower in the serial reactor (500-4500 ppm). For treated toluene (about 2000 ppm), 800-15000 ppm of CO_2 is produced in dry air, but lower concentrations in humid air (maximum 11000 ppm in negative HPGD and 6000 ppm in positive HPGD). The decomposition process of cyclohexanone and toluene are certainly different, a presence of moisture enhances the CO_2 formation in cyclohexanone but not in toluene.

CO produced in the cyclohexanone treatment as a function of R_V (Figure 5.3.8, right) has a slight maximum at about 2500 J/l for all four studied cases. CO formation is lower before the maximum because the removal efficiency of VOC is not very high. After the maximum it decreases again because the energy density is too high, hence CO transformation to CO_2 is enhanced. It explains the above mentioned trend of the $CO_2(R_V)$ curves which is steeper for higher R_V than in $\eta(R_V)$ curves. Produced CO ranges from 600 to 1600 ppm, a little lower in humid air.

CO production, as well as the CO_2 production, is higher for toluene treatment, especially in dry air where CO is formed in 500-2500 ppm range. It is lower in humid air which is similar to the cyclohexanone treatment. CO maximum in toluene treatment, though higher, occurs around R_V = 1500 J/l which is significantly lower than in cyclohexanone. This shows again a difference in the decomposition process of toluene and cyclohexanone.

Production of CO_2, CO and H_2O from organic compounds is characteristic for the combustion processes. [Kla93] One of the characteristic parameters of combustion and combustion-like processes is the ratio of produced CO and CO_2. A perfect combustion process produces just CO_2 and H_2O. Hence, the process approaches to the perfect combustion

when the CO/CO_2 ratio is low. CO, of course, is a noxious product, thus the process is better when CO production is minimal.

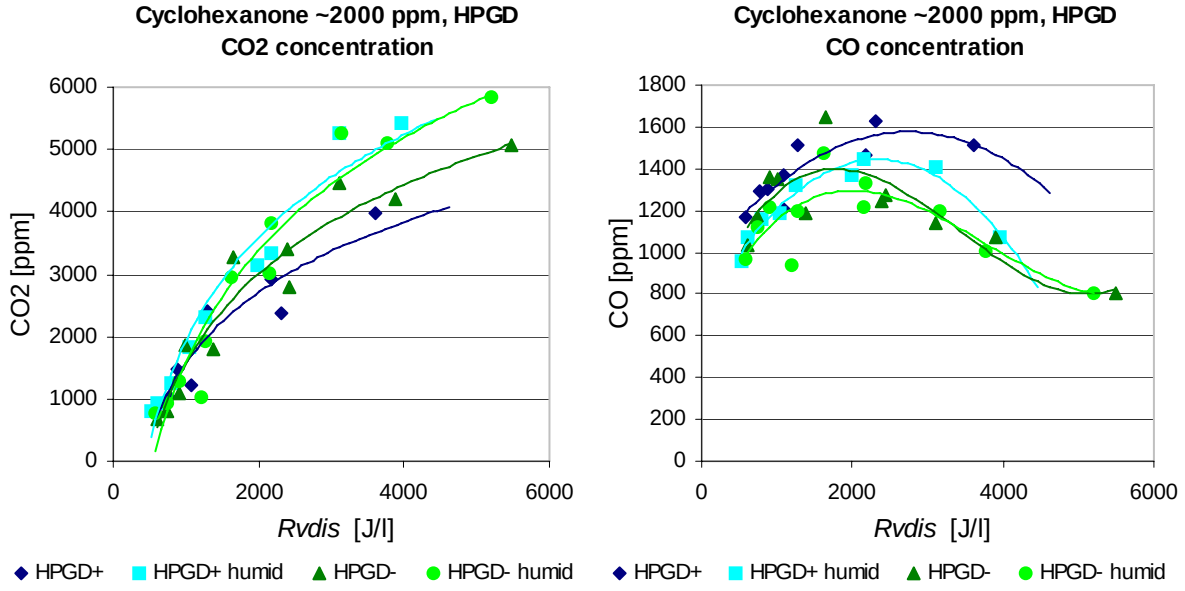

Figure 5.3.8 Formed CO_2 (left) and CO (right) concentrations as functions of the discharge energy density R_{Vdis}. Both polarities of HPGD in the 5-points glass tube reactor in dry and humid air.

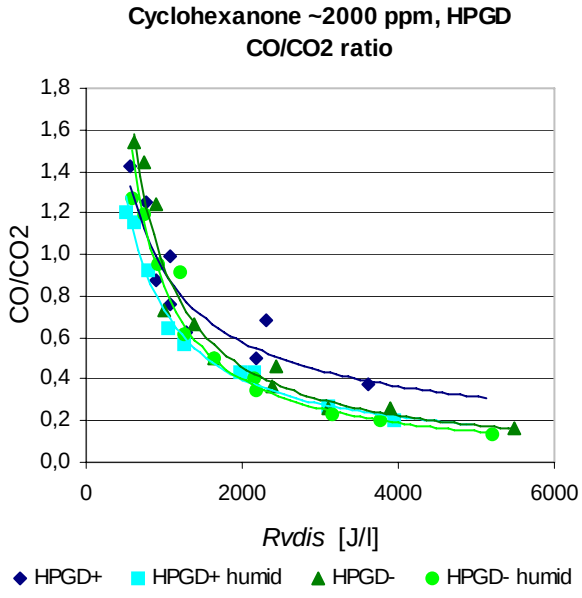

Figure 5.3.9 CO/CO2 ratio as a function of the discharge energy density R_{Vdis}. Both polarities of HPGD in the 5-points glass tube reactor in dry and humid air.

Figure 5.3.9 shows an exponential decrease of CO/CO_2 ratio as a function of the discharge energy density R_V characteristic for cyclohexanone (the same is observed for toluene). This ratio is lower in the process maintained in the humid air for both compounds and discharge polarities, the highest for positive polarity in dry air. In cyclohexanone treatment CO/CO_2 comes from about 1.5 at the lowest R_V to about 0.1 at the highest R_V, at R_V = 3000 J/l where we gain about 90 % of cyclohexanone destruction the CO/CO_2 ratio is about 0.3. In toluene treatment we get even lower CO/CO_2: from 1.2 to 0.05, at R_V=2000 J/l (η around 75%) CO/CO_2 = 0.2.

Obtained CO/CO_2 ratios are rather low in comparison with other plasma techniques of VOC removal [Odi98, Par99, Oga99]. A deVOC process induced by HPGD is close to the perfect combustion especially for high R_V. It is due to a high discharge temperature, remind chapter 3 dedicated to the study of HPGD, sections 3.3.5.2 and 3.4.5.

5.3.2.3 Total carbon balance

Total carbon balance is a special characteristics of VOC removal processes which tells how the total carbon (C) arriving into the process in the gas phase distributes to the outgoing gas-phase and other-phase carbon containing products. There are two ways how to express the carbon balance:

1. Gas carbon out-to-in ratio is a ratio of the total carbon in the gas phase getting out of the system to the total gas carbon going into the system. It considers **all** carbon which passes through the reactor. This characteristics was used e.g. in [Odi98, Par99]. In our experiments we treated always a pure organic compound (cyclohexanone or toluene, except a mixture treated in the pilot scale reactor, chapter 6). The outgoing gas-phase carbon is represented by the non-treated VOC and the carbon-containing gaseous products, such as CO_2 and CO. Other C-containing products detected in trace amounts (HCOH etc.) can be neglected. The total carbon out-to-in ratio is then given by the equation:

$$\frac{C_{\text{gas-out}}}{C_{\text{gas-in}}} = \frac{[CO_2] + [CO] + ic}{ic_0} \tag{5.3.1}$$

where $[CO_2]$ and [CO] are the concentration of produced CO_2 and CO, c is the final (output) VOC concentration, c_0 is the initial (input) VOC concentration, all in ppm; and

i is the number of C atoms in the concerned VOC molecule (*i*=6 for cyclohexanone, *i*=7 for toluene).

2. Treated carbon balance is a ratio of outgoing carbon in C-containing gaseous products to the total carbon treated in the process. This characteristics takes into consideration just the carbon **treated** in the process which is transformed partially to the gaseous and partially to other-phase products. It does not consider the unaffected carbon like the previous one. In our experiment where CO_2 and CO were the main C-containing gaseous products (we neglect other trace products), it is expressed by:

$$\frac{C_{\text{gas-product}}}{C_{\text{treated}}} = \frac{[CO_2]+[CO]}{i(c_0-c)} = \frac{[CO_2]+[CO]}{i\eta c_0} \qquad (5.3.2)$$

where η is the removal efficiency.

The difference between these two interpretations of the total carbon balance can be seen more clearly on the cake graph (Figure 5.3.10). $C_{gas\text{-}product}/C_{treated}$ = 100 % means that all treated C is converted to gaseous products, 0 % means that all treated C rests in other phases.

These two characteristics approach to each other when the VOC removal efficiency η approaches to 100 %, i.e. the final VOC concentration $c \rightarrow 0$. However, they might be very different when η is further from 100 %. In such case it is more appropriate to use the second characteristics taking into consideration just the treated carbon.

Figure 5.3.11 represents the dependencies of $C_{gas\text{-}out}/C_{gas\text{-}in}$ and $C_{gas\text{-}product}/C_{treated}$ ratios on the discharge energy density R_v for about 2000 ppm of cyclohexanone in dry and humid air treated by HPGD of both polarities. $C_{gas\text{-}out}/C_{gas\text{-}in}(R_V)$ curves have a minimum of about 65 % at 3000 J/l which implies that the formation of non-gaseous products is maximal at this R_V (35 % of the total C passing through the reactor goes to non-gaseous products). In reality, this is not true, the non-gaseous product are maximally formed at the lowest R_V as clearly seen from the curves $C_{gas\text{-}product}/C_{treated}(R_V)$. The fact that $C_{gas\text{-}out}/C_{gas\text{-}in}$ is high for low R_V is due to the low removal efficiency η. By other words, a great amount of non-treated VOC increases the ratio $C_{gas\text{-}out}/C_{gas\text{-}in}$. This demonstrates why $C_{gas\text{-}product}/C_{treated}$ is a better value to characterise the ratio of gas-phase products to all formed products.

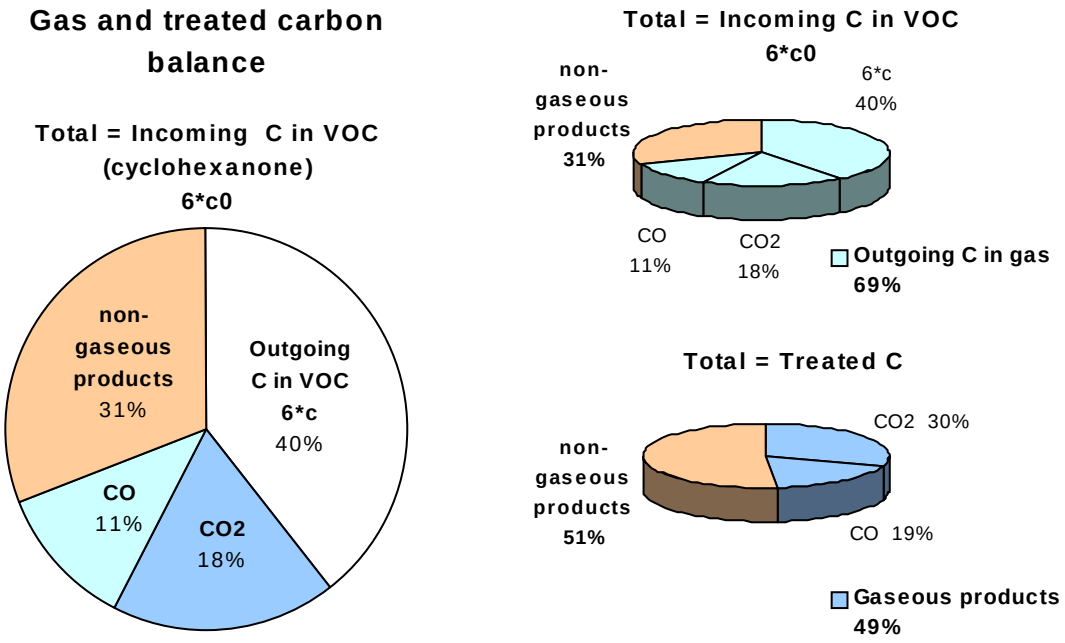

Figure 5.3.10 Cake graphs illustrating the difference between gas carbon out-to-in ratio $C_{gas\text{-}out}/C_{gas\text{-}in}$ and treated carbon balance $C_{gas\text{-}product}/C_{treated}$. An example of cyclohexanone treatment by negative HPGD in the 5-points glass tube reactor and humid air.

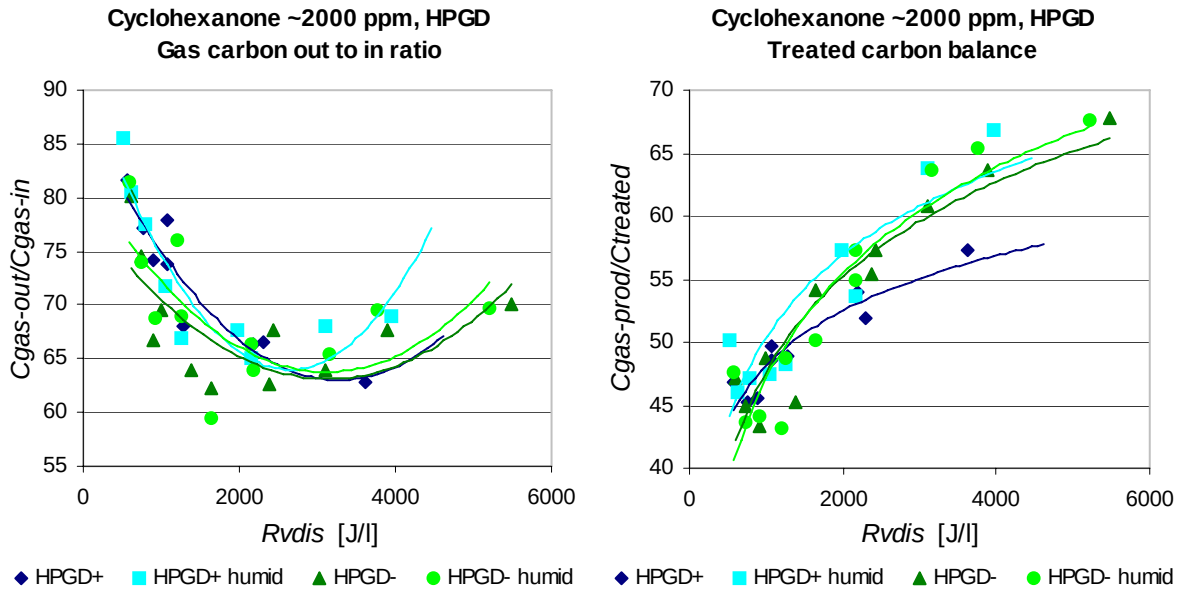

Figure 5.3.11 $C_{gas\text{-}out}/C_{gas\text{-}in}$ (left) and $C_{gas\text{-}product}/C_{treated}$ (right) ratios as functions of the discharge energy density R_{Vdis}. Both polarities of HPGD in the 5-points glass tube reactor in dry and humid air. Unit is %.

Result $C_{gas\text{-}product}/C_{treated}$ values for cyclohexanone removal process in HPGD are from 40 % for low R_v to 65 % for high R_V (i.e. from 35 to 60 % of the treated carbon is converted to non-gaseous products). $C_{gas\text{-}product}/C_{treated}$ is minimal (i.e. treated C is converted to non-gaseous products in a maximal rate) in the positive HPGD and dry air. In toluene treatment $C_{gas\text{-}product}/C_{treated}$ values are from 50 to 80 % (i.e. 20-50 % of C goes to non-gas phases), in the negative polarity and high R_V they approach to 100 % (0 % in non-gas phases). The more thermal process leads to the greater formation of gaseous products, at low energy density the process leads to the preferential formation of products in other phases.

In most of other plasma deVOC techniques the ratio of the treated carbon which transforms to non-gas phases does not usually exceed 25 %, though Anderson et al report 68 % (oxidation of styrene in the silent discharge). [And99] Hence, plasmas generated by HPGD presented here lead to rather high formation of non-gaseous products, especially at low energy densities. The question which appears is “what is better?”, either to produce gas-phase products or rather products in other phases? Most of people working with plasma environmental applications prefer gaseous products, the most desired are non-toxic CO_2 and H_2O and nothing else. Unfortunately, almost every VOC removal process is accompanied by CO and NO_x production and, moreover, some production of condensed products or aerosols is usually unavoidable. Furthermore, environmental applications producing CO_2 are also not ideal from the viewpoint of global environment, because CO_2 is a main contributor to the increase of the greenhouse effect on the Earth. All these facts reveal a new courageous approach to the pollution control techniques: non-gaseous products, especially if they are not toxic, might be better than the gaseous ones. Thus, results obtained in our experiments where a great ratio of the treated carbon transforms to non-gas phases are not bad. Even when the condensed products are toxic, they might be better than outgoing toxic gaseous ones, because they are separated from the gas and stored in the reactor or its pathways. Of course, the reactor has to be regularly cleaned which can be a technical problem, but it is usually feasible.

5.3.2.4 Water (H_2O)

Formation of H_2O goes with carbon oxides formed in the combustion-like deVOC processes. Produced concentration of H_2O as a function of discharge energy density in the process of cyclohexanone removal in HPGD is shown in Figure 5.3.12. A logarithmic tendency of the curves is present again for both compounds and all four cases (both polarities,

dry and humid air). In humid air, the initial H_2O concentration was subtracted from the final one to obtain really produced H_2O.

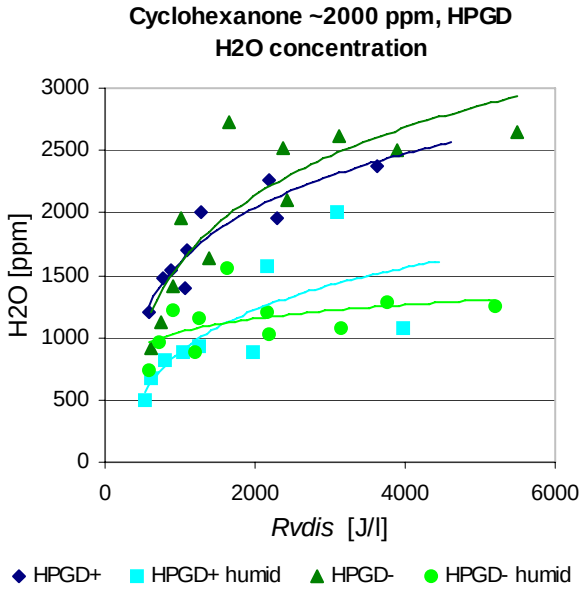

Figure 5.3.12 Formed H_2O concentration as a function of the discharge energy density R_{Vdis}. Both polarities of HPGD in the 5-points glass tube reactor in dry and humid air.

We observe a great difference between dry and humid air environment of the deVOC process for both involved compounds: H_2O in concentrations 1000-2700 ppm was produced in the cyclohexanone removal in dry air, while only 500-1500 ppm in humid air. Even more H_2O was produced in toluene removal: 500-5500 ppm in dry air and 0-2000 ppm in humid air. This surprising result shows that H_2O formation is not directly proportional to the number of hydrogen atoms in the removed molecule (8 in toluene, 10 in cyclohexanone, one would expect a lower H_2O formation in toluene removal), but it probably depends on more complicated plasmochemical mechanisms.

Significantly lower H_2O formation in humid air might be explained by a certain equilibrium of the processes concerning H_2O. It is gained at certain total H_2O concentration, regardless to the origin of H_2O presence, i.e. regardless if H_2O was produced by the discharge in the dry air or already present in the humid air. However, the whole process concerning H_2O is probably more complicated, because the working atmosphere of humid air results in slightly higher VOC removal efficiency and lower energy costs (remind section 5.3.1).

5.3.2.5 Nitrogen oxides (NO_x)

A typical feature of combustion-like processes, actually all processes with temperature over 800 °C occurring in air, is the production of nitrogen oxides (NO_x), especially NO_2 and NO. These gases are noxious due to their toxicity for living organisms. Most of plasma techniques for flue gas cleaning which use discharges with relatively high temperature face this problem. HPGD is not an exception, the deVOC process was always accompanied by NO_x production. In fact, HPGD operating in air produces NO_x even without the VOC (as shown in section 5.3.2.1, graphs in Figure 5.3.7), a presence of VOC influences the NO_x formation and leads to the additional formation of peroxy-acetyl-nitrates (PAN). White PAN aerosol was often observed in deVOC experiments with HPGD.

Graphs showing the dependence of produced NO_2 and NO concentrations on the discharge energy density for all four cases in the 5-point reactor are shown in Figure 5.3.13. We observe a rising tendency for both NO_2 and NO in both discharge polarities and in dry as well as humid air. The experimental points can be fitted by various types of curves, the best seem the exponential-like curves. This trend is not similar to the logarithmic one, observed in $CO_2(R_V)$ and $H_2O(R_V)$ graphs, which demonstrates that the NO_x production is not dependent on the VOC removal efficiency, just on the VOC presence in the system.

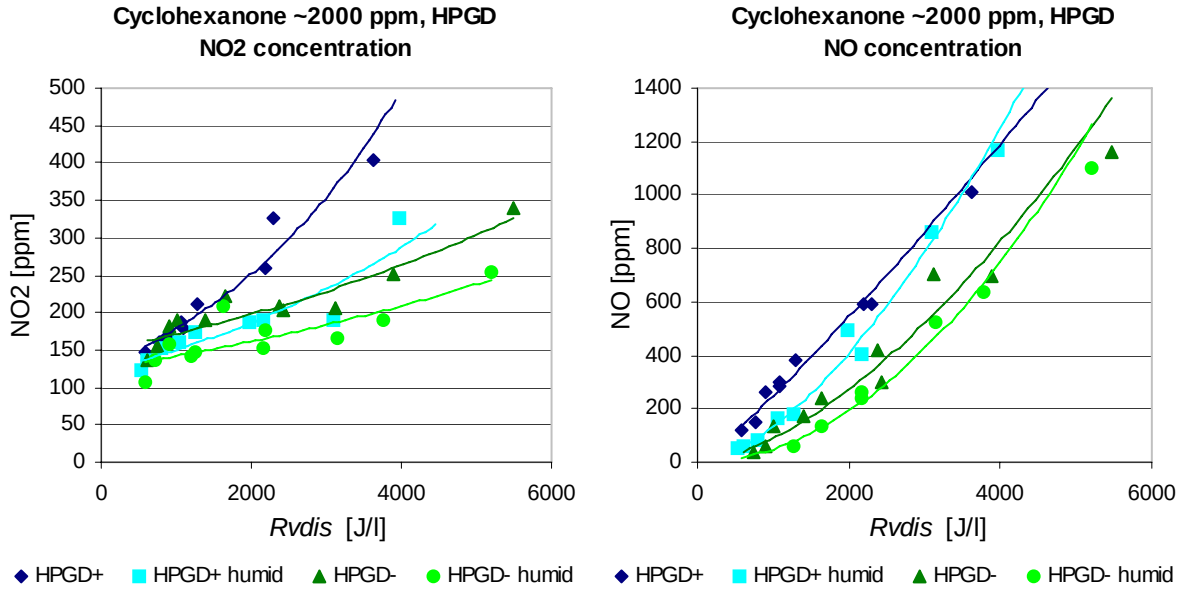

Figure 5.3.13 Formed NO_2 (left) and NO (right) concentrations as functions of the discharge energy density R_{Vdis}. Both polarities of HPGD in the 5-points glass tube reactor in dry and humid air.

NO_2 production in HPGD in the 5-discharge reactor is between 100 and 400 ppm, NO from 0 to 1200 ppm, except one case of toluene described below. A little higher concentrations were produced in the system with 10 parallel discharges and in the reactor with 5 serial discharges. In all reactors, the lowest NO_x production occurs in the negative HPGD in humid air and the highest in the positive HPGD in dry air. In dry air with toluene and positive HPGD up to 1400 ppm of NO_2 and NO were produced. Please, remind that real concentrations of produced gaseous NO_2 are in reality lower than the measured ones, because the basic IR band of NO_2 (at 1630 cm^{-1}), used for NO_2 evaluation, was superposed on the band of the nitrate group of formed PAN aerosol (explained in section 5.3.2.1). Unfortunately, due to the PAN formation we can determine the NO_2 concentration just with an uncertainty of about 10-20 %.

5.3.2.6 Comparison of 1, 2, 5 and 10-discharge systems from the viewpoint of gaseous products

We have already compared the systems with 1, 5, 10 and 2 distant discharges from the viewpoint of the removal efficiency (section 5.3.1.3) and found that two distant discharges are the most convenient system from the viewpoint of the efficiency per discharge. Graphs in Figures 5.3.14–5.3.16 show the production of the most typical gaseous products divided by the number of used points (discharges) as a function of the discharge power P_d per point (discharge) for the cyclohexanone treatment by the negative HPGD in humid air with flow Q = 1 l/min.

CO_2 production per point is about the same for 1 and 2-point systems, a little greater for 10 and 5 points (Figure 5.3.14, left). More thermal systems with 5 and 10 discharges enhance the CO_2 formation. However, an effect of certain saturation and CO_2 lowering occurs in the 10-discharge system, CO_2 formation is not dependent on P_d and is lower than in 5-discharge system. The saturation might be explained by the decreasing oxygen content, but a proper explication of the CO_2 lowering effect needs further investigations.

The greatest CO production per point (Figure 5.3.14, right) is for 1 point system, it decreases with number of used points. We could suspect that the first discharge forms a certain amount of CO, the second produces less and every next one even less of CO. This might be due to the decreasing oxygen content in the gas as it passes from one discharge to another, but it is not very probable, because CO_2 formation per point behaves oppositely. More likely, every involved discharge forms about the same amount of CO which might

slightly decrease with decreasing O_2, but CO is also decomposed in the discharges, the more discharges are active, the higher is the bulk gas temperature and the greater is the decomposition rate of CO. The temperature effect of CO decomposition is confirmed by the decreasing trend of CO(P_d) curves of 5 and 10-point systems. A major part of CO is probably transformed to CO_2.

The CO/CO_2 ratio behaves consequently (Figure 5.3.15, left), it is close to 1 for 1 point, 1-0.6 for 2 distant points, 0.6-0.2 for 5 points and 0.4-0.1 for 10 points. Although the system with 2 distant points is the best from the viewpoint of removal efficiency per point, it is not so convenient from the viewpoint of CO/CO_2 ratio, the lowest CO/CO_2 ratios are obtained in the more thermal systems with 5 or 10 discharges.

Treated carbon balance ($C_{gas\text{-}product}/C_{treated}$ ratio) is very interesting in the system of 2 distant points (Figure 5.3.15, right). It is lower than for 1 point, it lies in the interval 40-53 %, thus most of the treated carbon rests in non-gas phases, while in more thermal 5,10 and even 1 point system more than 50 % of the treated carbon transforms to gaseous products.

As discussed in section 5.3.2.3, products in solid or liquid phase which rest in the reactor may be considered to be more convenient than noxious gas-phase products (CO, NO_x), and even than non-toxic but greenhouse CO_2. In larger scales, of course, it requires to have solved the problem of reactor cleaning from the forming deposits and to avoid an outgoing of aerosols. Therefore, the system with several distant discharges is promising, though the CO/CO_2 ratio is higher.

NO_2 production per point is qualitatively very similar to the CO production (Figure 5.3.16, left). It is the highest for 1 point system and decreases with increasing number of points, although the highest total NO_2 production is in the 10-discharge system. In the 5 and 10-discharge systems NO_2 production per point decreases with the discharge power per point. It is probably due to higher discharge temperature which is responsible for the thermal decomposition of NO_2 and preferential formation of NO, e.g. according to the reaction:

$$NO_2 + N \rightarrow NO + NO \quad k = 3\times10^{-12}\exp(-300/T)\ cm^3s^{-1} \qquad [Bau82]$$

On the other hand, NO production per point increases with rising P_d per point (Figure 5.3.16, right) in all systems. NO is produced in the highest rate in the most thermal 10-discharge system. Greater bulk gas temperature in 5 and 10 discharge systems enhances the NO formation which is evident also from the steeper trends of the curves of 5 and 10-point

systems. It can be explained by the temperature dependent reactions leading to NO formation, e.g. the above mentioned reaction and the following ones:

$$N + O_2 \rightarrow NO + O \qquad k = 1.1\times10^{-14}\times T\times\exp(-3150/T)\ cm^3s^{-1}$$

$$O + NO_2 \rightarrow NO + O_2 \qquad k = 1.13\times10^{-11}\times(T/1000)^{0.18}\ cm^3s^{-1} \qquad [Kri87]$$

Of course, there occur much more reactions among a variety of species involved in the process. We present just the ones which are non-negligible and help to explain our experimental results. The detailed analysis of all plasmochemical reactions involved in the process requires a kinetic approach which is beyond the scope of this work.

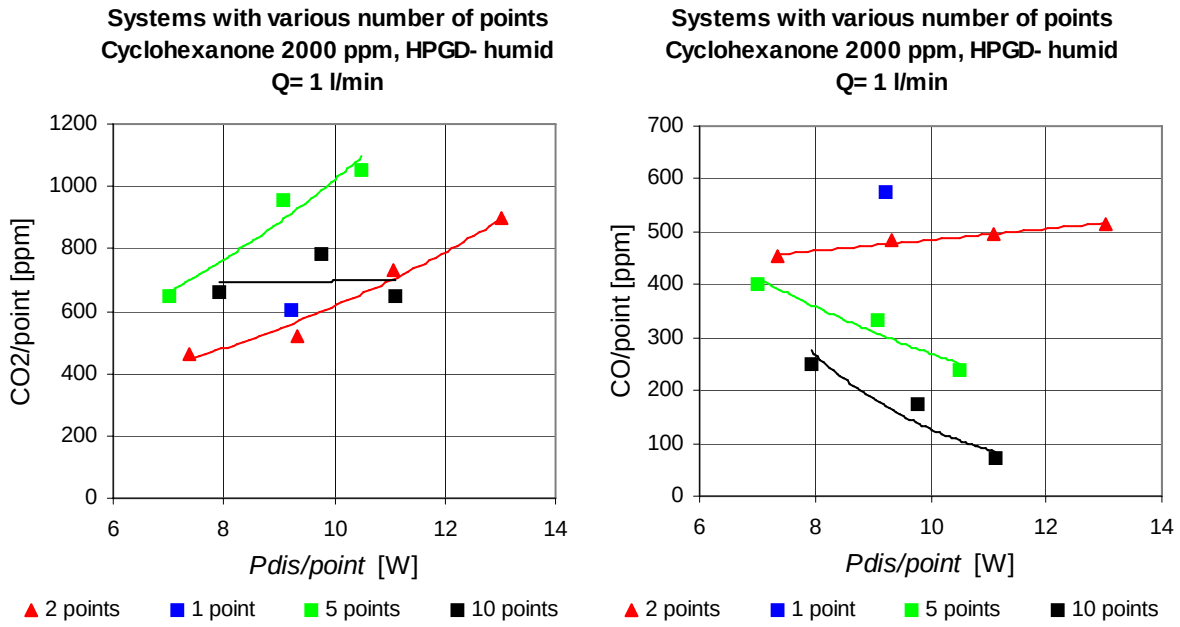

Figure 5.3.14 CO_2 (left) and CO (right) production per point as functions of the discharge power P_{dis} at fixed gas flow Q=1 l/min normalised to the number of working discharges. Systems with 1, 5, 10 discharges and 2 distant discharges (negative HPGD, humid air) in the glass tube reactors.

The conclusions of the comparison of systems with various number of operated discharges from the viewpoint of formed gaseous products are not so clear as from the viewpoint of removal efficiency. The lowest CO/CO_2 ratio was obtained in the more thermal 5- and 10-discharge systems, while the lowest NO_x production was achieved in the systems with 1 and 2 discharges. The VOC removal process occurring in the system with two distant discharges leads to the highest rate of non-gaseous products. Considering this fact and the best efficiency per discharge in this system, we suspect that the HPGD reactor adapted for an operation of several distant discharges might be a promising attempt for VOC removal.

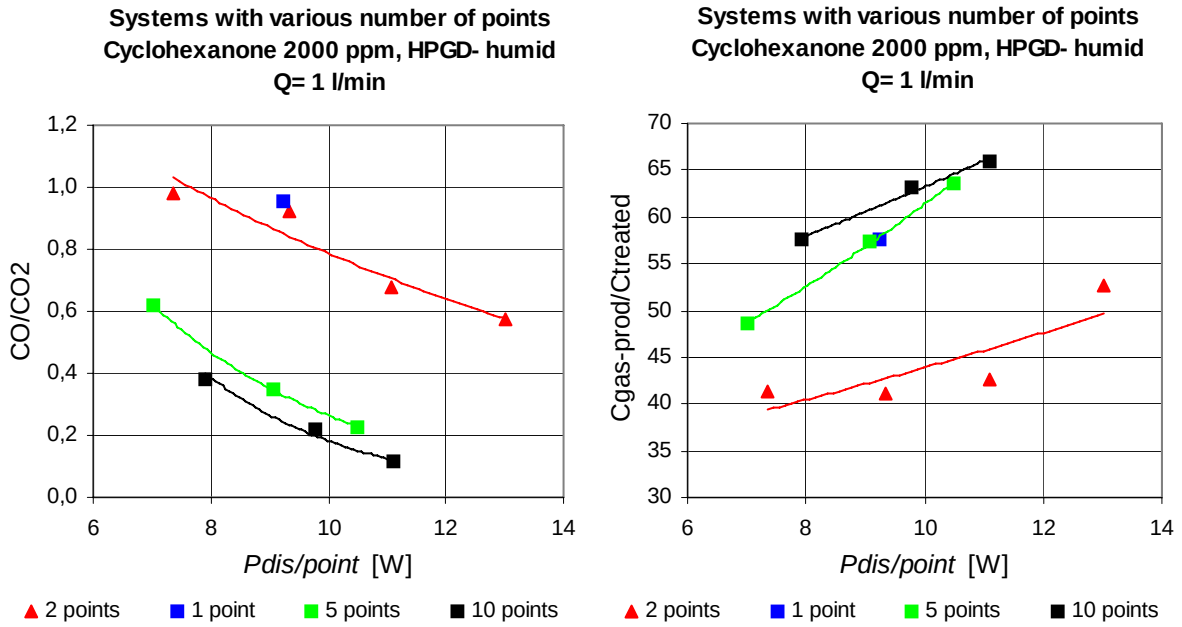

Figure 5.3.15 CO/CO_2 ratio (left) and treated carbon balance (right) as functions of the discharge power P_{dis} at fixed gas flow Q=1 l/min normalised to the number of working discharges. Systems with 1, 5, 10 discharges and 2 distant discharges (negative HPGD, humid air) in the glass tube reactors.

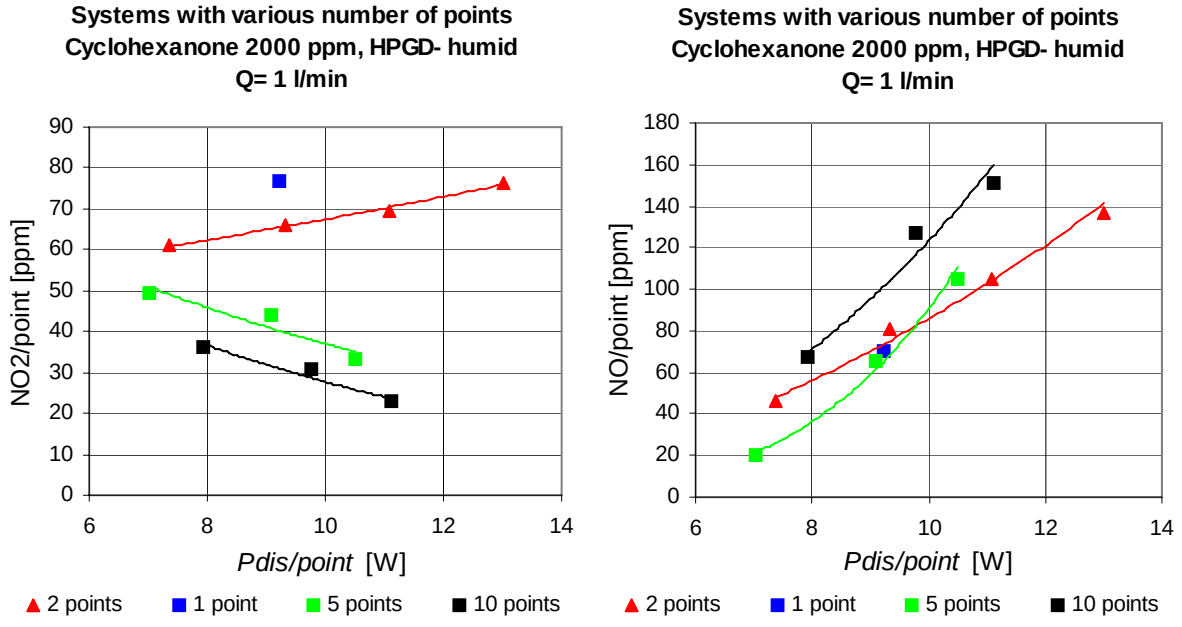

Figure 5.3.16 NO_2 (left) and NO (right) production per point as functions of the discharge power P_{dis} at fixed gas flow Q=1 l/min normalised to the number of working discharges. Systems with 1, 5, 10 discharges and 2 distant discharges (negative HPGD, humid air) in the glass tube reactors.

5.3.3 TS in the glass tube reactor with 5 parallel points

Physical properties of the transient spark were investigated in details in chapter 4, mainly in the point-to-plane configuration. We tried to apply this discharge to the removal of cyclohexanone and toluene in the reactor with 5 parallel points, the same reactor which was used for deVOC in HPGD. It allows to compare the effects of both studied discharges. These experiments were performed in dry and humid air. Just the positive polarity of TS was used, the negative TS was very difficult to establish and maintain.

5.3.3.1 Removal efficiency and energy costs

Figure 5.3.17 illustrates the removal efficiency η and energy costs R_{mol}, two basic characteristics of the VOC removal processes, as functions of the energy density R_V for cyclohexanone removal in dry and humid air (graphs for toluene are similar). Total energy costs R_{moltot} and total energy density R_{Vtot} were considered, because the precise measurement of the discharge power P_d in the pulsed TS is problematic (remind chapter 4.3.2) and the correct method of its measurement was not applied in all performed experiments. However, the total power P spent by the system was always correctly measured. Result curves of some representative cases of HPGD (usually the negative polarity in dry air case) were added into the graphs in order to compare the effects of the two discharges.

The first impression from the presented graphs is that lower energy densities R_V were reached in the TS, this discharge consumes less energy. The $\eta(R_V)$ dependence for both compounds (Figure 5.3.17, left) indicates that the TS curves are practically the same like the logarithmic-shaped curves of the HPGD, but TS takes place of the steeper growth at lower R_V, while HPGD is placed mainly in the part of the mild growth at higher R_V. The VOC removal efficiencies in both TS and HPGD are comparable, TS is a little more efficient than HPGD in the interval of R_V where both curves appear together. The maximal achieved efficiency in TS is 60-70 %, because higher R_V were not reached. Humid air slightly lowers the efficiency for both studied compounds.

The $R_{mol}(R_V)$ dependences for both compounds treated by TS (Figure 5.3.17, right) indicate a special trend which was not observed in HPGD, a fast growth of R_{mol} at very low R_V followed by a mild growth and then through an inflexion point by an exponential-like growth typical for HPGD. It is convenient to work in the part of the mild growth where an increase of the energy density R_V does not cause a dramatic growth of energy costs R_{mol}. TS is more

energetically efficient than HPGD, R_{mol} is lower in the interval of R_V where both curves appear together for both compounds, especially for cyclohexanone. Less than 100 eV/molecule of the energy costs obtained in TS is really a very low value, in comparison with HPGD as well as with other plasma techniques, e.g. dielectric barrier and silent discharges [ChM97, Odi99, Kra96, Bug96], surface discharges [Yam92, Ura97], pulsed corona [vHe98], capillary discharge [Koh98] and electron beam [Pau93]. Energy costs below 100 eV/molecule were obtained rarely, e.g. in pulsed corona [Kor98] and silent discharges [And99, Gau98]. Complex comparison of our results with the results of others will be provided in chapter 6.

A presence of water in TS increases the energy costs.

From the viewpoint of the initial VOC concentration, there is no difference between HPGD and TS for both cyclohexanone and toluene: no effect to the removal efficiency was observed in TS. Energy costs decrease with the rising initial VOC concentration as a logic consequence of the definition formula of R_{mol} (equation 2.4.4).

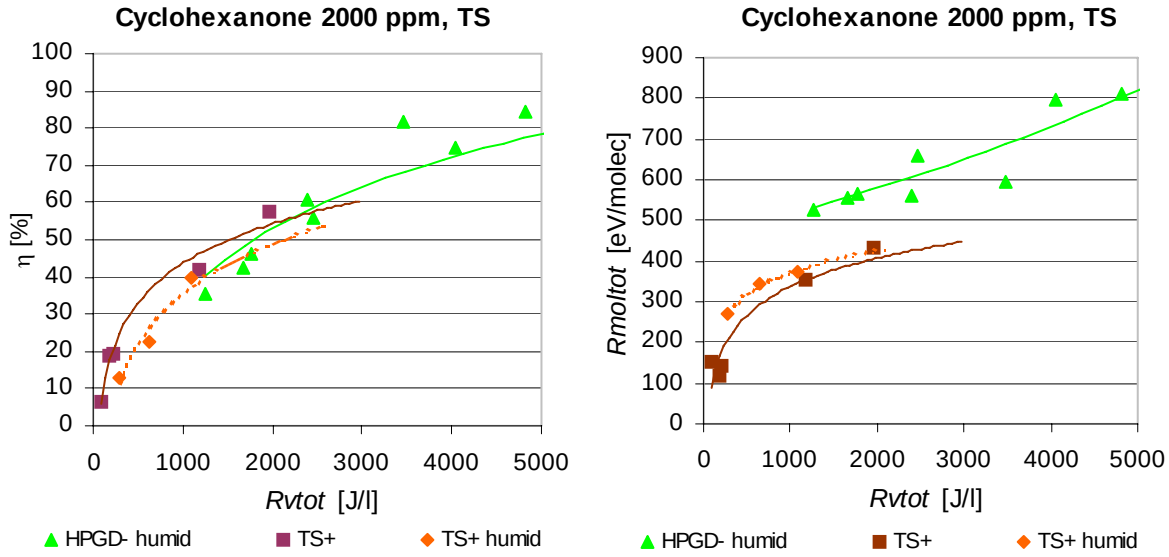

Figure 5.3.17 Removal efficiency η (left) and total energy costs R_{moltot} (right) as functions of the total energy density R_{Vtot}. Positive TS in the 5-points glass tube reactor in dry and humid air, compared with negative HPGD in dry air.

5.3.3.2 Effects of TS on dry and humid air without and with VOC

Similarly to HPGD, we examined how the TS discharge acts in dry and humid air without VOC from the viewpoint of the air composition changes. We used the 5-point reactor

with just one discharge operated. Then we charged air by about 2000 ppm of VOC representative (cyclohexanone) and investigated how it influences the gaseous products in the same system with one discharge.

Generally, TS in dry and humid air without VOC, as well as HPGD, forms nitrogen oxides (NO_x), especially NO and NO_2, in trace amounts also N_2O (dry) and HNO_2 (humid). NO_x formation (Figure 5.3.18, open points, dashed lines) increases with the discharge energy density, due to the increasing discharge and bulk gas temperature. A presence of moisture in air slightly reduces NO_2 formation, but increases NO formation, although it does not change the discharge properties, as discussed in chapter 3, section 3.3.8.1. Hence, the NO_x formation in TS in air is not purely dependent on the discharge temperature.

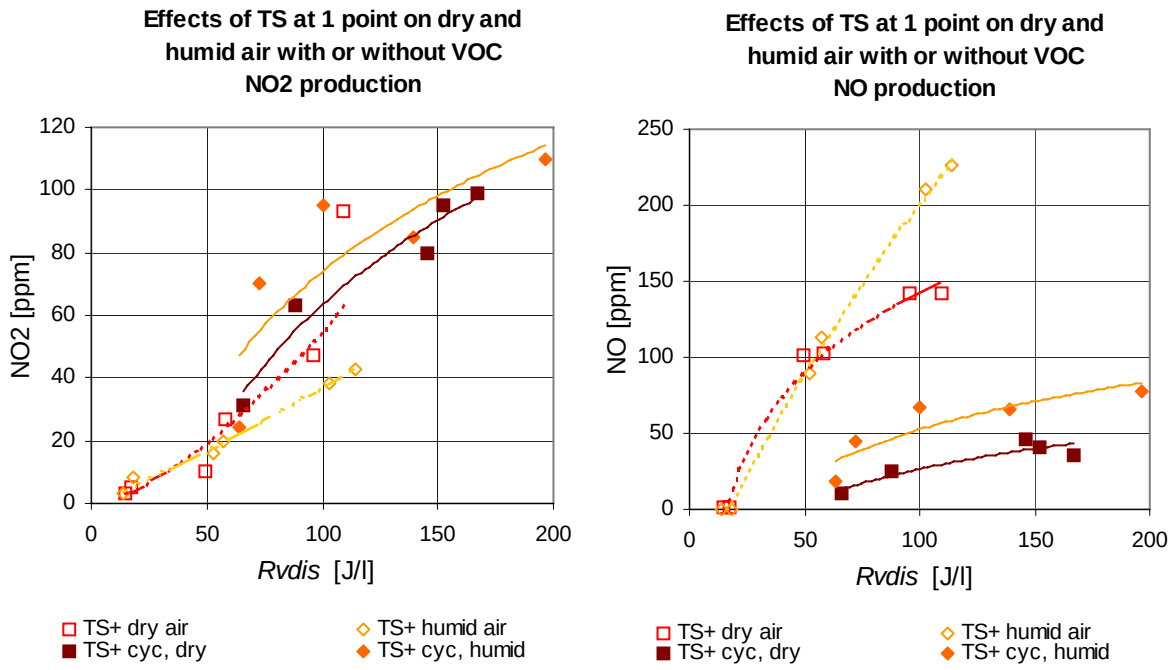

Figure 5.3.18 NO_2 (left) and NO (right) production by TS at 1 point in dry and humid air with (full points, solid lines) or without (open points, dashed lines) VOC (cyclohexanone ~2000 ppm) as functions of the discharge energy density R_{Vdis}.

When an organic compound (cyclohexanone) enters to this discharge system, it becomes more complicated, which was observed in HPGD too. The NO_2 formation is enhanced and the NO production is reduced in both dry and humid air (Figure 5.3.18, full points, solid lines). Both NO and NO_2 are formed in greater amount in humid air (with VOC), despite of lower NO_2 formation in humid air (without VOC), if compared with dry air. When

VOC is present the trends of NO_x(R_V) curves become logarithmic-like, an effect of saturation occurs. A white aerosol of PAN was sometimes observed in the reactor, as well as in HPGD. Its presence (nitrate group) enhances the basic IR band used for NO_2 evaluation, hence really produced NO_2 concentration is lower. This fact explains the measured increase of the NO_2 formation which in reality need not occur. Again, due to the PAN formation we cannot determine a precise value of NO_2 concentration.

The chemical influence of TS on air changes significantly when an organic compound is added, TS behaves similarly to HPGD. It occurs although an organic admixture has almost no effect to the discharge properties (observed in chapter 3, section 3.3.8.1). Like in HPGD, we found again that the discharge temperature is not the only factor influencing the chemical processes induced by the TS.

5.3.3.3 Gaseous products formed by TS in the 5-point reactor

VOC vapours treated by TS were converted to some gaseous and some solid (condensed) products, similarly to the HPGD treatment. The typical gaseous products (for about 2000 ppm of both cyclohexanone and toluene in both dry and humid air) were: carbon dioxide (CO_2), carbon monoxide (CO), water (H_2O), nitrogen dioxide (NO_2) and nitrogen oxide (NO). In trace amounts we often found formaldehyde (HCHO) and nitrous acid (HNO_2).

We traced graphs of the formed gaseous product concentrations as a function of total energy density R_V=R_{Vtot} of positive TS for all typical gaseous products. However, most of the result graphs are qualitatively similar to those ones obtained in the deVOC process in HPGD, so that just significantly different graphs will be presented in the following. So far, all results of these experiments will be noticed.

CO_2 in TS is formed in lower concentrations than in HPGD: 0-1500 ppm from cyclohexanone (R_{Vtot} = 0-2000 J/l) and 0-4000 ppm from toluene (R_{Vtot} = 0-4500 J/l). The logarithmic-like trend of its concentration as a function of energy density agrees with the trend of the removal efficiency. Its formation is slightly lower in humid air in both cyclohexanone and toluene, while in HPGD it was a case just for toluene.

On the other hand, CO in dry air is produced in higher concentrations than in HPGD, in humid air its formation is about the same like in HPGD, for both compounds. TS process in dry air leads to 300-2700 ppm of CO formed from cyclohexanone and 500-3500 ppm from toluene. Humid air significantly reduces its formation. Graph of the formed CO as a function

of energy costs R_{Vtot} (Figure 5.3.19, left) illustrates a very steep growth of CO with rising R_{Vtot}. A maximum was observed in the case of toluene, in cyclohexanone we did not reach higher energy costs, so we cannot state the existence of maximum although it is probable. The CO maximum was always found in HPGD treatment, but it was shifted to higher R_{Vtot}.

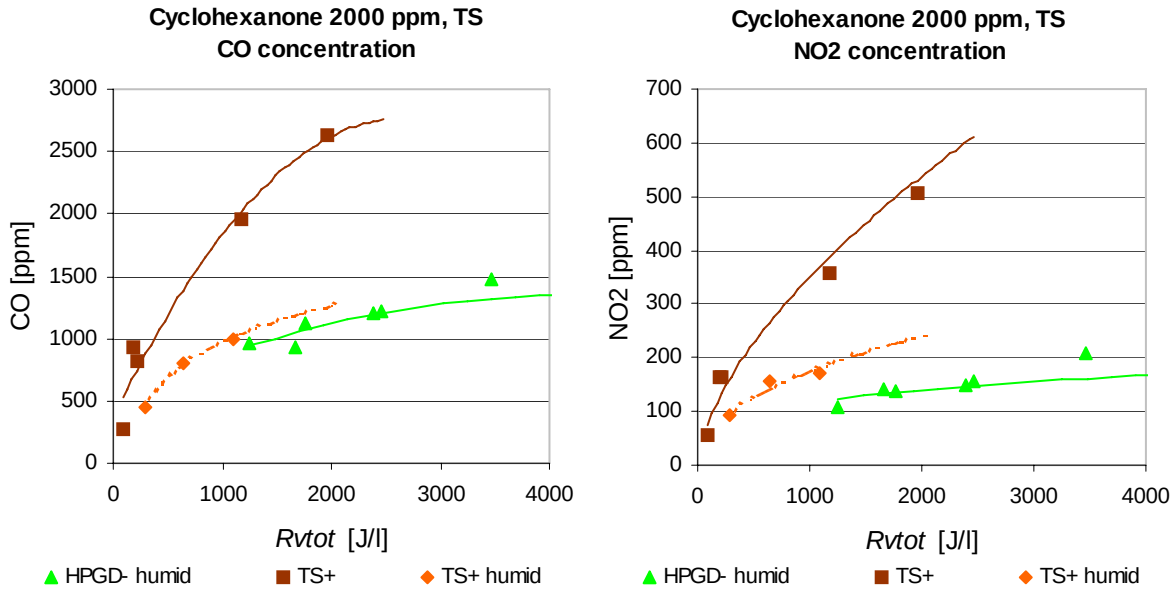

Figure 5.3.19 CO (left) and NO_2 (right) production as functions of the total energy density R_{Vtot}. Positive TS in the 5-points glass tube reactor in dry and humid air compared with negative HPGD in humid air.

As a consequence of lower CO_2 and higher CO formation, CO/CO_2 ratio in TS is much higher than in HPGD. It ranges in the intervals 1.5-4 for cyclohexanone and 0.7-7 for toluene. Thus, from the viewpoint of CO/CO_2 ratio, i.e. perfection of the combustion-like process, TS process of VOC removal is less convenient.

$C_{gas\text{-}product}/C_{treated}$ ratio characteristic for the TS treatment of cyclohexanone is about 45-60 % in dry air and 27-37 % in humid air. A greater rate of the attacked carbon is converted to gaseous products in toluene treatment: $C_{gas\text{-}product}/C_{treated}$ ratio is between 20 and 80 % for both dry and humid air. This ratio grows with rising R_{Vtot} for both compounds.

H_2O in TS is formed in lower concentrations than in HPGD, in dry as well as humid air. 2000 ppm of H_2O for cyclohexanone and 2500 ppm for toluene was a maximum in dry air. H_2O production is much weaker in humid air, similarly to HPGD, maxima of only 300 and 600 ppm were reached for cyclohexanone and toluene, respectively. In some experiments

in humid air we observed a decrease of the initial H_2O concentration, especially at low energy density. In such cases, a part of water present in the carrying air was consumed in the process.

From the viewpoint of NO_x production, VOC removal by TS is less convenient than by HPGD in dry air and about the same in humid air. NO_2 was formed within 50-500 ppm interval in dry air which is higher than in HPGD, but its concentration rises very steeply with rising energy density. This steep trend is significantly reduced in humid air and just 0-300 ppm of NO_2 was formed which is comparable with HPGD. (Figure 5.3.19, right) NO behaves by the same manner, its production is dramatic in dry air and reaches 900 ppm for cyclohexanone and 1100 ppm for toluene, but much lower and rather slight (maximum 200 ppm for cyclohexanone and 800 ppm for toluene) in humid air.

5.3.3.4 Conclusion

The conclusion of the comparison of HPGD and TS applied for cyclohexanone and toluene removal in the 5-point reactor are the following: from the viewpoint of the removal efficiency, these discharges are comparable and from the viewpoint of the total energy costs, TS is more effective. The colder plasma generated by the TS is certainly responsible for this fact, in TS there is less energy lost for the gas heating. Initial VOC concentration has no effect on the removal efficiency like in HPGD.

From the viewpoint of formed gaseous products, TS gives much higher CO/CO_2 ratio and in dry air also more NO_x. Humid air reduces the production of noxious CO and NO_x almost to the level of HPGD, but also yields a little lower removal efficiency and a little higher energy costs.

5.3.4 HPGD and TS in the Cu reactor with threaded rod

Copper tube reactor with threaded copper rod inner electrode (shown in Figure 4.2.2 in chapter 4.2 Experimental Set-Up for the Study of the Transient Spark) was developed in Bratislava in order to study the heterogeneous effects of the copper electrode surface on the plasmochemical processes involved in VOC removal, as well as in the CO_2 depletion and other applications [Mrv98b, Mac98c, Mrv99b]. It is adapted mainly for the transient spark which usually treats most of the reactor volume, its behaviour in this reactor was described in the chapter on TS, section 4.3.3 A special modification of the Cu tube reactor – transparent reactor with rectangular cross section and Cu threaded rod opposite to two plane

electrodes (described in this chapter, section 5.2.1.3 Additional discharge systems) was developed for the study of VOC removal by HPGD assisted by heterogeneous effects of the copper electrode surfaces. Similar effects of Cu surfaces reflected to the higher efficiency of NO_x, CO_x or VOC removal process were reported also elsewhere. [Gas98, Gas99, Mrv98a]

The construction of the Cu tube reactor (and rectangular reactor with Cu thread) allows a long contact of the treated gas with the Cu electrode surfaces, much longer than in the glass tube reactors, though they comprised the Cu plane electrode too. Due to a long contact of the treated gas with the Cu electrodes heterogeneous catalysis occurs during the VOC decomposition process, especially because of the length of the tube (50 cm), greater cross section of the tube resulting in slower flowing velocity and longer residence time, as well as the fact that both electrodes are made of Cu, even the thread which enlarges the surface of the HV electrode. Comparison of several parameters of the various reactors is given in Table 5.3.1.

Tests of the VOC removal in the Cu threaded rod reactor were performed in the Bratislava laboratory. Both polarities of the HPGD and the TS were applied to various initial concentrations of cyclohexanone, some tests were done also with toluene. We used dry air (in some experiments also humid air) as the carrying gas at various gas flows. The VOC decomposition process was characterised by the usual parameters: removal efficiency η, energy costs R_{mol} and specific energy density R_V. Total $R_{mol}=R_{moltot}$ and $R_V=R_{Vtot}$ (calculated from the total power consumed by the whole circuit) were considered, because we were not equipped for the precise measurements of the discharge power in Bratislava.

Reactor	***l* [cm]**	***S* [cm^2]**	**τ [s]**	***A* [cm^2]**
Glass tube with Cu plane	14	0.59	0.50	14
Cu tube with Cu thread	50	3.18	9.54	463
rectangular with Cu thread	50	6.72	24	333

Table 5.3.1 Comparison of some parameters of the glass tube and Cu tube reactors. l - active length, S - cross section, τ - active residence time of the gas (in the active part of the reactor, calculated for the gas flow rate 1 l/min), A - active surface of Cu electrode(s). Active means concerning Cu electrode(s), in Cu tube reactor both electrodes considered.

5.3.4.1 Removal efficiency and energy costs

The dependencies of the removal efficiency η and total energy costs R_{mol} on the specific total energy density R_V, input VOC concentration c_0 and residence time τ of the treated gas in the reactor are shown on the following graphs. Figure 5.3.20-24. They correspond to the cyclohexanone removal, the toluene removal gave similar results.

Achieved values of the decomposition rates η and energy costs R_{mol} are rather dispersed, η of cyclohexanone varied around 50 % in positive HPGD, 60 % in negative HPGD and around 50 % in both polarities of TS. Logarithmic interpolation curves were used in all following graphs, they seemed to fit best the dispersed measured values of η and $R_{mol.}$ Removal of toluene gave slightly lower efficiencies.

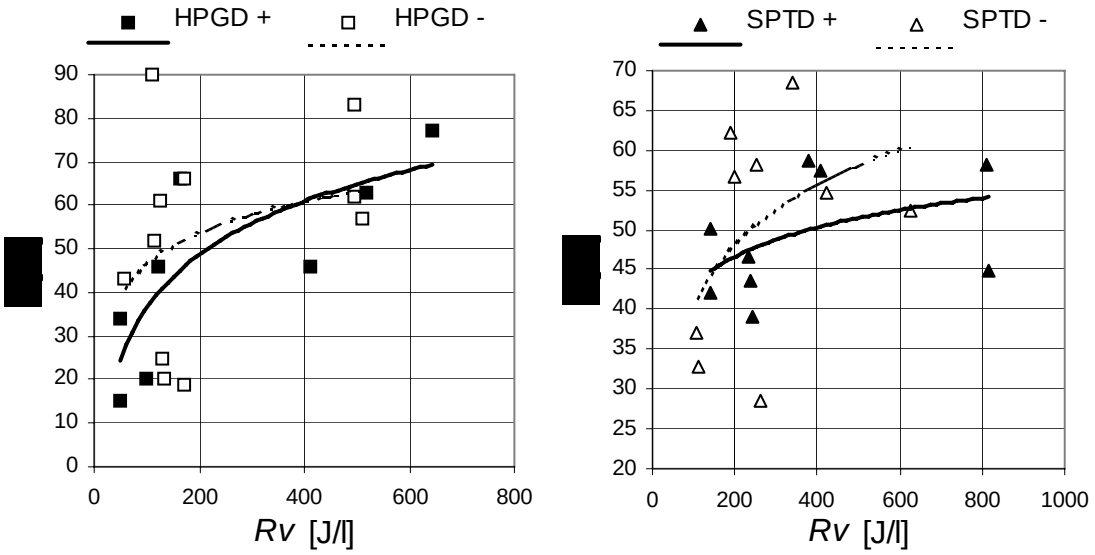

Figure 5.3.20. Removal efficiency η as a function of the energy density R_V, both polarities of HPGD and TS (=SPTD) applied for cyclohexanone removal in Cu tube reactors.

Figure 5.3.20 shows the cyclohexanone removal efficiency η as a function of the energy density R_V. For both polarities of HPGD and TS η grows with R_V. To obtain higher η we have to increase R_V, but doubled R_V does not double η, we observe the same saturation effect like in HPGD and TS in point-to-plane reactors which is typical for plasma deVOC processes. The highest η have been achieved in the negative HPGD (70%), the lowest in the positive TS (55%). Please, notice that the values of the total energy density R_V at which we obtained reasonable efficiencies (400-800 J/l, η up to 70 %) are much lower than in HPGD or

TS operated in the glass tube reactors (more than 2000 J/l). In fact, HPGD and TS operated in the Cu tube reactor should be comparable to the same discharges operated just on one unique point in the glass tube reactor, but the achieved η are highly above those ones, in particular for TS. They are comparable with results obtained on 5 active points. It confirms the reactor effect.

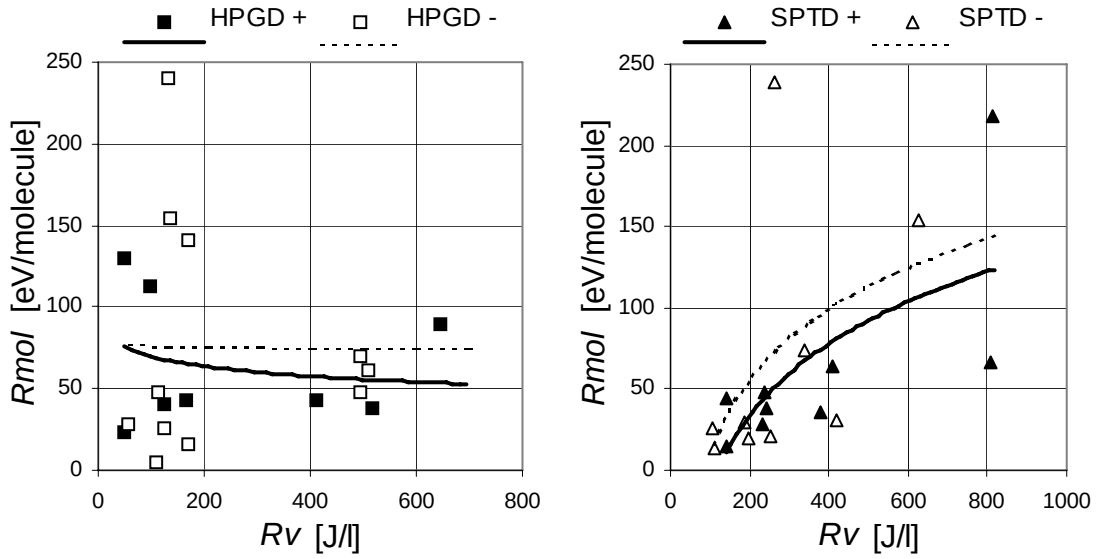

Figure 5.3.21 Energy costs R_{mol} as a function of the energy density R_V, both polarities of HPGD and TS (=SPTD) applied for cyclohexanone removal in Cu tube reactors

Figure 5.3.21 illustrates the energy costs R_{mol} as a function of the energy density R_V. The logarithmic lines interpolating the experimental points of both polarities of HPGD give approximately a constant function which means that the energy costs in HPGD are almost not influenced by the energy density, hence we could choose the regime with the highest efficiency regardless to R_V. This result is surprising and completely different from the behaviour of HPGD in the glass reactors. However, its reliability is questionable because of a great scatter in experimental points. On the other hand, a ”classical” rising trend of $R_{mol}(R_V)$ was observed in both polarities of TS. Thus, to decrease energy costs of the process R_{mol} it is better to work at low R_V, hence high gas flows or low total power. For $R_V < 200$ J/l the energy costs R_{mol} are lower in TS (10-50 eV/molecule, better in positive TS) than in HPGD (50-100 eV/molecule). For R_V around 300 J/l, TS and HPGD are similar from the point of view of R_{mol}. For $R_V > 400$ J/l the removal process was more energetically effective (lower R_{mol}) in HPGD (50-100 eV/molecule) than in TS (100-150 eV/molecule). The positive polarity of both discharges is more energetically efficient, it always gave lower R_{mol}. Obtained energy

costs are rather low, usually below 100 eV/molecule, which is better in comparison with the HPGD and TS processes in glass tube reactors as well as most of other plasma deVOC techniques (see overall comparison in chapter 6).

In both HPGD and TS operated in the glass reactors there was no effect of the initial VOC concentration c_0 to the removal efficiency η. On the contrary, we observed a concentration dependence of η in the discharges operated in the copper reactor, especially for HPGD, which is shown in Figure 5.3.22. η is rising with c_0 for HPGD, stronger in the negative polarity. It indicates that HPGD in Cu reactor is a more convenient method for higher initial VOC concentrations. The values of $\eta(c_0)$ of TS are too dispersed to do any conclusions. R_{mol} decreases with rising c_0 which is logic from the formula (2.4.4). This effect is event enhanced by the growth of η.

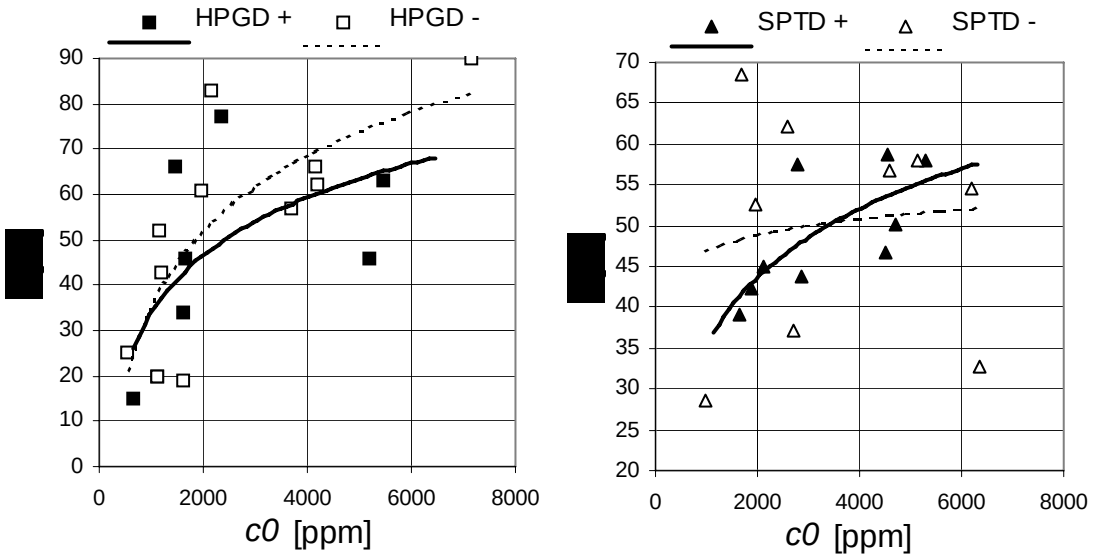

Figure 5.3.22 Removal efficiency η as a function of the initial concentration c_0, both polarities of HPGD and TS (=SPTD) applied for cyclohexanone removal in Cu tube reactors

Let us notice also Figure 5.3.23 and Figure 5.3.24 showing η and R_{mol} as functions of the residence time τ of the treated gas in the discharge chamber. τ is inversionally proportional to the gas flow Q which is practically reflected in the energy density R_V via formula 2.4.2, but τ is an important parameter of the process as well. η rises with growing τ in both discharges, for $\tau > 4$ s a saturation of η occurs. Hence, it is not convenient to work at very low gas flows. For $\tau < 4$ s the efficiency η is higher in TS than in HPGD, thus TS is a

more convenient method for low residence times (high gas flows). $R_{mol}(\tau)$ dependence demonstrates that R_{mol} is almost independent on τ in HPGD, while in TS R_{mol} grows with increasing τ. The lowest R_{mol} have been obtained in TS for very low $\tau < 1$ s. Such regime of the process is energetically very cheap, but η is relatively low (30-50 %). Putting more discharge tubes in series could improve this fact, it was a case in the pilot-scale reactor as will be shown later (chapter 6).

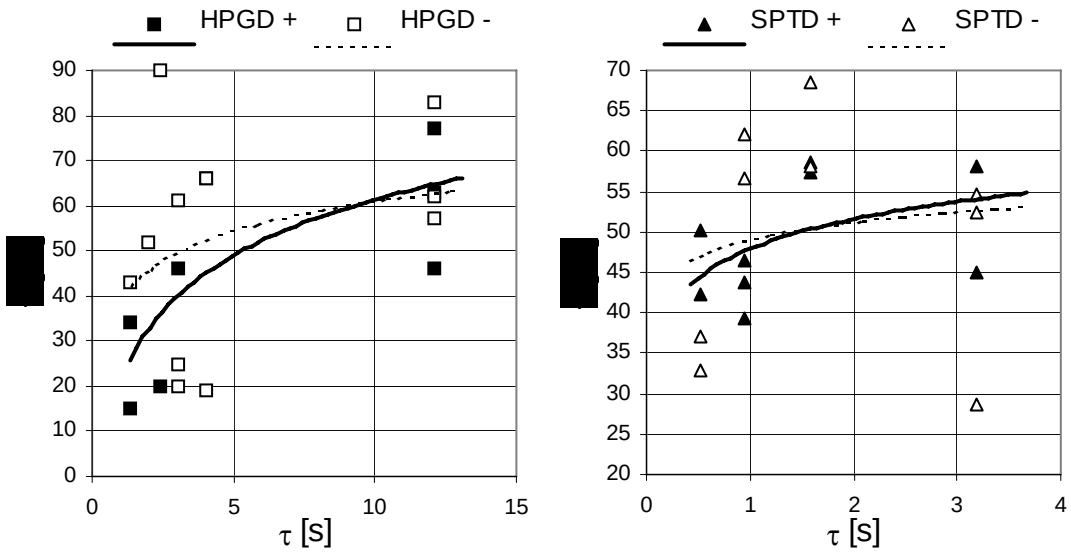

Figure 5.3.23 Removal efficiency η as a function of the residence time τ, both polarities of HPGD and TS (=SPTD) applied for cyclohexanone removal in Cu tube reactors

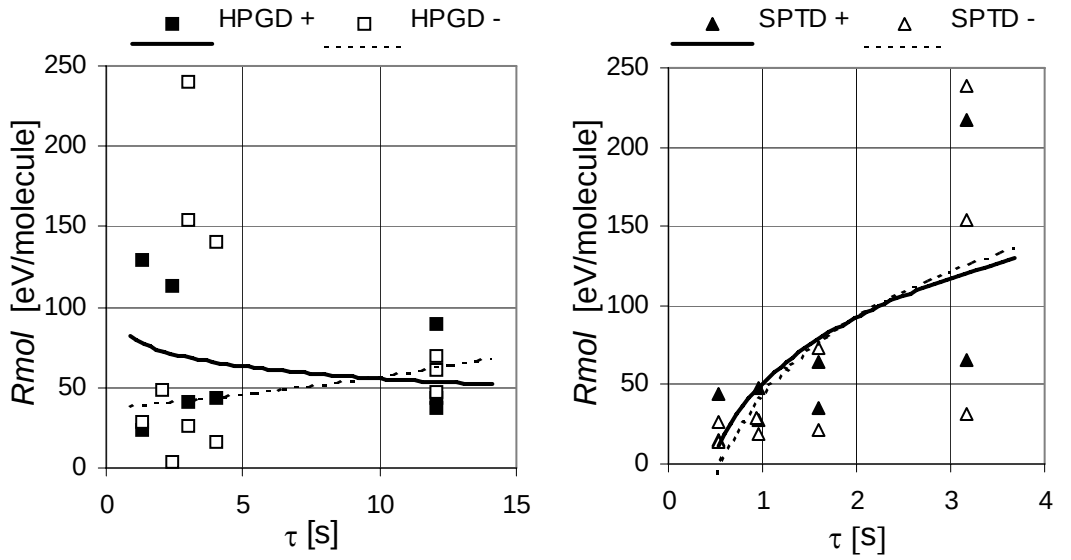

Figure 5.3.24 Energy costs R_{mol} as a function of the residence time τ, both polarities of HPGD and TS (=SPTD) applied for cyclohexanone removal in Cu tube reactors

5.3.4.2 Gaseous products of VOC removal in Cu tube reactors

VOC vapours treated by HPGD and TS operated in the Cu reactors were converted to some gaseous and some solid (condensed) products. Their character depends on the type of the discharge and its polarity, its energy density, residence time τ of the gas in the discharge volume and VOC type and its initial concentration c_0. Again we found typical gaseous products such as CO_2, CO, H_2O, NO_2, but new solid products appeared in some specific conditions.

The experiments with Cu reactors were performed in Slovakia where we used the spectrometer Specord M80 with lower resolution and higher detection limits than Bruker IFS 48 used in France (remind Table 5.2.2 in section 5.2.5.2). The species which were suspected, but not detected, might be present in concentrations under the detection limit.

In HPGD of both polarities and very long residence times (12 s) corresponding to high energy densities (800 J/l) we detected a strong CO_2 and H_2O production (about 4000 ppm) with some CO production (maximum 100 ppm). H_2O production was stronger in the negative polarity. NO_2 was formed in maximal concentrations 200 ppm. Other gaseous species such as NO, O_3, HNO_2 etc. were not detected. Such process is similar to the thermal VOC combustion with typical combustion products. It is also very similar to the HPGD operated in the glass tube reactors, but low CO and NO_x production in the copper reactor is advantageous in comparison with the glass reactors.

CO_2, H_2O and NO_2 productions decrease with decreasing residence time of the gas in HPGD, hence decreasing energy density, on the other hand new products appear, especially in the condensed phase. Formation of all gaseous products in Cu reactor is weaker than in glass reactors, which is due to lower energy density and the construction of the reactor.

VOC removal process induced by TS forms gaseous products similar to HPGD, but in lower concentrations. CO_2 (240 ppm), CO (160 ppm), NO_2 (maximum 80 ppm) and H_2O were produced in the positive TS at long residence times τ (3 s). Their creation was reduced to 100-120 ppm CO_2 and 25 ppm CO at short τ (0.5-1 s). The situation is similar in the negative TS, CO_2 (300-560 ppm), CO (100 ppm), NO_2 (maximum 40 ppm) and H_2O were produced at long τ and only 40-200 ppm of CO_2, traces of CO and some H_2O at short τ. Formation of condensed products was dominant in the TS, especially at short τ (low R_V).

In conclusion, when the residence time of the gas in the discharge is long, oxidation reactions prevail and the process is similar to the combustion (forming CO_2, H_2O, CO and NO_2). This has been observed especially in HPGD at long τ = 12 s. On the other hand, at

shorter residence times and particularly in TS, combustion products are formed in low concentrations and new VOC decomposition mechanisms leading mainly to the solid products become dominant.

5.3.4.3 Active molecular nitrogen and NCO radicals

The new IR band at 1370-1390 cm^{-1} always appeared in the gas product IR spectra, in positive polarity usually shifted to 1360 cm^{-1}, in negative to 1400 cm^{-1}. This band was present in especially strong intensity also in the spectrum of the solid product formed on the discharge electrodes (will be described in section 5.3.6). In the gas phase it corresponds to the long living NCO radical (formed from CO_2 after incorporation of electronically excited molecular nitrogen $N_2^* A^3\Sigma_u^+$) and related ON-NCO and OC-NCO intermediates. Let us analyse more precisely how NCO radicals are formed and what is the role of the active N_2.

Both HPGD and TS in air generate excited N_2 molecules, above all due to collisions of the ground state $X^1\Sigma_g^+$ with electrons to form resonant-radiative excited state $C^3\Pi_u$. C state deexcites to $B^3\Pi_g$ state resulting in the typical radiation of the discharge (2^{nd} positive N_2 system) observed by means of the emission spectroscopy (chapters 3 and 4). B state can deexcite to the metastable $A^3\Sigma_u^+$ state, it was confirmed by the presence of the 1^{st} positive N_2 system in the emission spectra of both discharges (sections 3.3.5.1, 3.4.5, 4.3.4.1, 4.3.5).

So, the first pathway of the $N_2^* A^3\Sigma_u^+$ formation can be traced schematically:

$$e^- + N_2\, X^1\Sigma_g^+ \rightarrow N_2\, C^3\Pi_u + e^- \rightarrow N_2\, B^3\Pi_g + h\nu \rightarrow N_2\, A^3\Sigma_u^+ + h\nu'$$

The necessary electron energy to produce C state is about 11 eV which can be achieved by electron impacts.

Another possible pathway of metastable A state generation proposed by Hanic et al. [Han00] and Kossyi et al. [Kos92] is a direct electron impact of the ground N_2 state (or consecutive electron impacts). The energy of A state at vibrational level v=0 is 6.17 eV, but vibrationally excited A state at v=3 with energy 6.75 eV is more probably generated due to the constant internuclear distance in the N_2 molecule during the collision (see Figure A.2.4 in Appendix 2). [Han00]

$$e^- + N_2\, X^1\Sigma_g^+ \rightarrow N_2\, A^3\Sigma_u^+ + e^-$$

However produced, the metastable state $N_2\ A^3\Sigma_u^+$ has a lifetime τ = 1.3-1.9 s [Lof77, She69, Mag92]. Due to this long lifetime, the stored energy can be reused in other reactions later and much further from its place of origin. That it why we call it also "active nitrogen". Moreover, the $N_2\ A^3\Sigma_u^+$ state is found to have the greatest population among all other active species in the streamer-induced discharges in air. [Fil00]

Now, let us analyse the formation of the NCO radicals which were detected in the IR spectra of gas-phase products in Cu reactors. These radicals are important intermediates in combustion process, in particular in the conversion of fuel nitrogen into nitrogen oxides and in the so-called "prompt" NO formation process. [Mll89] They are also intimately associated with the oxidation of N-containing hydrocarbons. [Per85] $NCO^{\bullet}$ radical is an important intermediate in various processes due to its very long lifetime, up to 24 h. [Cop92]

The main reaction pathways of $NCO^{\bullet}$ formation were introduced in chapter 2.5.3.3. M.Morvová et al. suggest mechanisms where CO_2 reacts with active $N_2^*\ A^3\Sigma_u^+$. ON-NCO and $NCO^{\bullet}$ radicals are then produced:

$$N_2\ A^3\Sigma_u^+ + O=C=O \nearrow O=N-N=C=O$$
$$\qquad\qquad\qquad\qquad\quad \searrow NO + {}^{\bullet}N=C=O$$

[Mrv98a, Mrv00, Kur97, Han00]

In our system, CO_2 is formed by the VOC combustion-like process and active N_2^* are generated in the discharge, hence the above mechanism of $NCO^{\bullet}$ formation is probable.

$NCO^{\bullet}$ radicals can react also with H_2O and H_2 and form bases of amino acids:

$$H_2O + {}^{\bullet}N=C=O \longrightarrow NH_2-\underset{\underset{O}{\|}}{C}-O-$$

$$H_2 + {}^{\bullet}N=C=O \longrightarrow NH_2-\underset{\underset{O}{\|}}{C}-$$

[Mrv00, Han00]

Reaction of $NCO^{\bullet}$ with H_2 may easily form a cyanuric acid HNCO. This intermediate enters to many other reactions, some of them lead to bases of amino acids as well.

$NCO^{\bullet} + H_2 \rightarrow H + H–N=C=O$ [Per85, Han00]

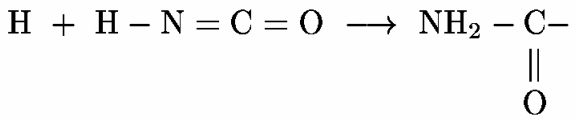

[Mrv00, Han00]

NO was not detected among the gaseous products in the Cu reactors. $NCO^{\bullet}$ radicals might be responsible for its vanishing, there are three possible exothermic reactions:

$NCO^{\bullet} + NO \rightarrow N_2O + CO$

$NCO^{\bullet} + NO \rightarrow N_2 + O + CO$

$NCO^{\bullet} + NO \rightarrow N_2 + CO_2$ [Per85, Bec97]

5.3.5 Solid products and deposits formed in the glass tube reactors

Removal process of cyclohexanone and toluene in HPGD and TS performed in the glass tube reactors lead to some gaseous products and some products in other phases - especially as solid deposits on the plane electrodes and liquid viscose deposits on the tube walls and output hoses leading the treated gas. An amorphous, very viscose deposit was caught also on the Cu passive planes put behind the output of the reactor.

Gaseous products formed in the glass tube reactors and involved mechanisms more or less similar to the combustion process have already been discussed for every treated compound and used discharge and reactor. A detailed analysis of the products in other phases and their development give another point of view on the involved mechanisms of the VOC decomposition process.

Infrared absorption spectroscopy (techniques for the analysis of surfaces, solid and liquid samples explained in sections 5.2.3.1, 5.2.4.3) was applied as the main analysis technique. It was combined with the electronic and optical microscopy. Spectral interpretations were done on the base of [Hol75, Smi99, WAIS, Zhu84, Nkm66, Ben68].

5.3.5.1 Liquid deposit on the glass tube walls (named deposit I)

Viscose liquid deposit of the yellow-brown colour was formed on the glass tube walls and in the output hoses leading the treated gas from the reactor. It is certainly formed by the collecting of aerosol particles and by the condensation of some gas-phase products on the cooler parts of the reactor (walls). Its formation was observed for both cyclohexanone and toluene and all used discharges operating in dry as well as humid air. The deposit I is of amorphous structure. It is very well soluble in acetone and ethanol, soluble in toluene and almost insoluble in water. Deposits of similar physical properties were found also by other authors who treated toluene [Par99] and styrene [And99].

General observation of the IR analysis is that the chemical composition of the deposit I forming from cyclohexanone is a little different from the composition of the toluene deposit I, but the deposit I forming from one compound is almost the same regardless to the used discharge and the presence of moisture in the carrying air. In other words, the discharge type and the humidity almost do not influence its composition. It indicates that the deposit I is the result of the common effect of all used discharges - high temperature and reactions of radicals and intermediates which appear in both used discharges and both applied polarities.

Typical IR spectra of the liquid deposit I formed from cyclohexanone and toluene are presented in Figure 5.3.25.

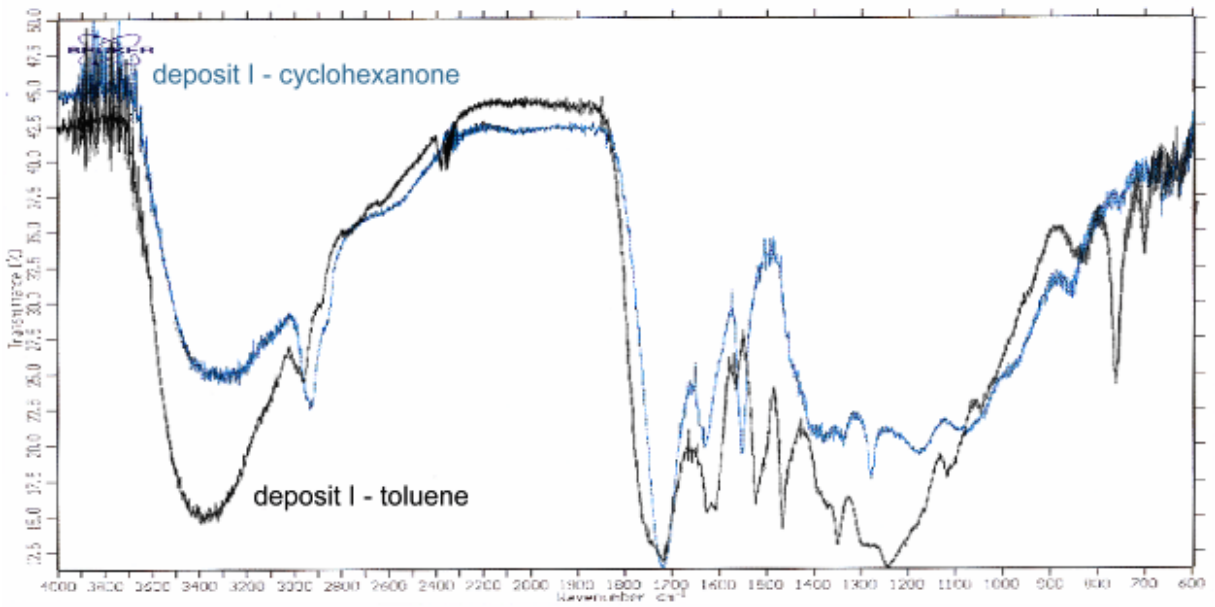

Figure 5.3.25 Typical IR spectrum of the liquid deposit I (on the glass walls) formed from cyclohexanone and toluene

The deposit I forming from cyclohexanone contains carbonyl (C=O), hydroxyl (OH), carboxyl (COOH), amine (NH, NH_2), amide (secondary -CO-NH- or tertiary -CO-N<) and methylene (CH_2) groups. Probable are also carboxylate ion (COO^-), ether group (C-O-C) and nitro group ($-NO_2$). Their presence in the IR spectra indicate that the deposit I is an amorphous condensate of amino acids, probably mixed with some other compounds (carboxylic acids, ethers, esters or nitro-compounds) or with characteristic groups of these compounds attached. 6-membered cyclohexanone very likely leads to the 6-carbon amino acids, e.g. lysine, arginine, histidine (their formation will be explained in more details in section 5.3.6.1). The liquid amorphous deposit I is very likely a mixture of several such amino acids.

The IR spectrum of the deposit I forming from toluene is rather similar to the cyclohexanone one; carbonyl, hydroxyl, carboxyl, amine, amide and CH_2 groups are definitely present in it. However, there are some new bands which can be assigned to the aromatic ring (ring vibrations at 1600 and 1500 cm^{-1}). Nitro groups seem to be more pronounced here which is due to the greater NO_2 formation in toluene treatment. In fact, an attachment of the nitro group ($-NO_2$) to the forming structure is rather probable, because NO_2 is produced by the process, and even more likely, formed PAN aerosol particles already containing nitro group can be incorporated into the deposit. The whole spectrum indicates again a presence of amino acids, but probably aromatic ones (e.g. amino-benzoic acid) with attached nitro groups. Nucleation of several aromatic rings may lead to the formation of polycyclic aromatic hydrocarbons (PAH) which were identified also by Parissi in toluene treatment by DBD [Par99], but our deposit I contains an amino acid component. The formation of amino acids and N atoms incorporation into the deposit I (and all the following ones) is probably associated with the role of active molecular nitrogen (described in sections 5.3.4.3 and 5.3.6.3)

5.3.5.2 Solid deposits on the Cu plane electrode

The copper low-voltage plane electrodes from the glass tube reactors were covered by solid deposits after the deVOC process of cyclohexanone and toluene. These deposits are a result of complicated heterogeneous plasmochemical reactions on the solid Cu surface-gas boundary. The gas flow, the electrode polarity and the distance from the discharge channel (high voltage electrodes were points, thus the discharge channels could be easily localised) are key factors influencing the deposit composition and the involved plasmochemical process,

since they reflect in the electric field, temperature and chemical environment. The deposit types depend on the treated compound, used discharge and its polarity and the presence of moisture which was not a case in the formation of previously mentioned liquid deposits I on the reactor walls. All these factors make their analysis very complicated, we scanned IR spectra from very many places on the low voltage Cu electrode (going from its beginning through spots where the discharge arrived to its end) after the treatment of each compounds in the specific environment (dry or humid air) by each discharge and its polarity.

Generally, all analysed deposits can be divided into three rough groups according to the place on the Cu plane electrode where they were formed.

1. Deposits formed directly in the place under the discharge channel (named ***deposits II***)

   These deposits are solid and rather hard, of black-brown colour, uneasy to remove from the electrode surface or to dissolve in usual solvents. Their common structural groups which were found in all discharges and environments in the IR spectra (see a representative spectrum in Figure 5.3.29) are hydroxyl (OH, strong broad band at 3600-3300 cm^{-1}), =C-O groups (sharp band at about 1300 cm^{-1}, possibly from N=C-O) and C-O, C-C and/or O-O groups (sharp band at 1045 cm^{-1}, probably from COOH or other structures). OH is stronger in humid environment and significantly enhanced in TS, due to higher OH radical formation.

   When the plane electrode was negatively charged (cathode, in positive HPGD and TS) we observed very clean holes and craters of the discharge with almost no deposits and hard black-brown deposits II in their very proximity. It is shown better in the microscopic photograph (Figure 5.3.26), deeper craters made by the discharge are evident from the scanning electrons image; backscattered electrons image demonstrates higher atomic number in the holes (clean Cu) and lower atomic number in the deposit II (C, N, O).

   Weak methylene (CH_2, about 2950 cm^{-1}), strong carbonyl (C=O, above 1700 cm^{-1}) and amide (amide I,II,III) groups appeared in the cathode deposits II. Amine bands (NH_2 or NH) were often superposed on the broad OH band (at 3400-3200 cm^{-1}). All these bands indicate a presence amino acids in the polymer form.

   When the plane electrode was positively charged (anode, in negative HPGD) there were no discharge craters observed, deposits II were formed almost homogeneously in a small spot under the point cathode. Carboxylate ion (COO^-) was determined in the IR spectra (two intense bands at 1560 and 1420 cm^{-1} corresponding to antisymmetric and symmetric COO^- vibration). These bands, together with OH, amine and C-O bands and

non-presence of C=O band, indicate bodies of amino acids in their zwitterionic form, mostly purged from hydrocarbon fragments (CH_2 etc.). These polymer structures are probably attached to the positively charged surface of the Cu electrode by the carboxylate anion.

Polymer structure of these deposits II based mainly on C, N, O but few H atoms is a result of the high discharge temperature. Incorporation of the atmospheric nitrogen into the hydrocarbon residues and their consequent attachment to the Cu electrode surface is followed by the pyrolysis-like process governed by the high temperature at the discharge proximity. It leads to polymerisation and release of the light fragments. Similar mechanisms of polymer formation were observed by Anderson et al. in the process of styrene decomposition in silent discharge plasma at increased temperature. [And99]

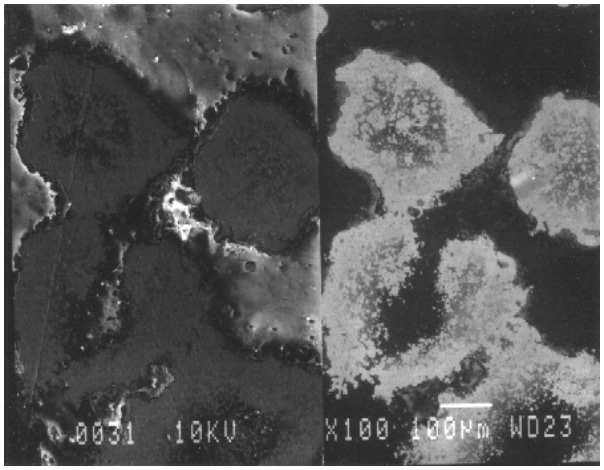

Figure 5.3.26 Electronic microscope photograph of the craters formed by positive TS and surrounding deposit II on the Cu cathode surface, magnification 100, left - scanning electrons image (SE), right - backscattered electrons image (BE) giving information on relative atomic number Z (lighter = higher Z, darker = lower Z)

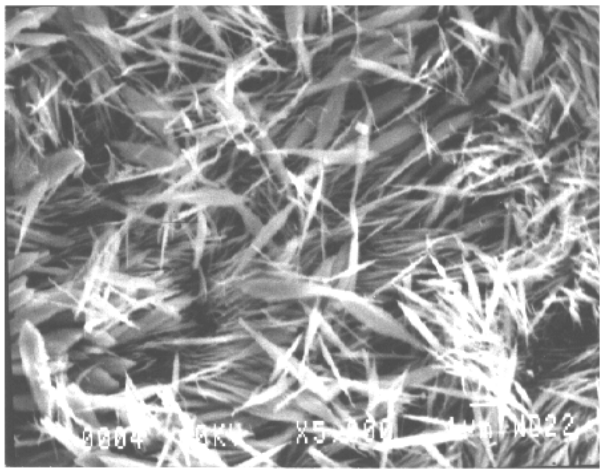

Figure 5.3.27 Electronic microscope photograph of the crystalline deposit on the Cu cathode surface of the positive HPGD formed in humid air, magnification 5000

X-ray element microanalysis (which was unfortunately not sensitive below atomic number 8, i.e. did not detect C and N) combined with IR spectroscopy in deformation region (700-200 cm^{-1}) added some more information on the structure of the deposits II. A mixture of CuO and Cu_2O with a possible presence of a non-stoichiometric Cu_xO_y is present in them, especially crystalline CuO on Cu cathodes. These crystalline mixtures of

copper oxides were observed also when HPGD and TS were operated in air without VOC, crystalline structure on the cathodes being supported by the electric field (please remind chapter 3 on HPGD, sections 3.3.6.1, 3.3.7, 3.4.3.2 and chapter 4 on TS, section 4.3.6.2). We observed an interesting behaviour of CuO crystals when the discharge was operated in humid air - crystals are longer and thinner, see Figure 5.3.27 and compare it with Figure 3.3.7 in section 3.3.6.1. N and C atoms from the previously described polymer structures of the deposits II can be bonded with Cu atoms from the surface as well as O atoms in Cu oxides, unfortunately Cu-N and Cu-C bonds were very difficult to distinguish in the complicated IR spectra.

1. Deposits formed in the surroundings of the discharge arrival place (named ***deposits III***)

   This kind of deposits was usually formed in the round or oval spot of about 1 cm diameter, the place where the discharge arrived was inside. Oval form is due to the gas flow which prolonged the spot in one direction. Typical look-up of these deposits observed microscopically was an amorphous, brown-grey sticky layer, its thickness depends on the duration of the process operation. (Figure 5.3.28) They were usually partially soluble in acetone and other solvents.

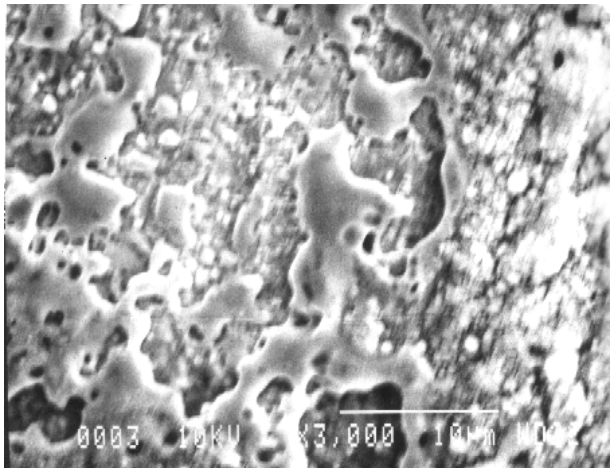

Figure 5.3.28 Electronic microscope photograph of the amorphous deposit III on the Cu anode surface of the negative HPGD, magnification 3000

The electrode polarity does not influence the chemical composition of the deposits III as significantly as in the case of deposits II. All these deposits contain specific OH, CH_2, C=O, amide, C-N, =C-O, -C-O and C-C groups determined in IR spectra (see a representative spectrum in Figure 5.3.29). Those formed from toluene comprise also

aromatic rings (identified ν CH above 3000 cm^{-1} and ring vibrations at 1600, 1500 and 1456 cm^{-1}). OH group is very pronounced in the deposits III forming in the humid environment and in TS discharge. Humid environment also suppresses the hydrocarbon fragments (CH_2 groups). Both these effects can be associated with OH radicals.

All identified groups indicate a presence of amino acids and carboxylic acids in the deposits III, toluene deposits III contain also aromatic components. Bands (at 2170 cm^{-1}) which can be assigned to carboimides (N=C=N) or nitriles (C≡N) were found in the deposits III from cyclohexanone treatment by the negative HPGD (i.e. on the anode) in dry air.

3. Deposits formed far from the discharge arrival (named ***deposits IV***)

Finally, this kind of deposits was formed in places more distant from the discharge channel, on the boundaries of the electrode. Their usual look-up was a thin grey solid layer, slightly rough, they were insoluble in typical solvents.

The chemical composition of these deposits does not crucially vary with the discharge type and polarity and the environment. Characteristic groups revealed by the IR spectroscopy are OH, C-N, =C-O, -C-O and C-C. Traces of aromatic rings were found in the deposit IV from toluene treatment in positive HPGD and dry air.

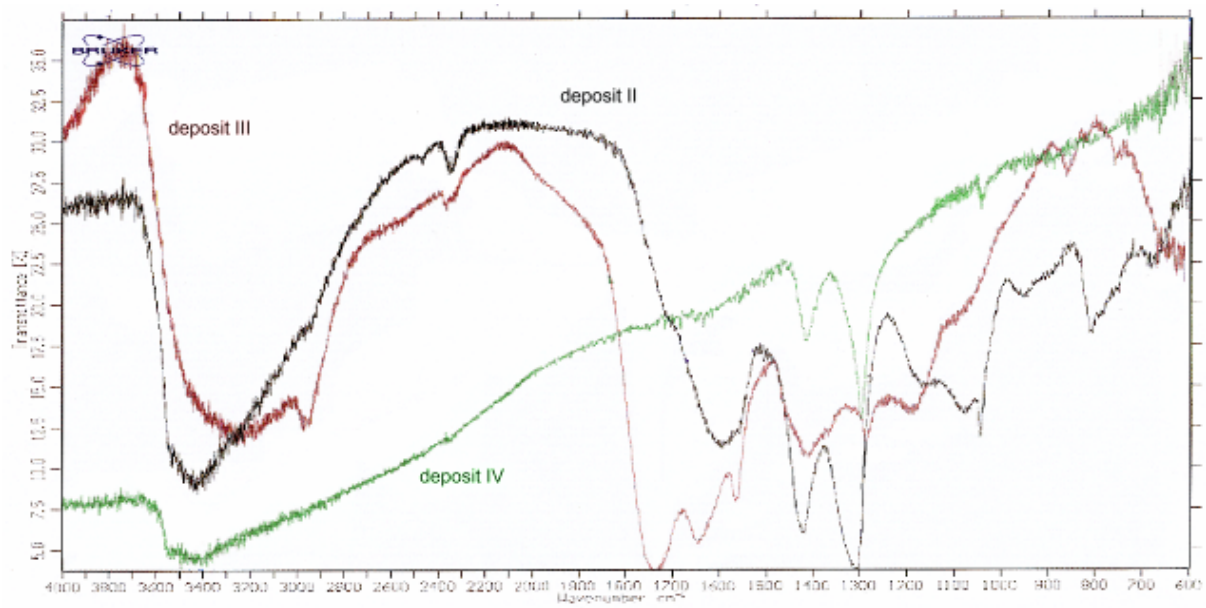

Figure 5.3.29 Representative IR spectra of the deposits II, III and IV formed on the Cu electrode surface.

However, identification of strong solitary IR bands at 1418 and 1300 cm^{-1}, typical for deposits IV (see spectrum in Figure 5.3.29), without a presence of other strong bands in the spectrum (except OH), is not easy. Therefore, an investigation of a real composition of the deposits IV needs much more work.

IR spectroscopy together with the electronic microscopy revealed also a presence of Cu_2O in the deposit IV. Surface Cu probably enters also to the organic deposit IV, by the way which is not clear yet. Mechanisms similar to those participating at the amino acid formation (they will be explained in section 5.3.6.3) might be employed.

5.3.5.3 Solid deposits on the passive Cu planes (named **deposits V***)*

As discussed in section 5.3.5.1, viscose liquid deposit I collected on the glass tube walls and in the output hoses leading the treated gas from the reactor. In order to analyse better this deposit and to investigate if even passive Cu surfaces have effects on the deposit properties, we put some Cu planes (outside of the reactor) into the output hoses - the surfaces of these passive planes with collected deposit I were then analysed by IR spectroscopy. The result of this analysis is surprising - the deposits I have slightly different properties, therefore, we renamed them to *deposits V*.

Deposits V, in comparison with deposits I, are more solid, they cover the Cu passive planes with an amorphous film which is more difficult to remove even with use of acetone and similar solvents. In other words, these deposits attach to the Cu surface better than to the glass of the discharge tube or plastics of the hoses.

IR spectra show some differences too (Figure 5.3.30): Strong carbonyl (C=O at 1725 cm^{-1}) band, typical for deposits I, is weak in deposits V (and shifted to 1712 cm^{-1}), but bands at 1550-1590, 1420 and 1307 cm^{-1} are very strong. These bands are characteristic for carboxylate ion COO^- and =C-O, respectively C-N groups. Other bands, such as OH, NH and CH_2 remain unchanged. OH bands are enhanced in humid air, this behaviour is typical for electrode deposits (II-IV), but not deposits I.

Deposits I were interpreted to be based on amino acids, with attached nitro ($-NO_2$) groups and aromatic rings (from toluene). COO^- and other bands in the spectra of deposits V indicate a zwitterionic form of amino acids, probably attached to the Cu surface by the COO^- group. However, there are no nitro groups in deposits V, just aromatic rings as a rest from toluene. Very weak bands (at 2170 cm^{-1}) which can be assigned to carboimides (N=C=N) or nitriles (C≡N) were found in the deposits V from cyclohexanone treatment by negative HPGD

in dry air. The bands of the same structures were present in deposits III in the same case (on the anode).

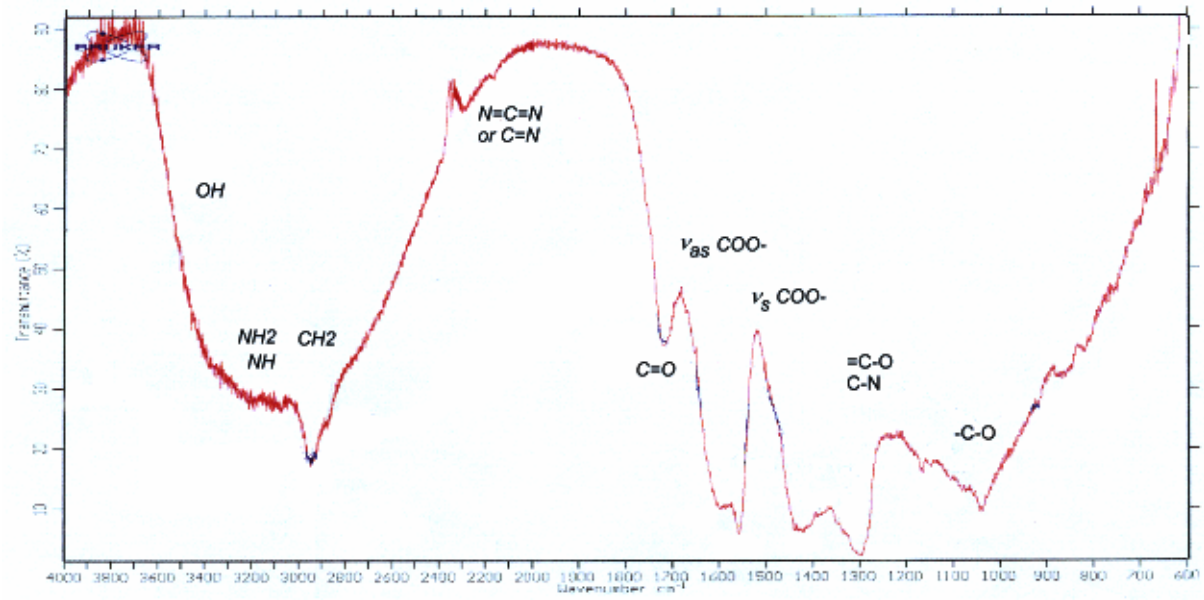

Figure 5.3.30 A representative IR spectrum of deposit V (from Cu passive plane), after HPGD- treatment of cyclohexanone

We propose the following explanation of the different properties of the deposits I and V. It is based on the fact that a non-negligible part of the gas particles treated by the discharge are charged. The dielectric glass walls of the reactor are charged negatively by mobile free electrons generated by the discharge. It results that they tend to attract positively charged particles and repel negatively charged ones up to the establishment of a certain equilibrium. It is likewise the principle of ambipolar diffusion [Fra56], although the discharge itself is constricted and does not touch walls. Therefore, particles with negatively charged COO^- groups cannot collect on the walls.

On the other hand, passive metal Cu planes are on the floating potential determined by the impact of negatively and positively charged particles (electrons likely do not exit from the reactor, since they collide with gas particles, hence they do not influence the potential on the passive planes). Species with negatively charged COO^- groups probably simply attach to the Cu surface, or, also possibly, Cu surface tends to behave as an electron donor and enhances the formation of the COO^- group. Polar bond between the Cu surface and the attached complex probably results in its solid phase and properties different from deposit I.

5.3.6 Solid products and deposits formed in the Cu tube reactor - heterogeneous processes on the Cu electrodes

Solid products were intensively formed in the removal process of cyclohexanone and toluene performed in Cu tube reactors, especially on the electrode surfaces. They were analysed by means of IR absorption spectroscopy, spectral interpretations on the base of [Hol75, Smt99, WAIS, Zhu84, Nkm66, Ben68, Sil91].

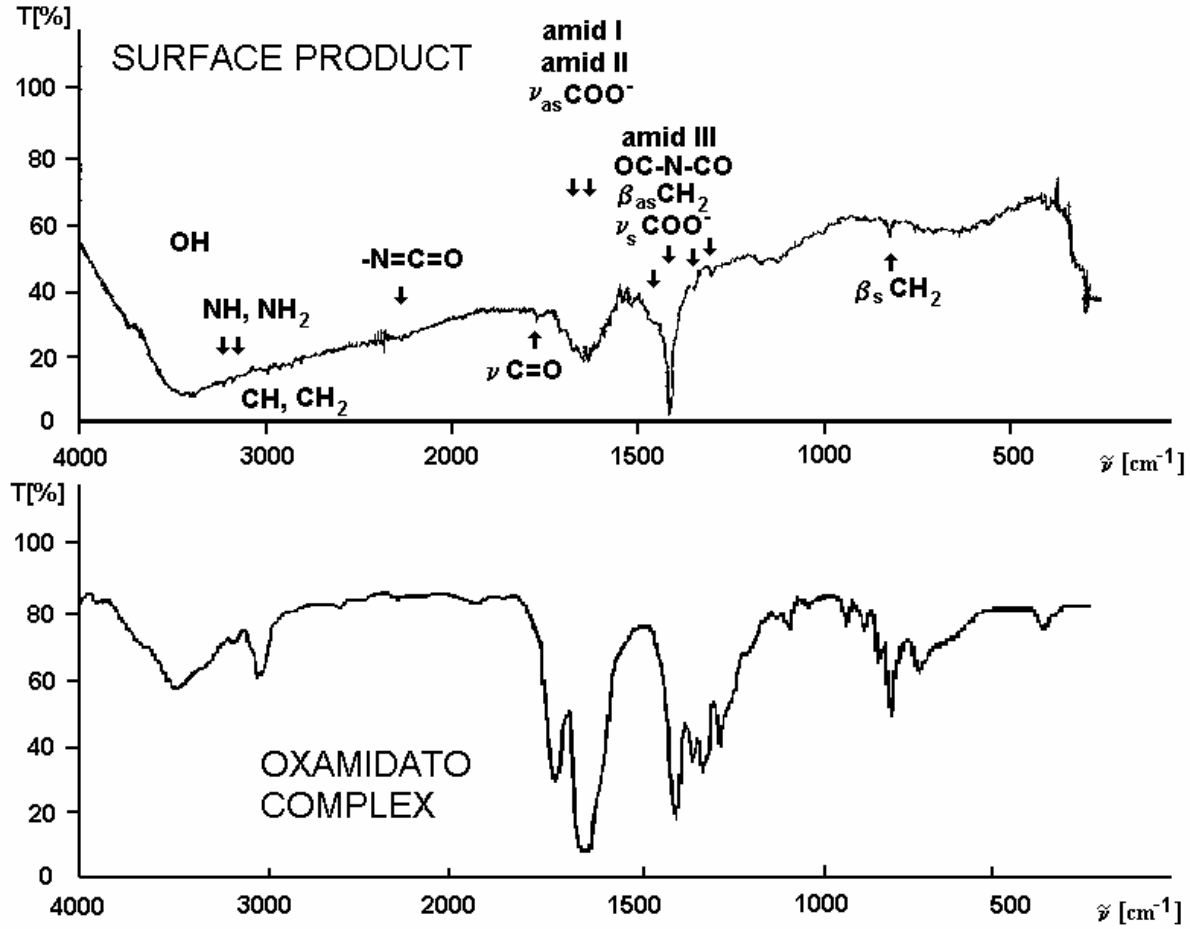

Figure 5.3.31 IR spectrum of the solid product formed on Cu electrode surfaces after cyclohexanone decomposition in both polarities of TS (up) compared with the spectrum of oxamidato complex from [Zhu84] (down).

General characteristics of all IR spectra of solid products formed on the discharge electrodes was a particularly strong band at 1370-1390 cm^{-1} (Figure 5.3.31). It appeared also in the gas product IR spectra, associated with the NCO radical (formed probably from CO_2 after incorporation of excited molecular nitrogen $N_2^* A^3\Sigma_u^+$) and related ON-NCO and OC-

NCO intermediates (as described in section 5.3.4.3). This spectroscopic band in the condensed phase is composed of the -N-CO groups present in amides (amide III band), imide group CO-N-CO, deformation β_s CH_2 and the stretching of carboxylate ion ν_s COO^-. The next strong and broad composed band at 1680-1580 cm^{-1} in the solid product spectrum corresponds to the amide I and II and ν_{as} COO^-. Other bands of medium and weak intensity in the solid product belong to stretching and deformation vibrations of CH_2, NH and NH_2 and OH groups. All these groups indicate a presence of amino acids in the product.

Obtained IR spectra of the gas phase and solid products allow to view some decomposition mechanisms of cyclohexanone and toluene and probable reaction pathways running in the discharge chamber.

Active N_2^* molecules (the long-living metastable state $A^3\Sigma_u^+$ with energy 6.17 eV, probably vibrationally excited to 6.75 eV) are key species governing the VOC decomposition process at shorter residence times, especially in the TS. They form NCO radicals and/or fix directly into the organic species. The N_2^* fixation is probably supported on the Cu surfaces, an enhanced N_2^* fixation in plasmas with a presence of various metals (Cu included) was reported in [Rap80].

5.3.6.1 Cyclohexanone decomposition mechanisms

A probable beginning of the cyclohexanone decomposition is the opening of its cycle, since the binding energy of C=O is high (C-C: 3.6-6.3 eV, C=O: up to 7.7 eV, see Table 2.5.1 in chapter 2.5). It may be initiated by various radicals, active N_2^* molecules with stored energy 6.75 eV are probably involved in this process. Then they are incorporated into the hydrocarbon residues.

Amino acids of C_6 type were detected in the solid product of cyclohexanone treatment formed on the electrode surfaces. Cyclohexanone leads especially to lysine NH_2-$(CH_2)_4$-$CHNH_2$-COOH which can be further converted to arginine NH_2-CNH-NH-$(CH_2)_3$-$CHNH_2$-COOH. We suggest the following reaction scheme of this process:

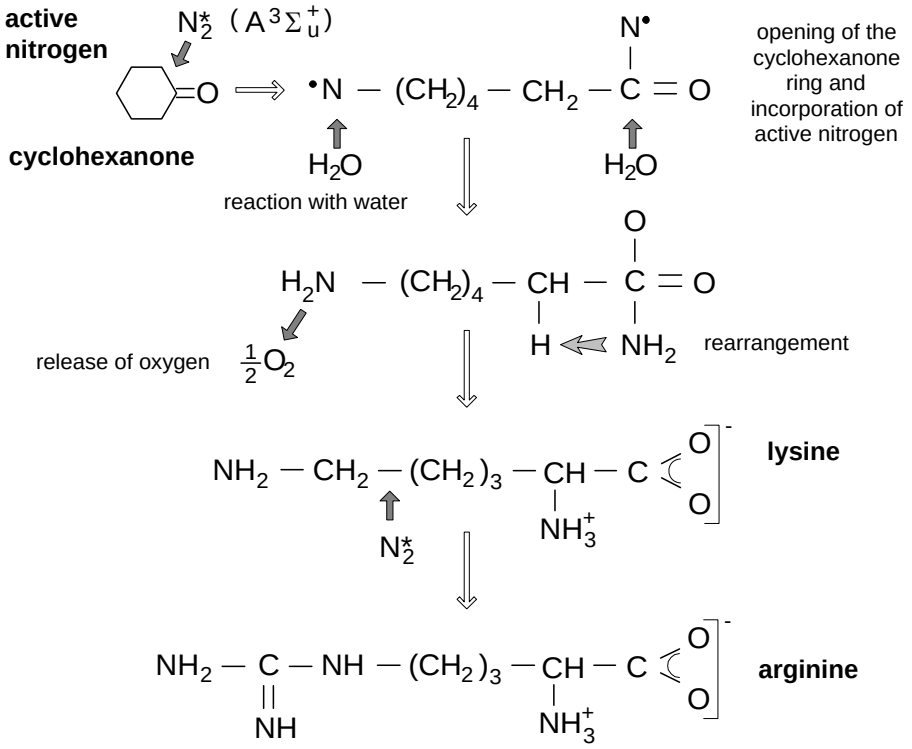

Lysine can be converted also to histidine $C_3N_2H_3$-CH_2-$CHNH_2$-COOH according to the suggested scheme:

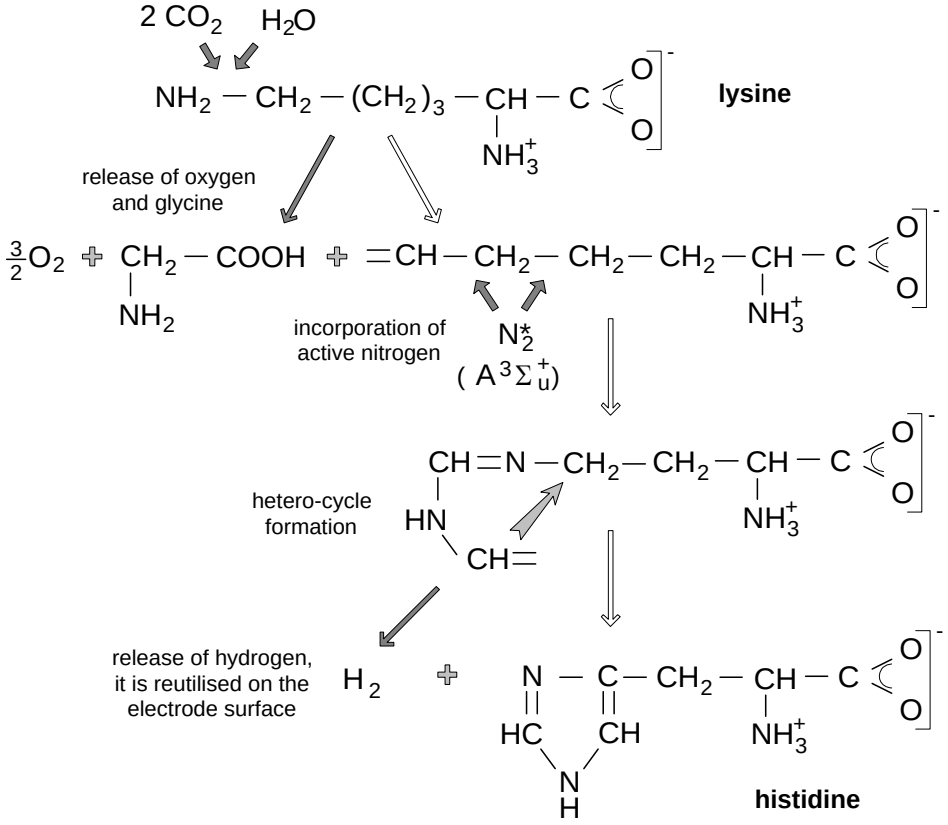

Amino acid histidine is probably formed directly on the Cu electrode surface, the surface reutilises released H_2 to form the oxamidato complex, it will be further explained in section 5.3.6.3.

Introduction of water into the discharge volume lead to the preferential production of carboxylic acids, especially adipic acid COOH-$(CH_2)_4$-COOH from cyclohexanone. It occurs due to the larger amount of OH radicals. The presence of the adipic acid in the product has been confirmed from IR spectra.

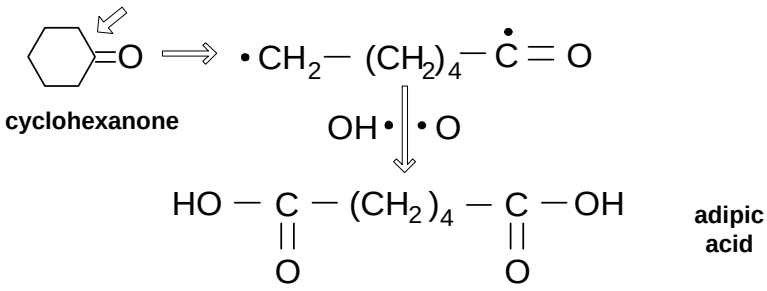

5.3.6.2 Toluene decomposition mechanisms

Aromatic toluene has a more stable ring with stronger bonds than trans-configurated cyclohexanone. A probable beginning of its decomposition is a -CH_3 group detachment induced by electron or radical impact, this bond has an energy 3.6-4.3 eV (Table 2.5.1). Ring opening requires greater amount of energy (5.4-5.5 eV), however, 6.75 eV of active N_2^* is sufficient to break the ring. The benzene ring usually splits into two C_3-parts, malonic acid anhydride $H_2C_3O_2$ can be formed after their oxidation. This intermediate enters to the heterogeneous processes occurring on the Cu electrode surface, it will be shown in the next section.

If the benzene ring is not destroyed, O and OH radicals may participate at carboxylic acids formation, e.g. benzoic acid. When active N_2^* is further incorporated into the structure, aromatic amino acids may be formed. They were detected in the IR spectra. The proposed reaction scheme leading to amino benzoic acid is:

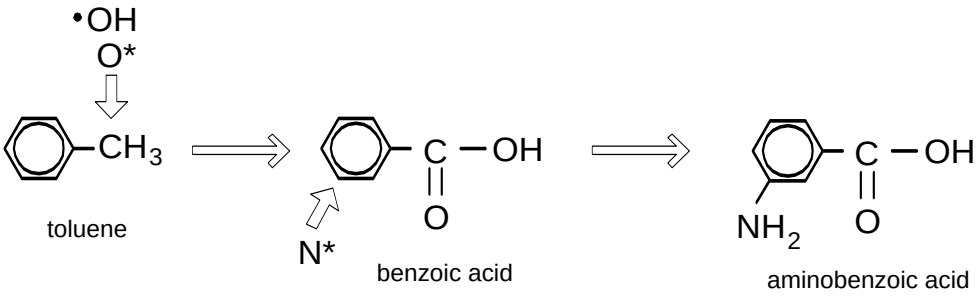

5.3.6.3 Heterogeneous effects of Cu electrode surfaces

The VOC removal processes initiated by HPGD and TS performed in the glass tube reactors and Cu reactors have several differences, as discussed in previous chapters. Briefly, in the glass reactors the deVOC process is similar to the combustion, although some other condensed products were formed. In Cu reactors, the major products are in the condensed phase (amino acids) and the process is energetically cheaper. Of course, oxidation and condensation reactions run together in both systems, the discharge type and injected energy determine which kind of reactions will prevail. However, the Cu electrode surfaces influence these processes by heterogeneous effects, as was reported by several authors [Hen96, Gas98, Kur97, Mrv98a, Mrv99a, Mrv00, Han00] and experimentally confirmed in our experiments. (The advantageous properties of the Cu reactors, especially the longer contact of the treated gas with the Cu surfaces were discussed in chapter 5.3.4, see also Table 5.3.1)

Now, we will try to provide some explications of the effects of Cu electrode surfaces in the plasmochemical processes of VOC decomposition and condensed products formation according to the results of our experiments and available literature.

Active N_2^* is incorporated into CO_2 or CO formed in oxidation process to create a long living NCO radical and ON-NCO and similar intermediates (remind chapter 5.3.4.3). These species are involved in the formation of electrode surface catalytic processes. An important part of this process is joined with the formation of oxamidato complexes on the Cu electrode surface, as shown in the following reaction scheme.

$$4\,(NCO^{*} + H) + Cu^{n+} \rightarrow (HNCO)_4 + Cu^{n+} \rightarrow$$

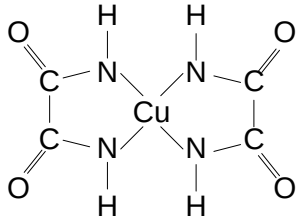

[Han00]

Hydrogen necessary for the above reaction is partially produced in the process of CH_2-group dehydrogenation during lysine to histidine conversion occurring in near electrode area (scheme in section 5.3.6.1).

The IR spectra of the surface products of deVOC processes in Cu reactors are very similar to the spectrum of oxamidato complex (as an example see Figure 5.3.31), identified amino acid components are superposed on the bands of the complex. A high dielectric constant of oxamidato complexes is responsible for their catalytic properties, previously described formation of other amino acids is enhanced by these surface properties, although an exact mechanism is not known.

Formed amino acids have their terminal group $-CH(NH_2)-COOH$ in an α–arrangement

which can be easily changed into a terminal zwitterion, i.e., $-CH(NH_3^+)-(COO)^-$

with groups $-NH_3^+$ and $-(COO)^-$. This can occur in the electric field of the discharge system, on the non-stressed electrode or by interaction with water.

The zwitterion amino acids formed on the Cu-containing electrode surfaces undergo polycondensation and/or dimerisation reactions to form amides, respectively imides and more complicated structures. This process can be schematically shown by the following way:

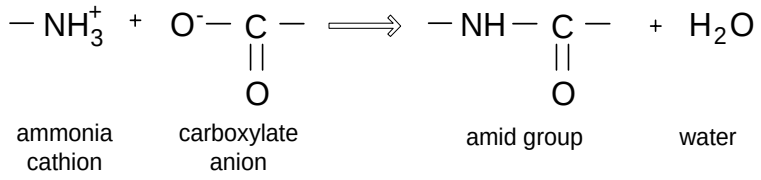

The polycondensates of amino acids attached to the oxamidato complex and other Cu-containing organo-metallic structures on the Cu electrode surface have properties different from pure amino acids, e.g. water insolubility, crystalline structure, mechanic hardness etc.

Let us finally mention reactions of NCO radicals and OC-NCO intermediates with C_3O_2 (decomposition product of toluene) on the electrode surfaces in the presence of water proposed by M.Morvová et al. [Mrv98a, Mrv00] They lead to the formation of a pyrrole ring. Pyrroles, and in particular cyclic tetra-pyrrole structures (e.g. porphyrin - a well known catalyst) formed from pyrrole groups, are photosensitive and can take part in the condensation

processes of amino acids formation. They bound on the Cu surface, as well as the oxamidato complexes. [Han00]

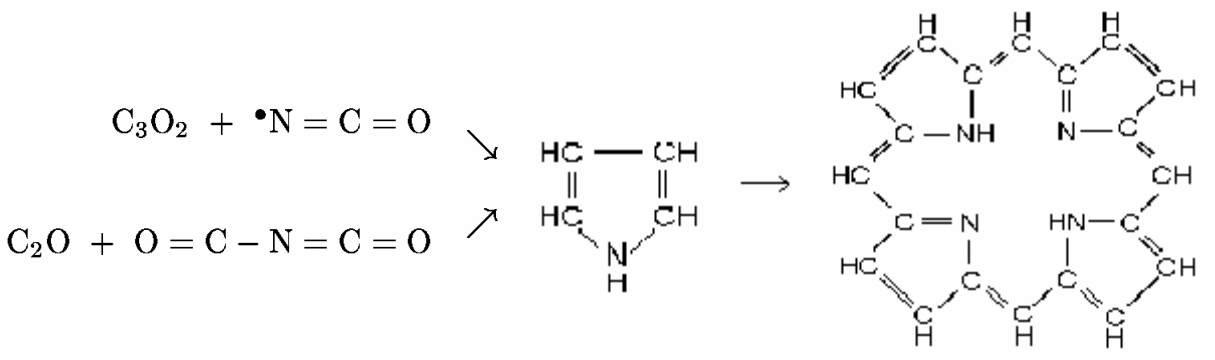

pyrrole cyclic tetrapyrrole – porphirine

The natural pyrrole ring based compounds are bases of the life important pigments (cyclic tetrapyrrole pigment with central atom Mg - chlorophyll, linear tetrapyrrole pigment with central atom Cu - phycocyanine, precursors of RNA basis cytosine and uracyl). A compound similar to the tetra-pyrrole structure formed on Cu electrodes - Phycocyanin (with Cu atom) is present in thylacoids of blue green algae Spirulina platensis and various types of cyanobacteria where this compound participate in the photosynthesis of amino acids. [Gla82]

We can say, that the process of amino acids formation on Cu electrode surface is somehow similar to the natural photosynthesis of amino acids in cyanobacteria. Cu electrode surface plays an important role in these processes, because it creates the organo-metallic compounds (oxamidato complex, tetra-pyrrole structures, etc.) effecting like catalysts for amino acids formation.

5.3.6.4 Energetic aspect of the deVOC processes in Cu reactors

The processes of the incorporation of active species of N_2^* and formation of amino acids require certain amount of energy (to produce nitrogen excites states). It is possible that the energy of radiation (UV and visible) emitted from the discharge, as well as the kinetic energy of the electrons created in the discharge via inelastic collisions with N_2 molecules are used. On the other hand, when the nitrogen active species are incorporated to more stable structures, some energy is released (these processes are exothermic) and can re-enter the reactions. This is a rough principle of the energy recycling in the studied systems. It helps to explain why the VOC decomposition rates (η and R_{mol}) in Cu reactors have not been

decreasing adequately to the decrease of the energy density (R_V) and why we have achieved such low energy costs (from 16 eV/molecule) in these systems. (Figure 5.3.20, Figure 5.3.21)

However, an exact thermochemical approach is needed to explain the energy recycling in details. A more detailed description of the exact role of heterogeneously effecting Cu electrode surfaces is a task for future as well, although we have provided some explications in the previous section.

5.4 VOC REMOVAL PROCESS IN OTHER ENVIRONMENTS - RESULTS AND DISCUSSION

5.4.1 Effect of the oxygen content to the VOC decomposition process in HPGD

Z. Falkenstein studied the effect of oxygen concentrations to the VOC removal process (toluene and TCE) induced by dielectric barrier discharge in air. Although one would expect that such a process works better when more oxygen is present since it is in a certain way similar to the combustion, the result of Falkenstein is rather surprising: he achieved the highest removal rates when the air contains just about 2 % and 0.3 % of O_2 for toluene and TCE removal, respectively. He explains this result by the optimal radical utilisation for VOC removal which occurs at low O_2 concentration, rather than ozone production. O_2 is a donor of fast reacting atomic oxygen, as well as a scavenger of atomic oxygen producing slow reacting ozone, its higher concentration enhances the O_3 production. [Fal99]

Similar result has been observed by Snyder et al. who decomposed chlorobenzene in DBD and found out that lower energy density is necessary to achieve the same removal efficiency (i.e. for the same work) at 2-3 % of O_2. They explain this effect by a lower ozone formation as well. Moreover, they found out that the VOC decomposition process works more effectively in Ar-O_2 mixture, rather than in N_2-O_2. It is caused by the reactions of O_2 with N_2 to form NO_x which consume reactive O radicals. [Sny98]

These results concerning O_2 content became a motive to investigate the VOC decomposition by the discharges involved in this work (HPGD and TS) in the atmosphere of air with various oxygen contents. We tried to find out if the process in these discharges behaves by the above mentioned manner and how does the O_2 content influence the involved plasma chemistry. We worked with toluene in oxygen rich atmosphere (30±2 % O_2, 70±2 %

N_2), oxygen poor atmosphere (5±2% O_2, 95±2 % N_2) and the atmosphere of pure N_2. The discharges were operated in the 5-point glass tube reactor, some experiments with TS were performed in the Cu tube reactor. These results were then compared with the results obtained in normal air with 21 % O_2 and 78 % N_2.

Anyway, this research stays a laboratory study, because most of real off-gases contain pollutants in normal air.

5.4.1.1 Effect of the oxygen content to the removal efficiency and energy costs

Graphs showing the removal efficiency η and discharge energy costs R_{mol} as functions of the O_2 content for negative HPGD are in Figure 5.4.1. We obtained similar graphs in the positive HPGD and in both polarities of TS. In the dry atmosphere we observed a maximum of efficiency and a minimum of energy costs at 5 % of O_2 (with uncertainty of 2 %). R_{mol} slightly increases with rising O_2, has a maximum at normal air and decreases again with O_2 rising to 30 %. A real efficiency maximum might be in the interval which was not covered by the measurements, probably between 0-5 % of O_2 (in accordance with [Fal99, Sny98], but maybe between 5-21 % of O_2. Yet, Figure 5.4.1 shows evidently that the VOC removal in the dry atmosphere with reduced oxygen content is more convenient than in normal air. From the viewpoint of energy costs it works better also in oxygen poor atmosphere than in normal air.

The efficiency is low and energy costs are high in pure N_2 (0 % O_2), but the fact that the VOC decomposition process works even without oxygen is interesting. It has already been reported in some works dealing with the plasma processing of chlorinated hydrocarbons, the authors explain the decomposition process by the effect of N radicals. [Ler95, Pen95]

Presence of water strongly influences the effect of O_2 content. The removal efficiency increases with O_2 rising from 0 to 5 %, then rests approximately constant. In normal air (21 % O_2) with the presence of moisture η is higher than in dry air. There is no efficiency maximum for reduced O_2 content what was observed in dry environment. The energy costs have a minimum at 21 % of O_2 (normal air) which is lower than the minimum in the dry atmosphere.

Anyway, there is a large scatter in experimental points shown in graphs in Figure 5.4.1. The oxygen content is not the only parameter affecting the removal efficiency η and the energy costs R_{mol}. As resolved from all experiments effectuated in normal air, the primary parameter which influences η and R_{mol} is the specific energy density R_V (power P divided by

gas flow Q). Therefore, if we want to study properly the influence of the oxygen content then we have to extract this parameter. It is possible to do by two ways: either fixing of R_V to the certain value not changing in all experiments or dividing the studied characteristics (η, R_{mol}) by R_V, by other words to do a certain normalisation of η and R_{mol}. The second method was applied, because it was too difficult to keep R_V at one fixed value.

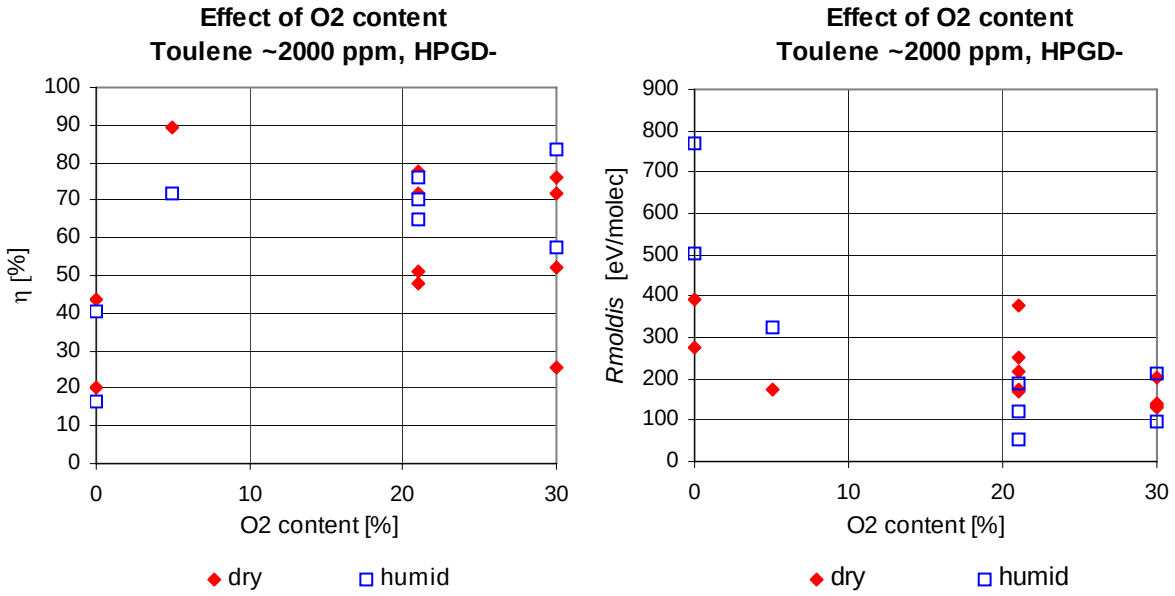

Figure 5.4.1 Effect of O_2 content on removal efficiency η (left) and discharge energy costs R_{mol} (right). Toluene treatment by negative HPGD in dry and humid N_2+O_2 gas.

Graphs from Figure 5.4.1 were changed by this way to those presented in Figure 5.4.2. The normalised efficiency η/R_V has no maximum neither in dry nor in humid atmosphere, it rises with O_2 content by a logarithmic-like trend. The normalised energy costs R_{mol}/R_V have slight minima at 5 and 21 % of O_2 corresponding to the dry and humid environments, respectively. There is no principal difference between the behaviours of R_{mol} and normalised R_{mol}/R_V.

This new point of view revealed a little different results in comparison with previous ones from Figure 5.4.1 (without normalisation). In reality, the VOC removal in the dry atmosphere with reduced O_2 content is just slightly more convenient than in normal dry air, but in humid air it works best at ambient O_2 content. The most convenient environment is the normal humid air, especially for low energy costs.

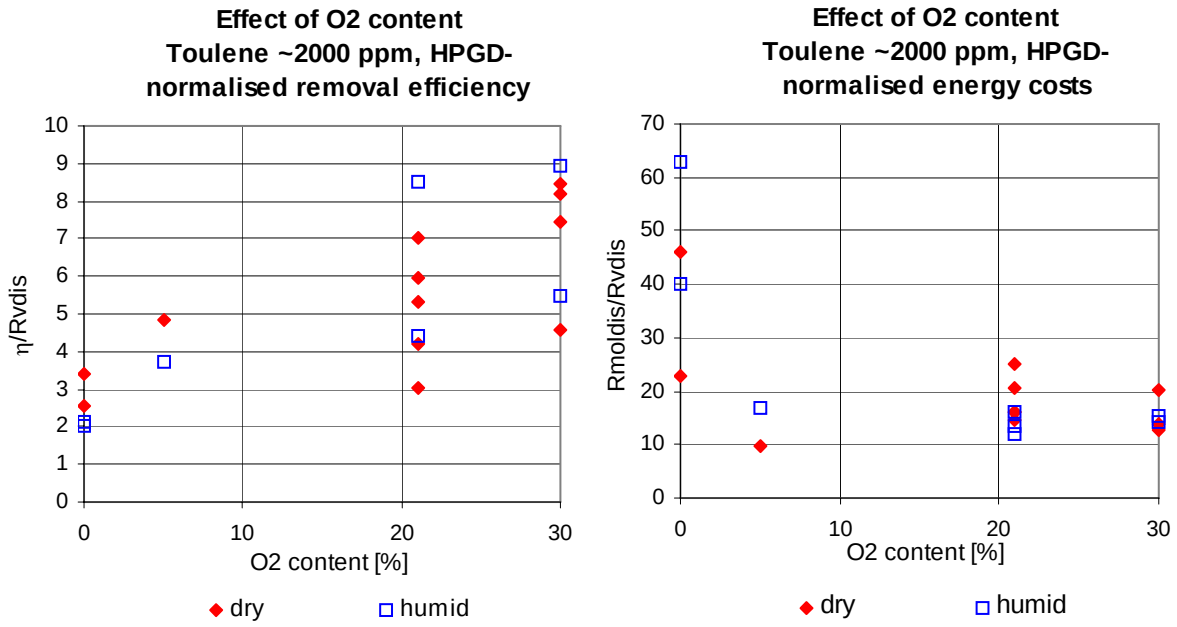

Figure 5.4.2 Effect of O_2 content on removal efficiency η (left) and discharge energy costs R_{mol} (right) normalised by energy density R_V. Toluene treatment by negative HPGD in dry and humid N_2+O_2 gas.

5.4.1.2 Effect of the oxygen content to the gaseous products

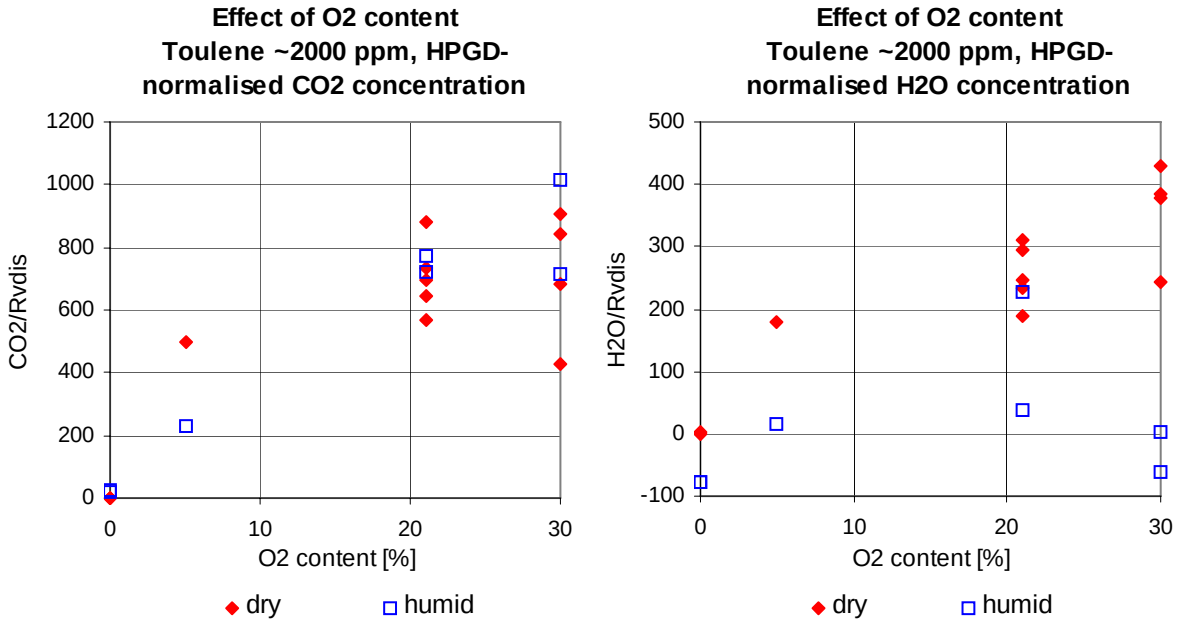

Figure 5.4.3 Effect of O_2 content on produced CO_2 (left) and H_2O (right) concentrations normalised by energy density R_V. Toluene treatment by negative HPGD in dry and humid N_2+O_2 gas.

The O_2 concentration in the working atmosphere influences the gaseous products formed by the VOC removal process in HPGD and TS, especially the typical products (CO_2, CO, H_2O, NO_2, NO), since they all contain oxygen. Their formation and some new gaseous products (HCN, C_2H_2) were investigated. Normalisation in a sense of division by the energy density R_V was applied again in order to extract the parameter R_V (explained in the previous section).

Graph showing normalised CO_2 formation as a function of O_2 content is presented in Figure 5.4.3 (left). Evidently, CO_2 formation rises with O_2 content, in humid atmosphere almost linearly, but in the dry atmosphere we observe a saturation (logarithmic-like trend). CO production behaves very similarly, there is not such a difference between the trends in the dry and humid atmosphere.

The graph of normalised H_2O formation as a function of O_2 content is interesting (Figure 5.4.3, right). In the dry atmosphere there is a rising logarithmic-like trend very similar to CO_2. The H_2O formation in air in all types of discharges and reactors was always lowered in the humid air, i.e. if some water has already been present (remind sections 5.3.2.4, 5.3.3.3, 5.3.4.2). We observe the same effect now, but the trend of the "humid" curve is completely different from the "dry" one, H_2O maximum occurs at 21 % O_2 (normal air) and the H_2O formation decreases at higher O_2 content.

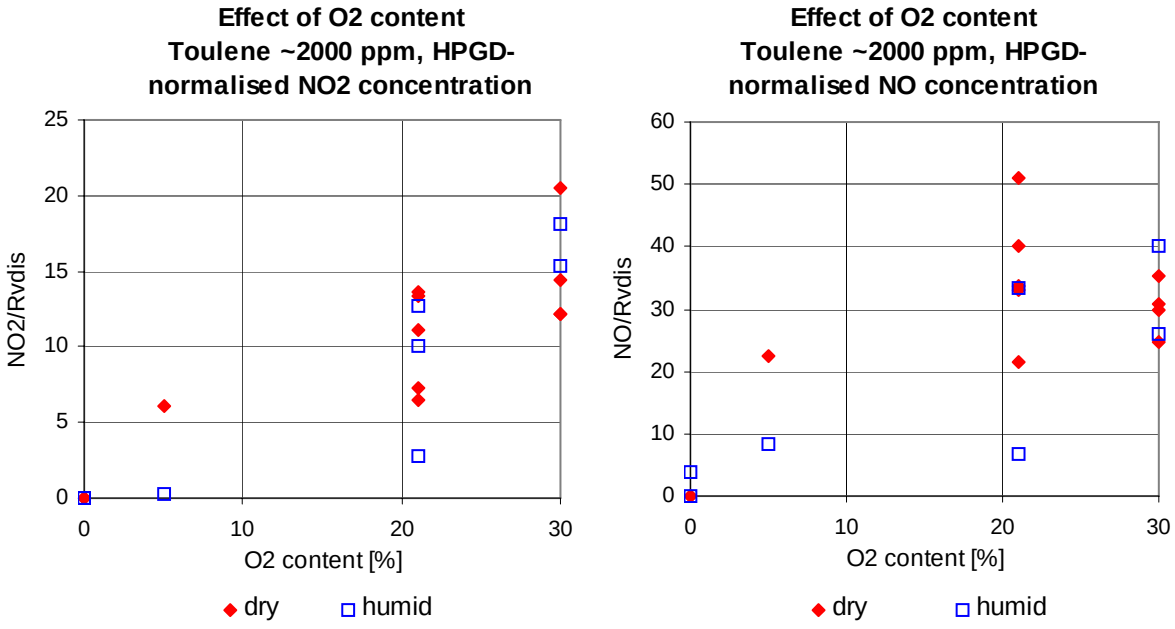

Figure 5.4.4 Effect of O_2 content on produced NO_2 (left) and NO (right) concentrations normalised by energy density R_V. Toluene treatment by negative HPGD in dry and humid N_2+O_2 gas.

The NO_x formation rises with the O_2 content as well, NO_2 slightly exponentially (Figure 5.4.4, left), especially in the humid atmosphere, and NO rather logarithmically (Figure 5.4.4, right).

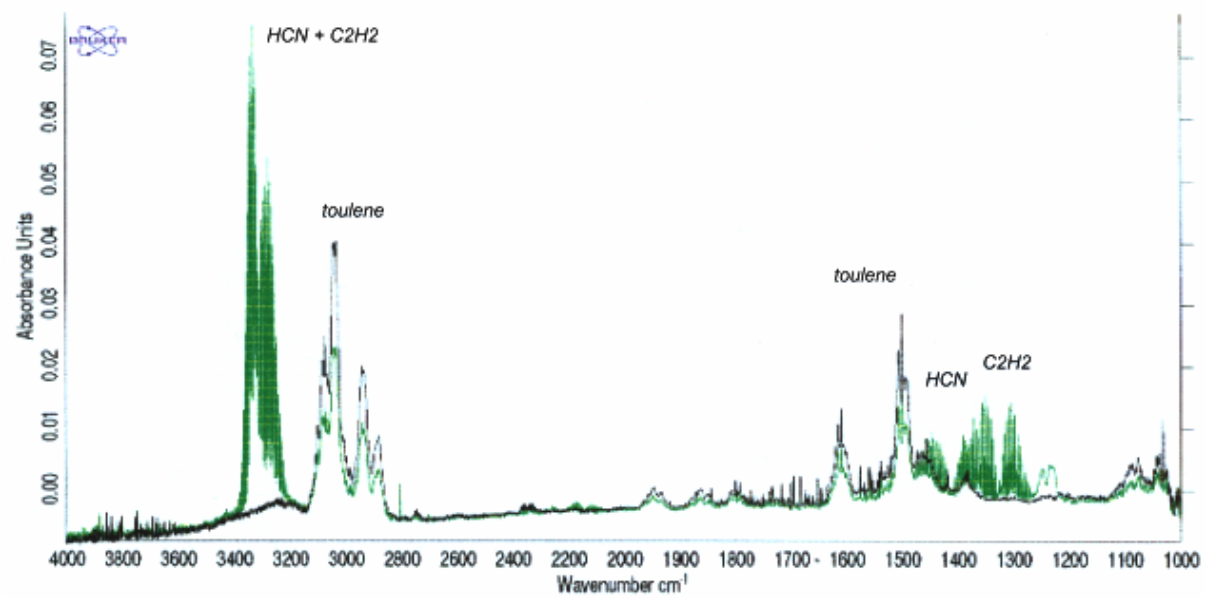

Figure 5.4.5 Typical IR spectrum of toluene before (black) and after (green) treatment in dry N_2 in positive HPGD

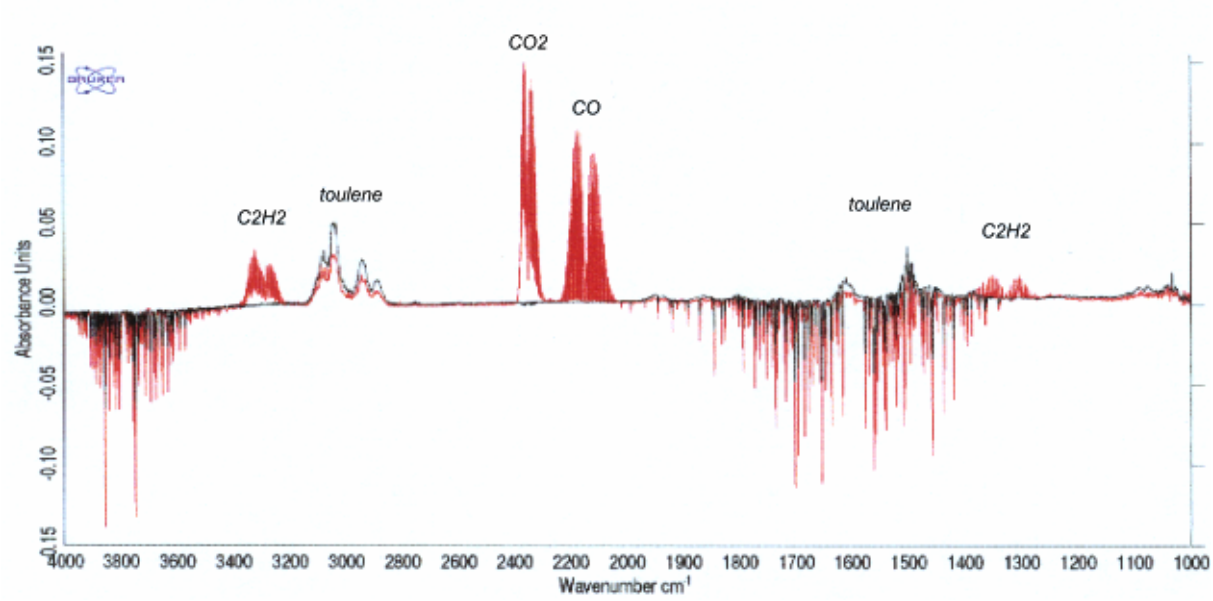

Figure 5.4.6 Typical IR spectrum of toluene before (black) and after (red) treatment in humid N_2 in positive HPGD

In the dry atmosphere at 0 % O_2, i.e. in pure N_2, there was obviously no formation of the above mentioned oxygen containing products. On the other hand, new products appeared, mainly hydrogen cyanide (HCN) and acetylene (C_2H_2).

In the humidified N_2, HCN formation was suppressed and C_2H_2 formation enhanced. Some CO_2, CO and NO were found in low concentrations too, the necessary oxygen was supplied by the present H_2O which was consequently consumed (negative H_2O at 0 % O_2). The typical IR spectra of the gaseous products of toluene decomposition process in dry and humidified N_2 are shown in Figure 5.4.5 and Figure 5.4.6.

5.4.1.3 Solid and liquid products formed in oxygen rich and poor air and in N_2

Solid and liquid products of the deVOC process in normal air - deposits appearing on the walls (deposits I), Cu plane electrode (deposits II-IV) and passive Cu planes (deposits V) produced by HPGD and TS in the glass tube reactors were analysed in details in section 5.3.5. The same processes operated in oxygen rich and oxygen poor atmospheres lead to the very similar solid and liquid products - liquid deposits I based on amino acids, aromatic rings and nitro-groups, and solid deposits on the Cu electrode and passive Cu planes, mainly similar to previously described deposits III and V based on aromatic amino acids as well. The only significant difference occurred in oxygen poor atmosphere - all deposits on Cu surfaces contained the 2170 cm^{-1} band in the IR spectra assigned to carboimides (N=C=N), or even more likely to nitriles (C≡N, cyano-group). Such functional groups were found in small amounts also in the deposits III and V from cyclohexanone treatment by negative HPGD in dry air. Their presence here is very probable, because C≡N groups were formed even in the gas phase, as HCN.

On the other hand, solid products formed in N_2 and N_2+H_2O atmospheres with toluene were completely different. A black powder deposit grew quickly on both electrodes in pure N_2. The deposit had a porous structure, after a gentle knocking on the discharge chamber it fell down as a fine powder. A thin black layer of probably amorphous structure stayed fixed to the electrodes, even after removing the powder. The same deposit was formed in the one-point discharge chamber used for the study of HPGD and TS physical properties (see sections 3.3.8.3, 4.3.7.2). Infrared absorption analysis showed no bands in 4000-600 cm^{-1} region which gives rise to a hypothesis that the deposit could be a soot of pure carbon, probably amorphous (symmetric C-C groups are inactive in IR). Pure carbon formation from VOC in N_2 atmosphere is very probable, because the process is similar to the pyrolysis (carbonisation),

the discharge works as the thermal source. Arc discharges are typically employed for the pyrolysis of the hydrocarbons and polymers, carbon in various modifications is a typical final product. [Huc98, Huc00] It is possible that the carbon produced in our process might have properties of an active carbon due to its porous structure. Certainly, it needs further investigations. There was no deposit on the glass walls in dry N_2 environment.

A black powder soot was formed in humidified N_2 too, but a thin black layer which rests on the Cu electrodes and passive planes surfaces in not just a pure carbon. IR spectroscopy determined amine (NH, NH_2), C-N and C-O groups on the electrode and typical zwitterionic structures of amino acids on the Cu passive planes (COO^- and amide bands). A layer of the same structure, particularly based on amino acids was observed on the Cu electrodes of Cu tube reactor after TS toluene treatment in both dry and humid N_2. A thin layer of a liquid deposit on the glass reactor walls has formed in humid N_2, it has approximately the same structure as a usual deposit I from toluene treated in air. However, an additional intense band at 2170 cm^{-1} was typical for all spectra of these deposits, it is associated with nitrile (cyano) group (C≡N).

5.4.1.4 Conclusion

The results of Falkenstein and Snyder et al. [Fal99, Sny98] mentioned at the beginning of this chapter were not fully confirmed in our experiments with HPGD and TS, though we worked with toluene which is the same VOC, rather similar to chlorobenzene respectively. We observed just a slight decrease of the process energy costs in the atmosphere with reduced O_2 and no moisture. Falkenstein explains the efficiency maximum at 2 % of O_2 by the optimal radical utilisation for VOC removal which occurs at low O_2 concentration. On the contrary, at higher O_2 concentration, slowly reacting ozone is produced which scavenges fastly reacting atomic oxygen.

Ozone was never detected among the products in our experiments with HPGD and TS, neither in air, nor in other environments. First reason is certainly a relatively high discharge temperature (2000 K for HPGD, 1000 K for TS) which is responsible for immediate O_3 decomposition even once it is formed. Intermediate O_3 may scavenge the fast reacting atomic oxygen, but it is recuperated as soon as O_3 is decomposed. Second mechanism of immediate utilisation of eventually formed O_3 is its incorporation to peroxy-acetyl-nitrates (PAN) which are often produced. Atomic O used for O_3 formation is not recuperated in this case, they are

used ineffectively. A weak lowering of discharge energy costs at reduced O_2 content in dry environment can be explained by this way.

On the other hand, in humid environment, OH radicals (formed especially from present H_2O) seem to be more important in the VOC decomposition mechanisms than the O radicals. Hence, reducing of O_2 content has no sense.

However, there exist mechanisms responsible for ineffective utilisation of O radicals in both dry and humid environments : NO_x formation growing with rising O_2 content. This is the only serious argument for working with reducing atmosphere when we operate HPGD and TS in glass tube reactors.

A fast preliminary study of the effect of O_2 content to the VOC removal in Cu tube reactor with threaded rod electrode showed that the effect of energy costs lowering in the slightly reducing atmosphere (N_2/O_2 = 95/5) was stronger than in the glass tube reactors with point-to-plane electrodes. Amino acids were intensively formed on the Cu electrode surface, in oxygen poor atmosphere, as well as in N_2+VOC environment. It might be interesting to investigate the effect of O_2 content to VOC removal parameters and formed products in Cu tube reactors in more details, since all plasmochemical mechanisms are rather different in these systems due to the heterogeneous effect of Cu electrode surfaces. (section 5.3.6.3). Furthermore, according to some results of M. Morvová et al., the process of CO_x reducing and formation of amino acids and other interesting compounds occurs preferentially in the reducing atmosphere, e.g. combustion exhaust, CO_2-N_2-H_2O system. [Mrv98b, Mrv00] Formation of amino acids in the CO_2-N_2-H_2O atmosphere irradiated by a synchrotron radiation was found also by Y. Utsumi et al. [Uts98]

Similar processes responsible of formation of amino acids in strong and middle reducing primitive Earth atmosphere lead to the origin of life on Earth, they were described by S. L. Miller. [Mil53, Mil92]

5.4.2 Simultaneous VOC and NO_x removal in HPGD

The second series of experiments concerned in this chapter was aimed at the simultaneous removal of VOC and NO_x. It was motivated by the studies of some authors working with various kinds of discharges, who found that VOC and NO_x can be removed simultaneously and that a presence of NO_x improves the VOC removal and vice versa. [Kal96, Yos96, Nie96, Nie98, Gas00]

We investigated the effect of NO_x presence in dry and humid air to the removal process of VOC (about 2000 ppm of toluene) in HPGD of both polarities operated in the 5-points reactor. Pure NO from the pressure bottle was diluted in air in such a ratio to obtain approximately 1000 ppm. Practically, it reacts quickly with atomic oxygen to form NO_2, about 500 ppm of NO and 500 ppm of NO_2 entered to the reactor.

HPGD of both polarities operating in air, as well as in air enriched by VOC, produces NO_x (remind sections 5.3.2.1 and 5.3.3.2), VOC and H_2O presence influences their concentrations and NO-to-NO_2 repartition. When NO_x are already present in the input air what was the objective of this study, their concentration increases after the HPGD treatment. This occurs in both polarities of HPGD, in dry as well as humid air, if VOC is present or not. However, VOC presence influences relative amounts of result NO and NO_2, it enhances NO_2 and reduces NO formation. It seems that, besides VOC presence which strongly affects the plasmochemical processes, the main parameters influencing the NO_x production are the discharge temperature and the energy delivered to the treated volume (energy density), regardless to the initial NO_x presence or non-presence. The VOC removal is fairly affected by the initial presence of NO_x.

Hence, we can conclude that HPGD, this discharge with relatively high temperature effective for VOC removal, is absolutely inconvenient for NO_x removal. It creates, rather than decomposes NO_x. The simultaneous decomposition of VOC and NO_x does not work, just VOC are removed, NO_x are formed.

On the other hand, we did not study the effects of TS to simultaneous VOC and NO_x removal, especially in Cu tube systems. It probably works, NO_x in combustion exhaust containing CO, CO_2 and CH_4 were successfully reduced in the systems with heterogeneously catalysing Cu electrode surfaces and streamer-to-spark transition discharge (regime practically equal to TS). [Mrv00]

5.5 SUMMARY AND CONCLUSIONS OF THE LABORATORY TESTS OF VOC REMOVAL

The whole chapter 5 was dedicated to the laboratory tests of VOC removal in the new types of non-thermal plasmas generated by HPGD and TS of both polarities. Most of the experiments were carried out in dry or humidified air charged by various concentrations of VOC representatives - cyclohexanone and toluene. We used several types of plasma reactors, in particular the glass tube reactor with 5 parallel points and the Cu tube reactor with the threaded rod electrode. We investigated how various discharge and gas flow parameters influence the VOC decomposition (deVOC) process from the viewpoint of the removal efficiency, energy costs and formed products. Some reaction mechanisms leading to the product formation were proposed.

5.5.1 Summary: VOC removal in air - glass tube reactors

VOC removal process induced by both discharges in the glass reactors is not dependent on the initial VOC concentration from the viewpoint of removal efficiency, but working with higher initial concentration always reflects in the lower energy costs. Removal efficiency rises logarithmically with the energy dissipated in the reactor volume (energy density R_V), it reaches 95 %. The energy costs rise exponentially with the same parameter, they vary in the range 200-1000 eV/molecule. Main gaseous products of the process are CO_2, CO, H_2O, NO_2 and NO, their concentrations depend on the initial VOC concentration, presence of moisture in the carrying air and mainly R_V. The VOC removal process, especially in HPGD, is partially similar to the combustion characterised by relatively low CO/CO_2 ratio. A non-negligible part of the treated carbon from VOC goes to the condensed products, in some specific conditions it rises up to 60 %. Although the discharge polarity influences the process very fairly, the negative HPGD in humid air gives the highest removal efficiencies, the lowest energy costs and the lowest concentrations of noxious output gases. The presence of humidity improves the process, especially by reducing the NO_x production.

TS, in comparison with the more thermal HPGD (both in glass reactors) works with weaker R_V and consequently gives lower removal efficiencies (60-70 %), but at lower energy costs (even below 100 eV/molecule). In dry air, it produces less H_2O but more NO_2 and CO which is disadvantageous, increased CO formation results in higher CO/CO_2 ratio. In humid

air, it is comparable with HPGD.

By a comparison of reactors with 1, 5, 10 and 2 distant discharges we studied an effect of non-linearity of the deVOC process, i.e. a saturation of removal efficiency with increasing injected energy (R_V). Maximal efficiency per discharge was obtained in 2-distant-discharges system, maximal total efficiency was reached in 5 and 10-discharge system. This study opened a new way how to construct the plasma reactor based on HPGD: reactor with about 5 discharges distant one from another. Putting them electrically in series results in lowering of the total energy costs, because less energy is lost in the external resistances.

5.5.2 Summary: VOC removal in air - Cu tube reactors

Long Cu tube reactors, characterised by larger Cu surfaces and longer residence time of the treated gas in the active volume have different effects on deVOC process than the glass reactors with point-to-plane discharge configuration, though the same discharges are used. Achieved removal efficiencies (50-60 %), though lower than in glass tube reactors with 5 working discharges, are obtained at lower injected energy (R_V = 50-800 J/l). Moreover, the energy costs in these systems are considerably lower (16-100 eV/molecule) than in glass reactors, particularly in TS. The influence of the discharge polarity on the efficiency and the energy costs is weak at both discharges.

Another advantage of the Cu reactors in comparison with glass reactors is a lower formation of the noxious gaseous products such as NO_x, mainly at low residence times of the treated gas in the reactor volume. When the energy density of the involved discharge is high the process is similar to the combustion (with a dominant formation of CO_2, H_2O, CO and NO_2, but in lower concentration than in glass reactors), especially in more thermal HPGD. On the other hand, processes initiated with active N_2^* molecules (metastable state $A^3\Sigma_u^+$) and formation of NCO radicals leading to the solid products based on amino acids become dominant at lower energy densities. Amino acids and other condensed phase products (amides, imides) created in particular on the Cu electrode surfaces are non-toxic and more convenient from the point of view of the global Earth environment than the gaseous combustion products, CO_2 included.

Large Cu electrode surfaces in Cu reactors heterogeneously influence the deVOC processes and participate at the amino acids formation. They are certainly involved also in the recycling of energy in the plasmochemical processes based on the incorporation of active nitrogen species into CO_2 and hydrocarbon residues, which results in very low energy costs.

Excited N_2 species probably work as energy reservoirs in this process.

Active nitrogen and Cu electrode surfaces play some role also in the deVOC processes in the glass reactors with Cu plane electrode. However, this role is less important, since the Cu electrode surface is small and the injected energy in these discharge systems is relatively high, thus the combustion processes prevail. Amino acids detected in the deposits on the plane Cu electrode surface as well as on the glass walls of the reactor and on the Cu passive planes confirm an occurance of these processes in every case.

5.5.3 Synthesis: Three effects participating at VOC removal

Removal efficiencies achieved in VOC removal by HPGD and TS might seem rather high realizing that both these discharges are strongly constricted and occupy a small part of the discharge chamber. We suggest the following explanation of this phenomenon: VOC are treated in the rector by three effects which cooperate and lead to their removal:

1. thermal decomposition occurring in the close surroundings of the discharge channel due to a high temperature - a minor part of the passing gas is treated directly by this way
2. volume reactions induced by radicals formed by the discharges occurring in further and cooler parts of the reactor - most of the passing gas is treated by this way
3. surface reactions on the copper electrodes - a significant amount of the passing gas gets in touch with electrodes due to the hydrodynamic turbulences in the reactor

Furthermore, the discharges, especially TS, quickly move in the discharge tube, axially (along the discharge tube) and radially (around the stressed electrode). These motions enhance the contact of the passing gas with the discharges and increase the turbulences which results in more effective VOC treatment.

The reactor type and the injected energy are basic parameters determining which of these three effects will dominate. Type of the formed products is a result of the dominating process as well.

5.5.4 Summary: VOC removal process in other environments

A study of the deVOC process initiated by HPGD and TS in the slightly reducing air atmosphere (5 % O_2 in N_2) did not confirm results of some authors who achieved evidently higher VOC removal efficiencies [Fal99, Sny98]. Improvement of VOC removal in

such an atmosphere is rather weak in glass reactors, but stronger in Cu reactors where the slightly reducing atmosphere enhances the amino acids formation. DeVOC process in such an atmosphere is logically associated with lower CO_x and NO_x formation due to the lack of oxygen.

Increased oxygen content (30 %) does not seem to influence the deVOC process. An interesting result is that the VOC decomposition occurs also in pure N_2, though not as effectively as in air. It leads above all to HCN and acetylene in the gas phase and to the pure carbon as the solid product. Amino acids are formed in N_2+VOC atmosphere just in the Cu reactor with TS.

Finally, the tests of simultaneous removal of VOC and NO_x by HPGD in glass tube reactor did not succeed. HPGD is convenient just for VOC removal, it forms rather than destroys NO_x.

5.5.5 Conclusion: It works!

The large experimental study of the VOC removal by transition types of electric discharges (pulseless HPGD and pulsed TS) in various reactors in laboratory scale, practically the essential part of this thesis, confirmed an applicability of HPGD and TS for this purpose. It implies that the new types of the non-thermal plasmas generated in these discharges are effective for the VOC removal and able to compete with other non-thermal plasma applications for pollution control. Our results were included into some selected results from the Table 2.4.1 (chapter 2.4) giving a general view on the typical VOC removal plasma techniques, see Table 6.5.1 in chapter 6. They are comparable with mostly employed techniques based on pulsed corona discharge and dielectric barrier discharge. Especially the results obtained in Cu reactors characteristic with low energy costs are interesting.

HPGD and TS used for the pollution control are neither typical non-thermal plasma applications, nor fully thermal plasma processes, but something in-between them. The thermal decomposition as well as the radical induced volume reactions and heterogeneous surface reactions participate at the VOC removal.

6.

TESTS OF THE VOC REMOVAL IN THE SMALL PILOT-SCALE DISCHARGE REACTOR

6.1 INTRODUCTION

Interesting results of VOC removal induced by TS in the Cu tube reactor obtained from the laboratory measurements become a motive to construct a small pilot-scale discharge reactor (for 50 Nm^3/h) based on Cu tubes. The tests of this reactor were performed on the by-pass of the off-gas system of one production hall where cyclohexanone and some other VOC (ethyl acetate, ethyl benzene, toluene, xylene) are used in the process of the false brilliant jewellery production.

Most of the two weeks time in the factory was spent by an adjustment of the reactor to the suitable electrical and gas flow parameters. The main measurement of VOC removal itself, when an authorised group measured the composition and concentrations of the compounds present in the off-gas, took one long day, six hours in each discharge polarity.

6.2 EXPERIMENTAL SET-UP OF THE BY-PASS MEASUREMENTS

6.2.1 Small pilot-scale reactor

The discharge reactor (Figure 6.2.1) consists of two main sectors, each with 12 parallel 50 cm long coaxial discharge tubes. Inner electrodes are represented by cooper rods with a thread (6 mm diameter), outer electrodes are brass cylindrical tubes with 18 mm inner diameter. These discharge tubes are very similar to those used in the laboratory measurements, brass is a copper containing metal. The two sectors of the reactor form a U-shape, the first sector leads the gas down and the second one up. The whole device is equipped with two fans before and after the reactor, two gas flowmeters posed similarly, and hermetically closable holes for various probes. The ultrasonic aerosolator system and the high voltage electrode cleaning system were unfortunately out of function during the time of the measurements.

A d.c. high voltage of both polarities was applied to all discharge tubes from the high voltage power supply giving up to 20 kV, maximum power 500 W, 50 Hz transformation frequency. Each HV electrode was equipped by its own series resistance in the range 1.8-5.8

MΩ. Characteristic internal capacity of each discharge tube ranges in the order of tens of pF (30-50 pF). Total discharge current (sum of the currents in all discharge tubes) and voltage were measured by d.c. meters.

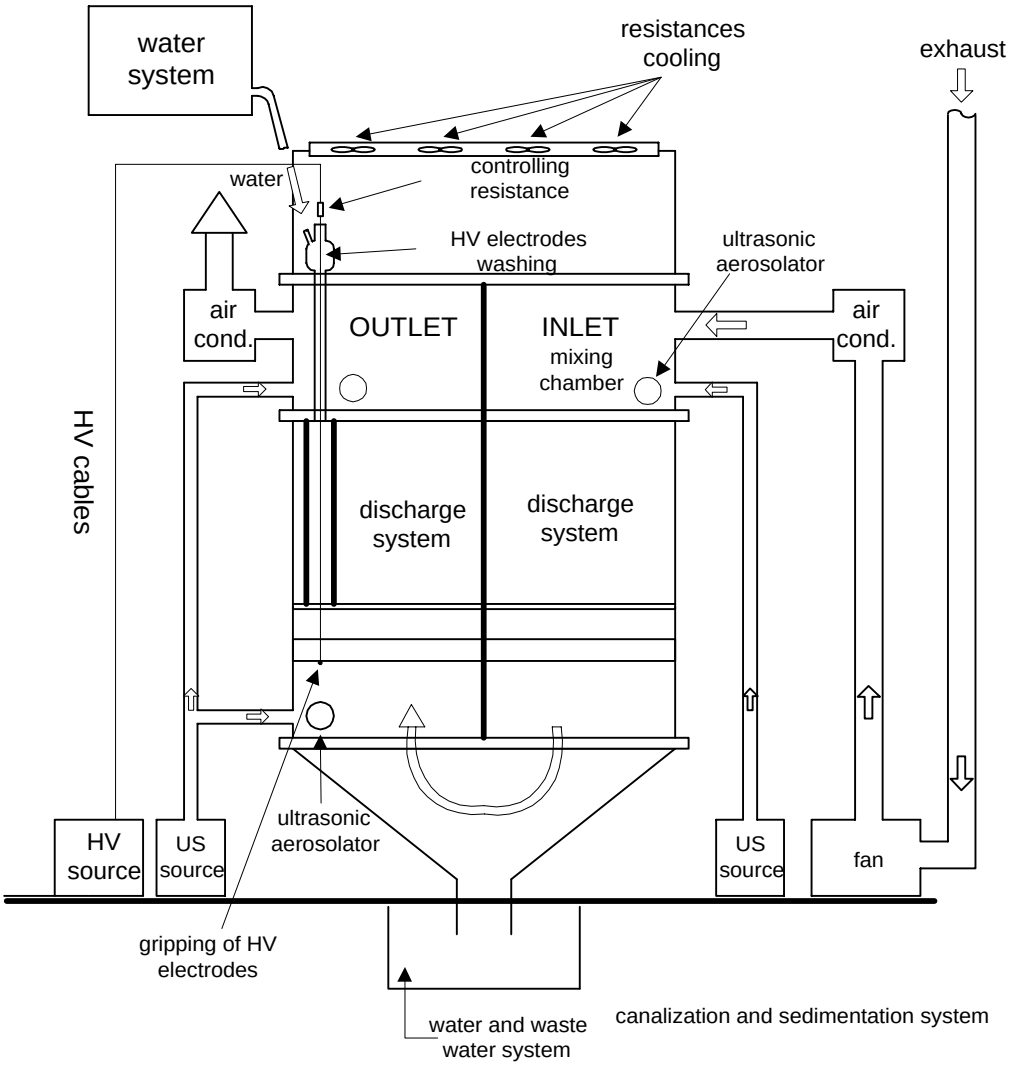

Figure 6.2.1 Scheme of the small pilot-scale discharge reactor

6.2.2 Gas flow system

The off-gas of the production hall was composed of air at ambient temperature enriched by vapours of cyclohexanone and some other VOC (ethyl acetate, ethyl benzene, toluene, xylene) and the exhaust of the natural gas combustion.

The flap valve at the beginning of the by-pass did not enable a very large choice to regulate the gas flow. The total by-pass flow was about 1.72 m^3/min at maximum, about 0.8

m^3/min at minimum. We tried to put it to the minimum value in order to decrease the gas flow rate, because the gas flow in one discharge tube was about ten times greater than in the laboratory measurements. Anyhow, the total by-pass flow depended on the operation of the hall, it varied with the day time.

The gas flow was measured by the two flowmeters before and after the reactor. They were certificated with approximately 1-2% uncertainty in the range about 60 m^3/h (it was the range where we measured). It must be mentioned that the main measurement in the negative discharge polarity was maintained in the morning, while in the positive polarity in the afternoon when the operation in the hall decreased and the by-pass gas flow lowered. The corresponding flowing velocities and residence times in the discharge tubes are given in the following table.

	Q [m^3/min]	Q [m^3/h]	v [m/s]	τ [s]
negative TS	0.83	48	5.08	0.1
positive TS	0.58	33	3.56	0.14

Table 6.2.1 Gas flow parameters during the main measurement in the small pilot-scale reactor. Q – total gas flow rate, v – flowing velocity in one discharge tube, τ – residence time of the gas in one discharge tube

We have also measured the velocity profiles in the flow system, in the input and output pipeline of the by-pass. This was realised by the TESTO TERM probes working on the principle of the heated stick.

6.2.3 Diagnostics

A direct diagnostics of the gaseous products of the deVOC process was performed by an authorised group of measurers from VUANCH (Research Institute of Inorganic Chemistry in Ústí nad Labem, Czech Republic). They used the gas chromatography, high precision liquid chromatography (HPLC), mass spectrometry and calculation of the total carbon. The samples before and after the reactor were taken by an isokinetic acquisition (explained in chapter 5.2.2) using small membrane pumps. The components of the non-treated and treated exhaust were caught in the tubes filled by activated carbon. The total amount of organic carbon was measured by an on-line gas chromatograph calibrated on cyclohexanone.

The diagnostics of the solid products formed in the reactor was done by means of the IR spectroscopy (KBr pellet technique), optical and electronic microscopy, thermogravimetry (universal V 1.9 D TA instrument using mass and differential thermal analyser MTA & DTA), HPLC and X-ray diffraction (Cu Kα radiation, 40 kV, 20 mA).

6.3 RESULTS OF THE TESTS IN THE SMALL PILOT-SCALE DISCHARGE REACTOR

Effects of the TS on cyclohexanone in the mixture with some other VOC (toluene included) and products of natural gas combustion were verified in the small pilot scale discharge reactor. The results of these tests are promising.

6.3.1 VOC removal efficiency, energy density and energy costs

Initial VOC concentrations were rather low if compared with the laboratory measurements. The results are concluded in Table 6.3.1. The VOC concentrations in mg/m^3 and result values of energy costs are calculated with regard to the total carbon, H and O are not taken into account, the concentration in ppm are related to whole molecules.

Obtained removal efficiencies are similar to those achieved by TS in the laboratory Cu discharge chambers. Energy densities R_V were extremely small due to very high gas flow Q, higher efficiencies might be achieved if R_V were in the same order as in the laboratory tests, because every treated molecule had to pass through two discharge tubes (down and up sectors). Energy costs R_{mol} = 155 eV/molecule (negative polarity) are acceptable, in the positive polarity they were higher due to the very low VOC concentration (energy costs always rise with decreasing VOC concentration as a logic result of formulas 2.4.3 and 2.4.4, this phenomenon has already been discussed in several places of this work, e.g. sections 2.4.1.3, 5.3.1.1, 5.3.4.1 and 5.5.1).

Too strong gas flow rates, inhomogeneous velocity profiles of the gas in the by-pass pipelines, as well as a non-presence of moisture (due to not working ultrasonic aerosolator and HV electrode rinsing system), may be reflected in some efficiency decrease of the reactor. If all these technical problems were removed, we might expect higher efficiencies of the device.

polarity		positive			negative	
	c0 (C)	c0	η	c0 (C)	c0	η
VOC	*mg/m3*	*ppm*	*%*	*mg/m3*	*ppm*	*%*
cyclohexanone	27.4	9.3	52.5	70.8	24.0	56.9
ethyl acetate	5.2	2.6	48.6	24.7	12.6	34.2
ethyl benzene	1.4	0.4	50.8	5.7	1.4	31.4
toluene	0	0.0	-	1.4	0.4	100.0
xylene	3.2	0.8	62.3	14.7	3.7	34.8
total carbon	37.2	-	54.5	117.3	-	48.1
P [W]		133			120	
Q [l/min]		580			830	
τ [s]		0.28			0.2	
Rv [J/l]		14			9	
Rm [kWh/kg]		189			43	
Rmol [eV/molec]		686			155	

Table 6.3.1 Results of the VOC removal in the small pilot-scale reactor. VOC concentrations in mg/m^3 and values of energy costs are calculated with regard to the total carbon

6.3.2 Products

Gaseous products of the process such as CO_2, H_2O, CO and NO_x were formed in negligible concentrations.

Approximately 100 g of the solid product of the deVOC process was found in the discharge reactor after about 50 hours of its total operation. The discharge tubes (LV electrodes), HV thread electrodes and all surrounding spaces inside the reactor were covered by a layer of a beige powder, of a fractal structure on microscopic level. (Figure 6.3.1) It is insoluble in water and very slightly soluble in usual solvents (isopropanol, acetone, toluene, benzene). The flake chains of the powder contain many hollows, the powder floats after putting into water, later, when the hollows fill with water it slowly sinks.

The IR spectrum of the product made by the KBr pellet technique (Figure 6.3.2) and HPLC chromatograph (Figure 6.3.3) are shown. The HPLC analysis (6 molar HCl was applied for the extraction at 100 °C during 24 h) confirmed a presence of some types of amino acids, such as arginine (H_2N- CNH-NH-$(CH_2)_3$-CH-NH_2-COOH), histidine ($C_5H_8N_3COOH$) and methionine (CH_3S-CH_2-CH-NH_2-COOH). The former two were formed also in laboratory experiments with Cu tubes (from cyclohexanone), the latter was not detected in the laboratory tests, because there was no sulphur. S in methionine comes from mercaptanes present in the natural gas combustion exhaust which was a part of the treated gas.

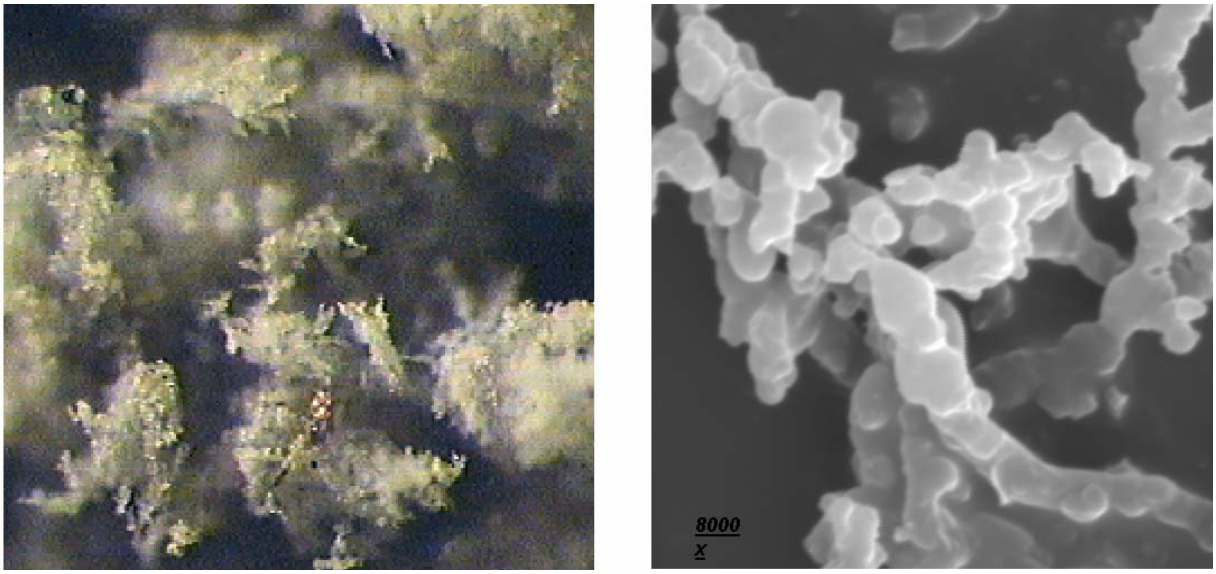

Figure 6.3.1 Microscopic photographs of the solid product formed in the small pilot-scale reactor. Left - optical microscope, magnification 500; right - scanning electron microscope, magnification 8000.

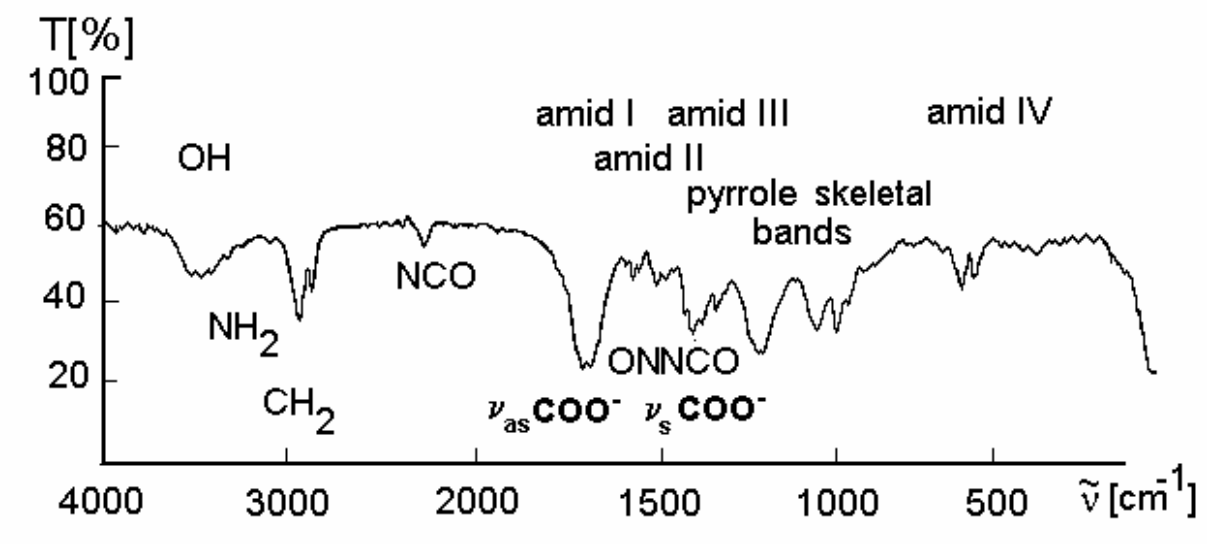

Figure 6.3.2 IR spectrum of the solid product formed in the small pilot-scale reactor with interpretation of the bands

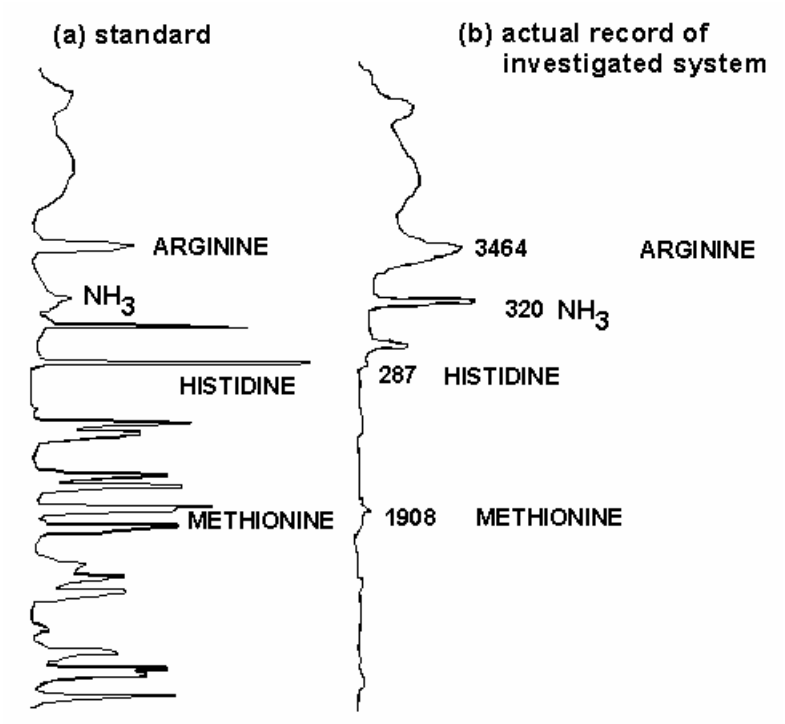

Figure 6.3.3 HPLC chromatograph of the solid product formed in the small pilot-scale reactor compared with the standard of some amino acids

IR analysis showed additionally a presence of other amino acids such as alanine, glycine, serine and aspartic acid (Figure 6.3.4).

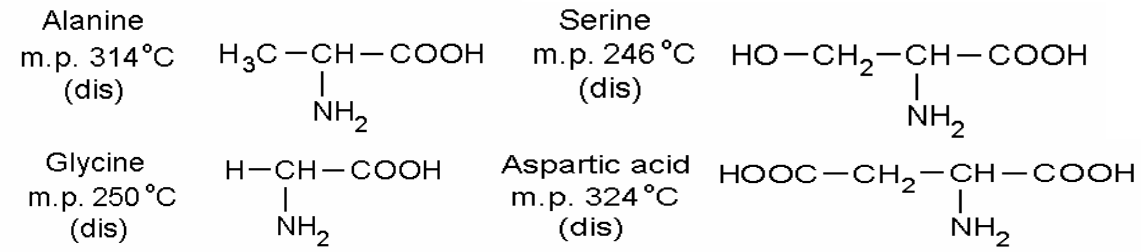

Figure 6.3.4 Other amino acids identified in the solid product formed in the small pilot-scale reactor with their melting (dissociation) points (m.p.)

The thermogravimetric analysis of the solid product was based on its thermal decomposition in air to clarify the decomposition process and to find out the combustible portion of the sample. The dynamic thermal decomposition in air (Figure 6.3.5) starts even below 100°C and ends by an intensive loss of weight between 290-320°C joined with the dissociation of amino acids. The total loss of mass at 320°C is approximately 85 %. On

isothermal heating at 320°C, the loss of mass increased to 99 %. The incombustible residue is CuO. This analysis confirmed that the main component of the powder (95-99%) is a solid condensate of amino acids.

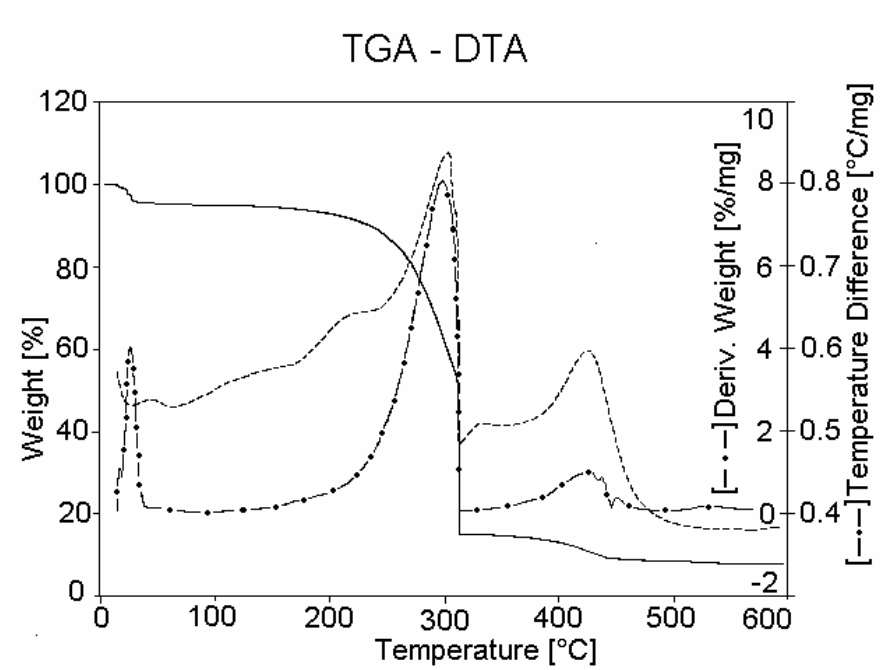

Figure 6.3.5 Thermal analysis of the solid condensate of amino acids (TGA, DTA, DTG)

The difficulty experienced in dissolving the amino acids from their solid condensate (by boiling under the pressure in 6 molar HCl), indicates strong binding forces and cohesion in the condensate. The studied condensate can be therefore considered as non-linear proteinoid with a high flexibility of peptide units **[Kar81]**. Its X-ray diffraction analysis validated the amorphous character.

Involved plasmochemistry initiated by TS in such a composed gas mixture system is very complicated, but it is based on the active nitrogen incorporation and formation of amino acids enhanced by some way by the heterogeneous reactions on Cu-containing electrode surfaces, as well as in air+cyclohexanone mixture used in the laboratory tests. The working atmosphere was slightly reducing due to the presence of natural gas exhaust in air which decreased the oxygen content. It helps to explain why the processes leading to the amino acids formation were preferred (being aware of some results obtained in Cu tube reactors in oxygen poor air, chapters 5.4.1.4 and 5.5.4), while typical combustion products (CO_2, CO, H_2O, NO_x) were formed just in negligible concentrations.

6.4 CONCLUSION OF THE PILOT-SCALE TESTS

The results of the tests of the small pilot-scale reactor for VOC removal confirmed a possibility of the application of transient spark in such a type of Cu-based reactor for the treatment of large volumes of VOC polluted air. The process is energetically cheap and relatively effective even at high gas flows through the reactor. The most important result is that the there are almost no noxious gases produced, the major product of this process is an intoxic polymer in the solid phase based on the condensate of amino acids.

6.5 OUR LABORATORY AND PILOT-SCALE RESULTS IN COMPARISON WITH OTHER PLASMA TECHNIQUES OF VOC REMOVAL

Table 6.5.1 concludes results of various plasma techniques of the removal of aromatic (mainly toluene) and carbonyl containing (acetates, ketones) VOC together with our laboratory and pilot-scale results of the removal of cyclohexanone and toluene in HPGD and TS. It is practically derived from the overall view of plasma deVOC techniques given in Table 2.4.1 (chapter 2.4.2) with the essential of our results added.

Removal efficiency (removal rate) is usually given as a main parameter of the deVOC process, some authors also indicate specific energy density and energy costs. However, very few works provide all these parameters, so it is difficult to do compare one with another. Moreover, a large variety of important parameters specific for each process, such as the gas composition, pressure and temperature, initial VOC concentrations, formed products, etc. make the comparisons almost impossible.

The new types of the non-thermal plasmas generated by HPGD and TS are effective for the VOC removal and able to compete with other non-thermal plasma techniques for pollution control in the laboratory as well as in the pilot scale. Low energy costs, almost no noxious gas output and solid products based on amino acids (obtained in Cu reactors and pilot-scale reactor) are particularly interesting.

Plasma technique [authors]	Treated compound	Initial concentration c_0 [ppm]	Gas (ambient air if not specified)	Flow Rate Q [l/min]	Energy density R_v [J/l]	Removal Efficiency η [%]	Energy costs R_m [kWh/kg]	Products
Electron beam								
[Pau93]	acetates, ketones toluene,xylene benzene	~ 400				60 – 90 (alif.) 60 – 80 (arom.) 20 – 40 (benzene)	25 – 100 71 – 111 55 – 167	aerosols (52%), CO_2 (20-10%), CO (10%), VOC (24%)
d.c. Corona Discharge								
[Mrv93]	styrene					82 – 99 (- polarity) 60 (+ polarity)		copolymers
[Jaw96]	mixture-petrol	3500				80 – 90		CO_2, H_2O, CO, NO_x
[Huc00] (streamer-to-spark regime)	benzene		air N_2 Ar	20 20 12		64 (+), 77 (-) 18 (+), 5 (-) 100 (+), 87 (-)	44 (+); 19.5 (-) 12.4 (+); 1.3 (-) 52 (+); 4.7 (-)	condensate of amino acids
Pulsed Corona Discharge								
[Yam93]	toluene		air, N_2			100		solid product
[vHe98] (pilot scale)	biogas-toluene, styrene, …	125 – 450 (tol) 30 – 190 (sty)	dry air (850°C)	1667	147	90	40	CO, particles tars
[Frc98] (+ catalysis)	butyl acetate, …	< 100	air (30 – 400°C)		36 – 54	99		CO_2, H_2O, organic acids aldehydes
[Kor98]	toluene	~330	dry & humid air	45	120-175	90	~29.3	CO_2, O_3, particles, ?
Dielectric barrier discharge (silent discharge)								
[ChM97]	toluene MEK	50 – 400	dry & humid air (25-100°C)	3 – 4		65 – 75 45 – 80	196 625	CO_2, CO, NO_x, HCHO, C, H_2, solid product
[Kra96]	toluene	100	dry air	5.3		98	77	CO_2, CO, particles
[Par99,Odi98] [Odi99]	toluene isopropanol	1000 – 2400	dry air	2.5 – 5		80 – 91 99	46 – 106 169	CO_2, CO, NO_2, NO particles, acetone
[And99]	styrene	5370 1000	Ar / O_2 (8 %) (90, 300°C)	1 – 20	750 – 2060 0 – 900		31 – 44	solid product, CO_2, CO, H_2O, other VOC
[ChM95]	formaldehyde	100	dry & humid air		600	97		
[Sny98]	chlorobenzene	250-1000	air, Ar + O_2 160°C various O_2 contents		1500-2000 500-1000	90-99 (air) >99 (Ar + O_2)		CO, CO_2 (CO/CO_2 = 1-3)
Surface Discharge & Ferroelectric packed bed								
[Yam92]	toluene	229	dry air	0.8		95	44	CO, CO_2, O_3, NOx, particles
[Ura97]	toluene	2000	dry air	1		75	39	CO_2, particles

Plasma technique [authors]	Treated compound	Initial concentration c_0 [ppm]	Gas (ambient air if not specified)	Flow Rate Q [l/min]	Energy density R_v [J/l]	Removal Efficiency η [%]	Energy costs R_m [kWh/kg]	Products
[Oga99]	benzene	< 50 – 200	synthetic air	0.2	3000	100		O_3, NO_x, CO_2, CO
[Fut98]	benzene toluene cyclohexene		dry & humid air, N_2	0.5-3	20000 5000 18000	75 65 90		CO_2, CO in N_2: cyclohexanone, cyclohexene oxide, aldehydes
Microwave and Radio-frequency (RF) discharge								
[Kud00]	cyclohexane		O_2 (120, 20°C)	0.06	10656		45	alcohols, ketones, H_2O, H_2O_2
[Tep95]	toluene		He+O_2 (25-70 kPa)	0.15 – 0.4		99.9		CO_2, H_2O, carbon black
DC glow discharge								
[Aki96]	toluene	10 – 15	dry & humid air (66°C)	25		90		
[McC99] (low pressure)	benzene	300 – 400	He, Ne, Ar (266-2930 Pa)	1	250 – 300 50	60 – 70 60 (pulsed)		
Gliding Arc								
[Cze96] (laboratory and pilot scale)	xylene (pilot) toluene MEK	200 1800 2000		2000 33.3 53.3		75 92 66	80 (related to C) 60 100	CO_2, CO, ?
[Opa00]	toluene ethyl acetate	200 – 600	dry & humid air	58 – 66	< 1620	46 60		
Other plasmas								
[Koh98] (capillary dis.)	toluene	50-2300	dry air	<<1-6		< 85	200-500	CO_2, CO, H_2O, NO_2, HNO_3, aerosol
This work								
HPGD Glass tube reactor	cyclohexanone toluene	1000 – 6000 1000 – 3000 (~2000 usually)	dry & humid air	0.5-6 0.5-10	1000 – 5000 1000 – 5000	50 – 90 40 – 80	54.9 – 219.8 29.3 – 204.8	CO_2, CO, H_2O, NO_2, NO, condensate of amino acids + aromatic nitrates from toluene
TS Cu tube reactor	cyclohexanone toluene	600 – 6000 (~2000 usually)	dry & humid air	2-18	200 – 800 200 – 600	46 – 55 50 – 60	8.24 – 33 (+) 13.73 – 35.7 (-)	CO_2, CO, H_2O, NO_2, solid product (amino acids)
TS Pilot-scale	cyclohexanone + other VOC	42.1 (-) 13.1 (+)	ambient air with combustion exhaust	830 (-) 580 (+)	9 (-) 14 (+)	56.9 (-) 54.5 (+)	43 (-) 189 (+)	solid product (amino acids)

Table 6.5.1 Comparison of results of the deVOC processes in various plasma techniques with our laboratory and pilot-scale results. Blank cells mean that the data were not available. MEK = methyl-ethyl ketone.

CONCLUSIONS AND PERSPECTIVES

The presented work, motivated by a rising trend of environmental problems of atmospheric pollution, especially by volatile organic compounds (VOC), had two essential objectives:

(1) To investigate new regimes of streamer-induced electric discharges operating in air at atmospheric pressure and generating non-thermal plasmas applicable for the removal of VOC.

(2) To apply these discharges for the VOC removal in various reactors and under various conditions, to explore the involved process from both, physical and chemical point of view, and to find out an optimal design and working conditions of the plasmochemical reactors for VOC removal working with these new discharges.

Concerning the first point, the experimental investigation of the new discharge regimes and their physical properties was done in air and some other environments at atmospheric pressure. Both discharges are generated by a d.c. high voltage of both polarities applied between two metal electrodes of a point-to-plane geometry. Results which gave rise to the simplified theories of a nature and running mechanisms of the discharges were obtained by means of UV-VIS emission spectroscopy, by measurements of electric discharge parameters and by other diagnostic techniques, such as electronic and optical microscopy applied for the analysis of electrodes.

The pulseless filamentary high pressure glow discharge (HPGD) is a normal glow discharge, regardless to the polarity of the point electrode. It is maintained pulseless due to the equilibrium between ionisation, electron attachment and recombination, as well as electrical heating and thermal cooling equilibrium. This condition is guaranteed by the external electric circuit, especially by a suitable choice of the series resistance. The gas temperature in the discharge is relatively high (900-2300 K), it rises with rising discharge current and changes along the discharge channel. However, the generated plasma is out of the local thermodynamic equilibrium (LTE) in the studied range of currents (1-5 mA), as resolved from the difference between rotational and vibrational discharge temperatures.

The transient spark (TS) is a pulsed discharge working in the regime of streamer-to-spark transition and in the kHz frequency range. Electric parameters of the circuit, especially the low gap capacity which discharges through the gap, determine the transient character of the spark pulse. It results that TS does not develop into an arc and does not reach LTE conditions, but generates a non-thermal plasma with medium gas temperatures (500-1700 K).

In comparison with the high pressure glow discharge, TS with suitable electric parameters generates colder plasma (further from the LTE) than the HPGD. As well as the HPGD it can be used as a special non-thermal plasma application where medium temperatures are needed, but the plasmochemical processes induced by the TS are somewhat different than those induced by the HPGD.

The second point concerns the specific applications of such discharges to the removal of VOC. Two basic kinds of plasma reactors were used for the laboratory tests of VOC removal in HPGD and TS of both polarities - the multipoint glass tube reactors with point-to-plane configuration and the Cu tube reactors with threaded rod HV electrode. Most of these experiments were carried out in dry or humidified air charged by various concentrations of VOC - cyclohexanone and toluene, varying the discharge and the gas flow parameters. The VOC decomposition (deVOC) process was investigated in some other environments as well. We used the IR absorption spectroscopy as the main technique for the diagnostic for treated VOC and formed products in all phases.

Three basic parameters of the VOC decomposition process (deVOC) were observed for every specific experimental condition: the removal efficiency, the energy costs and the formed products. They were always referred to the energy dissipated in the reactor volume (specific energy density R_V).

In general, the deVOC process induced by both discharges in all used reactors is not dependent on the initial VOC concentration from the viewpoint of the removal efficiency, but working with higher initial concentration always reflects in the lower energy costs. Removal efficiency rises logarithmically and energy costs rise exponentially with the energy density R_V. The influence of the discharge polarity is weak at both discharges. On the other hand, the reactor type, especially Cu electrode surfaces strongly influence the deVOC process.

In the glass reactors, HPGD gains the removal efficiencies up to 95 % and the energy costs in the range of 200-1000 eV/molecule (at R_V = 1000-5000 J/l). TS, in comparison with the more thermal HPGD, works with weaker R_V (200-800 J/l) and consequently gives the lower removal efficiencies (60-70 %), but also the lower energy costs (even below 100 eV/molecule).

The main gaseous by-products of the deVOC process in the glass reactors are CO_2, CO, H_2O, NO_2 and NO, their concentrations depend on the initial VOC concentration, presence of moisture in the carrying air and mainly R_V. The VOC removal process, especially

in HPGD, is partially similar to a combustion characterised by a relatively low CO/CO_2 ratio. A non-negligible part of the treated carbon from VOC goes to condensed products. The presence of humidity improves the process in both discharges, especially by reducing the NO_x production.

It was found out that the process in the glass multipoint reactors works better when the discharges are relatively distant from one another, because the radicals have a sufficient maturation time to induce the plasmochemical deVOC reactions. Moreover, it is suitable to put the gaps electrically in series, since it results in energy saving, thus lowering the total energy costs.

The Cu tube reactors, characterised by larger Cu surfaces and longer residence time of the treated gas in the active volume, have different effects on the deVOC process than the glass reactors, though the same discharges are used. Achieved removal efficiencies (50-60 %) are obtained at lower injected energy (R_V = 50-800 J/l) and the energy costs are considerably lower (16-100 eV/molecule) than in the glass reactors, particularly in colder TS.

Another advantage of the Cu reactors in comparison with glass reactors is a lower formation of noxious gaseous products such as NO_x, especially in TS at low residence times of the treated gas in the reactor volume. Processes initiated by active N_2^* molecules leading to the solid products based on amino acids become dominant at the lower energy densities. Amino acids and other condensed phase products (amides, imides) are non-toxic and thus more convenient from the point of view of the global effects. Environmental consequences of such products are reduced compared to the gaseous combustion products, CO_2 included. They are formed in particular on the Cu electrode surfaces which heterogeneously influence the deVOC processes and are certainly involved also in the mechanisms of N_2 fixation resulting in low energy costs. Excited N_2 species generated by the discharge probably work as energy reservoirs.

We investigated also the effects of other environments to the deVOC process, especially N_2 atmosphere with various oxygen contents. A slightly oxygen reduced air atmosphere (5 % O_2 in N_2) weakly improves the VOC removal in glass reactors, but stronger in Cu reactors where the amino acids formation is enhanced. The process in such an atmosphere is associated with lower CO_x and NO_x formation due to a lack of oxygen. On the other hand, the increased oxygen content (30 %) does not seem to influence the deVOC process. An interesting result is that the VOC decomposition occurs also in pure N_2, though not as efficiently as in air. It leads above all to HCN and acetylene production in the gas

phase and to a pure carbon as a solid product. Amino acids are formed in N_2+VOC atmosphere just in the Cu reactor with TS.

Let us summarize in the following ways. The large experimental study of the properties of transition types of electric discharges (pulseless HPGD and pulsed TS) and their application to the VOC removal in various reactors in laboratory scale confirmed their applicability for this purpose. Both objectives of the work were fulfilled.

The new types of the non-thermal plasmas generated by HPGD and TS are effective for the VOC removal and able to compete with other non-thermal plasma applications for pollution control. Results obtained in Cu reactors, characteristic of low energy costs and leading to the amino acids formation, are particularly interesting.

HPGD and TS used for the pollution control are not typical non-thermal plasma applications, they are somewhere in-between cold non-thermal plasmas of corona discharges and hot thermal plasmas. The thermal decomposition as well as the radical induced volume reactions and heterogeneous surface reactions participate at the VOC removal. The reactor type, the value of the injected energy and the residence time are basic parameters determining which of these three effects dominates. The nature of the formed products is a result of dominating processes as well.

The results of the tests of the small pilot-scale reactor (designed for 50 Nm^3/h) confirmed a possibility of application of the transient spark in such a type of Cu-based reactor for the treatment of large volumes of air polluted by VOC. The process is energetically cheap and relatively effective even at high gas flows through the reactor. It is to be emphasised that there are almost no noxious gases produced, the major product of this process is a non-toxic polymer in the solid phase based on the condensate of amino acids.

Let us finally identify some of the future perspectives of this approach. The presented work touches several scientific areas - from plasma physics and discharge diagnostics through plasma chemistry to the hetero-phase organic chemistry and surface phenomena. Of course, all areas of such a large topic could not have been investigated in exhaustive ways. A great attention have been paid to some aspects while of them, others were only flew over. This opens many new questions and several new directions of future investigations.

Let us emphasise for example the deVOC processes and the discharge phenomena in the atmosphere of N_2 or N_2 with poor oxygen content - it might be interesting and also

practical to apply the studied discharges to the treatment of combustion exhausts containing VOC (car emissions) or other mixture gases with a lack of O_2. A more detailed study of the discharge behaviour and temperatures in the mixed atmospheres (air+H_2O, air+VOC, combustion exhaust) might be also useful in order to find out all influences of the gas composition to the discharge properties. The control of the discharge properties by means of the external electric circuit also opens an interesting area of research.

The VOC removal itself could be further studied as well, for example a step-by-step analysis of the products and intermediates developing in the active reactor zone would enable a complex kinetic and thermochemical approach to the plasmochemical processes and all mechanisms participating at VOC removal. In particular, a detailed analysis of the processes and heterogeneous reactions occurring on electrode surfaces and their role in the formation of solid products (especially those based on amino acids) might be very interesting and useful, not only for the purposes of plasma techniques of pollution control, but also with regard to the biological processes such as photosynthesis and the origin of life on the Earth.

From the practical and industrial application point of view, HPGD was tested only in laboratory scales, important information obtained from these tests might be used to design and test the HPGD pilot-scale reactor. On the other hand, TS has already been successfully tested in the small pilot-scale reactor. However, the operation of this reactor might be even improved if all technical problems were eliminated. Similar reactor suitable for much larger treated volumes could be then suggested.

APPENDICES

A.1 APPENDIX 1 – CONCENTRATION UNITS AND THEIR CONVERSION

In the chemistry of gases and the atmospheric chemistry we usually find two different quantities and corresponding units describing the concentrations of some gas component. The first one is a relative concentration c given for example in % (per cent), ppm (parts per million) or ppb (parts per billion). The second one is a mass concentration c_m (mass per volume) given e.g. in mg.m^{-3}. Sometimes we find also a molar concentration c_{mol} (number of moles per volume) given in mol.l^{-1} or mol.m^{-3}.

The relative concentration c in ppm is given by the ratio of the number of particles of the inspected gas component N_i to the total number of all particles N:

$$c\ [\mathrm{ppm}] = 10^6 \frac{N_i}{N} \tag{A.1.1}$$

Such definition is however not very practical for calculations. Let us remind a general feature of ideal gases, that one mole of any gas takes always the same volume, whatever the kind of molecules. Gases at normal conditions can be approximately regarded as ideal gases, thus we can rewrite the above definition to the ratios of volumes.

$$c\ [\mathrm{ppm}] = 10^6 \frac{V_i}{V} \tag{A.1.2}$$

This is the reason why ppm is often written as ppmv – volume parts per million, or we talk about volume %. Considering the same important feature of gases we can write also [Kre98]:

$$c\ [\mathrm{ppm}] = 10^6 \frac{c_{mol}}{Y} \tag{A.1.3}$$

where c_{mol} [mol.m^{-3}] is a molar concentration of the inspected gas component and Y is a number of moles in one m^3 of a gas. Y is given just by the pressure p [Pa] and temperature T [K] via the state equation (A.1.4), it is universal for any gas due to the above mentioned general feature of gases.

$$Y = \frac{p}{RT} \tag{A.1.4}$$

R = 8.314 J.mol^{-1}.K^{-1} is the universal gas constant.

Molar and mass concentration of the gas component are linked via its molar mass M:

$$c_{mol}\ [\mathrm{mol.m^{-3}}] = \frac{c_m\ [\mathrm{g.m^{-3}}]}{M\ [\mathrm{g.mol^{-1}}]} \tag{A.1.5}$$

Replacing c_{mol} and Y in (A.1.3) we get the conversion between ppm and g.m^{-3}:

$$c\ [\mathrm{ppm}] = 10^6 \frac{R\ [\mathrm{J.mol^{-1}K^{-1}}]\ T\ [\mathrm{K}]}{p\ [\mathrm{Pa}]} \frac{c_m\ [\mathrm{g.m^{-3}}]}{M\ [\mathrm{g.mol^{-1}}]} \tag{A.1.6}$$

Y is practically an inverted value of V_{mol}, molar volume of a gas (volume of one mole) which is also universal for all gases and depends only on p and T. For instance, at normal conditions (atmospheric pressure and T = 273 K (O °C)), V_{mol} = 22.41 mol/l. Conversion formula (A.1.6) can be thus rewritten to

$$c\ [\mathrm{ppm}] = 10^6 \frac{V_{mol}\ [\mathrm{mol.l^{-1}}]\ c_m\ [\mathrm{mg.m^{-3}}]}{M\ [\mathrm{g.mol^{-1}}]} \tag{A.1.7}$$

- **Examples**:

  cyclohexanone c = 2000 ppm c_m = 8.158 g.m^{-3} (M = 98.14 g.mol^{-1})

  toluene c = 2000 ppm c_m = 7.659 g.m^{-3} (M = 92.14 g.mol^{-1})

  (calculated at T = 293 K and p = 101 kPa)

- **Remark**: We worked with relative concentration units (ppm) in the whole presented thesis, but mass concentration units (mg.m^{-3}) had to be used in the calculation of the energy costs (R_m, R_{mol}, see formulas 2.4.3, 2.4.4 in chapter 2.4.1) of the VOC removal process, conversion was done according to the formula (A.1.6).

Reference

[Kre98] Kreissl B. (1998) *"Influence des lignes de transport à haute tension sur la chimie atmosphérique en corrélation avec les conditions météorologiques"*, Thèse de doctorat de l'Université Paris VI

A.2 APPENDIX 2 – EMISSION SPECTROSCOPY OF N_2 MOLECULES

Emission spectroscopy in UV-visible spectral region is a powerful technique of plasma and gas discharge diagnostics. In this work it was used above all for the determination of vibrational and rotational discharge temperatures. Emission spectra of N_2 molecules (2^{nd} positive system of N_2) were measured for this purpose.

Please, note that all physical quantities in the following will be marked in *Italic* font, vector quantities will be distinguished by ***Bold Italic***.

A.2.1 Basic information

Let us remind some basic information on quantum mechanics. An electromagnetic radiation can be thought as having wave-like or particle-like properties. Considered as wave it is usually specified by the wavelength λ, in spectroscopies the wavenumber ν is commonly used:

$$\nu = \frac{1}{\lambda} \qquad [\mathrm{cm}^{-1}] \tag{A.2.1}$$

Light considered as particles, alias photons, has a specific energy given by the Planck's equation:

$$E = \frac{hc}{\lambda} = hc\nu \tag{A.2.2}$$

where h is the Planck's constant (h = 6.63×10^{-34} Js) and c is the velocity of light (c = 3×10^{8} ms^{-1}). The energy of the radiation is directly proportional to the wavenumber. [Atk94]

Potential energy of molecules is composed of the energy of electrons in the molecule, the energy of vibrations and the energy of rotations:

$$E = E_e + E_v + E_r \tag{A.2.3}$$

In a spectroscopy, we traditionally use the spectroscopic terms, i.e. energies expressed like wavenumbers. They are defined as follows:

electronic term $$T_e = \frac{E_e}{hc} \quad \text{(A.2.4)}$$

vibrational term $$G(v) = \frac{E_v}{hc} \quad \text{(A.2.5)}$$

rotational term $$F(J) = \frac{E_r}{hc} \quad \text{(A.2.6)}$$

where v and J are quantum numbers of vibration and rotation, respectively.

A spectral line then corresponds to the change of the energy of the upper state *E'* to the energy of the lower state *E"*:

$$\nu = T_e' - T_e'' + G(v') - G(v'') + F(J') - F(J'') \quad \text{(A.2.7)}$$

A.2.2 Electronic states of molecules

Electronic states of molecules are determined by the electrons of the atoms in the molecule. A projection of angular orbital moments ***L*** on the internuclear axis of the molecule determines the total orbital moment of the molecule (orbital quantum number Λ). Λ can have the following values:

$$\Lambda = 0, 1, 2, ..., L$$

According to the values of the molecule orbital quantum number Λ we mark electronic states of the molecules by the following symbols:

Λ =	0	1	2	3	...
electronic state (term) symbol	Σ	Π	Δ	Φ	...

Similarly, spin orbital moment $\boldsymbol{\Sigma}$ of a molecule is formed by the projection of the sum of spin vectors $\boldsymbol{S}$ on the internuclear axis of the molecule. Spin quantum number Σ (do not confuse with symbol Σ for the molecular state with Λ=0) of a molecule can have values:

$$\Sigma = -S, -S+1, ..., S-1, S$$

The multiplicity of the term due to the spin is 2S+1. Singlet states have 2S+1=1, triplet states have 2S+1=3.

Coupling of the orbital angular moment vector $\boldsymbol{\Lambda}$ and the spin vector $\boldsymbol{\Sigma}$ of the molecule form its total angular moment $\boldsymbol{\Omega}$ with a corresponding quantum number Ω.

$$\Omega = | \Lambda + \Sigma |$$

The electronic state of the molecule can be then written using these quantum numbers:

$${}^{2S+1}\Lambda_{\Omega}$$

Majuscule Greek symbols for Λ are employed. This nomenclature is similar to that one used for atoms (${}^{2S+1}L_J$). However, instead of Ω, symbols g or u are often used. They indicate even (g, gerade) or odd (u, ungerade) wave functions. Symbols + and - used as right superscripts mean symmetric (+) or antisymmetric (-) wave functions.

Furthermore, symbol X is used for the ground state and symbols A, B, C, ... or a, b, c, ... for the excited states, the former with the same multiplicity as the ground state, the latter with the different multiplicity. [Cha96]

Ground state of N_2 molecule can be then written like $X^1\Sigma_g$, excited N_2 states are e.g. $C^3\Pi_u$, $B^3\Pi_g$, $A^3\Sigma_u^+$.

The transition between electronic states of molecules are governed by the selection rules:

$\Delta\Lambda = 0 \pm 1$	
$\Delta\Omega = 0 \pm 1$	but $0 \rightarrow 0$ is forbidden
$\Delta\Sigma = 0$	
$g \leftrightarrow u$	for homonuclear molecules only

Possible transitions between Σ and Π states in homonuclear molecules are then:

$$\Sigma_g^+ \leftrightarrow \Sigma_u^+ \qquad \Sigma_g^- \leftrightarrow \Sigma_u^- \qquad \Pi_g \leftrightarrow \Sigma_u^+ \qquad \Pi_u \leftrightarrow \Sigma_g^+$$
$$\Pi_g \leftrightarrow \Sigma_u^- \qquad \Pi_u \leftrightarrow \Sigma_g^- \qquad \Pi_g \leftrightarrow \Pi_u$$

[Mrr68]

A.2.3 Rotational spectra of diatomic molecules

Energy of the rotational state of the molecule derived by quantum mechanics is given by the equation (A.2.8) and the rotational term consequently by (A.2.9):

$$E_r = hcBJ(J+1) \tag{A.2.8}$$

$$F(J) = BJ(J+1) \tag{A.2.9}$$

where J is the rotation quantum number and B is the rotational constant defined like:

$$B = \frac{h}{8\pi cI} \tag{A.2.10}$$

I is the moment of inertia of the molecule, for diatomic molecules given by:

$$I = \mu r^2 \tag{A.2.11}$$

with the reduced mass $\mu = mm'/(m+m')$ and the internuclear distance r.
Using (A.2.9) for $J' \rightarrow J''$ transition we get the difference of two rotational terms:

$$\nu = BJ'(J'+1) - BJ''(J''+1) \tag{A.2.12}$$

The selection rules for rotational transitions are

$$\Delta J = 0, \pm 1 \qquad \text{with } 0 \rightarrow 0 \text{ transition forbidden.} \tag{A.2.13}$$

Taking *J”*=*J’*+1 according to the selection rule (A.2.13) we get

$$\nu = 2BJ' \tag{A.2.14}$$

This condition causes that rotational lines are equidistant.

Energies of rotational states of molecules with more than 2 atoms can be solved regarding these molecules as spherical or symmetric tops. [Atk94]

A.2.4 Vibrational spectra of diatomic molecules

A diatomic molecule can be in first approximation regarded as a harmonic oscillator. Solving this problem by means of quantum mechanics results in the equations for the vibrational energy and vibrational term, respectively:

$$E_v = hc\omega_e(v + \frac{1}{2}) \tag{A.2.15}$$

$$G(v) = \omega_e(v + \frac{1}{2}) \tag{A.2.16}$$

with the vibrational quantum number v = 0, 1, 2, ... and the fundamental frequency of the oscillator $c\omega_e$. ω_e has a dimension of wavenumber [cm^{-1}].

However, diatomic molecules do not behave as harmonic oscillators, equations (A.2.15, A.2.16) have to be corrected by the anharmonicity factors:

$$G(v) = \omega_e(v + \frac{1}{2}) - x_e\omega_e(v + \frac{1}{2})^2 + y_e\omega_e(v + \frac{1}{2})^3 + \cdots \tag{A.2.17}$$

Typical potential energy curve of a real diatomic molecule (Morse curve) is shown in Figure A.2.1.

Specific selection rule for the vibrational transitions is

$$\Delta v = \pm 1 \tag{A.2.18}$$

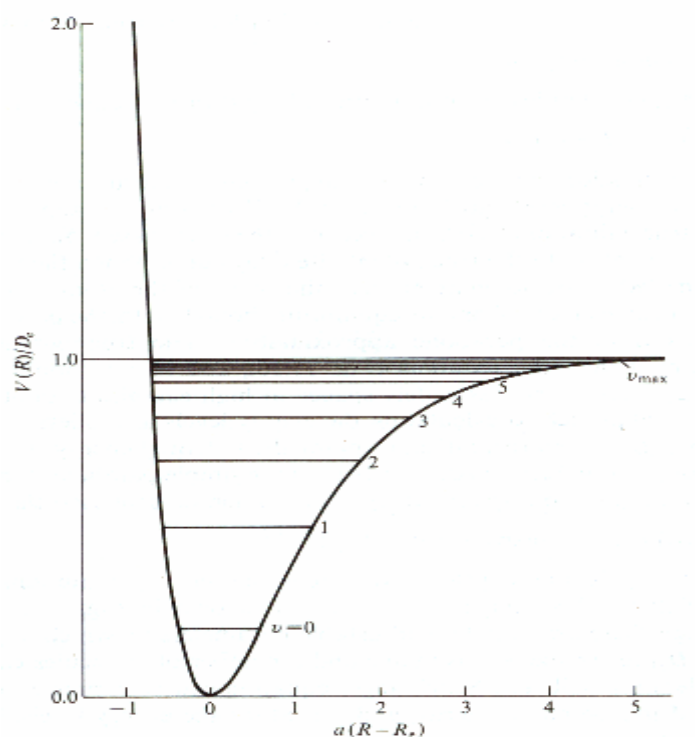

Figure A.2.1 Morse potential energy curve of a diatomic molecule with non-equidistant vibrational levels **[Atk94]**

The basis of this rule can be traced to the conservation of angular moment of the combined photon + molecule system. Hence, the wavenumber of the spectral line corresponding to the transition between two adjacent vibrational levels is:

$$\nu = \omega_e \tag{A.2.19}$$

in the harmonic oscillator, or

$$\nu = \omega_e - 2(v+1)x_e\omega_e + \cdots \tag{A.2.20}$$

if the anharmonicity is taken into account. Non-equidistant vibrational levels of a diatomic molecule are shown in Figure A.2.1. However, so called gross selection rule (the dipole moment must change during a vibration if it is to be spectroscopically active) forbids the vibrational transitions of N_2 molecule within one electronic state, because N_2 molecule has no permanent dipole moment. Homonuclear diatomic molecules are vibrationally active if only electronic states change at the same time. [Atk94]

A.2.5 Vibrational-rotational spectra of diatomic molecules

Real molecules behave as vibrating rotators, vibrational and rotational transitions occur simultaneously, we observe vibrational as well as rotational spectra. Vibrational-rotational term of a diatomic molecule can be expressed like a sum of vibrational (A.2.17) and rotational (A.2.9) terms:

$$G(v,J) = G(v) + F(J) = \omega_e(v+\frac{1}{2}) - x_e\omega_e(v+\frac{1}{2})^2 + B_v J(J+1) - D_v J^2(J+1)^2 \qquad \text{(A.2.21)}$$

if just the quadratic term of the anharmonicity correction is considered. Rotational constant B is characteristic for each vibrational state, we write B_v. The expression $D_v J^2(J+1)^2$ is a correction of the rotational term (A.2.9) due to the centrifugal distortion of the elastic bond between the nuclei. However, D_v is about 10^{-4} times smaller than B_v and can be neglected in further considerations.

We get a vibrational band containing many rotational lines, they are superposed on the band. The wavenumber of the rotational lines of the vibrational band corresponding to the transition $v' \rightarrow v''$ is given by:

$$\nu = G(v') - G(v'') + B'_v J'(J'+1) - B''_v J''(J''+1) \qquad \text{(A.2.22)}$$

Let us remind the selection rules for rotational and vibrational transitions (equations (A.2.13) and (A.2.18)).Transitions with $\Delta J = -1$ and $\Delta v = +1$ make so called P branch of the vibrational-rotational spectrum, transitions with $\Delta J = +1$ and $\Delta v = +1$ make the R branch. $\Delta J = 0$ and $\Delta v = +1$ make the Q branch. When we neglect also the anharmonicity factors, the wavenumbers corresponding to the three branches of the spectrum are:

$\nu = \omega_e - 2BJ$ P branch (A.2.23)

$\nu = \omega_e$ Q branch (A.2.24)

$\nu = \omega_e + 2B(J+1)$ R branch (A.2.25)

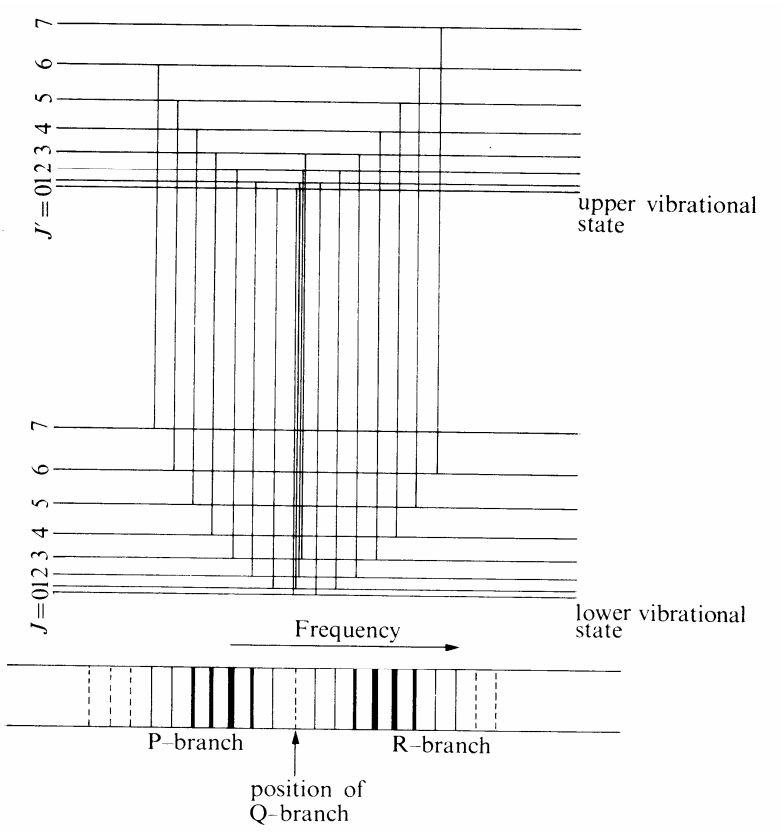

Figure A.2.2 Formation of P,Q and R branches of the vibrational-rotational spectrum **[Atk94]**

Rotational constants B_v for v and v+1 states are slightly different which results that Q branch appears as a cluster of very closely spaced lines. The three branches are illustrated in Figure A.2.2. The separation between the rotational lines in P and R branches of a vibrational transition gives the value of the rotational constant B_v, and so useful information can be obtained from the vibrational-rotational spectrum without needing to take a pure rotational spectrum which is in the microwave region. [Atk94]

Q branch appears only in electronic-vibrational-rotational spectra, i.e. when an electronic transition occurs together with vibrational-rotational transitions, otherwise transitions characterised by $\Delta J = 0$ are forbidden. The wavenumbers of spectral lines are then determined by equation (A.2.7). Figure A.2.3 demonstrates electronic, vibrational and rotational states of a diatomic molecule which give rise to the electronic-vibrational-rotational spectrum.

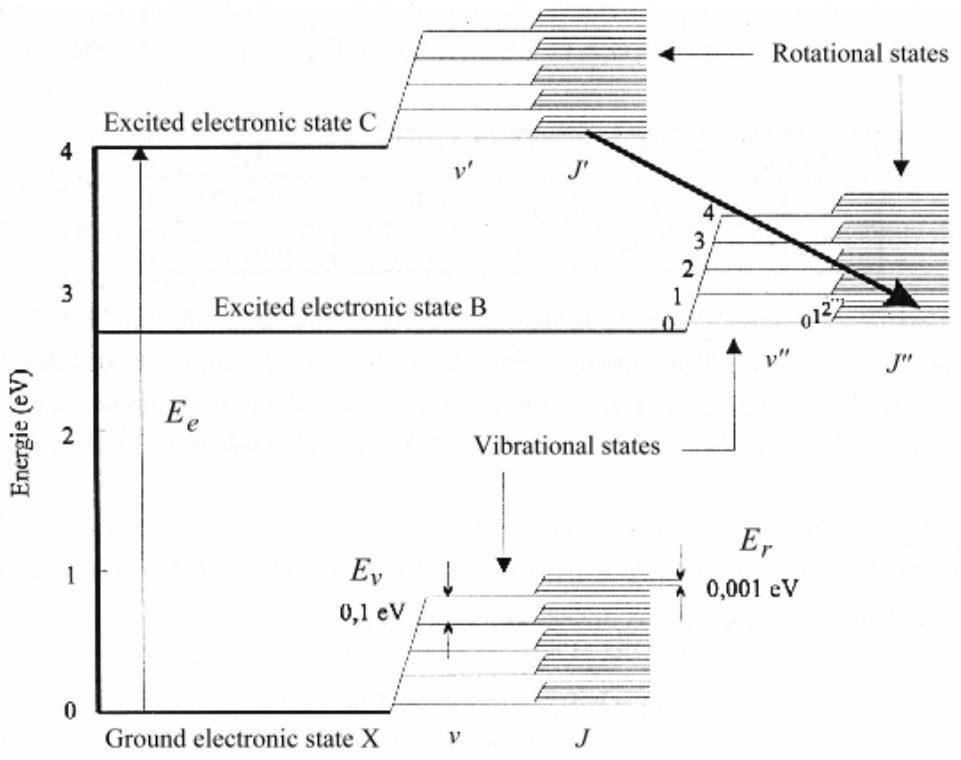

Figure A.2.3 Electronic, vibrational and rotational states of a diatomic molecule (e.g. N_2) giving rise to the electronic-vibrational-rotational spectrum **[Cha96]**

A.2.6 N_2 molecules - electronic-vibrational-rotational spectra

N_2 molecules are symmetric with no permanent dipole moment. They emit vibrational-rotational spectra only if electronic transitions occur at the same time. Most of the electronic states of N_2 molecule (and N_2^+ ion) are shown on the potential energy diagram of N_2, Figure A.2.4.

The most important electronic transitions occurring in plasmas generated by our discharges (HPGD and TS) are the following:

- excitatation of the ground N_2 state by an electron impact

$$e + N_2\ X^1\Sigma_g^+ \rightarrow N_2\ C^3\Pi_u + e$$

- radiative resonant deexcitations of the upper states

$N_2\ C^3\Pi_u \rightarrow N_2\ B^3\Pi_g + h\nu$ 2^{nd} positive system of N_2

$N_2\ B^3\Pi_g \rightarrow N_2\ A^3\Sigma_u^+ + h\nu$ 1^{st} positive system of N_2

where $h\nu$ is an energy of the emitted light (photon). It lies in the UV-visible spectral region for both mentioned systems. “System” means an ensamble of many vibrational bands induced by various vibrational transitions which accompany the electronic transition. Rotational lines are superposed on the vibrational bands. N_2 emits typical electronic-vibrational-rotational spectra.

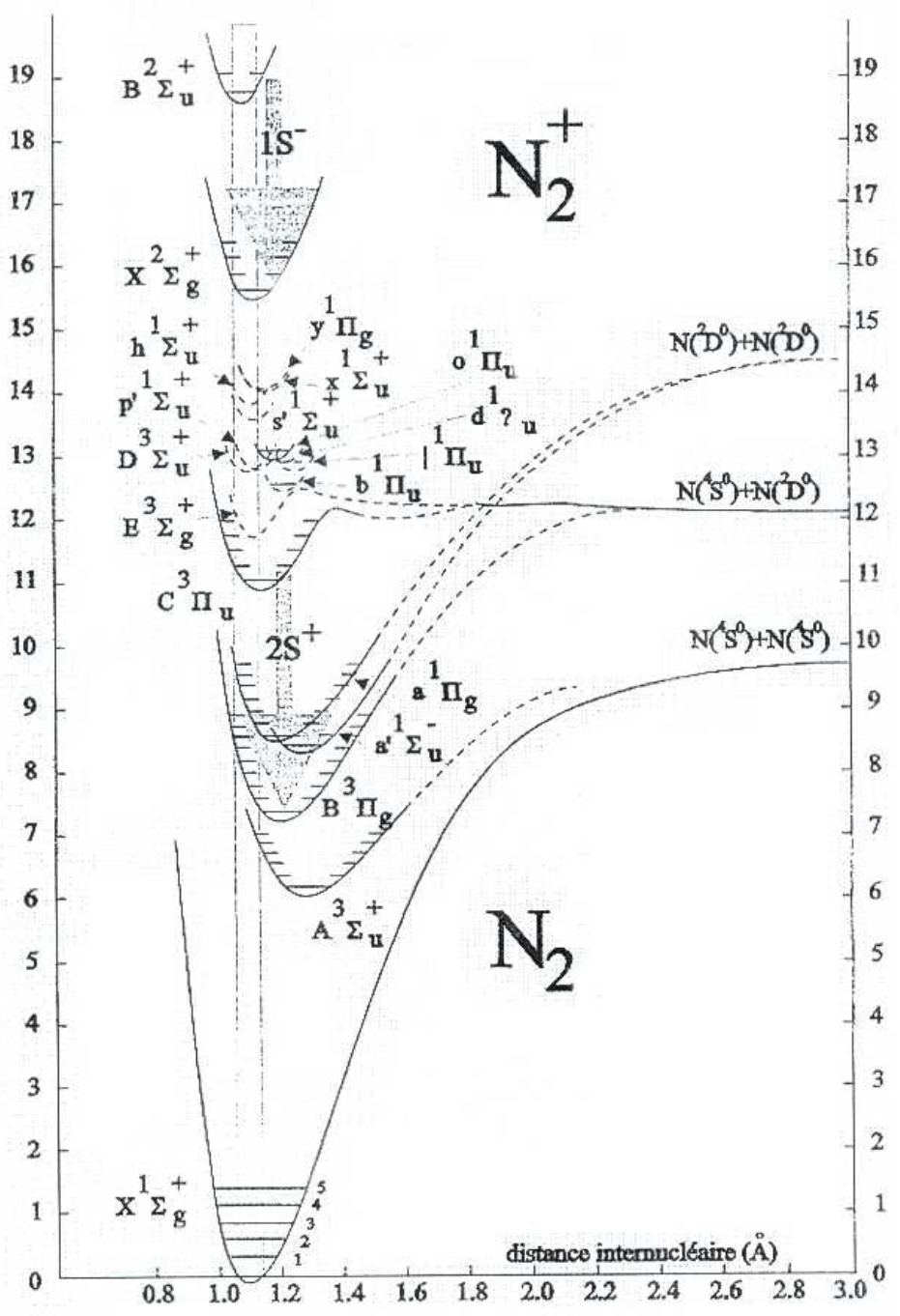

Figure A.2.4 Diagram of the potential energy and states of the N_2 molecule **[Har77]**

Band wavelengths of the 2nd and 1st positive systems are listed in Table A.2.1; an example of the emission spectrum of the 2nd positive N_2 system is shown in Figure A.2.5. Excited states $C^3\Pi_u$ and $B^3\Pi_g$ are resonant-radiative with short lifetimes ($3\text{-}5\times10^{-8}$, 8×10^{-6} s). $A^3\Sigma_u^+$ is a metastabe state with a very long lifetime (1.3-1.9 s), beacuse the transition to the ground state ($N_2\ A^3\Sigma_u^+ \rightarrow N_2\ X^1\Sigma_g^+$) is forbidden. [Lof77].

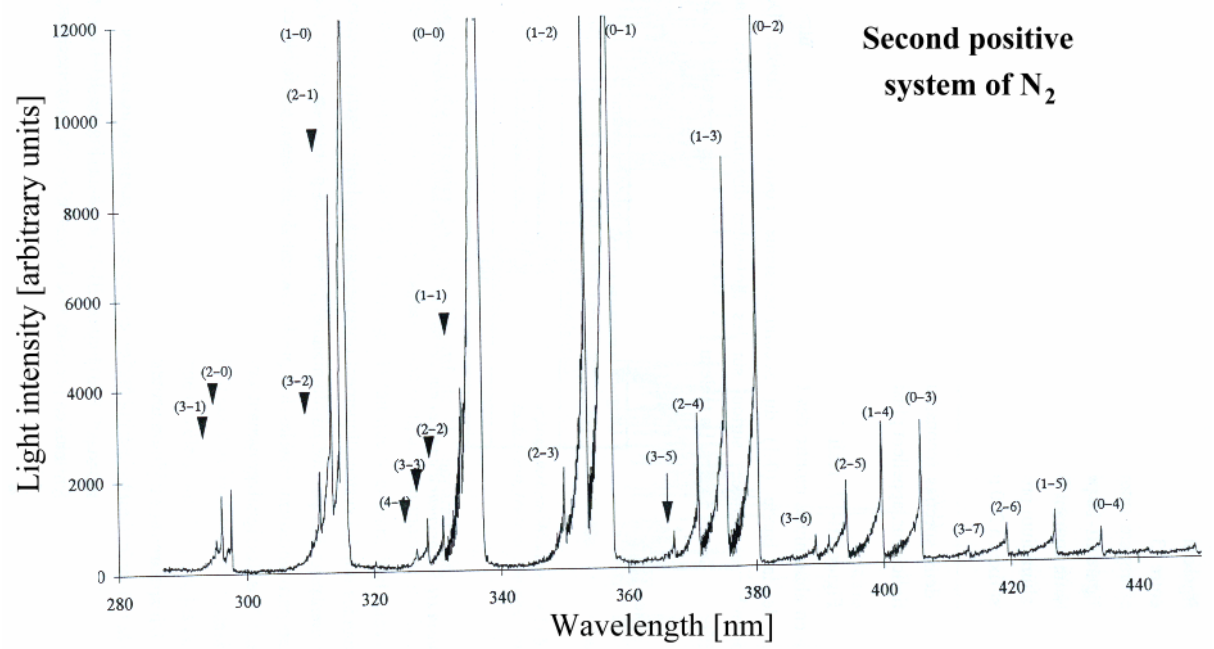

Figure A.2.5 Example of the emission spectrum of N_2 - 2nd positive system.

2nd positive system of N_2			**1st positive system of N_2**		
Transition v'-v''	**Wavelength [nm]**	**Spontaneous emission probability**	**Transition v'-v''**	**Wavelength [nm]**	**Relative band intensity (max. 10)**
4-0	268.65	-	12-7	537.28	3
4-1	281.43	0.0726	11-6	540.71	3
3-0	281.98	0.024	10-5	544.23	3
4-2	295.32	0.355	12-8	575.52	7
3-1	296.2	0.262	11-7	580.43	7
2-0	297.68	0.152	10-6	585.44	8
4-3	310.4	0.104	9-5	590.6	8
3-2	311.67	0.233	8-4	595.9	8
2-1	313.6	0.371	7-3	601.36	7
1-0	315.93	0.44	6-2	606.97	7
4-4	326.81	0.11	5-1	612.74	3
3-3	328.53	0.117	12-9	618.52	3

2-2	331.0	0.0337	11-8	625.28	3
1-1	333.9	0.021	10-7	632.29	7
0-0	337.13	0.485	9-6	639.47	9
3-4	346.9	0.0059	8-5	646.85	10
2-3	350.05	0.0669	7-4	654.48	10
1-2	353.67	0.206	6-3	662.36	9
0-1	357.69	0.321	5-2	670.48	8
4-6	364.17	0.0518	4-1	678.86	6
3-5	367.19	0.0868	3-0	687.5	2
2-4	371.05	0.151	7-5	716.48	2
1-3	375.54	0.185	6-4	727.33	3
0-2	380.49	0.134	5-3	738.66	5
4-7	385.79	0.0865	4-2	750.39	7
3-6	389.46	0.117	3-1	762.62	7
2-5	394.3	0.117	2-0	775.32	6
1-4	399.84	0.0895	5-4	820.48	3
0-3	405.94	0.042	3-2	854.18	6
4-8	409.48	0.0951	2-1	872.23	8
3-7	414.18	0.0778	1-0	891.16	10
2-6	420.05	0.062	4-4	936.2	3
1-5	426.97	0.0395	3-3	959.9	3
0-4	434.36	0.0134	0-0	1042	10

Table A.2.1 2nd and 1st positive systems of N_2 - wavelengths of the band heads, corresponding vibrational transitions and other characteristics. **[Har77, Pea50]**

A.2.7 Determination of rotational and vibrational temperatures from the spectra of the 2nd positive N_2 system

Rotational and vibrational temperatures T_r and T_v give a valuable information on the type of generated plasma, if $T_r = T_v$ a plasma is in the local thermodynamic equilibrium.

Intensity of rotational lines in the vibrational-rotational spectrum depends on the population of molecules N_J excited to the rotational state with the quantum number J. This population $N_J(v)$ of the rotational level J at vibrational state v is governed by the Botzmann distribution:

$$N_J(v) = \frac{N_v}{Q_r}(2J+1)e^{-B_v J(J+1)\frac{hc}{kT}} \tag{A.2.26}$$

where N_v is a total population of the vibrational level v and Q_r is the partition function given by:

$$Q_r = \sum_{J=0}^{\infty} (2J+1) e^{-B_v J(J+1)\frac{hc}{kT}} \tag{A.2.27}$$

The intensity of the rotational line in the vibrational band is given by the expression:

$$I_{J',J''} = D\ N_{J'}\ \nu^4_{J',J''}\ S_{J',J''} \tag{A.2.28}$$

where $S_{J',J''}$ is the line strength, $\nu_{J',J''}$ is the wavenumber of $J' \rightarrow J''$ transition. $N_{J'}$ is the population of the upper rotational level and D is a constant depending on units and geometry of the experimental set up. Putting (A.2.26) into (A.2.28) and expressing by Hönl-London factors $H_{J',J''}$ we get a new expression for the intensity:

$$I_{J',J''} = I_{v',v''} \frac{\nu^4_{J',J''}}{\nu^4_{v',v''}} \frac{H_{J',J''}}{g' Q_r}\ e^{-\frac{B_{v'} J'(J'+1)hc}{kT}} \tag{A.2.29}$$

with a statistical weight g' and the wavenumber of the vibrational band origin $\nu_{v',v''}$. By taking natural logarithms it is possible to obtain the rotational temperature T_r from the slope of a plot of ln ($I_{J',J''}$ / $\nu_{J',J''}{}^4 H_{J',J''}$) against $J'(J'+1)$. [Mrr68]

In reality, we used a program (described in [Che94a, Cha96]) which generated a simulated spectrum and compared it with the measured one to determine T_r. However, the principle of T_r determination used in the program is approximately the same.

Vibrational temperature can be measured by a similar way. The integrated intensity over a vibrational band can be written similarly:

$$I_{v',v''} = D\ N_{v'}\ \nu^4_{v',v''}\ S_{v',v''} \tag{A.2.30}$$

where $S_{v',v''}$ is the band strength and $N_{v'}$ is the population of the upper vibrational level. D is a constant depending on units and geometry of the experimental set up. The band strengths $S_{v',v''}$ are given by the Franck-Condon factors $q_{v',v''}$. Assuming Boltzmann distribution we can write for the population of the upper vibrational state:

$$N_{v'} = \frac{N}{Q_v}\, e^{-G(v')\frac{hc}{kT}} \tag{A.2.31}$$

where N is the total population of molecules in a given electronic state. Q_v is the vibrational partition function given by:

$$Q_v = \sum_{v=0}^{\infty} e^{-\frac{E_v}{kT_v}} \tag{A.2.32}$$

After putting (A.2.31) into (A.2.30) and doing a natural logarithm we get:

$$\ln \frac{I_{v',v''}}{\nu^4_{v',v''}\, S_{v',v''}} = -\frac{G(v')}{0.6925T} + \text{ constant} \tag{A.2.33}$$

A plot of ln ($I_{v',v''}$ / $\nu_{v',v''}{}^4$ $S_{v',v''}$) against $G(v')/0.6925$ should give again a straight line with a slope $-1/T_v$. Vibrational temperature T_v can be thus determined from this line. [Mrr69]

We used a program based on the above described principle to calculate T_v.

In the case of the local thermodynamic equilibrium (LTE), the distribution function of the population in an excited state is the same as in a fundamental state, it is based on the Botzmann distribution (just with some modifications of the rotational constant B_v for the rotational distribution).

Plasma generated by the discharges studied in this work is, however, out of the LTE. The time constants of the collisions are not sufficient to obtain a thermalisation of the present excited species. Radiative depopulation of the excited N_2 states (joined with a light emission) occurs more probably than their thermal deexcitation by collisions. Hence, the Boltzmann distribution function which was used to write the populations of rotational and vibrational states may not be completely correct. Some precautions have to be taken into account when determining T_r and T_v.

The energies between rotation levels are of the same order of magnitude as the energy corresponding to the neutral speed, thus a quick relaxation of the rotational energy towards a thermal equilibrium with the neutral species happens. Therefore, the rotational temperature of the ground state should quickly relax to the neutral gas temperature, and the intensity

distribution of the rotational components into a molecular band may be used to derive T_r [Che94b].

On the other hand, the determination of the vibrational temperature is more delicate, because the energies between vibrational levels are much higher than the thermal energy of neutral species and the relaxation of the vibrational excited stated will preferentially occur by radiation. The T_v that we measured is practically just an apparent vibrational temperature. This problem is in more details discussed in chapters 3.4.5 and 4.3.5.

A.2.8 References

[Atk94] Atkins P.W. (1994) *Physical Chemistry*, Oxford University Press, 5th edition

[Cha96] Champain H. (1996) *"Stabilité des décharges couronne dans le SF_6 en régime établi. Spectroscopie de la décharge et phénomènes aux électrodes"*. Thèse de doctorat de l'Université Paris XI

[Che94a] Chelouah A., Marode E., Hartmann G., Achat S. (1994) J. Phys. D: Appl. Phys **27**, 940-945

[Che94b] Chelouah A., Marode E., Hartmann G. (1994) J. Phys. D: Appl.Phys **27**, 770-780

[Har77] Hartmann G. (1977) *"Spectroscopie de la décharge couronne: étude des mécanismes de collision dans le dard"* Thèse de doctorat de l'Université Paris XI

[Lof77] Lofthus A., Krupenie P. H. (1977) J. Phys. Chem. Ref. Data **6**, 113-307

[Mrr69] Marr G.V. (1968) *Plasma spectroscopy*, Elsevier Publ. Comp., Amsterdam, London, New York

A.3 APPENDIX 3 - INFRARED ABSORPTION SPECTROSCOPY

The infrared (IR) spectroscopy is a powerful diagnostic technique widely used for qualitative and quantitative analysis of chemical samples in all phases. It is applicable also to complicated molecules and polymers, it is possible to distinguish the bonds and characteristic atomic groups. Raman spectroscopy is often employed as the complement to the IR spectroscopy. [Atk94]

The infrared absorption spectroscopy was used as a main analytical technique in this work. It was applied for the detection and quantitative analysis of VOC and other gaseous products of the VOC removal process, as well as for the analysis of all other products in solid or liquid phase.

Please, note that all physical quantities in the following will be marked in *Italic* font, vector quantities will be distinguished by ***Bold Italic***.

A.3.1 Basic information

Let us start with some basic information on quantum mechanics. Light (electromagnetic radiation) can be thought as having wave-like or particle-like properties. Considered as wave it is usually specified by the wavelength λ, in infrared spectroscopy the wavenumber ν is commonly used:

$$\nu = \frac{1}{\lambda} \qquad [\mathrm{cm}^{-1}] \tag{A.3.1}$$

Light considered as particles, alias photons, has a specific energy given by the Planck's equation:

$$E = \frac{hc}{\lambda} \tag{A.3.2}$$

where h is the Planck's constant (h = 6.63×10^{-34} Js) and c is the velocity of light (c = 3×10^{8} ms^{-1}). Putting formula (A.3.1) into (A.3.2) we get

$$E = hc\nu \tag{A.3.3}$$

This equation shows that the energy of the radiation is directly proportional to the wavenumber. [Atk94, Smt99]

The infrared radiation, alias heat, has an energy corresponding to the changes of vibrational and rotational molecular states. Rotational energies of the molecules are lower than the vibrational ones. According to the energy of radiation we divide the infrared part of the spectrum into three basic regions. Their view with specific wavelengths, wavenumbers and energies is given in Table A.3.1.

Infrared region	**wavenumber** ν **[cm^{-1}]**	**wavelength** λ **[m]**	**energy** E **[eV]**
far infrared (FIR)	10 - 700	10^{-3} - 1.4×10^{-5}	1.2×10^{-3} - 8.7×10^{-2}
Middle infrared (MIR)	700 - 4000	1.4×10^{-5} - 2.5×10^{-6}	8.7×10^{-2} - 5×10^{-1}
near infrared (NIR)	4000 - 12000	2.5×10^{-6} - 8.3×10^{-7}	5×10^{-1} - 1.5

Table A.3.1 View of the infrared regions

The energy (wavenumber) of an electromagnetic radiation determines what kind of excited molecular states will be generated by its absorption. According to these energies, three types of molecular spectra can be obtained [Atk94]

1. rotational spectra corresponding to the change of the rotational molecular states, the vibrational states may stay unchanged. Energies of these states differ very little (~10^{-4} eV. $\nu \sim 1\text{cm}^{-1}$), thus the energy of the radiation necessary to cause the transition is small and the wavelengths are from microwave region.
2. rotational-vibrational spectra corresponding to the simultaneous change of the rotational and vibrational molecular states. The rotational terms are superposed on the vibrational ones. The radiation of such energies has the wavelengths from the far (deformation) and middle infrared region.
3. vibrational spectra referring to the change of the vibrational molecular states, transition from the ground state to one of the excited states. Energies of the radiation inducing such transitions are in the range of all IR regions (FIR. MIR and NIR).

A.3.2 Two conditions necessary for the infrared absorption

The electromagnetic radiation of some specific frequency (wavenumber ν respectively) can vibrationally excite a molecule only when its frequency is equal to the characteristic resonance frequency of the molecule, by other words when the following condition is fulfilled:

$$\Delta E_v = hc\,\nu \tag{A.3.4}$$

where ΔE_v is a vibrational energy level difference in the molecule, h is the Planck constant and c is the speed of light. The same condition is valid for the rotational excitation of the molecule. If the radiation has a wavenumber which does not satisfy this condition, a molecule cannot be excited. Practically, all spectroscopies as analysis techniques are based on this very important condition. [Smt99]

A vibration of the molecule need not necessarily be accompanied by an infrared absorption band. An IR absorption occurs only when the vibration causes a change in the charge distribution within a molecule. This is the second necessary condition for IR absorption. Dipole moment $\boldsymbol{\mu}$ (vector quantity) is a measure of the charge asymmetry of the molecule.

$$\boldsymbol{\mu} = q\,\boldsymbol{r} \tag{A.3.5}$$

where q is a charge and $\boldsymbol{r}$ is a vector connecting atoms in the molecule (interatomic distance). Molecules with permanent dipole moment (asymmetric polar molecules with inhomogeneous charge distribution. e.g. H_2O) are always active in infrared, their $\boldsymbol{\mu}$ interacts with the electric vector of an electromagnetic radiation and they absorb the radiation (if the first condition (A.3.4) is fulfilled. of course). Some molecules have no permanent dipole moment (symmetric polar molecules with homogeneous charge distribution. their $\boldsymbol{\mu}$=0. e.g. CO_2), but can get a dipole moment induced by an interaction with an electromagnetic radiation, they vibrate by such a way that the charges within them distribute inhomogeneously (asymmetric vibrations). We can write the second condition for IR absorption simply:

$$\frac{\partial \mu}{\partial x} \neq 0 \qquad \text{(A.3.6)}$$

where $\partial \boldsymbol{\mu}$ is a change in dipole moment and ∂x is a change in bond distance. A molecular vibration can be IR active only when it causes a spatial change of the dipole moment of a molecule. This condition is responsible for IR inactivity of diatomic mono-element molecules such as O_2, N_2, but also very symmetric C-C structures. [Smt99]

On the other hand, the larger the charge distribution change within a molecule, the stronger the absorption. Accordingly, the bands of hydrocarbons composed only of C and H atoms are generally weak, but bands associated with bounds connecting atoms that differ considerably in their electronegativities, e.g. C-N. C-O. C=O. C≡N. are usually quite strong. [Nak77]

A.3.3 Model of harmonic oscillator, its consequences and other effects

Let us consider the factors that determine the position of absorption bands. A diatomic molecule composed of atoms with masses *m* and *m'* can be regarded as a harmonic oscillator. Solving this system as two balls joined with a spring according to the Hooke's and the second Newton's laws we get the wavenumber ν at which the molecule absorbs the IR radiation:

$$\nu = \frac{1}{2\pi c}\sqrt{\frac{f\left(m+m'\right)}{mm'}} \qquad \text{(A.3.7)}$$

where *c* is the velocity of light and *f* [N/m] is a force constant (bond strength). It is evident from the previous equation that wavenumber ν, thus the band position in the IR spectrum, is determined by the bond strength *f* and the reduced mass of the atoms linked with the bond. The stronger the bonds and the smaller the reduced mass, the higher the absorption wavenumber of the particular bond, i.e. more energy is required to vibrate the bond. [Smt99]

For example, the bond strengths increase from single to double to triple bounds and the absorption bands go towards higher wavenumbers. Strong polar bonds also result in high *f*. hence high ν. [Nak77]

The mass effect to the position of the absorption band in the IR spectrum is determined (always from the equation (A.3.7)) by the inversion value of the reduced mass, i.e. the difference of masses of concerned atoms. The reduced mass is maximal ($m/2$) when $m = m'$, ν is low consequently. The model of two basketballs joined with a spring can be applied, they vibrate with a low frequency. Examples are C-C, C-N and C-O stretching vibrations which appear in 900-1300 cm^{-1} IR region. On the other hand, when $m << m'$, the reduced mass is minimal, a model of a basketball and a ping-pong ball can be applied, the vibational frequency, hence ν, is high. An example are C-H, N-H and O-H bonds which usually absorb above 3000 cm^{-1}. It is even more clearly seen on the deuteration effect: the stretching vibration of the O-H bond is at 3600 cm^{-1} but lowered to 2630 cm^{-1} in the O-D bound where the bond strength f is the same. The bending frequencies can be qualitatively treated in the same fashion. [Nak77, Smt99]

However, this was just a simplified model of a harmonic oscillator which can approximately determine a wavenumber of the vibration. Real 2-atomic molecules behave as anharmonic oscillators, the anharmonicity being stronger with greater mass difference of concerned atoms. The vibrations of real molecules with 3 and more atoms are even more complicated. Individual bonds within a molecule never vibrate independently with respect to the remaining part of the molecule, exciting of one bond in such a molecule leads to the partial excitation of another bonds, the bands positions vary from case to case. These effects are called vibrational interactions. [Smt99]

An extreme example of the vibrational interaction is known as Fermi resonance. Two vibrations of similar ν and proper symmetry "repel" each other appearing in wavenumbers above and below where they are normally expected. Vibrations that normally would not appear in the spectrum can "steal" intensity via Fermi resonance and appear in the spectrum. When an overtone or combination band is located near a fundamental frequency of the same symmetry. the band intensity of the former may be anomalously enhanced or bands may be split. [Smt99]

Many other effects that make the IR spectral interpretation difficult occur. One of them is so called electronic effect which causes changes of the force constant f due to the electronic structure of the molecule, and consequently induces shifts in wavenumber. An example is shifted ν of C-H band in O=C-H structures (aldehydes), because electronegative oxygen pulls electron density away from C-H bond, weakening it and reducing the C-H force constant. [Smt99]

Effects of association. These phenomena occur when two bonds of the same symmetry are closely located either within one molecule (intramolecular associations. named also coupling), or with other molecule in the surroundings (intermolecular associations). The respective bands are strong and the absorption occurs in the same region. A typical example of the intermolecular association are hydrogen bonds or influences of the solvents (e.g. C=O interferences with OH and NH_2). [Hol75]

A.3.4 Vibrations and rotations of molecules

Typical IR spectra of molecules are vibrational spectra, sometimes with rotational bands superposed on the vibrational ones (vibrational-rotational spectra)

A.3.4.1 Vibrations of molecules

There exist two basic kinds of molecule vibrations: stretching and bending vibrations.

1) Stretching (valence) vibrations marked ν.

Stretching vibrations (stretches) may be illustrated using the CH_2 group as a model (Figure A.3.1). They are generally rather energetic, thus associated absorption bands are at higher wavenumbers in the MIR region.

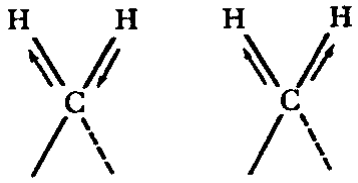

asymmetric stretch ν_{as} symmetric stretch ν_s

Figure A.3.1 Stretching vibrations of the CH_2 group

2) Bending (deformation) vibrations marked δ.

Bending vibrations (alias deformations) of CH_2 and CH_3 groups taken as models are shown in Figure A.3.2, Figure A.3.3. More complicated atomic groups vibrate by approximately the same fashion as CH_2 and CH_3. Some other types of deformations, typical for other

groups, e.g. cyclic molecules, may occur. (Figure A.3.4) The deformations are generally less energetic than stretches, thus associated absorption bands lay at lower wavenumbers.

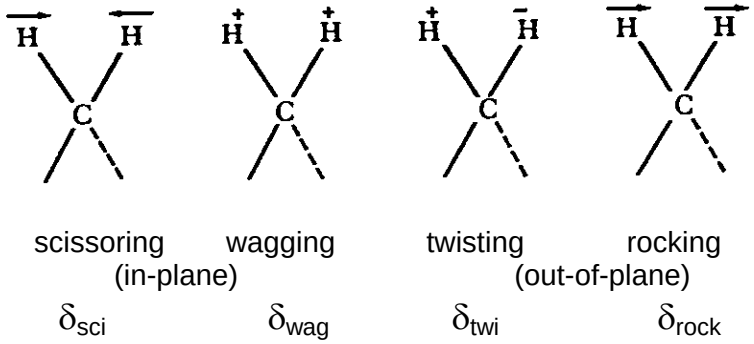

Figure A.3.2 Bending (deformation) vibrations of CH_2 group

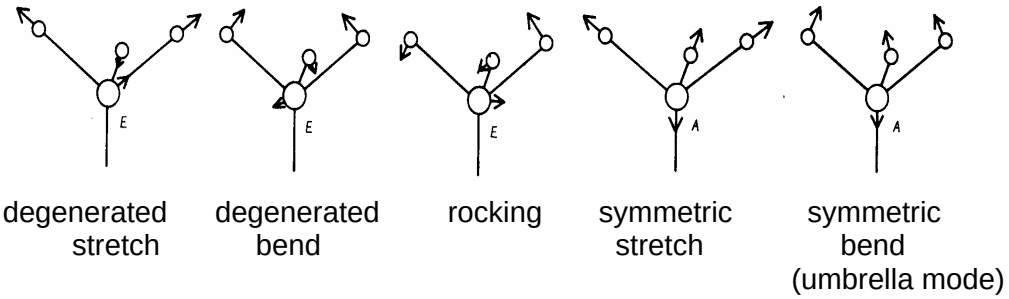

Figure A.3.3 Vibrations of CH_3 group

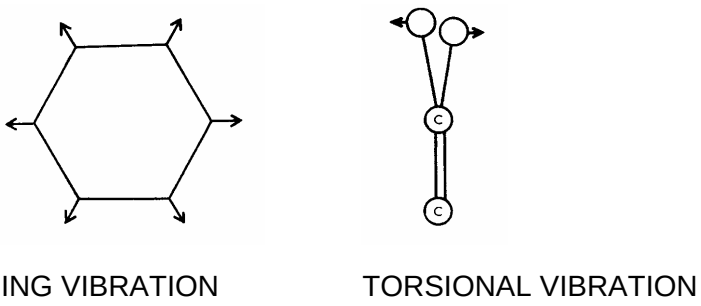

Figure A.3.4 Breathing (skeletal) and torsional vibrations

A.3.4.2 Rotations of molecules

Rotations of molecules go together with their vibrations, molecules behave as vibrating rotators (rotors). Rotors can be linear, symmetric, asymmetric or spherical. They are characterised by the total angular moment *J*. Rotations of molecules are explained in

Appendix A.2, chapters A.2.3 (Rotational spectra of diatomic molecules) and A.2.5 (Vibrational-rotational spectra of diatomic molecules). Detailed description of the vibrations and rotations of molecules is given by quantum mechanics, for example by P.W.Atkins in [Atk94].

As was already mentioned at the beginning of this appendix, rotational energies of the molecules are lower than the vibrational ones. That is the reason why equidistant rotational lines are superposed on the vibrational bands. It can be obviously seen on high resolution IR absorption spectra of simple molecules such as CO, NO, CO_2 and NO_2.

A.3.5 Absorption

When a radiation transmits through the matter able to absorb it, its intensity decreases. The dependence of the monochromatic radiation intensity on the absorption in the homogeneous environment characterised by the concentration c given in volume per cent (ppm or ppb respectively), the extinction coefficient ε [m^{-1}] (rate of the absorption in one unit of the compound) and the optical length l [cm] is described by the Lambert-Beer law [Atk94]:

$$I = I_0 e^{-cl\varepsilon} \tag{A.3.8}$$

where I_0 is the initial intensity and I is the intensity after absorption (Figure A.3.5). The law is valid just in a certain range of concentrations.

The new physical quantities are introduced in spectroscopy: transmittance T and absorbance A, both dimensionless, usually given in %. T is given by the following formula:

$$T(\nu) = \frac{I}{I_0} \tag{A.3.9}$$

This is for the case of one beam spectrometers assuming $T = 1$ for I_0. The double beam spectrometers have $T = T_b < 1$ for I_0. T_b is the background transmittance. Then (A.3.9) modifies to (A.3.10):

$$\frac{T(\nu)}{T_b(\nu)} = \frac{I}{I_0} \tag{A.3.10}$$

Fourrier transform infrared (FTIR) spectrometer Bruker IFS 48 is an example of one-beam spectrometer, dispersive spectrometer Specord M 80 is a double beam spectrometer. Both were used in this work.

Absorbance *A* (optical density) is defined by the formula:

$$A(\nu) = \ln \frac{T_b}{T} = \ln\left(\frac{I_0}{I}\right) \qquad \text{(A.3.11)}$$

thus $$A(\nu) = cl\varepsilon \qquad \text{(A.3.12)}$$

Lambert-Beer law (A.3.8) is sometimes given with an exponent of 10, absorbance *A* is then defined by a decadic logarithm of the same term. The formula (A.3.12) is important for calculation of the concentration *c*. It was applied for the calculation of concentration of cyclohexanone and toluene, VOC concerned in this work, as well as for all other gases produced by the VOC removal process (see Tables 5.2.1 and 5.2.2 in chapter 5.2.5).

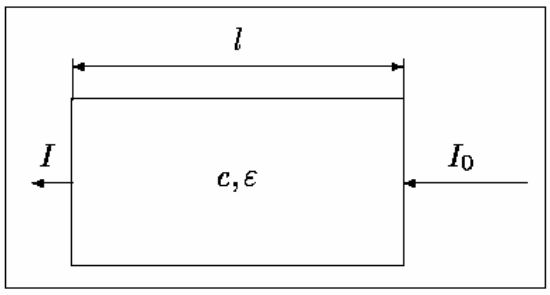

Figure A.3.5 Lambert-Beer law - Absorption of the light intensity I_0

A.3.6 Interpretation of the IR bands

There are several general factors necessary to take into account when IR spectra are interpreted. We note the most important ones, all other effects such as associations (inter- and intra-molecular), electronic effects and Fermi resonance (already explained in section A.3.3) must be considered as well.

A.3.6.1 Band intensity

Intensities of the absorption bands are divided into 5 categories. These notations. which are often made subjectively by visual inspection of the spectrum, correspond to the apparent molecular absorption coefficient ε_a with values viewed in Table A.3.2. ε_a is given by formula (A.3.13) where c is the concentration in moles per litre, l is the cell thickness in cm and I_0 and I are the intensities of entering and transmitted light. Accordingly, $\log_{10}\left(\frac{I_0}{I}\right)_\nu$ is the apparent optical density obtained when the instrument is set to the wavenumber ν, it is not the true absorbance involved by Lambert-Beer law (A.3.8). [Nak77]

$$\varepsilon_a = \frac{1}{cl}\log_{10}\left(\frac{I_0}{I}\right)_\nu \qquad \text{(A.3.13)}$$

Intensity	abbreviation	ε_a
very strong	vs	>200
strong	s	75-200
medium	m	25-75
weak	w	5-25
very weak	vw	0-5

Table A.3.2 Intensities of the IR absorption bands according to the apparent absorption coefficient ε_a [Nak77]

A.3.6.2 Types of the absorption bands

- Characteristic bond and group bands. These reflect bonds and functional groups present in the compounds. Characteristic absorption bands appear with a relatively high intensity in the range characteristic for a certain group of atoms (e.g. -CH_2) and are useful for a primary identification of the group. They cover the whole MIR region, metal-organic bonds have bands in the deformation (FIR) region (below 700 cm^{-1}).
- Deformation vibrations. Appearance of the deformation bands in spectra gives a complementary information to the characteristic group bands. However, they are also necessary for the interpretation. They define valence angles within the molecule. Their position in the spectra is in the region under 2000 cm^{-1}.

- Skeletal vibrations. The region of wavenumbers 1350 $cm^{-1} > \nu > 650$ cm^{-1} correspond to the skeletal vibrations of the molecules. i.e. breathing vibration modes of rings and cycles.
- Overtones. Overtones having approximately twice frequency of the normal vibration will occasionally be observed as weak bands. They may be useful for instance at the interpretation and differentiation of CH bands from the region 3000-2800 cm^{-1} as appeared in the NIR region.
- Combination tones. Weak bands occasionally appearing at frequencies that are a sum or a difference of two or more fundamental bands. Thus, bands at x and y cm^{-1} may give rise to weak bands at $x+y$ or $x-y$ cm^{-1}. Weak combination tones of CO_2 appearing at 3600-3800 cm^{-1} region (ν_{as} at 2350 cm^{-1} + $2\times\delta_{as}$ at 667 cm^{-1}) helped at the calibration of the main CO_2 bands in this work, see chapter 5.2.5.3.

[Nak77, Hol75, Ben68]

A.3.6.3 Positive and negative spectral interpretation

The spectrum can be interpreted by seeing which absorption bands are present in it – the positive interpretation, or which bands are absent – the negative interpretation. Usually, both approaches are used at the same time. [Soc94]

A.3.7 References

[Atk94] Atkins P.W. (1994) *Physical Chemistry*, Oxford University Press, 5th edition

[Ben68] Bentley F.F., Smithson L.D., Rozek A.L.: *Infrared Spectra and Characteristic Frequencies ~700-300 cm-1*, John Wiley & Sons, New York, London, Sydney 1968

[Hol75] Holly S., Sohár P. (1975) *Absorption spectra in the infrared region*, Akademiai Kiado Budapest

[Nak77] Nakanishi K. (1977) *Infrared Absorption Spectroscopy*, Holden Day Inc.

[Smt99] Smith B.: *Infrared Spectral Interpretation*, CRC Press, 1999

[Soc94] Socrates G. (1994) *Infrared characteristic group frequencies*, table and charts, John Willey & sons Inc.

[WAIS] *Working atlas of infrared spectroscopy* (1972) Butterworths, London

REFERENCES

[Aki93] Akishev Yu. S., Deryugin A. A., Kochetov I. V., Napartovich A. P., Trushkin N. I. (1993) J. Phys. D: Appl. Phys. **26**, 1630-1637

[Aki96] Akishev Yu. S., Napartovich A. P., Trushkin N. I.:*"Decomposition of VOC at ppm levels using DC glow discharge plasmas"* Int. Symp. on High Pressure Low Temperature Plasma Chemistry **HAKONE V,** Mílovy, Czech Republic, Sep 1996, pp. 123-124

[Alb71] Albugues F., Birot A., Blanc D., Brunet H., Galy J., Millet P., Millet P. (1971) J. Chem. Phys. **61**, 7, 2695

[AMTS97] Annual Meeting Technical Sessions SYMPOSIUM - Session **28**, 19 November 1997, San Gabriel C

[And99] Anderson G.K., Snyder H., Coogan J. (1999) Plasma Chem. Plasma Proc. **19** (1), 131-151

[Ans97] Anshumali, Winkleman B.C., Sheth A (1997) J. Air & Waste Manage. Assoc. **47**, 1276-1283

[Ati92] Atkinson R., Baulch D.L., Cox R.A., Hampson R.F. jr., Kerr J.A., Troe J. (1992) J. Phys. Chem. Ref. Data **21**, 1125

[Atk94] Atkins P.W. (1994) *Physical Chemistry,* Oxford University Press, 5th edition

[Bad65] Badareu E., Popescu I.: *Gaz Ionisés, Décharges dans les gaz*, Ed. Editura Technica, Bucuresti, & Ed. Dunod, Paris (1965)

[Bai92] Bailey A., Stanley A.W., Williams M.R.: *"Gas phase decomposition of organic vapours in dc corona discharges"* 10th Int. Conf. on Gas Discharges & their Application, Swansee (1992), pp. 356-359

[Bak84] Baker L.E.: *"Solvent disposal"* in Solvent problems in industry, Elsevier applied science publishers LTD (1984), pp. 185-193

[Bas75] Bastien F., Haug R., Lecuiller M. (1975) J. Chimie Physique **72**, 105

[Bau82] Baulch D.L., Cox R.A., Crutzen P.J., Hampson R.F., Jerr J.A., Troe J., Watson R.T. (1982) J. Phys. Chem. Ref. Data **11**, 1259

[Bec97] Becker K.H., Kurtenbach R., Schmidt F., Wiesen P. (1997) Ber. Bunsenges. Phys. Chem. **101**, 128-133

[Ben68] Bentley F.F., Smithson L.D., Rozek A.L.: *Infrared Spectra and Characteristic Frequencies ~700-300 cm^{-1}*, John Wiley & Sons, New York, London, Sydney 1968

[Bla78] Blair D.T.A. (1978) *"Breakdown Voltage Characteristics"*, Electrical Breakdown of Gases, eds J.M.Meek and J.D.Craggs, New York, Willey & Sons, 533-654

[Bor98] Borra J.-P., Goldman A., Goldman M., Boulaud D. (1998) J. Aerosol Sci. **29**, No 5/6, 661-674

[Bra98] Brablec A., Slavíček P., Klíma M., Kapička V.: *"High pressure RF discharge: Spectral diagnostics and perspective apllication"* 11th Symp. on Elementary Processes and Chemical Reactions in Low Temperature Plasma, eds. M.Morvová & K.Hensel, Contrib. Papers **2**, 188-191, Low Tatras, Slovakia, June 1998

[Bro65] Browning E. (1965) *Toxicity and metabolism of industrial solvents*, Elsevier publishing company, Amsterdam, London, New York

[Bro80] Brož J., Roskovec V., Valouch M.: *Physical and Mathematical Tables (Fyzikální a matematické tabulky)*, SNTL Praha 1980

[Bug96] Bugaev S.P., Kuvshinov V.A., Sochugov N.S., Khryapov P.A.: *"Oxidative conversion of methane in a plasmochemical reactor with a simulated phase transition of the reaction*

products" Int. Symp. on High Pressure Low Temperature Plasma Chemistry **HAKONE V,** Mílovy, Czech Republic, Sep 1996, pp. 145-149

[Cha96] Champain H. (1996) *"Stabilité des décharges couronne dans le SF_6 en régime établi. Spectroscopie de la décharge et phénomènes aux électrodes"*, Thèse de doctorat de l'Université Paris XI

[ChD89] Chang D.P.Y., Guensler R., Uyeminami D., Schroeder E.D., Caballero R., Griffith P.: *"Efficiency of activated carbon bed odor control systems for VOC removal"* Proc. of 82nd Annual Meeting & Exhibition, Air & Waste Management Association, Anaheim California, June 1989, pp. 2-13

[Che94a] Chelouah A., Marode E., Hartmann G., Achat S. (1994) J. Phys. D: Appl. Phys. **27**, 940-945

[Che94b] Chelouah A., Marode E., Hartmann G. (1994) J. Phys. D: Appl. Phys. **27**, 770-780

[ChJ93a] Chang J.S.:*"Energetic electron induced plasma processes for reduction of acid and greenhouse gases in combustion flue gas"*, Non-Thermal plasma techniques for pollution control, eds B.M.Penetrante & S.E.Schultheis, NATO ASI series, Part **A**, pp. 1-32, Springler-Verlag Berlin Heidelberg 1993

[ChJ93b] Chang J.S., Kohno H., He W., Berezin A.A., Looy P.C., Iijima K., Honda S., Matsumoto Y., Shibuya A.: *"Dissociation of methane by atmospheric glow discharges in a capillary tube plasma reactor"* Int. Symp. on High Pressure Low Temperature Plasma Chemistry **HAKONE IV**, Bratislava, Slovakia, Aug-Sep. 1993, pp. 171-176

[ChJ97] Chang J.S., Myint T., Chakrabarti A., Miziolek A. (1997) *"Removal of carbon tetrachloride from air stream by a corona torch plasma reactor"* Jpn. J. Appl. Phys. **36**, part 1, No 7B, 5018-5024

[ChM95] Chang M.B., Lee C.C. (1995) *"Destruction of formaldehyde with dielectric barrier discharge plasmas"* Envin.Sci.Technol. **29**, 181-186

[ChM97] Chang M.B., Chang C.C. (1997) *"Destruction and removal of toluene and methyl-ethyl-ketone from gas streams with silent discharge plasma"* AIChE J. **43**, No 5, 1325-1330

[Chn84] Chen F.F.: *Introduction to plasma physics*, Plenum Press, New York 1974 (Czech translation, Academia Praha, 1984)

[ChR88] Chang R., Tikkanen W.: *The Top Fifty Industrial Chemicals*, Random House, New York, 1988

[Coo46] Coops J., Mulder D., Dienske J.W., Smittenberg J. (1946) *"The heats of combustion of a number of hydrocarbons"*, Rec. Trav. Chim. Pays/Bas **65**, 128. [all data]

[Cop92] Cooper W. F., Hershberg J. F. (1992) J. Phys. Chem. **96**, 771-775

[Cze94] Czernichowski A., Opalinska T., Potapkin B.V.:*"Plasma assisted oxidation of chloroform in gliding discharges"* Int. Flame Days, No **46**, Biarritz, France, March 1994

[Cze96] Czernichowski A., Ranaivosoloarimanana A. (1996) Chemtech **26** (4), 45-49

[Cze98] Czernichowski A., Hajossy R.: *"Energetics of selected plasma-chemical processes in electric discharges"* 11th Symp. on Elementary Processes and Chemical Reactions in Low Temperature Plasma, eds. M.Morvová & K.Hensel, Invited Papers, pp. 7-25, Low Tatras, Slovakia, June 1998

[Don98] Donó A., Martinucci S., Paradisi C., Scorrano G., Rea M.: *"Decomposition of chlorinated VOC in air at ambient temperature and pressure in a pulsed corona reactor and in an APCI source"* Int. Symp. on High Pressure Low Temperature Plasma Chemistry **HAKONE VI,** Cork, Ireland, Aug-Sep 1998, pp. 31-36

[Dut63] Dutton J., Llewellyn-Jones F., Rees D.B. (1963) *"The determination of attachment and ionisation coefficients in air"* Proc. Phys. Soc. of London **85**, 909

[EEU99] *Environment in the European Union at the turn of the century* (1999) European Environmental Agency

[Eli87] Eliasson B., Hirth M., Kogelschatz U. (1987) *"Ozone synthesis form oxygen in dielectric barrier discharge"* J. Phys. D: Appl. Phys. **20**, 1421

[Emd92] Emdee J.L., Brezinsky K., Glassman I. (1992)*"A kinetic model for the oxidation of toluene near 1200 K"* J. Phys.Chem. **96**, No 5, 2151-2161

[Fal99] Falkenstein Z. (1999) J. Appl. Phys. **85**, No 1, 525-529

[Fil00] Filimonová E.A., Amirov R.H.: *"Modelling of C_2H_2 removal for different conditions of streamer discharge organization in air"* Int. Symp. High Pressure Low Temperature Plasma Chemistry **HAKONE VII**, eds. H.-E.Wagner, J.F.Bhenke, G.Babucke, Proc. **1**, 174-178; Greisfwald, Germany, Sep 2000

[Fil98] Filimonová E.A., Amirov R.H., Francke K.-P., Rudolph R.:*" Removal of ethene from synthetic air using pulsed corona discharge"* 11th Symp. on Elementary Processes and Chemical Reactions in Low Temperature Plasma, eds. M.Morvová & K.Hensel, Contrib. Papers **2**, 212-215, Low Tatras, Slovakia, June 1998

[Fra56] Francis G.: *"The Glow Discharge at Low Pressure"* Encyclopedia of Physics, Vol. **XXII**, Gas Discharges II, ed S.Flügge, Spriger-Verlag, Berlin-Heidelberg, 1956; 53-208

[Frc98] Francke K.P., Miessner H., Rudolph R., Rutkowski J.: *"Removal of VOCs by plasmocatalysis"* 11th Symp. on Elementary Processes and Chemical Reactions in Low Temperature Plasma, eds. M.Morvová & K.Hensel, Contrib. Papers **1**, 63-64, Low Tatras, Slovakia, June 1998

[Fri99] Fridman A., Nester S., Kennedy L.A., Saveliev A., Mutaf-Yardimci O. (1999) Progress in Energy and Combustion Science **25**, 211-231

[Frk93] Frank N.W., Hirano S.: *"The history of electron beam processing for environmental pollution control and work performed in the US",* Non-Thermal plasma techniques for pollution control, eds B.M.Penetrante & S.E.Schultheis, NATO ASI series, Part **B**, Springler-Verlag Berlin Heidelberg 1993; pp. 1-26

[Fut97] Futamura S., Zhang A., Yamamoto T. (1997) J. Electrostatics **42**, 51-62

[Fut98] Futamura S., Zhang A., Einaga H.: *"Involvement of active oxygen species in plasma chemical decomposition of volatile hydrocarbons"* The Asia-Pacific Workshop on Water and Air Treatment by Advanced Techn.: Innovation and Commercial Appl., Proceedings, 87-90, December 1998

[Gal79] Gallimberti I. *Invited Lecture*, Proceedings 9th Int. Conf. Phen. Ion. Gas, Grenoble, France 1979 & Journal de Physique, Supp **40**, C7, 193

[Gas00] Gasparik R., Ihara S., Satoh S., Yamabe C. (2000) Reports of the Faculty of Science and Engineering, Saga University **29**, No 1, 25-46

[Gas98] Gasparik R., Yamabe C., Ihara S., Satoh S. (1998) Jpn. J. Appl. Phys. **37**, 5786-5788

[Gas99] Gasparik R.: *"Electrode materials and initial gas composition effects on NOx treatment using dc positive streamer corona"*, PhD thesis, Saga University, Japan, 1998

[Gau98] Gaurand I., Hibert C., Nikravech M., Motret O., Pavé D., Pouvesle J.M.: *"Pulsed dielectric barrier discharge processing of TCE"* Int. Symp. on High Pressure Low Temperature Plasma Chemistry **HAKONE VI,** 260-264; Cork, Ireland, Aug-Sep 1998

[Ghe98] Gherardi N., Gat E., Gouda G., Massines F. Proc. Int. Symp. on High Pressure Low Temperature Plasma Chemistry **HAKONE VI**, 118-122, Cork, Ireland, Aug-Sep 1998

[GHGT98] 4th Int. Conf. on Greenhouse Gas Control Techn., Interlaken, Switzerland, Aug-Sep 1998, various contributions

[Gla82] Glaser A.N. (1982) Ann. Rev. Microbiol. **36**, 173-198

[Glb95] Glarborg P., Kubel D., Kristensen P.G., Hansen J., Dam-Johansen K. (1995) *"Interactions of CO, NO_x and H_2O under post flame conditions"* Combus. Sci. Techn. **110-111**, 461-485

[Gls95] Goldston R.J., Rutherford P.H.: *Introduction to Plasma Physics*, IOP Publishing Ltd 1995

[Gol83] Goldman A., Amouroux J.: *"Plasma Chemistry"*, Electrical Breakdown and Discharges in Gases, eds E.E.Kundhart, L.H. Luessen, NATO ASI series **B 89b**, Plenum Press, New York, 1983

[Gol93] Goldman M, Goldman A. (1993) High Temperature Chem. Process **2**, 215-220

[Gri98] Gritsinin S.I., Kossyi I.A., Misakyan M.A., Silakov V.P., Temchin S.M.:*"Freons and the products of their transformation evolution in electric discharges"* Europeen Conf. on the Atomic and Molecular Phys. of Ionized Gases **ESCAMPIG XIV,** Malahide, Ireland, Aug 1998, pp. 478-479

[Haf95] Hafez R., Samson S., Marode E.: *"A prevented spark reactor for pollutant control. Investigation of NO_x removal"* **12th ISPC**, Minneapolis, USA, 855-861

[Han00] Hanic F., Morvová M., Morva I. (2000) J. Thermal Analysis Calorimetry **60**, 1111-1121

[Har64] Hartmann G. (1964) *"Analyse temporelle ultra-rapide de phénomènes transitoires et faiblement lumineux"*, Mémoire Ingénieur du CNAM, Paris

[Har77] Hartmann G. (1977) *"Spectroscopie de la décharge couronne: étude des mécanismes de collision dans le dard"* Thèse de doctorat de l'Université Paris XI

[HCP] Handbook of Chemistry and Physics, ed. Weast R C, Astle M J, 60th edition 1979-1980, CRC Press

[Hen96] Hensel K., Morvová M. (1996) Contrib. Plasma Phys. **36**, 1, 51-61

[Hll74] Hollahan J.R., Bell A.T.: *Techniques and Applications of Plasma Chemistry*, John Willey & Sons - Interscience, New York 1974

[Hlz98] Holzinger R., Warneke C., Hansel A., Jordan A., Lindinger W.: *"Diagnostics of biomass burning plumes: a source of VOC ..."* Europeen Conf. on the Atomic and Molecular Phys. of Ionized Gases **ESCAMPIG XIV,** Malahide, Ireland, Aug 1998, pp. 530-531

[Hol75] Holly S., Sohár P.: *Absorption spectra in the infrared region*, Akademiai Kiado Budapest, 1975

[Hou94] Houghton J.: *Global warming, the complete briefing*. Lion Publishing, Oxford, UK (1994)

[Hsi95] Hsiao M.C., Merritt B.T., Penetrante B.M., Vogtlin G.E., Wallman P.H. (1995) *"Plasma assisted decomposition of methanol and TCE in atmospheric pressure air streams by electrical discharge processes"* J. Appl. Phys **78** (5), 3451-3456

[HsL98] Hsieh L.-T., Lee W.-J., Chen Ch.-Y., Wu Y.-P. G., Chen S.-J., Wang Y.-F. (1998) J. Hazardous Materials **B 63**, 69-90

[Huc00] Huczko A., Lange H., Sioda M., Rżanek-Boroch Z., Morvová M. (2000) Czech. J. Phys. **50**, No 5, 615-622

[Huc98] Huczko A., Sioda M., Kaminski A., Lange H.: *"Arc plasma pyrolysis of carbon bearing reactants"* 11th Symp. on Elementary Processes and Chemical Reactions in Low Temperature Plasma, eds. M.Morvová & K.Hensel, Contrib. Papers **1**, 83-86, Low Tatras, Slovakia, June 1998

[IPCC] International Panel on Climate Change 1995 - the science of climate change, summary for policymakers and technical summary of the working group I report. Cambridge University Press, Cambridge, UK, 1996

[Ito93] Ito T., Ehara Y., Onouchi H.: *"New type of ozonizer by superposition of silent discharge and surface discharge."* Int. Symp. on High Pressure Low Temperature Plasma Chemistry **HAKONE IV**, Bratislava, Slovakia, Aug-Sep. 1993, pp. 7-12

[Jaf95] Jaffrezic X. (1995) *"Etude de l'ammorcage de la combustion..."*, Thèse de doctorat de l'Université Paris XI

[Jas00] Jasinski M., Szczucki P., Dors M., Mizeraczyk J., Lubanski M., Zakrzewski Z.: *"Application of coaxial-line-based microwave torch ..."* Int. Symp. High Pressure Low Temperature Plasma Chemistry HAKONE VII, Greisfwald, Germany, Sep 2000, eds. H.-E.Wagner, J.F.Bhenke, G.Babucke; Proc. vol. **2**, 496-500

[Jaw96] Jaworek A., Krupa A., Czech T. (1996) J. Phys. D: Appl. Phys. **29**, 2439-2446

[Jor96] Jordan A., Prazeller P., Holzinger R., Hansel A., Panlson J.F., Lindinger W.: *"VOC compounds in urban air and indoor air investigated by PTR-MS"* Europeen Conf. on Atomic and Molecular Phys. of Ionized Gases **ESCAMPIG XIII,** Poprad, Sovakia, Aug 1996, pp. 383-384

[Kal96] Kalyana S., White S., Finney W.C., Locke B.R., Clark R.J.: *"Reaction products and chemical pathways for ethylene breakdown in simulated combustion gases in a pulsed corona reactor"* Int. Symp. on High Pressure Low Temperature Plasma Chemistry **HAKONE V,** Mílovy, Czech Republic, Sep 1996, pp. 77-81

[Kan98] Kando M.:*"Microwave discharge at atmospheric pressure and its application to the production of fullerene"* 11th Symp. on Elementary Processes and Chemical Reactions in Low Temperature Plasma, eds. M.Morvová & K.Hensel, Invited Papers, 73-92. Low Tatras, Slovakia, June 1998

[Kar81] Karle I.L., in *The Peptides*, eds. E.Gross & J.Meienhofer, Vol. **4**, Academic Press, New York 1981, p. 1

[Kla93] Klaeyle M. (1993) *"Etude cinétique des processus de dégradation thermique ..."*, Thèse de doctorat de l'Université Lille I

[Kog93] Kogelshatz U.:*"UV production in dielectric barrier discharges for pollution control"*, Non-Thermal plasma techniques for pollution control, eds B.M.Penetrante & S.E.Schultheis, NATO ASI series, Part **B**, 339-354, Springler-Verlag Berlin Heidelberg 1993

[Koh98] Kohno H., Berezin A., Chang J.S., Tamura M., Yamamoto T., Shibuya A., Honda S. (1998) IEEE Trans. Industry Appl. **34**, No 5, 953-966

[Kon97] Konnov A.A.: *"NO formation rates in natural gas combustion"* 4th Int. Conf. on Techn. & Combustion for a Clean Env., Vol. **1**, 1-9, Lisbon, Portugal, July 1997

[Kor98] Korzekwa R.A., Grothaus M.G., Hutcherson R.K., Roush R.A., Brown R. (1998) Review of scientific instruments **69**, No 4, 1886-1892

[Kos92] Kossyi I.A., Kostinsky A.Yu., Matveyev A.A., Silakov V.P. (1992) Plasma Sorces Sci. Technol. **1**, 207-220

[Kra96] Krasnoperov L.N., Krishtopa L.G., Bozzelli J.W. (1996) J. Advanced Oxid. Tech., 583-595

[Kre98] Kreissl B. (1998) *"Influence des lignes de transport à haute tension sur la chimie atmosphérique en corrélation avec les conditions météorologiques"*, Thèse de doctorat de l'Université Paris VI

[Kri87] Krivonosova O.E., Losev S.A., Nalivaiko V.P., Mukoseev Yu.K., Shalatov O.P. (1987) *Plasma Chemistry* **14**, ed B. Smirnov, Moscow, Energoatomizdat, p. 3-31

[Krw98] Krawczyk K., Rusniak J., Schmidt-Szalowski K.: *"Decomposition of CCl_4 in silent discharge stabilised by a dielectric barrier"* Int. Symp. on High Pressure Low Temperature Plasma Chemistry **HAKONE VI,** Cork, Ireland, Aug-Sep 1998, pp.42-46

[Kud00] Kudrjashov S.V., Sirotkina E.E., Loos D.: *"Oxidation of n-C5-C8 hydrocarbons and cyclohexane in the barrier discharge"* Int. Symp. High Pressure Low Temperature Plasma Chemistry **HAKONE VII**, Greisfwald, Germany, Sep 2000, eds. H.-E.Wagner, J.F.Bhenke, G.Babucke; Proc. vol. **2**, 257-261

[Kur97] Kurdel M., Morvová M.: (1997) *"DC corona discharge influence on chemical composition in mixtures of natural gas with air and combustion exhaust with air"* Czech. J. Phys. **47**, No 2, pp. 205-215

[Lar98] Larsson A. (1998) J. Phys. D: Appl. Phys. **31**, 1100-1108

[Ler95] Lerner B., Birmingham J., Tonkyn R., Barlow S., Orlando T.: *"Decomposition of TCE by a large scale high flow packed-bed gas phase corona reactor"* 12th Int. Symp. on Plasma Chemistry, Minneapolis, USA, 697-703

[Les94] Lesueur H., Czernichowski A., Chapelle J. (1994) *"Electrically assisted partial oxidation of methane"* Int. J. Hydrogen Energy **19**, No 2, 139-144

[Lin96] Lindinger W., Hansel A.: *"Analysis of trace gases at ppb levels by PTR-MS"* Europeen Conf. on Atomic and Molecular Phys. of Ionized Gases **ESCAMPIG XIII,** Poprad, Sovakia, Aug 1996, pp. LII-LV

[Lin98] Lindinger W.: *lecture at the* 11th Symp. on Elementary Processes and Chemical Reactions in Low Temperature Plasma, not in the Proceedings, Low Tatras, Slovakia, June 1998

[LlJ56] Llewellyn-Jones F.: *"Ionization Growth and Breakdown"* Encyclopedia of Physics, Vol. **XXII**, Gas Discharges II, 1-52, ed S.Flügge, Spriger-Verlag, Berlin-Heidelberg, 1956

[Loe65] Loeb L.B. : *Electrical coronas, their basic physical mechanisms*, University of California Press, Berkeley, Los Angeles 1965

[Lof77] Lofthus A, Krupenie P H (1977) J. Phys. Chem. Ref. Data **6**, 113-307

[Lou76] Loudet M., Grimaud M., Metras F., Pfister-Guillouzo G. (1976) *"Interactions intramoleculaires en serie cyclohexanique partie II. Spectres photoelectroniques de chloro-2-cyclohexanones"*, J. Mol. Struct **35**, 213

[Low95] Lowke J.J., Morrow R. (1995) *"Theoretical analysis of removal of oxides of sulphur and nitrogen in pulsed operation in electrostatic precipitators"* IEEE Trans. Plasma Sci. **23**, No 4, 661-671

[Lu92] Lu K.-T.; Eiden G.C.; Weisshaar J.C. (1992) J. Phys. Chem. **96**, 9742

[Mac98a] Machala Z., Morvová M., Marode E., Morva I.:*"Removal of aromatic VOCs using high pressure pulseless glow discharge"*, 11th Symp. on Elementary Processes and Chemical Reactions in Low Temperature Plasma, Contrib. Papers **2**, 227-231, eds. M.Morvová & K.Hensel, Low Tatras, Slovakia, June 1998

[Mac98b] Machala Z., Marode E., Morvová M.:*"Study of the high pressure pulseless (d.c.) glow discharge"* Int. Symp. on High Pressure Low Temperature Plasma Chemistry **HAKONE VI,** Cork, Ireland, Aug-Sep 1998, pp. 303-307

[Mac98c] Machala Z., Morvová M., Marode E.:*"Removal of cyclohexanone using high pressure pulseless glow discharge"* Int. Symp. on High Pressure Low Temperature Plasma Chemistry **HAKONE VI,** Cork, Ireland, Aug-Sep 1998, pp. 250-254

[Mac00] Machala Z., Morvová M., Marode E., Morva I.:*"Removal of Cyclohexanone in Transition Electric Discharges at Atmospheric Pressure"*, accepted in J. Phys. D: Appl. Phys. (2000)

[Mag92] Magne L., Cernogora G., Veis P. (1992) J. Phys. D: Appl. Phys. **25**, 472

[Mar75] Marode E. (1975) J. Appl. Phys, I, II, **46**, 2005

[Mar79] Marode E., Bastien F., Bakker M. (1979) J. Appl. Phys. **50**, 140

[Mar86] Marode E., Bastien F., Hartmann G. (1986) NATO Series ASI, Serie **B 149**, 95

[Mar93] Marode E., Goldman A., Goldman M.: *"High pressure discharge as a trigger for pollution control"* Non-Thermal plasma techniques for pollution control, eds B.M.Penetrante & S.E.Schultheis, NATO ASI series, Part **A**, Springler-Verlag Berlin Heidelberg 1993; pp. 167-190

[Mar98] Marode E., Djermoune D., Samson S., Deniset C.: *"Modelling of the chemical dynamics in a streamer induced discharge"* 11th Symp. on Elementary Processes and Chemical Reactions in Low Temperature Plasma, eds. M.Morvová & K.Hensel, Invited Papers 93-109, Low Tatras, Slovakia, June 1998

[Mas98] Massines F. and Gouda G. (1998) J. Phys. D: Appl. Phys. **31**, 3411-3420

[McC99] McCorkle D.L., Ding W., Ma Ch.-Yu, Pinnaduwage L.A. (1999) J. Phys. D: Appl. Phys. **32**, 46-54

[Met84] Metcalfe I., Wilkins C.S.H.: *"Solvent recovery using activated carbon"* in Solvent problems in industry, Elsevier applied science publishers (1984), pp.163-170

[Mez98] Mezei P., Cserfalvi T., Jánossy M., Szöcs K., Kim H.J. (1998) J. Phys. D: Appl. Phys. **31** 2818-2825

[Mil53] Miller S.L. (1953), *"A Production of Amino Acids Under Possible Primitive Earth Conditions"* Science **117**, 528-529

[Mil92] Miller S.L. in *"Major Events in the History of Life"*, Ed. J.W.Schopf, Jones & Bartlett, Boston, 1992, Chap.1, pp. 1-28

[Mll89] Miller J.A., Bowman C.T. (1989) Prog. Energy Combust. Sci. **15**, 287

[Mor97a] Morrow R. (1997) J. Phys. D: Appl. Phys. **30**, 614-627

[Mor97b] Morrow R. (1997) J. Phys. D: Appl. Phys. **30**, 3099-3114

[Mou92] Moussou P., Marode E. (1992) J. Phys. D: Appl. Phys. **25**, 1205-1209

[Mra96] Moras F., Brisset J.-L.: *"Air corona oxidation of halogenated hydrocarbons"* Int. Symp. on High Pressure Low Temperature Plasma Chemistry **HAKONE V,** Mílovy, Czech Republic, Sep 1996, pp. 87-91

[Mrc98] Marec J., Leprince P. (1998) J. Phys. IV France **8**, Pr7-1 – Pr7-17

[Mrr68] Marr G.V.: *Plasma spectroscopy*, Elsevier Publ. Comp., Amsterdam, London, New York 1968

[Mrt95] Martišovitš V.: *Introduction to Plasma Physics*, lecture for students of plasma physics at the Faculty of Mathematics and Physics, Comenius University Bratislava, Slovakia (attended in 1995)

[Mrv93] Morvová M., Morva I., Kurdel M. (1993) *"The Use of Corona Discharge for Rubber Crush Drier Exhaust Control"* Contrib. of Plasma Phys. **33**, 4, 285-295

[Mrv98a] Morvová M. (1998) *"DC corona discharges in CO_2-air and CO-air mixtures for various electrode materials"* J. Phys. D: Appl. Phys. **31**, 1865-1874

[Mrv98b] Morvová M., Hanic F., Morva I.: *"Chemical and physical processes in conversion of the gaseous system CO_2-N_2-H_2O into a solid condensate of amino acids"* 11th Symp. on Elementary Processes and Chemical Reactions in Low Temperature Plasma, eds. M.Morvová & K.Hensel, Contrib. Papers **2**, 237-241, Low Tatras, Slovakia, June 1998

[Mrv98c] Morvová M., Morva I., Machala Z.: *"Environmental application of spontaneously pulsing discharge with corona geometry and developed arc phase"*, 13th Symposium on Physics of switching Arcs, Vol. **II**: Invited Papers, Techn. University Brno 1998, 239-260

[Mrv99a] Morvová M. (1999) Czech. J. Phys. **49**, No 12, 1703-1719

[Mrv99b] Morvová M., Morva I., Machala Z., Janda M.: *"Removal of Aromatic Ring Based VOC Using Electric Discharge and Electrode Catalysis"*, Proc. of 14th **ISPC**, vol. **V**, 2533-2538, eds. M.Hrabovský, M.Konrád, V.Kopecký, Prague, Czech Republic, August 1999

[Mrv00] Morvová M., Hanic F., Morva I. (2000) J. Thermal Analysis and Calorimetry **61**, 273-287

[Msd93] Masuda S.: *"Destruction of gaseous pollutants and air toxics by surface discharge induced plasma chemical process and pulsed corona induced plasma chemical process"* Non-Thermal plasma techniques for pollution control, eds B.M.Penetrante & S.E.Schultheis, NATO ASI series **B**, 199-209; Springler-Verlag Berlin Heidelberg 1993

[Mur84] Murcar W.G., Boden J.C.: *"Heat recovery from solvent incineration"* in Solvent problems in industry, Elsevier applied science publishers 1984, pp. 171-184

[Nak77] Nakanishi K.: *Infrared Absorption Spectroscopy,* Holden Day Inc. 1977

[Ncl62] Nicolls R.W. (1962) J. Quant. Spect. Radiat. Trans. **2**, 433

[NCPSR] *Národný klimatický program SR (National Climate Program of Slovak Republic)*, **I**, No 1, Bratislava 1994, part by D.Závodský et al.

[Nee89] Neely W.C., Newhouse E.I., Pathirana S., Worley S.D. (1989)*"An AM1 SCF study of the of formaldehyde with atomic O"* Chem. Phys. Letters **155**, No 4-5, 381-384

[Nee93] Neely W.C., Newhouse E.I., Clothiaux E.J., Gross C.A.:*"Decomposition of complex molecules using silent discharge plasma processing"* Non-Thermal plasma techniques for pollution control, eds B.M.Penetrante & S.E.Schultheis, NATO ASI series **B**, Springler-Verlag Berlin Heidelberg 1993; pp. 309-320

[New94] Newhouse E.I., Neely W.C., Clothiaux E.I., Rogers J.W.: *"The silent discharge plasma decomposition of trichlorethylene"* Extended abstract of I & EC Special Symp. of the Am. Chem. Soc. Atlanta, GA, USA, September 1994

[Nic94] Nicolas F., Loiseau J.F., Ecrilbengoa A.E., Peyrous R. (1994) J. Phys. D: Appl. Phys. **31**, 3108-3119

[Nie96] Niessen W., Russ H., Schruft R., Nieger M.: *"Modelling of the removal of NO from exhaust by Dielectric Barrier discharge"* Int. Symp. on High Pressure Low Temperature Plasma Chemistry **HAKONE V,** Mílovy, Czech Republic, Sep 1996, pp. 102-105

[Nie98] Niessen W., Wolf O., Schruft R., Nieger M. (1998) J. Phys. D: Appl. Phys. **31**, 542-550

[Nkm66] Nakamoto K.: *Infrared spectra of inorganic and coordination compounds*, John Wiley & Sons, Inc. New York, London (russian translation Mir, Moscow 1966)

[Odi98] Odic E. (1998) *"Etude d'une décharge moyenne fréquence avec barrière dielectrique, ..."*, Thèse de doctorat de l'Université Paris VI

[Odi99] Odic E., Paradisi M., Rea M., Parissi L., Goldman A., Goldman M.:*"Abatement of organic pollutants by corona discharge plasma"*, NATO ARW on Modern Problems of Electrostatics with Applications in Environment Protection, NATO ASI Series **I**, eds I.Inculet and R.Cramarius., Plenum Press 1999, 143-160

[Oga99] Ogata A., Shintani N., Mizuno K., Kushiyama S., Yamamoto T. (1999) IEEE Trans. Industry Appl. **35**, No 4, 753-759

[Oka93] Okazaki S., Kogoma M., Uehara M., Kimura Y. (1993) J. Phys. D: Appl. Phys. **26**, 889

[Opa00] Opalinska T., Pawlowski S., Sekulska A.: *"Decomposition of VOC in a Gliding arc"* Int. Symp. High Pressure Low Temperature Plasma Chemistry HAKONE VII, Greisfwald, Germany, Sep 2000, eds. H.-E.Wagner, J.F.Bhenke, G.Babucke; Proc. vol. **2**, 388-392

[Par98] Parissi L., Odic E., Goldman A., Goldman M., Borra J.P.:*"Formation of particulate by-products by nucleation mechanisms in VOC combustion processes monitored by a dielectric barrier discharge"* Int. Symp. on High Pressure Low Temperature Plasma Chemistry **HAKONE VI,** Cork, Ireland, Aug-Sep 1998, pp. 52-56

[Par99] Parissi L. (1999) *"Etude d'un procedé de traitement d'air chargé en composés organiques volatils ..."*, Thèse de doctorat de l'Université Paris VI

[Pau93] Paur H.-R.:*"Removal of volatile hydrocarbons from industrial off-gas"* Non-Thermal plasma techniques for pollution control, eds B.M.Penetrante & S.E.Schultheis, NATO ASI series **B**, Springler-Verlag Berlin Heidelberg 1993; pp. 77-89

[Pea50] Pearse R.W.B., Gaydon A.G.: *The Identification of Molecular Spectra*, Champan & Hall LTD. London 1950

[Pen95] Penetrante B.M., Hsiao M.C., Bardsley J.N., Merritt B.T., Vogtlin G.E., Wallman P.H., Kuthi A., Burkhart C.P., Bayless J.R. (1995) *"Electron beam and pulsed corona processing of CCl_4 in atmospheric pressure gas streams"* Phys. Let. **A 209**, 69-77

[Pen97a] Penetrante B.M, Bardsley J.N., Hsiao M.C. (1997) *"Kinetic analysis of non-thermal plasmas for pollution control"* Jpn. J. Appl. Phys. **36**, part 1, No 7B, 5007-5017

[Pen97b] Penetrante B.M., Hsiao M.C., Bardsley J.N., Merritt B.T., Vogtlin G.E., Kuthi A., Burkhart C.P., Bayless J.R. (1997) *"Identification of mechanisms for decomposition of air pollutants by non-thermal plasma processing"* Plasma Sources Sci. Technol. **6**, 251-259

[Per85] Perry R.A. (1985)*"Kinetics of the reactions of NCO radical with H_2 and NO using laser photolysis - laser induced flourescence"* J. Chem. Phys. **82**, No 12, 5485-5488

[Pnn84] Penning C.: *"Solvent recovery by distillation"* in Solvent problems in industry, Elsevier applied science publishers LTD, 1984, pp. 151-162

[Poi97] Pointet K., Renou-Gonnord M.F., Milliet A., Jaudon P. (1997)*"Quantification of PAHs in diesel engine combustion by GC/MS"* Bull. Soc. Chim. France **134**, 133-140

[Pol80] Polak L.S.: *Theoretical and experimental plasmochemistry*, Moscow 1980 (in Russian)

[Por96] Porteus A. (1996) *Dictionary of environmental science and technology*. Wiley, Chichester, UK

[Rai91] Raizer Yu. P.: *Gas Discharge Physics*, Springer-Verlag Berlin Heidelberg 1991 (respectively Russian original, Nauka, Moscow, 1987)

[Rap80] Rapakoulias D., Amouroux J. (1980) Revue Phys. Appl. **15**, 1251-1259

[Rdd93] Ruddy E.N., Carrol L.A. *"Select the best VOC control strategy"* Chem. Engeneering Progress, July 1993, pp. 28-35

[Rea93] Rea M., Yan K.: "*Energization of Pulse Corona Induced Chemical Processes*", Non-Thermal plasma techniques for pollution control, eds B.M.Penetrante & S.E.Schultheis, NATO ASI series **A**, Springler-Verlag Berlin Heidelberg 1993; pp. 191-204

[RECOVI] *La Réduction des Emissions de Composés Organiques Volatils dans l'Industrie*, Ademe, Ministère de l'environnement, France, ISBN 2-908035-21-9

[Ree65] Rees J.A. (1965) *"The behaviour of free and attached electrons in oxygen"* Australian J. Phys. **18**, 41-57

[Ree78] Rees J.A. (1978) *"Fundamental Processes in Electrical Breakdown of Gases"*, Electrical Breakdown of Gases, eds J.M.Meek and J.D.Craggs, New York, Willey & Sons, 1-128

[Rog72] Rogoff G.L. (1972) Phys. Fluids **15**, 1931

[Ros93] L.A.Rosocha, G.K.Anderson, L.A.Bechtold, J.J.Coogan, H.G.Hech, M.Kang, W.H.McCulla, N.A.Tennant, P.J.Wantuck: *"Treatment of hazardous organic wastes using silent discharge plasma"* Non-Thermal plasma techniques for pollution control, eds B.M.Penetrante & S.E.Schultheis, NATO ASI series **B**, Springler-Verlag Berlin Heidelberg 1993; pp. 281-307

[Rud00] Rudolph R., Francke K.-P., Miessner H.: *"Plasma catalyytic treatment of hydrocarbons in air flows"* Int. Symp. High Pressure Low Temperature Plasma Chemistry **HAKONE VII**, Greisfwald, Germany, Sep 2000, eds. H.-E.Wagner, J.F.Bhenke, G.Babucke; Proc. vol. **2**, 417-421

[Sch93] Scheytt H., Esrom H., Prager L., Menhert R., von Sonntag C.: *"UV light and electron beam induced degradation of trichloethylene"* Non-Thermal plasma techniques for pollution control, eds B.M.Penetrante & S.E.Schultheis, NATO ASI series **B**, Springler-Verlag Berlin Heidelberg 1993; pp. 91-102

[Scl93] Schlienger M.P.:*"Plasma arc processing of solid and liquid wastes"*, Non-Thermal plasma techniques for pollution control, eds B.M.Penetrante & S.E.Schultheis, NATO ASI series, Part **A**, Springler-Verlag Berlin Heidelberg 1993; pp. 43-48

[Sha71] Shahin M.N. (1971) Reaction under plasma condition, Wiley, New York, **II**-14

[She69] Shemansky D.E. (1969) J. Chem. Phys. **51**, 689-700

[Sho97] Schoenbach K.H., El-Habachi A., Shi W., Ciocca M. (1997) Plasma Sources Sci. Technol **6**, 468-477

[Shv98] Shvedchikov A.P., Belousova E.V., Ponizovskii A.Z., Ponizovskii L.Z. (1998) High Energy Chemistry **32**, No 6, 411-415

[Sig78] Sigmond R. S. (1978) *"Corona Discharge"*, Electrical Breakdown of Gases, eds J.M.Meek and J.D.Craggs, New York, Willey & Sons, 319-384

[Sig84] Sigmond R. S. (1984) J. Appl. Phys. **56**, 1355

[Sig94] Sigmond R. S. (1994) *"The residual streamer channel : return strokes and secondary streamers"* J. Appl. Phys. **56,** No 5, 1355-1370

[Sil91] Silverstein R.M., Bassler G.C., Morril T.C.: *Spectrometric Identification of Organic Compounds*, John Willey & sons, 1991

[Ska93] Skalný J.D., Sobek V., Lukáč P.: *"Negative corona induced decomposition of CCl_2F_2"* Non-Thermal plasma techniques for pollution control, eds B.M.Penetrante & S.E.Schultheis, NATO ASI series **A**, Springler-Verlag Berlin Heidelberg 1993; 151-166

[Smi96] Smith F.L., Sorial G.A., M.T. Suidan, A.W. Breen, Biswas P., Brenner R.C. (1996) *"Development of Two Biomass Control Strategies for Extended, Stable Operation of Highly Efficient Biofilters with High Toluene Loadings"* Environ. Sci. Technol. **30**, 1744-1751

[Smt99] Smith B.: *Infrared Spectral Interpretation*, CRC Press, 1999

[Smu98] Smulders E.H.W.M, van Heesch B.E.J.M, van Paasen S.S.V.B. (1998) IEEE Trans. Plasma Science **26**, No 5, 1476-1484

[Sny98] Snyder H.R., Anderson G.K. (1998) IEEE Trans. Plasma Sci. **26**, No 6, 1695-1699

[Soc94] Socrates G. (1994) *Infrared characteristic group frequencies,* table and charts, John Willey & sons Inc.

[Soo97] Soontjens C.D., Holmberg K., Westerholm R.N., Rafter J.J. (1997)*"Characterization of PAC in diesel exhaust particulate responsible for aryl hydrocarbon receptor activity"* Atmospheric Environment **31**, No 2, 219-225

[SSz93] Schmidt-Szalowski K., Jodzis S.: *"Influence of dielectric packing on characteristics of ozone generation"* Int. Symp. on High Pressure Low Temperature Plasma Chemistry **HAKONE IV**, Bratislava, Slovakia, Aug-Sep. 1993, pp. 37-42

[Tep95] Teplý J., Dressler M., Janča J., Tesař C. (1995) Plasma Chem. Plasma Proc. **15**, No 3, 465-479

[Tho70] Tholl A (1970) Z. Naturforsch. **259**, 420

[Tim50] Timmermans J.: *Physico-Chemical Constants of Pure Organic Compounds*, Elsevier publishing company, Inc. 1950

[UNFCCC] UNITED NATIONS FRAMEWORK CONVENTION ON CLIMATE CHANGE, Kyoto, Dec. 1-10. 1997

[Ura97] Urashima K. Chang J.S., Ito T. (1997) IEEE Trans. Ind. Appl. Soc., New Orleans, USA, 1969-1974

[Uts98] Utsumi Y., Takahashi J. (1998) Jpn. J. Appl. Phys. **37**, L 1268-1270

[vBe92] van Beem E.J.: *"Solvent VOC emission abatement"* XXIst FATIPEC Congress, Amsterdam, June 1992, pp. 158-161

[vHe98] van Heesch E.J.M., Pemen A.J.M., van Paasen S.V.B., Ptasinski K.J., Zacharias P.: *"Hot biogas conditioning using pulsed corona"* Int. Symp. on High Pressure Low Temperature Plasma Chemistry **HAKONE VI,** Cork, Ireland, Aug-Sep 1998, 21-25

[WAIS] *Working Atlas of Infrared Spectroscopy* (1972) Butterworths, London

[War98] Warneke C., Karl T., Judmaier H., Hansel A., Jordan A., Lindinger W.:*"Acetone, Methanol and other parcially oxidised VOC emissions from dead plant matter by abiological processes : Significance for atmospheric chemistry"* Europeen Conf. on Atomic and Molecular Phys. of Ionized Gases **ESCAMPIG XIV,** Malahide, Ireland, Aug 1998, pp. 534-535

[Wat78] Waters R.T. (1978) *"Spark Breakdown in Non-uniform Fields"*, Electrical Breakdown of Gases, eds J.M.Meek and J.D.Craggs, New York, Willey & Sons, 385-532

[Wol72] Wolf G. (1972) *"Thermochemische Untersuchungen an cyclischen Ketonen"*, Helv. Chim. Acta **55**, 1446-1459

[Wue93] Wuebbles D. J. (1993) *Global climate change due to radiatively active gases*, in Global atmospheric chemical change, eds. C.N.Hewitt, W.T.Sturges, Elsevier

[Yam92] Yamamoto T., Ramanathan K., Newsome J.R., Plaks N., Ramsey G.H. (1992) IEEE Trans. Ind. Appl. **28**, No 3, 528-534

[Yam93] Yamamoto T., Lawless P.A., Owen M.K., Ensor D.S., Boss C.: *"Decomposition of VOC by a packed-bed reactor and pulsed corona plasma reactor"* Non-Thermal plasma techniques for pollution control, eds B.M.Penetrante & S.E.Schultheis, NATO ASI series **B**, Springler-Verlag Berlin Heidelberg 1993; pp. 223-237

[Yam97] Yamamoto T. (1997) *"VOC decomposition by nonthermal plasma processing - new approach"* J. Electostatics **42**, 227-238

[Yos96] Y.Yoshioka et al.: *"An effective oxidation of NO of low concentration in large quantity air flow by silent discharge process"* Int. Symp. on High Pressure Low Temperature Plasma Chemistry **HAKONE V,** Mílovy, Czech Republic, Sep 1996, pp. 67-71

[Zhu84] Zhubanov B. A., Agashkin O. V., Ruchina L. B.: *Atlas of IR Spectra of Heterocyclic Monomers and Polymers*, Nauka Alma Ata, 1984